# Computer Aided Analysis of Mechanically Fastened Composite Laminates

by

Surachate Chutima

A Dissertation submitted for the degree of Doctor of Philosophy

in the Faculty of Engineering, University of London

Department of Mechanical Engineering

University College London

May 1996

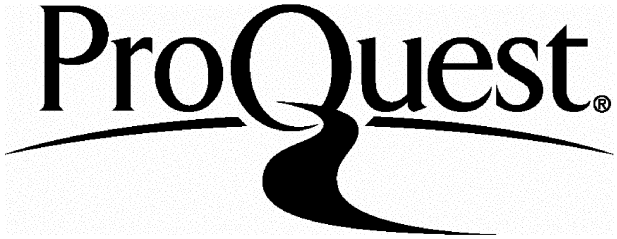

# ABSTRACT

The procedures adopted in the design of mechanically fastened joints between polymer based composite laminates have evolved from the results of a number of experimental investigations as well as some simplified analytical simulations. However, the universal applicability of experimental data is limited, since the type of material, the lamina stacking sequence and the geometric configuration of a joint can vary widely in practice. Similarly there are shortcomings in using an analytical approach to evaluate the stress distribution and joint strength since certain modelling constraints are required to minimize the complexity of the assessment. However, recent advances in modelling techniques have enabled more realistic constraints to be applied, thereby, ensuring greater confidence in the design of this type of joint.

In this study general finite element models are proposed for two dimensional and three dimensional analysis of mechanically fastened composite laminates joined in a double lap fashion. In a two dimensional analysis, the material properties of the fibre and matrix were used, in conjunction with classical laminate theory, to compute the ply properties and, subsequently, the laminate properties, for a variety of ply lay-ups and orientations. These results were then used for each discrete element in the model representing the complete laminate. Finite element analysis was applied to the composite laminate connected in a double lap configuration with a single pin fastening; this was subsequently extended to assess the performance of multi-fastened joints.

From this preliminary investigation three dimensional models were constructed to accurately determine the effect of in-plane loading in the vicinity

of the bolt-laminate contact zone and the interlaminar stresses between adjacent plies in the composite laminate. As in the two dimensional analysis the material properties for each element were computed from the ply material properties in combination with the ply orientation. The laminate properties were subsequently formulated from layering of these elements. Bending and clamping effects as well as interlaminar shear and through thickness stresses were examined using these models.

The results obtained for a range of parametric constraints, viz.; the laminate properties, fastener configuration and interfacial friction, showed good agreement with previously published experimental work. This study confirmed that a design methodology may be developed for mechanically fastened composite laminates utilising commercially available computer code together with appropriate modelling techniques, which must incorporate a full three dimensional stress analysis.

**TO MY FAMILY**

**and THE MEMORY OF MY PARENT**

**CHATCHAVAN CHUTIMA**

# ACKNOWLEDGMENTS

I would like to express my gratitude to my supervisor, Dr. Alvin P. Blackie, for his supervision, enthusiasm, encouragement and valuable suggestions throughout this research.

I also gratefully acknowledge the financial support provided by the Thai Government during the period of my studies. The cooperation from the Thai Government Students' Office is also acknowledged.

A special thanks to my wife, Cattaleeya, my daughter, Chutinan and my son, Vajarah for their support, love, encouragement and patience.

I am also indebted to my parents, Chatchavan and Pensri, and my brothers for their love and kindness.

Finally, thanks to the staff of the Department of Mechanical Engineering, University College London, especially the computer system manager, Mr. Mark Iline and Mr. Joe Fletcher for their help.

# CONTENTS

# LIST OF TABLES

# LIST OF FIGURES

# NOTATION

| Symbol | Description |
|---|---|
| [A] | extensional stiffness matrix for the laminate |
| [B] | coupling stiffness matrix for the laminate |
| C | stiffness component |
| [D] | bending stiffness matrix for the laminate |
| $d$ | hole diameter |
| $d_{bo}$ | bolt diameter |
| E | modulus of elasticity |
| e | distance from the centre of the hole to the edge of the laminate |
| F | force |
| $F$ | components of the strength tensor |
| G | in-plane shear modulus |
| h | distance from the mid plane |
| [K] | structure stiffness matrix |
| $k$ | torque coefficient |
| M | moment resultant per unit width |
| N | force resultant per unit width |
| $n$ | total number of layers in the laminate |
| $p_w$ | clamping pressure |
| Q | reduced stiffness component |
| [$R$] | structural load matrix |

| Symbol | Description |
|---|---|
| $R$ | interlaminar shear strength |
| $r, \theta$ | Polar coordinates |
| S | compliance component |
| $S$ | laminate in-plane shear strength |
| [T] | translation matrix |
| T | bolt tightening torque |
| $t$ | laminate thickness |
| $u$ | displacement vector |
| $w$ | laminate strip width |
| $w_a$ | outside diameter of the washer |
| $X$ | laminate longitudinal strength |
| $x, y, z$ | Cartesian coordinates |
| $Y$ | laminate compressive strength |
| z | distance from the midplane in the thickness direction |
| $\beta$ | prescribed tolerance stress magnitude |
| $\gamma$ | shear strain |
| $[\delta]$ | nodal displacement matrix |
| $[\Delta\delta^0]$ | incremental displacement matrix |
| $\delta$ | displacement component |
| $\varepsilon$ | normal strain |
| $\theta$ | angular position |
| $\kappa$ | curvature component |

| Symbol | Description |
|---|---|

| | |
|---|---|
| $\lambda$ | clearance ratio |
| $\mu$ | static coefficient of friction |
| $\nu$ | Poisson's ratio |
| $\sigma$ | normal stress component |
| $\tau$ | shear stress component |

**SUBSCRIPT**

| | |
|---|---|
| 1, 2, 3 | material principal directions |
| C | compressive |
| f | fibre |
| *k* | layer number in the laminate |
| Lc, Lt | longitudinal compressive and tensile, respectively |
| m | matrix (resin) |
| s | shear |
| T | tension |
| Tc, Tt | Transverse compressive and tensile, respectively |
| v | lamina volume |
| x, y, z | global direction |

**SUPERSCRIPT**

| | |
|---|---|
| *0* | initial position |
| n | increment number |

# CHAPTER 1

# INTRODUCTION

## 1.1 OBSERVATIONS

The utilization of composite materials for a variety of structural purposes has increased with astonishing speed in the last few decades and consequently joining techniques between two or more structural components has become one of the major concerns in research and development as well as design. Conventional mechanical fastening methods have been utilized, although the use of adhesive technology is now quite widespread. Despite the advantages offered by adhesive bonding, mechanically fastened joints are essential to enable a convenient means of assembly, for the replacement of structural parts or to implement dismantling of sections where regular inspection and or repair is required. The common types of joint design used in mechanical fastening of composites are shown in Figure 1.1.

One of the basic functions of mechanically fastened joints is to transfer loads from one structural component to another via the fasteners. The joint strength is dependent on the contact stress distribution developed at the fastener-hole interface. The generalized design methodology for the joining of ductile materials, such as steel, is incapable of providing rational guidelines for the anisotropic and heterogeneous characteristics of a composite material, since in this case a comprehensive stress analysis is required. The most successful and

reliable way to determine the strength of mechanically fastened composite laminates is by full scale experimental examination. However, the ability to tailor laminate properties to match a specific design requirement would be extremely expensive and time consuming using this method. This has encouraged investigators to conduct research concerned specifically with the stress analysis and strength prediction of mechanically fastened composite joints.

The detailed stress or strain distributions in the proximity of a loaded bolt in a composite material can be determined by means of a complex variable formulation (Oplinger and Gandhi 1974), fracture mechanics (Eisenmann 1976) or numerical analysis (Waszczak and Cruse 1971). Most of the analytical investigations of mechanically fastened composite structures are aimed at providing precise stress resultants to enable strength prediction which may then be incorporated in rational design methodologies. Since strength prediction by fracture mechanics methods requires considerable experimental investigation, this presents severe limitation on its application. Furthermore, due to the complexities of the problem, which involves many influential factors, for example: laminate type, ply orientation, stacking sequence and joint configuration, the analytical procedures in predicting joint strength are frequently semi-empirical. For these reasons numerical analysis may be considered as the most appropriate technique to handle these complexities.

The significant influence of joint geometry (e.g., the bolt diameters, laminate width, edge distance and thickness) on the strength and the failure mode

of single bolted joints has been reported by Hart-Smith (1980). Figure 1.2 shows a variety of failure modes that can occur in single fastened double lap composite laminates. Smith (1985) demonstrated that the damage mechanism in composite laminates was extremely complex and essentially distinct from that occurring in metals, though failure modes are similar.

Effective design of mechanically fastened composite joints requires reliable and accurate methods to predict the joint strength. Procedures for determination of strength and the resultant failure mechanism can be considered from either a microscopic or macroscopic point of view. Moreover, it is known that failure patterns for composite joints are more difficult to establish than for joints between isotropic materials because they are more susceptible to the joint variables, such as fastener configuration, joint geometry and material complexity (Curtis, 1993).

The methods for predicting joint strength fall into essentially three categories based on the following: fracture mechanics, damage mechanics or failure criteria. The method based on fracture mechanics requires determination of the energy necessary for development of a single crack. This is not strictly feasible since a single crack can not characterise the complex damage zone in a composite joint. The damage mechanics method covers all the techniques based on the identification of a particular failure mode and the subsequent effort to model such behaviour (Kortschot, 1990). Since this approach relies on predictive models of the physical behaviour,

rather than mathematical formulations, this demands micromechanical detail that is very costly and difficult to incorporate in strength prediction models for composite joints. For this reason, most of the design procedures use simple, approximate, failure theories, or, a two-parameter model, to predict strength.

## 1.2 STATEMENT OF THE PROBLEM

Analytical and numerical techniques based on a two-dimensional approach have been used extensively for performing stress analysis or for investigating the strength and fracture of mechanically fastened composite joints. However, previous analytical strength prediction methods, which are mostly based on semi-empirical procedures, have provided conservative estimates when compared with results from experimental investigations (Poon 1986).

This is due to the fact that in conventional analytical procedures the following assumptions are made, giving less than optimum design: a cosine pressure distribution at the interface, rigid pin contact and smooth surface contact. Moreover, the benefits that may be obtained by suitable selection of the stacking sequence in a composite laminate, to control the magnitude of the through thickness and interlaminar shear stresses, has not been fully realised using two-dimensional modelling. Consequently, an adequate stress investigation procedure, which includes a full contact stress analysis, based

on a more realistic three-dimension model, may offer considerable advantages.

## 1.3 THE OBJECTIVES OF THIS STUDY

The main objective of this study is to conduct a more comprehensive stress evaluation of mechanically fastened composite laminates, subjected to in-plane loading, than has previously been reported. Effects of a range of parametric constraints, viz; the laminate properties, fastener configuration and interfacial friction, on the stress distribution within the laminate will also be quantified. Subsequently, the results obtained from this analysis will be used to determine the resultant ply stress and thereby ascertain the onset and location of ply failure and delamination within the laminate. Rational design guidelines for mechanically fastened composite laminates joined in a double lap fashion are also considered.

## 1.4 SCOPE AND LIMITATIONS

In this analysis commercially available finite element code is utilized to ensure the general applicability of the modelling technique employed. Initially, two-dimensional models, for a single and multi fastened composite laminates joined in double lap configuration, were constructed. The orthotropic shell element has been used in Representative Volume Element (RVE) modelling (Wood, 1994). Gap elements have been utilised to model the contact condition at the fastener-hole interface. A double lap joint configuration, having a perfect

fit pin with circumferential friction at the bolt-hole interface, has been considered.

However, this technique is incapable of evaluating the interlaminar normal and shear stresses, thus a three-dimensional model was developed for a more extensive assessment of the local stress distribution and to determine the onset of failure in the laminate. A replica model of a double lap joint composite laminate, connected by a perfect fit bolt, having layered elements equal to individual ply thickness, was investigated. Friction at the hole boundary between the bolt and laminate, in the circumferential direction, as well as the friction at the laminate plate interface in the loading direction was considered.

The novel analytical aspects of the modelling technique adopted are: three-dimensional modelling based on a layerwise theory that enables evaluation of the global stiffness matrix on a ply-by-ply basis; utilization of gap elements to model the contact condition at the joint interfaces; the ability to incorporate bolt tightening torque in the model; and finally, failure analysis which includes an assessment of the interlaminar normal and shear stresses.

## 1.5 ORGANIZATION OF THE THESIS

The material in this thesis is organized in the following sequence. A review of the relevant literature is given in chapter two. This includes both previously published experimental and analytical studies concerned with mechanically

fastened composite laminates and incorporates topics relating the effect of joint geometry: width (for single fastener), pitch distance (for multi-fastener), edge distance, as well as laminate material properties, stacking sequences, washer size and bolt tightening torque, on the stress distribution and joint strength.

Laminate theory relevant to this analysis is discussed in chapter three. The following chapter includes a description of the two-dimensional modelling exercise adopted for a single fastened, double lap, composite laminate joint. The results and conclusions for this particular model are given in the final section of this chapter. Chapter five includes a similar analysis applied to the problem of multi-row pinned joints and the results and conclusion for this configuration are included in the final part of this chapter. Design guidelines for multi-fastened composite laminates, based on the optimum load transferred, are also provided.

Chapter six contains a description of the three-dimensional model for a single bolt, double lap, composite laminate joint and includes validation of the modelling technique and a comprehensive stress investigation. Failure initiation for a specific joint geometry has also been considered. Results and discussion of this work is presented in the last part of this chapter. The final chapter contains the conclusions of this entire study and includes a comparison of the results obtained in the two-dimensional and three-dimensional modelling exercise as well as considerations for further work.

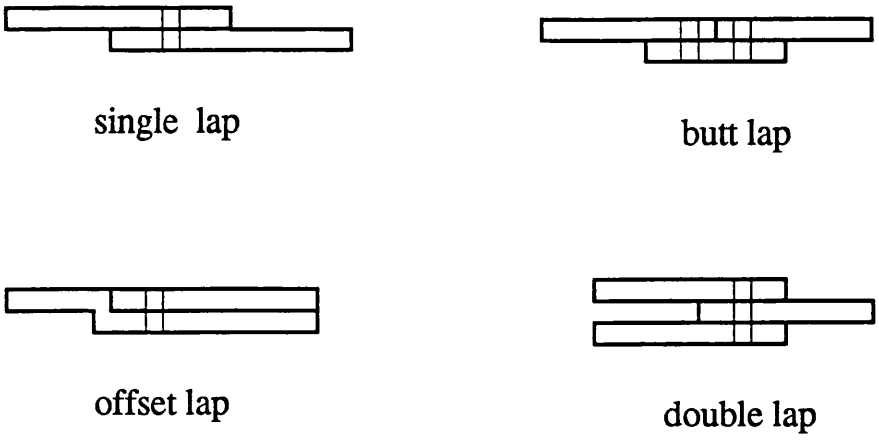


Figure 1.1 Designs of mechanically fastened joints

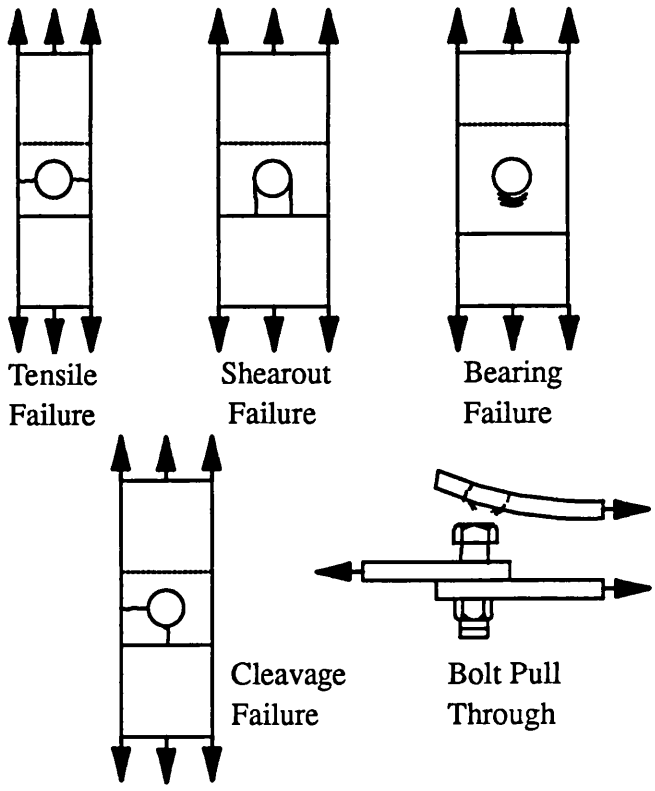


Figure 1.2 Failure modes of double lap composite joints

# CHAPTER 2

# LITERATURE REVIEW

## 2.1 INTRODUCTION

In this chapter previously published state-of-the-art experimental and analytical investigations are surveyed. The review is drawn from the range of general classical experimental examinations as well as the advanced three-dimensional analysis of mechanically fastened joints. The following chapter is divided into two sections on this basis: experimental and analytical investigations of mechanically fastened composite joints.

## 2.2 EXPERIMENTAL EXAMINATIONS OF MECHANICALLY FASTENED COMPOSITE JOINTS

Most of the information provided in design guidance notes for mechanically fastened composite laminates has been obtained from experimental investigations of specific laminate constructions. One of the earliest investigations was undertaken by Lehman and Hawley (1969) to evaluate the performance of CFRP joints for aircraft structures. The empirical methods derived from this and other similar studies has required a tremendous effort in testing and inspection. More recently, major effort has been expended on developing analytical based design methods that can handle the complex analysis associated with modelling the behaviour of mechanically fastened joints.

However, as a consequence of the numerous variables involved analytical approaches are in the early state of evolution and comparison with experimental results is needed to validate the methodology used.

The variables that have a significant influence on joint strength can be categorized into three major groups: material properties, fastener configurations and joint geometry. The following review presents the results of published experimental work on these topics.

### 2.2.1 INFLUENCE OF MATERIAL PROPERTIES ON JOINT STRENGTH

Carbon, glass, boron or Kevlar are the commonly used reinforcing fibres embedded in a resin matrix to form a layer of a prepeg. The fibres may be arranged either unidirectional or in two principal orthogonal directions, as in woven roving, or as randomly chopped short strands. Laminates are produced from stacking the layers of prepegs, usually in a specific sequence or lay-up. The elastic properties of fibrous composite laminates depends strongly on this stacking sequence, as well as the fibre volume fraction, orientation and on the properties of both the fibre and resin within the plies.

**Fibre stacking sequence**

The plies of a laminate can be stacked in more than one combination for any given thickness to provide various laminates having particular mechanical properties. Pagano and Pipes (1971) confirmed that the interlaminar stresses in the vicinity of an unloaded hole, for laminates loaded in tension, are influenced by the stacking sequence of the piles.

The effects of stacking sequence on the strength of mechanically fastened composite laminates has been examined by many investigators. Matthews et al. (1976) investigated riveted joints and found that the bearing strength of a 90° and ±45° lay-up was significantly lower than that for a 0° and ±45° lay-up.

Collings (1977) has concluded from work on 0° and ±45° CFRP laminates joined by a single bolt, that the bearing strengths were significantly lower for stacking sequences having 0° piles grouped together. The tensile strengths were slightly different, but the measured shear strengths were approximately the same for laminates having the same composition but different stacking sequences.

Quinn and Matthews (1977) have examined pin-loaded joints in GFRP laminates and showed that rearrangement of the stacking sequence can lower the bearing strength by 30%, compared with the maximum bearing strength that can be achieved.

Garbo and Ogonowski (1981) and Ramkumar and Tossavainen (1984) have shown that the bearing strength under the tensile loading decreases when the percentage of adjacent plies, having the same fibre orientation, is increased.

**Fibre orientation**

Collings (1977) concluded that for bolted joints between CFRP laminates optimal bearing strength was achieved when the percentage of 0° plies is in the range of 55% to 80%, balanced by ±45°plies to reduce the stress concentration at the loaded hole. For optimum tensile strength the ratio of 0° to 45° piles was 2:1, while an equal percentage of both plies was required for optimum shear strength.

Ramkumar and Tossavainen (1984) tested AS I/3501-6 graphite/epoxy and found that under tensile loads gross tensile strength, gross tensile failure strain and bearing strength increased when the percentage of ±45° plies was increased from 40% to 60%. The failure mode changed in this optimal range from a shear-out mode to a local bearing failure mode. In compression tests the failure strain increased with an increase in percentage of ±45° plies, but gross compressive strength and bearing strength decreased. The local bearing failure mode was found to be independent of the lay-up sequence.

For glass fibre/epoxy laminates Kretsis and Matthews (1985) showed that 0°/±45° laminates gave better bearing strengths than other lay-ups investigated.

Marshall et al. (1989) considered the bearing strength in $(0°/90°)_s$ and $(90°/0°)_s$ glass reinforced polyester laminates and concluded that those with outer layers having 90° orientations fail at higher applied stresses.

Recently, Hamada et al. (1995) demonstrated that for a quasi-isotropic carbon-epoxy laminate having plies of 0° orientation on the outer surfaces and alternate 90° and ±45° plies in the centre provided the highest bearing strength.

### 2.2.2 EFFECTS OF FASTENER CONFIGURATION

The term fastener configuration as used here refers to the type of fastener, clamping pressure, washer size, bolt friction and tolerance between the hole and fastener. Bolt fasteners are of major interest since they are suitable for high load transfer applications, they are easy to install and may be used to control the clamping pressure. Pin fasteners are often considered as a type of bolt with zero clamping pressure for the purposes of comparison.

#### Effect of tightening torque

The beneficial effect of a lateral pressure or bolt pre-load on joint strength has been widely reported. Stockdal and Matthews (1976) concluded that the strength of a glass epoxy was dramatically increased when the clamping pressure is increased.

The remarkable influence of bolt tightening on joint strength was demonstrated in the work of Crews (1981). In this study the bearing strength increased by approximately a factor of two when the tightening torque was applied to a value recommended for structural applications.

Godwin et al. (1982) also reached the same conclusion for bolted composite laminates and showed that the joint strength was increased with increasing bolt torque.

Hodgkinson (1985) demonstrated the significance of a bolt tightness factor for both single lap and double lap KFRP joints.

Eriksson (1990) reported that a tightening torque of 5.4 Nm increased the joint strength by a factor of 1.5 times that obtained from finger tightening a fastener on a specimen of the same configuration. Moreover, it was shown that for a specimen clamped to a torque of 0.6 Nm the maximum bearing strength was obtained in a laminate having the largest proportion of plies oriented in ±45° direction.

Cooper and Turvey (1995) demonstrated that the critical laminate width and edge distance, normalized with respect to the hole diameter ($w/d$ and $e/d$) for mechanically fastened pultruded GRP was dependent on the bolt clamping torque.

These finding reference the earlier work of Collings (1977 and 1982) and Garbo and Ogonowski (1981) which reports that the degree of lateral constraint was the most important factor governing joint strength and recommended a clamping pressure of 22 $MN/m^2$ to develop full strength.

**Effect of washer size**

Stockdale and Matthews (1976) found that failure load in a mechanically fastened laminate to be proportional to the ratio of the outer and inner diameters of the washer when the clamping pressure was maintain at a constant level.

Godwin and Matthews (1980) noted that the degree of clamping pressure was determined by the washer size and demonstrated that the joint strength of a CFRP laminate increased when washers were used. Later, Godwin et al. (1982) showed that replacing the washer by a GRP plate produced insignificant changes in failure loads.

Abd-El-Naby and Hollaway (1993a.) showed the behaviour of the bolted joint of a pultruded glass/epoxy depends on the size of the clamping area and the washer material.

**Effect of bolt friction and tolerance**

In reality both friction and clearance exist at the interface between the laminate and the fastener. However, only analytical investigations have been conducted to determine the effect of variable friction between the fastener and the hole interfacial surface area. Three conditions may occur in defining the bolt and hole tolerances: clearance fit, perfect fit and interference fit. Cole et al. (1982) recommended that only clearance fit (-0.000 to +0.004 inch) fasteners should be considered in joining composite laminates.

Stockdale and Matthews (1976) compared results obtained from standard washers and interference fit washers and showed that the joint strengths were almost the same, the only difference being in the behaviour of the load-displacement curve on initial loading. Nevertheless, it was considered important to ensure that the washer is a close fit to the bolt. Godwin et al. (1982) has suggested that an oversize hole would reduce the strength of the joint.

## 2.2.3 CONSEQUENCES OF JOINT GEOMETRY

The joint geometry describes the type of joint, joint thickness, laminate width and end distance. A number of authors have investigated the dependency of joint strength on these variables. The following section presents a review of the literature especially concerned with these parameters.

**Effect of joint configurations**

Most mechanically fastened composite materials are constructed using a lap joint configuration. Smith et al. (1986) considered two types of joint design: single lap and double lap configurations. The results from this study showed that for a single lap joint the additional complication of an applied bending moment causes a reduction in joint strength. Conservatively, it was recommended that a safety factor of 1.25 should be applied to the strength of single lap joints when compared with double lap joints of the same laminate.

Hart-Smith (1980 and 1987) reached the same conclusion showing that double lap joints give higher strengths than single lap joints, which suffer as a consequence of the eccentric nature of loading. It was proposed that in design a reduction of 20% must be applied to the strength of double lap joints to obtain the equivalent strength for a single lap joint.

In the experimental analysis of Ramkumar and Tossavainen (1984) single lap joints gave gross tensile bearing loads 17-20% lower than double lap joints.

Hodgkinson (1985) concluded that for KFRP laminates double lap joints produced higher joint strengths than single lap joints for the same laminate material.

**Influence of joint thickness**

To determine the role of joint thickness on strength, the results from various studies should be normalized for effective comparison. Collings (1977) used this approach and normalized the thickness to an equivalent laminate containing 60% of fibre, by volume, but considered this technique as unsuitable when the fibre volume fraction is low.

Garbo and Ogonowski (1981) showed the effect of laminate thickness on bearing strength of a graphite/epoxy laminate. The results from both tension and compression tests showed an increase in bearing strength when the laminate thickness was increased.

For single lap joints, Ramkumar and Tossavainen (1984) showed that the strength of a 60-ply laminate was lower than a 20-ply laminate, by approximately five percent.

Godwin et al. (1982) demonstrated that decreasing the ratio between the bolt diameter to laminate thickness ($d_{bo}/t$) resulted in an increase in bearing strength.

Collings (1982) produced the same result for pin loaded holes, however, in a later work (1985) the author suggested the use of a $d_{bo}/t$ ratio greater than 1.5 to avoid fastener failure.

**Effect of laminate width**

In the studies concerned with the effect of laminate width on joint strength, most investigators have attempted to correlate the dimensionless ratio of strip width to hole diameter (*w/d*) with joint strength for single lap and double lap joints. A minimum *w/d* ratio is required to achieve full strength according to Matthews et al. (1976), Collings (1977), Garbo and Ogonowski (1981) and Ramkumar and Tossavainen (1984). Smith (1985), Smith et al. (1986) and Hart-Smith (1987) have also shown that the laminate width exerts a considerable influence on joint strength, particularly in a single fastened joint.

In an experimental investigation using CFRP laminates of 0°±45°, Matthews et al. (1976) suggested a minimum value for *w/d* of 4 to develop full bearing strength.

Collings (1977) recommended a *w/d* ratio of 8 for CFRP with ±45° lay-ups and a *w/d* ratio of 5 for pseudo-isotropic lay-ups to achieve full bearing strength. It was found that the 0°/90° laminates were more sensitive to a change in *w/d* than ±45° laminates.

Garbo and Ogonowski (1981) have shown that for a AS/350-6 graphite-epoxy an increase in hole diameter caused a reduction in bearing strength and gross joint failure strain over the stress range investigated.

Hayer and Liu (1983) showed that the stress concentration, which was based on the nominal bearing stress, was increased when the *w/d* ratio was increased.

Ramkumar and Tossavainen (1984) investigated over 318 statically tested coupons of AS I/3501-6, graphite-epoxy, in both single lap and double lap joint configurations. The results indicated that for a *w/d* ratio over 6 the bearing strength remained relatively constant. For a *w/d* ratio below 4 the failure mode occurred as a net section failure across the hole while for ratios greater than 4, the failure mode was primarily shear-out for 50/40/10 laminates having a 0°, ±45° and 90° lay-up. In contrast failure of 30/60/10 laminates was predominantly via a bearing mode. The effects of hole diameter on joint strength for both single lap and double lap configurations were found to be similar.

Smith (1985) conducted an experimental study to investigate the strength of a range of quasi-isotropic CFRP bolted double lap joints. The results showed that the bearing strength of the laminate was sensitive to the laminate width. In contrast, Smith and Pascoe (1985) demonstrated that for a cross ply laminate $(0°/90°)_{2s}$ the bearing strength was unaffected by the laminate width. A similar conclusion was made in the later work by Smith et al. (1986) for single lap joints using cross ply laminates.

Hart-Smith (1987) derived empirical expression for multi-fastened joints based on the experimental results obtained from testing a single pin fastened

elastic-isotropic material. An interesting observation in this work was the reported incidence of non-uniform bearing stresses through the laminate thickness.

**Effect of end distance**

The joint strength and failure mode are also influenced by the magnitude of the end distance (*e*) between the hole centre and the edge of the laminate. To promote bearing failure and avoid net tension failure modes it is considered desirable to adopt a minimum value for the *e/d* ratio.

Collings (1977 and 1987) has proposed a relationship between end distance to diameter ratio and bearing strength for different CFRP laminates. A minimum *e/d* ratio of 5 was required to develop full bearing strength for all ±45° CFRP lay-ups, whereas a minimum *e/d* ratio of 3 was preferred for a pseudo-isotropic lay-up.

Pradhakaran (1982) showed in a quantitative assessment that the maximum shear stress decreased as a result of increasing the end distance on a quasi-isotropic and unidirectional glass-epoxy laminate.

Ramkumar and Tossavainen (1984) found that for a AS I/3501-6 graphite/epoxy unidirectional prepeg material, the bearing strength of all lay-ups increased with *e/d* ratio, up to a value of 4 or 5.

Hyer and Liu reported comparable results with those obtained by Pradhakaran (1982) using quasi-isotropic (Hyer and Liu, 1984) and orthotropic (Hyer and Liu, 1985) glass-epoxy laminates.

Kretsis and Matthews (1985) concluded that the minimum *e/d* ratios required for full bearing strength were dependent on bolt diameter, joints with large bolt diameters requiring lower *e/d* values.

Smith (1985) showed that for a double lap quasi-isotropic CFRP laminate the end distance has negligible effect on the bearing strength. On the contrary, Smith and Pascoe (1985) have shown that failure of $(0°/90°)_{2s}$ laminates to be sensitive to the joint end distance. The identical conclusion has been shown for single lap cross ply laminates in the later work of Smith et al. (1986).

Hart-Smith (1987) have also provided information on the influence of end distance on the modes of failure in composite laminates.

### 2.2.4 MULTI-FASTENED JOINTS

Some experimental examinations of multi-fastened composite laminates have been performed to determine the effect of fastener arrays and joint geometry on the resultant strength of the joint.

Oplinger (1978) reported a remarkable increase in the gross section strength for glass/epoxy laminates of ±45° lay-ups, fastened using three pins in a single row compared with a single pin joint. A similar comparison for 0°/90° lay-up showed only slightly higher strengths in the multi-fastened configuration.

Agarwal (1980) has shown that for multi-fastened bolted joints the net section failure increased slightly (5 to 10 percent) by increasing the number of fastener rows.

Tests undertaken on multi-bolt glass-reinforced plastic (GRP) joints by Godwin et al. (1982) showed that two bolts in a row perpendicular to the loading direction resulted in higher failure strengths than two bolts aligned with the loading direction. For a single row of bolts a pitch value of 2.5d and an *e/d* ratio of 5 were given as the necessary requirements to achieve optimum joint strength; in this particular case a tensile failure mode predominated. For the case of bearing mode failures they reported an optimum pitch distance of five or six times the pin/bolt diameter. A similar value was proposed by Hart-Smith (1980) in joints containing CFRP laminates.

Using photoelasticity on a joint having two pins aligned with the loading direction, Hyer and Liu (1983) showed that the inboard hole sustains the higher tensile stress concentration factor compared with the outboard hole.

Hodgkinson (1985) suggested that the ratio of pitch to bolt diameter should be greater than, or equal to, four for Kevlar reinforced plastic, joined in double lap fashion with bolts aligned with the loading direction. For bolts in a line perpendicular to the loading direction, $p/d$ ratios greater than or equal to 6 were recommended.

An experimental investigation of multiple-fastener arrays in a composite laminate was also conducted by Herrera-Franco and Cloud (1986). In this study high-sensitivity Moire interferometry was used on glass-reinforced epoxy plates with two pins in tandem, two pins in a row and a 3-hole pattern. In the case of two pins in tandem, subjected to tensile loads, the results showed that the maximum tensile strain at the edge of the inboard hole was 2.9 times larger than the maximum tensile strain at the edge of the outboard hole.

In a complimentary study, Cohen et al. (1989) conducted an experimental investigation on thick IM7G graphite fibre laminate joints and showed that the percentage of plies of a specific orientation, pin diameter, row spacing and pitch distance, can substantially alter the failure mode of a multi-fastened composite laminate. Increasing the percentage of $\pm 45°$ plies for a multi-fastened joint raised the joint strength of thick Hercules IM7G graphite fibre laminate by a considerable margin.

Zimmerman (1991) determined the stress concentration factors in GFRP multi-bolt joints and showed that there was considerable interaction between various stress components in the vicinity of the hole boundary.

Abd-El-Naby and Hollaway (1993b.) reported experimental results for pultruded GRP fastened using two bolts in series and showed that failure occurred in bearing and tensile modes at loads double that of a single-bolt specimen.

## 2.3 ANALYTICAL INVESTIGATIONS OF MECHANICALLY FASTENED COMPOSITE JOINTS

The analytical method used in this study is based on mathematical models which employ a certain type of approximations to represent the physical problem. These models can be examined using either classical analysis techniques, based on two-dimensional anisotropic theory of elasticity, as given by Lekhnitskii (1968), or modern numerical analysis such as the finite element and boundary element methods.

### 2.3.1 CLASSICAL ANALYSIS

A classical work which accounts for the effect of friction on the behaviour of pin jointed composites was given by Oplinger and Gandhi (1974) by using continuum mechanics, based on complex variables, including Hoffman's specified

distortion failure criterion. A prescribed cosine displacement of the contact boundary was assumed at the interface representing friction between the pin and laminate. The effect of tolerance was also considered in this work. As non-linear shear behaviour was not incorporated in the analysis, considerable discrepancy was noted in comparing the analytical results for the shear failure mode with those obtained experimentally.

Eisenmann (1976) has successfully predicted the strength of bolted joints based on an analysis incorporating a fracture mechanics approach. The principal of this method is to calculate a characteristic dimension, based on the laminate tensile strength and Mode I fracture toughness, which defines the damage zone around the hole boundary. This characteristic is the same, in principal, as the concept employed in the earlier work of Whitney and Nuismer (1974). Unfortunately, this method requires extensive experimental testing and consequently presents severe limitation in its practical application.

De Jong (1977) presented a superposition solution to simplify an approximate expression for the stress distribution on the hole boundary in a pin loaded orthotropic plate of infinite width. The normal stresses were calculated from displacements of the loaded section on the hole boundary. In subsequent work pin friction was incorporated in the analysis which was applied to both infinite (De Jong, 1982) and finite (De Jong, 1987) width anisotropic plates. This work showed that the contact stress on the bearing plane was reduced as the numerical value of the friction coefficient increased.

Agrawal (1980) showed that the assumed cosine pressure distribution for pin loaded laminates was related to the experimental contact pressure. Changing the pattern of the contact stress was shown to exert a considerable effect on the predicted bearing strength using the average stress failure criterion. However, this method is regard as unsuitable for non-linear elastic materials.

Garbo and Ogonowski (1981) used the first term of the cosine series for the contact stress and the superposition technique, employed by De Jong (1977), to investigate the strength of mechanically fastened composite lap joints. The analytical procedure was subsequently implemented in a computer program called BJSFM (Bolted Joint Stress Field Model). This program also enables the strength for the first ply failure to be determined using the Tsai-Hill, Hoffman, Tsai-Wu, maximum stress and maximum strain failure criterion.

A similar program, 'A4EJ', was developed by Hart-Smith (1981) based on semi-empirical bolted joint analysis. The assumed load transfer through the mechanical fasteners was defined in terms of the relative displacement between the fastener and the laminate.

More recently, Hayer and Klang (1984), using a complex variable, found that the stress distribution on the hole boundary of a finite width laminate plate was significantly affected by: the laminate properties, interfacial friction and the bolt-hole clearance. This work was extended to the more complicated problem of a joint containing an elastic pin. The results showed that increasing the

interfacial friction tended to decrease the maximum radial stress on the bearing plane ($\theta = 0°$) and the maximum circumferential stress occurred near the end of the contact zone (i.e. values of $\theta$ between 75° and 85°). Nevertheless, this method was limited to the analysis of a two dimensional problem.

Mangalgiri (1984) studied the interfacial contact condition in an infinite orthotropic laminate loaded by perfect fit rigid pin using the inverse technique. The investigation demonstrated that the contact angle between the pin and plate was a non-linear function of the load. This technique was subsequently modified for the same contact problem to incorporate in-plane loading in any given directions, with respect to the bearing plane (Mangalgiri and Dattaguru 1986).

Smith et al. (1986) predicted the bearing strength of double-lap joints subjected to net-tension loading by evaluating the stress distribution along the net-tension plane using a point stress criterion. Reasonably good agreement was obtained with the earlier reported results of Smith (1985).

Wilson and Tsujimoto (1986) also used the point stress hypothesis to predict the strength and failure mode of mechanically fastened composite laminates, in conjunction with a customized failure criteria. In this study a cosine contact stress distribution was assumed at the interface and it was concluded that a reasonably accurate result was achieved for a range of plate widths ranging from $2d$ to $8d$.

Smith et al. (1987) used a simple three-dimensional analytical approach to model the clamping pressure in a bolted composite laminate joint. The clamping pressure was shown to improve the bearing strength by a greater amount than the extra load transferred due to friction. However the lack of suitable experimental data to support this work limited the applicability of this semi-empirical method.

### 2.3.2 NUMERICAL ANALYSIS

The advantages of utilizing closed-form solutions in the analysis of contact problems of this type are their accuracy and computational efficiency. However, there is a major disadvantage: solutions become increasingly more complicated when fewer assumptions are considered in the model (Jurf and Vinson, 1990). Despite this, the suitability of using a numerical method to evaluate the complex behaviour of mechanically fastened composite laminates is well recognized.

The boundary element method has been less often applied to this problem compared with finite element method since the features of this technique can not be as readily applied to interfacial analysis.

However, this method has been utilized in several cases. Zhang and Ueng (1984) used a complex stress function, which satisfies the displacement boundary condition at the hole interface, to obtain an analytical solution of the local contact stress for a pin-loaded hole in an orthotropic laminate. A more efficient boundary element method was utilized by Mahayerin and Sikarskin (1986) in the

analysis of mechanically fastened composite structures. More recently, Lin and Lin (1993) using a two-dimensional boundary element method, in conjunction with Yamada-Sun (1978) failure criterion, predicted the strength of uniform loaded bolted joints between orthotropic plates.

Finite element analysis provides a more appropriate method of modelling the interfacial contact and there are several examples of its application. Waszczak and Cruse (1971) predicted the local strength of a mechanically fastened joint between composite laminates using a two-dimensional finite element method. A cosine-distributed contact pressure was assumed for a rigid pin, although friction was not considered in this analysis. The maximum stress criterion, the maximum strain criterion and the Tsai-Hill distortional failure criterion was used to predict the joint strength which resulted in a value 50% lower than that obtained experimentally. A subsequent investigation by Waszczak and Cruse (1973) used the first term of cosine distribution of the normal stress to represent the bolt load, in conjunction with a superposition technique, to estimate the finite plate stresses but on this occasion did not evaluate the joint strength.

In an early attempt to model the non-linear behaviour of a composite laminate Humphris (1978) used a finite element model that recalculated the effective stiffness matrix of each element as individual plies failed. The Tsai-Hill failure criterion was used to predict the strength of the laminate at successive load increments and at the time represented a novel approach to the failure analysis of fibre reinforced composites.

Wilkinson et al. (1981) used a method based on an incremental load procedure in conjunction with the application of a stress-strain transformation matrix to study the effect of friction between a rigid fastener and an orthotropic plate. Rowlands et al. (1982) continued this work and applied a similar analysis to the problem of multi-bolted laminates. In this study the contact area was found to be dependent on the pin tolerance and subsequently was considered as a superior method of analysis compared with that obtained using the cosine pressure assumption. Later, Rahman et al. (1991) adopted the Tsai-Hill, Tsai-Wu and Cowin failure criteria to predict the ultimate strength of multifastened wood members. In this study failure initiation as opposed to the failure strength was predicted at 10 to 25% of the ultimate structural strength of the material.

An alternative method of predicting joint strength was employed by Wilson and Pipes (1981) using the point stress hypothesis, in association with a maximum stress criterion, to predict the shear-out strength in a composite laminate. The analysis was undertaken using SAP V finite element code and showed that for $w/d$ ratios > 5.25 shear-out failure was the predominant failure mode for all the values of $e/d$ ratios investigated.

Chang et al. (1982) used the Yamada-Sun failure criterion together with the characteristic length, initially introduced by Waddoups et al. (1971), to determine the joint strength in a composite laminate. This method was extended by Chang et al. (1984a) to investigate the strength of a multi-pin joint which was

subsequently implemented in a finite element program (BOLT) for the design of this type of joint configuration (Chang et al. 1984b).

In the classical work of Matthews et al. (1982) a three-dimensional analysis was performed on a smooth pin laminate model, using twenty node hybrid iso-parametric elements, which was solved using an iterative loading technique. The results for three clamping cases showed the important contribution of the through thickness, direct and shear stresses in determining the behaviour of the joint.

Tsiang and Mandell (1985) used a polynomial failure criteria (Tsai-Hill, Azzi-Tsai and Hoffman) to examine the failure initiation index for in-plane tensile loaded double lap joints. Two cases were examined for glass and graphite fibre-reinforced epoxy laminates and included either frictionless conditions, or, with infinite friction and no sliding at the fastener interface. The same assumptions were analysed in the work by Conti (1986) and Serabian and Oplinger (1987) which were concerned with evaluating the stress distribution in the vicinity of the hole boundary. Generally good agreement was obtained in comparisons between these results and experimental observations.

Crews and Naik (1986) employed the inverse iteration technique with the NASTRAN finite element code to model the displacement constraint at the pin-plate interface. The result obtained from tensile loading showed the combined effect of bearing and bypass loads may be correlated with the damage developed

on the net tension plane. Conversely, compressive bypass loads were shown to reduce the bearing strength and promote bearing failure in the laminate.

Eriksson (1986) investigated the contact stress in composite laminates using the ASKA code, based on a transformation matrix method (a routine in the general purpose FE computer program from SAAB-SCANIA AB and IKOSS GmbH). In this study the effects of the elastic properties of the laminate, clearance, friction, and loading as well as bolt stiffness, on the stress distribution at the hole boundary were considered. This study concluded that the most important influence on the peak stresses was due to interfacial friction and bolt clearance, while pin elasticity was considered to exert only a minor role.

The effect of contact friction between a pin and a graphite and epoxy laminate on the resulting stress distribution in the vicinity of the hole boundary, was also considered by Tsujimoto and Wilson (1986). A two dimensional elasto-plastic finite element analysis was used, with the simplifying assumption of a rigid pin. A non-linear ply-by-ply failure analysis was undertaken using the average stress and Hill yield criterion. Varying the friction coefficient was reported to have a significant effect on the failure mode. The results obtained from this study were in good agreement with those obtained experimentally, with the best correlation established for the model containing a rigid frictionless pin.

Chang and Chang (1987) determined the strength of a pin jointed composite laminate using a progressive modelling technique, although this

evaluation was limited to only net-tension and shear-out failure mechanism, since the model is incapable of incorporating an assessment of through thickness stresses.

Hyer et al. (1987) examined the influence of pin elasticity, clearance and friction at the interface on the stress distribution in a double lap joint containing a pin fastening. The principal conclusion of this work was that pin elasticity was found to have an insignificant effect on the stress distribution on the hole boundary.

This work was re-examined by Yogeswaran and Reddy (1988) where a mixed variational Lagrangian multiplier method was employed in a finite element model. In this case a dynamic and a static friction coefficient was introduced in the model as part of the contact analysis. Despite the differences in the analytical technique the results from this work compared well with that of Hyer et al. (1984).

In the work of Marshall et al. (1989), twenty node orthotropic elements were utilised to model a double lap joint composite structure. A displacement boundary condition was employed in considering four clamping conditions for a carbon-fibre-reinforced epoxy (CFRP) and glass-reinforced polyester laminate (GRP). Variations in the normal interfacial stress, generated under the washer area, were identified. Quantitative comparisons with experimental work on bearing failures in pin-loaded laminates showed good agreement with these

results. An interesting observation in this study was that the contact angle at the pin-laminate interface was found to change through the laminate thickness which was taken to be indicative of nonuniform elastic deformation of the pin.

Jurf and Vinson (1990) used a two dimensional finite element technique, similar to that adopted by Crews et al. (1981) to study failure of bolted joints between Kevlar/epoxy and graphite/epoxy laminates. The predicted joint strength was found to be consistent with the values obtained in a corresponding experimental investigation.

In an attempt to significantly reduce the computational time involved in solving bolt-laminate contact problems Murthy et al. (1990) utilized a condensed stiffness matrix of the joint together with an iteration technique. This technique was subsequently utilized by Murthy et al. (1991) in conjunction with the Yamada-Sun failure criteria to predict the strength of a joint constructed from anisotropic graphite/epoxy laminates.

Lessard (1991) employed the technique of progressive damage modelling to investigate the failure mechanisms in the pinned jointed CFRP. A rigid pin was modelled using a radial displacement method. The influence of joint geometry, ply lay-up sequence and fibre-matrix composition on the failure mode of the joint was investigated. Unfortunately, the results of this work have limited applicability in joint design since only a small number of joint geometries were studied.

Serabian (1991) carried out a three-dimensional non-linear finite element investigation on a pin loaded laminate and showed that the stress distribution was changed as the load applied through a perfect fit pin was increased. The contact angle also changed with the applied load attaining a maximum value of 80°. Although an in-plane load was applied to the joint out-of-plane deflections were reported, which was also confirmed by Serabian and Anastasi (1991). A point of interest to note was that the radial contact stress on the outer surface of the laminate appeared to be higher than at the mid-plane position.

Graham et al. (1994) demonstrated the effect of bolt clamp-up pressure and washer friction on the magnitude and distribution of global in-plane strain for a CFRP quasi-isotropic laminate. It was concluded that the joint strength was increased by pre-loading the bolt since a high proportion of the applied load was transferred directly from the plate through the washer to the fastener.

Three-dimensional finite element analysis of a bolted joint between a CFRP laminate and a rigid fixture was undertaken by Benchekchou and White (1995) using (a) cheese-headed bolts and (b) countersunk bolts. The results from this analysis showed good agreement with the experimental work conducted in the same investigation. It was concluded that the results from the stress analysis may be used to predict the fatigue initiation site in XAS/914 CFRP laminates.

Chen and Lee (1995) investigated the effects of friction, stacking sequence and bolt head profile on the stress distribution in vicinity of the hole boundary of

a composite laminate. A three-dimensional finite element technique was used to predict the strength of a bolted composite joint based on an incremental restricted variational principal (the transformation matrix of three-dimensional contact kinematics) and the Ye delamination criterion (Ye, 1988). The results were shown to be compatible with the experimental data conducted in the same study.

An identical technique was utilized by Chen et al. (1995) for bolt fastened composite laminates. In general, the results obtained compared favourably with experimental works of Smith et al. (1986) and Marshall et al. (1989). However, the friction at the laminate plate interface and the washer-plate interface was not considered.

Lessard and Mahmood (1995) used a two-dimensional finite element model to investigate damage propagation in pin jointed graphite/epoxy laminates. Despite the assumption of a perfect fit rigid pin the results showed a good correlation with the earlier experimental work of Lessard et al. (1992)

Ramakrishna et al. (1995) investigated the behaviour of pultruded sandwich composite laminates connected by a single pre-loaded bolt. Radial load was applied to the hole boundary to simulate two-dimensional pin contact. The characteristic distance in conjunction with the Yamada-Sun failure criteria was used to determine the joint strength. The laminate having the pultrusion direction

normal to the longitudinal axis, with an optimum *w/d* ratio of 7, gave the highest strength, which was consistent with the results obtained experimentally.

An alternative approach was conducted by Schulz et al. (1995) using a finite element code to model the tensile failure mode in bolted laminate joints. In this analysis a fracture mechanics approach was adopted, based on the maximum circumferential stress failure criterion (Erdogan and Sih, 1963), applied to a pseudo flaw size. Although a cosine contact stress distribution was assumed in this modelling exercise, the accuracy of this solution was considered to be compatible with the result obtained by Hart-Smith (1977) and Chang et al. (1982).

The work undertaken on composite joints with a single fastener has tended to concentrate on evaluating the contact stress on the hole boundary as well as the joint strength. However, in the case of multifastened joints the principal concern has been an assessment of the load distribution. In these studies, such as in the early work of Wang and Han (1988), specific two-dimensional finite element procedures have been developed to investigate the load transferred to the fastener.

Fan and Qiu (1993) incorporated friction and fitting tolerances in their model of a multi-fastened joint in an attempt to produce a more realistic solution for a multi-fastened composite laminates. The analysis included a Faber expansion in conjunction with the assumption of a cosine contact stress between

the laminate and a rigid pin. The conclusions of this work were somewhat unsatisfactory since the modelling technique was not validated and the many assumption adopted limited the applicability of this work.

Oakeshott and Matthews (1994) have modelled the load distribution of multi-fastened joints using a finite element method. In contrast to the model developed by Wang and Han (1988), this model allowed bending to be included in the analysis. However, the effect of friction and clearance at the fastener-composite interface was neglected.

This was partly addressed in the work by Rahman (1994) which included contact friction analysis of multi-fastened composite laminates. The effect of varying the in-plane geometry, bolt clearance, bolt friction, relative motion and load ratios between adjacent bolts, were incorporated in a two-dimensional stress analysis of a double-bolted model.

The work of Abd-El-Naby et al. (1991) was specifically concerned with the effects of friction on the load distribution in multi-fastened joints and showed that for a two-pinned composite joint interfacial friction has an insignificant effect in changing the load distribution on the pins.

Cohen et al. (1995) used single-fastener test data, in conjunction with finite element analysis and the average stress criterion, to predict the strength of a multi-fastened joint. In this analysis the ABAQUS finite element code was utilized and a

rigid pin joint was assumed. The predicted joint strength was shown to be within 1% of the results obtained experimentally. However, predicting failure initiation, using the average stress criterion, was not nearly as accurate.

Griffin et al. (1995) investigated the stress distribution and load transfer in multi-fastened composite joints. A two dimensional finite element model was used to represent a composite plate joined to steel outer laps by a number of rigid, frictionless, pins in a double lap fashion. This analysis showed that the load transferred by each pin was in good agreement with the experimentally determined values conducted by Cohen et al. (1989).

The extended interior penalty method was employed by Kim and Kim (1995) to model the contact pressure in multi-pin composite laminates joined to a rigid fixture. For a quasi-isotropic laminates joined by two, perfect fit, rigid pins in tandem, the results showed that the percentage of load transferred via the inboard pin was 63.4% for a frictionless case and 64.2% when a friction coefficient of 0.2 was adopted.

A review of the literature reveals that a considerable amount of effort has been expended in attempts to obtain a satisfactory analytical procedure for investigating the behaviour of mechanically fastened composite joints. A more reliable, accurate, and widely applicable technique is still challenging researchers in this field. The current study is an attempt to address some of these shortcomings.

# CHAPTER 3

# THEORETICAL ANALYSIS OF COMPOSITE LAMINATES

## 3.1 INTRODUCTION

This chapter provides the theoretical background for the investigation of mechanically fastened composite laminates. An understanding of the theory given here is necessary to successfully model the physical characteristics and behaviour under load of a composite laminate joint. Two major topics are involved in the analysis: the mechanics of composite materials and finite element analysis for contact mechanics.

## 3.2 MECHANICS OF COMPOSITE MATERIALS

Two techniques were used to construct the laminate properties in this study: representative volume element (RVE), and replica (layerwise) modelling techniques, the advantages and limitations of these techniques have been discussed elsewhere (Wood, 1994). In the REV technique unidirectional ply properties are used to construct the laminate properties by employing laminate plate theory. From any defined stacking sequence the compliance of the laminate may be derived. The laminate properties are then assigned to the element representing the laminate in the model. The two dimensional laminate properties are different from three-dimensional laminate properties in that the properties in relation to z-direction are not considered in the former case.

For the layerwise technique the unidirectional ply properties are also utilized, however, these properties are applied directly to each elemental layer representing specific lamina orientation. Local element constituents are then transformed to a global coordinate system and assembled to form the laminate properties.

### 3.2.1 UNIDIRECTIONAL LAMINA

Chamis (1974) has reviewed approaches to the micromechanical behaviour of a composite lamina. One of these approaches involved a simplification of the firbre-matrix interactions in the unidirectional lamina (Holister and Thomas, 1966) where the basic assumptions are as follows:

1. Fibres are perfectly aligned and uniformly distributed throughout the matrix.
2. Perfect bonding exists between fibres and matrix.
3. The matrix is free of voids.
4. Applied loads are either parallel to or normal to the fibre direction.
5. The lamina is initially in a stress-free state (i.e., no residual stresses are present).
6. Both fibres and matrix behave as linearly elastic materials.

The stress of unidirectional lamina can be calculated using the theoretical micromechanic behaviour of a lamina, material properties of fibre and matrix and the percent of fibre content, as given by Jones (1975):

$$\sigma_1 = \sigma_f v_f + \sigma_m v_m \tag{3.1}$$

where $\sigma_1$ is average tensile stress in the composite, $\sigma_f$ and $\sigma_m$ are fibre and matrix stresses, respectively, $v_f$ and $v_m$ are fibre and matrix volume, respectively. Dividing both sides of equation (3.1) by longitudinal strain of composite, the longitudinal modulus for the composite, $E_1$, can be written as

$$E_1 = E_f v_f + E_m(1-v_f) \tag{3.2}$$

where $E_f$ and $E_m$ are the elastic moduli for fibre and matrix, respectively. Equation (3.2) is called the rule of mixture. This equation shows that the composite longitudinal modulus is an intermediate value between the fibre and matrix moduli.

The major Poisson's ratio, $\nu_{12}$, transverse modulus, $E_2$, minor Poisson's ratio, $\nu_{21}$ and shear modulus are given as:

$$\begin{aligned} \nu_{12} &= \nu_f v_f + \nu_m v_m \\ E_2 &= \frac{E_f E_m}{E_f v_m + E_m v_f} \\ \nu_{21} &= \frac{E_2}{E_1}\nu_{12} \\ G_{12} &= \frac{G_f G_m}{G_f v_m + G_m v_f} \end{aligned} \tag{3.3}$$

where $G_{12}$ is in-plane shear modulus.

Since in the manufacturing process none of the assumption made is completely valid, these equation provide only approximate values for the elastic properties of a continuous fibre 0° lamina. Chamis and Sendeckyj (1968) showed that the value of $E_1$ and $\nu_{12}$ predicted by the above equation agree well with the experimentally determined values, whereas, $E_2$ and $G_{12}$ are lower than the results obtained from experimental investigations.

### 3.2.2 STRESS-STRAIN RELATION

The relation between stress and strain in general continuum is given by generalized Hook's law as follows (Daniel and Ishai, 1994):

$$\begin{bmatrix} \sigma_{11} \\ \sigma_{22} \\ \sigma_{33} \\ \sigma_{23} \\ \sigma_{31} \\ \sigma_{12} \\ \sigma_{32} \\ \sigma_{13} \\ \sigma_{21} \end{bmatrix} = \begin{bmatrix} C_{1111}\ C_{1122}\ C_{1133}\ C_{1123}\ C_{1131}\ C_{1112}\ C_{1132}\ C_{1113}\ C_{1121} \\ C_{2211}\ C_{2222}\ C_{2233}\ C_{2223}\ C_{2231}\ C_{2212}\ C_{2232}\ C_{2213}\ C_{2221} \\ C_{3311}\ C_{3322}\ C_{3333}\ C_{3323}\ C_{3331}\ C_{3312}\ C_{3332}\ C_{3313}\ C_{3321} \\ C_{2311}\ C_{2322}\ C_{2333}\ C_{2323}\ C_{2331}\ C_{2312}\ C_{2332}\ C_{2313}\ C_{2321} \\ C_{3111}\ C_{3122}\ C_{3133}\ C_{3123}\ C_{3131}\ C_{3112}\ C_{3132}\ C_{3113}\ C_{3121} \\ C_{1211}\ C_{1222}\ C_{1233}\ C_{1223}\ C_{1231}\ C_{1212}\ C_{1232}\ C_{1213}\ C_{1221} \\ C_{3211}\ C_{3222}\ C_{3233}\ C_{3223}\ C_{3231}\ C_{3212}\ C_{3232}\ C_{3213}\ C_{3221} \\ C_{1311}\ C_{1322}\ C_{1333}\ C_{1323}\ C_{1331}\ C_{1312}\ C_{1332}\ C_{1313}\ C_{1321} \\ C_{2111}\ C_{2122}\ C_{2133}\ C_{2123}\ C_{2131}\ C_{2112}\ C_{2132}\ C_{2113}\ C_{2121} \end{bmatrix} \begin{bmatrix} \varepsilon_{11} \\ \varepsilon_{22} \\ \varepsilon_{33} \\ \varepsilon_{23} \\ \varepsilon_{31} \\ \varepsilon_{12} \\ \varepsilon_{32} \\ \varepsilon_{13} \\ \varepsilon_{21} \end{bmatrix} \quad (3.3)$$

and

$$\begin{bmatrix} \varepsilon_{11} \\ \varepsilon_{22} \\ \varepsilon_{33} \\ \varepsilon_{23} \\ \varepsilon_{31} \\ \varepsilon_{12} \\ \varepsilon_{32} \\ \varepsilon_{13} \\ \varepsilon_{21} \end{bmatrix} = \begin{bmatrix} S_{1111} & S_{1122} & S_{1133} & S_{1123} & S_{1131} & S_{1112} & S_{1132} & S_{1113} & S_{1121} \\ S_{2211} & S_{2222} & S_{2233} & S_{2223} & S_{2231} & S_{2212} & S_{2232} & S_{2213} & S_{2221} \\ S_{3311} & S_{3322} & S_{3333} & S_{3323} & S_{3331} & S_{3312} & S_{3332} & S_{3313} & S_{3321} \\ S_{2311} & S_{2322} & S_{2333} & S_{2323} & S_{2331} & S_{2312} & S_{2332} & S_{2313} & S_{2321} \\ S_{3111} & S_{3122} & S_{3133} & S_{3123} & S_{3131} & S_{3112} & S_{3132} & S_{3113} & S_{3121} \\ S_{1211} & S_{1222} & S_{1233} & S_{1223} & S_{1231} & S_{1212} & S_{1232} & S_{1213} & S_{1221} \\ S_{3211} & S_{3222} & S_{3233} & S_{3223} & S_{3231} & S_{3212} & S_{3232} & S_{3213} & S_{3221} \\ S_{1311} & S_{1322} & S_{1333} & S_{1323} & S_{1331} & S_{1312} & S_{1332} & S_{1313} & S_{1321} \\ S_{2111} & S_{2122} & S_{2133} & S_{2123} & S_{2131} & S_{2112} & S_{2132} & S_{2113} & S_{2121} \end{bmatrix} \begin{bmatrix} \sigma_{11} \\ \sigma_{22} \\ \sigma_{33} \\ \sigma_{23} \\ \sigma_{31} \\ \sigma_{12} \\ \sigma_{32} \\ \sigma_{13} \\ \sigma_{21} \end{bmatrix} \tag{3.4}$$

where $\sigma_{ij}$ and $\varepsilon_{ij}$ are stress and strain components, respectively (where $i, j$ = 1,2,3), $C_{ijkl}$ and $S_{ijkl}$ are stiffness components and compliance components, respectively (where $i, j, k, l$ = 1,2,3). Clearly, the compliance matrix $\left[S_{ijkl}\right]$ is the inverse of the stiffness matrix $\left[C_{ijkl}\right]$.

Using a contracted notation for stress, strain, stiffness and compliance tensors in mechanics of composites for example:

$$\begin{aligned} \sigma_{ii} &= \sigma_i \\ \sigma_{ij} &= \tau_{ij} \\ \varepsilon_{ii} &= \varepsilon_i \\ 2\varepsilon_{ij} &= \gamma_{ij} \; ; \; i, j = 1, 2, 3 \end{aligned} \tag{3.5}$$

in conjunction with the symmetric stiffness and compliance matrices. The state of stress (or strain) at a point can be described by six components of stress (or

strain), and the stress-strain equations. (3.3) and (3.4) are expressed in terms of 21 independent stiffness (or compliance) constants.

However, in the case of an orthotropic material the number of independent elastic constants is reduced to nine, as various stiffness and compliance terms are inter-related. For the specially orthotropic material having a reference coordinate system along principal planes of material symmetry the stress-strain relation can be written as

$$\begin{bmatrix} \sigma_1 \\ \sigma_2 \\ \sigma_3 \\ \tau_{31} \\ \tau_{23} \\ \tau_{12} \end{bmatrix} = \begin{bmatrix} C_{11} & C_{12} & C_{13} & 0 & 0 & 0 \\ C_{12} & C_{22} & C_{23} & 0 & 0 & 0 \\ C_{13} & C_{23} & C_{33} & 0 & 0 & 0 \\ 0 & 0 & 0 & C_{44} & 0 & 0 \\ 0 & 0 & 0 & 0 & C_{55} & 0 \\ 0 & 0 & 0 & 0 & 0 & C_{66} \end{bmatrix} \begin{bmatrix} \varepsilon_1 \\ \varepsilon_2 \\ \varepsilon_3 \\ \gamma_{31} \\ \gamma_{23} \\ \gamma_{13} \end{bmatrix} \tag{3.6}$$

and

$$\begin{bmatrix} \varepsilon_1 \\ \varepsilon_2 \\ \varepsilon_3 \\ \gamma_{31} \\ \gamma_{23} \\ \gamma_{12} \end{bmatrix} = \begin{bmatrix} S_{11} & S_{12} & S_{13} & 0 & 0 & 0 \\ S_{12} & S_{22} & S_{23} & 0 & 0 & 0 \\ S_{13} & S_{23} & S_{33} & 0 & 0 & 0 \\ 0 & 0 & 0 & S_{44} & 0 & 0 \\ 0 & 0 & 0 & 0 & S_{55} & 0 \\ 0 & 0 & 0 & 0 & 0 & S_{66} \end{bmatrix} \begin{bmatrix} \sigma_1 \\ \sigma_2 \\ \sigma_3 \\ \tau_{31} \\ \tau_{23} \\ \tau_{12} \end{bmatrix} \tag{3.7}$$

For thin laminates loaded in the plane of the laminate, the composite laminate can be considered to be under a condition of plane stress with all stress components in the out-of-plane direction (3-direction) being zero, i.e.,

$$\begin{aligned} \sigma_3 &= 0 \\ \tau_{23} &= 0 \\ \tau_{13} &= 0 \end{aligned} \tag{3.8}$$

Thus, the in-plane stress-strain relationship for an orthotropic layer under plane stress can be expressed in term of only four independent elastic parameters. The orthotropic stress-strain relation (equation 3.6) reduce to

$$\begin{bmatrix} \sigma_1 \\ \sigma_2 \\ 0 \\ 0 \\ 0 \\ \tau_{12} \end{bmatrix} = \begin{bmatrix} C_{11} & C_{12} & C_{13} & 0 & 0 & 0 \\ C_{12} & C_{22} & C_{23} & 0 & 0 & 0 \\ C_{13} & C_{23} & C_{33} & 0 & 0 & 0 \\ 0 & 0 & 0 & C_{44} & 0 & 0 \\ 0 & 0 & 0 & 0 & C_{55} & 0 \\ 0 & 0 & 0 & 0 & 0 & C_{66} \end{bmatrix} \begin{bmatrix} \varepsilon_1 \\ \varepsilon_2 \\ \varepsilon_3 \\ \gamma_{31} \\ \gamma_{23} \\ \gamma_{12} \end{bmatrix} \tag{3.9}$$

which can be written as

$$\begin{bmatrix} \sigma_1 \\ \sigma_2 \\ \tau_{12} \end{bmatrix} = \begin{bmatrix} Q_{11} & Q_{12} & 0 \\ Q_{12} & Q_{22} & 0 \\ 0 & 0 & Q_{66} \end{bmatrix} \begin{bmatrix} \varepsilon_1 \\ \varepsilon_2 \\ \gamma_{12} \end{bmatrix} \tag{3.10}$$

where reduced stiffnesses $Q_{ij}$ are

$$Q_{ij} = C_{ij} - \frac{C_{i3} - C_{j3}}{C_{33}} \quad (i, j = 1, 2, 6) \tag{3.11}$$

and equation (3.7) can be written as

$$\begin{bmatrix} \varepsilon_1 \\ \varepsilon_2 \\ \gamma_{12} \end{bmatrix} = \begin{bmatrix} S_{11} & S_{12} & 0 \\ S_{12} & S_{22} & 0 \\ 0 & 0 & S_{66} \end{bmatrix} \begin{bmatrix} \sigma_1 \\ \sigma_2 \\ \tau_{12} \end{bmatrix} \tag{3.12}$$

where [S] is the compliance matrix.

**Relation between Mathematical and Engineering Constants**

The stress-strain relationship in equation (3.7) can be expressed in terms of engineering constant as follows:

$$\begin{bmatrix} \varepsilon_1 \\ \varepsilon_2 \\ \varepsilon_3 \\ \gamma_{23} \\ \gamma_{31} \\ \gamma_{12} \end{bmatrix} = \begin{bmatrix} \frac{1}{E_1} & -\frac{\nu_{21}}{E_2} & -\frac{\nu_{31}}{E_3} & 0 & 0 & 0 \\ -\frac{\nu_{12}}{E_1} & \frac{1}{E_2} & -\frac{\nu_{32}}{E_3} & 0 & 0 & 0 \\ -\frac{\nu_{13}}{E_1} & -\frac{\nu_{23}}{E_2} & \frac{1}{E_3} & 0 & 0 & 0 \\ 0 & 0 & 0 & \frac{1}{G_{23}} & 0 & 0 \\ 0 & 0 & 0 & 0 & \frac{1}{G_{13}} & 0 \\ 0 & 0 & 0 & 0 & 0 & \frac{1}{G_{12}} \end{bmatrix} \begin{bmatrix} \sigma_1 \\ \sigma_2 \\ \sigma_3 \\ \tau_{23} \\ \tau_{31} \\ \tau_{12} \end{bmatrix} \tag{3.13}$$

However, in a case of a thin, unidirectional, lamina a state of plane stress may be applied. The reduced stiffness and compliance component in equation (3.10) and (3.12) can be expressed in terms of the engineering constants as follows:

$$
\begin{aligned}
S_{11} &= \frac{1}{E_1} \\
S_{11} &= \frac{1}{E_1} \\
S_{12} &= -\frac{\nu_{12}}{E_1} = -\frac{\nu_{21}}{E_2} \\
S_{66} &= \frac{1}{G_{12}}
\end{aligned}
\tag{3.14}
$$

and

$$
\begin{aligned}
Q_{11} &= \frac{E_1}{1-\nu_{12}\nu_{21}} \\
Q_{11} &= \frac{E_2}{1-\nu_{12}\nu_{21}} \\
Q_{12} &= \frac{\nu_{12}E_2}{1-\nu_{12}\nu_{21}} = \frac{\nu_{21}E_1}{1-\nu_{12}\nu_{21}} \\
Q_{66} &= G_{12}
\end{aligned}
\tag{3.15}
$$

Thus, this clearly shows that in considering the in-plane stress-strain relationship, four independent constants are needed to characterize the unidirectional lamina, such as the four reduced stiffnesses $Q_{11}$, $Q_{22}$, $Q_{12}$ and $Q_{66}$; or four compliances $S_{11}$, $S_{22}$, $S_{12}$ and $S_{66}$; or four engineering constants $E_1$, $E_2$, $G_{12}$ and $\nu_{12}$ ($\nu_{21}$ is equal to $\nu_{12}$ as the compliance matrix is symmetric).

**Transformation of Stress and Strain**

In the case where the lamina principal axes (1, 2) do not coincide with the in-plane loading or global axes (x, y), as shown in Figure 3.1, the stress and strain components referred to the principal material axes (1, 2) can be expressed in terms of those referred to the loading axes (x, y) by the following transformation relationship:

$$\begin{bmatrix} \sigma_1 \\ \sigma_2 \\ \tau_{12} \end{bmatrix} = [T] \begin{bmatrix} \sigma_x \\ \sigma_y \\ \tau_{xy} \end{bmatrix} \tag{3.16}$$

and

$$\begin{bmatrix} \varepsilon_1 \\ \varepsilon_2 \\ \frac{1}{2}\gamma_{12} \end{bmatrix} = [T] \begin{bmatrix} \varepsilon_x \\ \varepsilon_y \\ \frac{1}{2}\gamma_{xy} \end{bmatrix} \tag{3.17}$$

where the transformation matrix [T] is given by

$$[T] = \begin{bmatrix} m^2 & n^2 & 2mn \\ n^2 & m^2 & -2mn \\ mn & -mn & m^2 - n^2 \end{bmatrix} \tag{3.18}$$

and $m = \cos\theta$, $n = \sin\theta$. The angle $\theta$ is measured counterclockwise from the $x$-axis to the 1-axis. The laws of stress and strain transformation are independent of material properties, i.e., they are same for isotropic or anisotropic materials.

The transformation matrix for the stress-strain relationship is needed to transform the stress-strain equation (3.10 and 3.12) from the principal material axis to the arbitary axis $x$ and $y$ for more practical propose. The stress-strain relationship expressed in arbitary axis $x$ and $y$ is,

$$\begin{bmatrix} \sigma_x \\ \sigma_y \\ \tau_{xy} \end{bmatrix} = \begin{bmatrix} Q_{xx} & Q_{xy} & Q_{xs} \\ Q_{yx} & Q_{yy} & Q_{ys} \\ Q_{sx} & Q_{sy} & Q_{ss} \end{bmatrix} \begin{bmatrix} \varepsilon_x \\ \varepsilon_y \\ \gamma_{xy} \end{bmatrix} \tag{3.19}$$

From the transformation equation (3.16) the relationship between the transformed stiffness $[Q]_{xy}$, in the abitary direction, and the principal stiffness $[Q]_{1,2}$ is,

$$\begin{bmatrix} Q_{xx} & Q_{xy} & 2Q_{xs} \\ Q_{yx} & Q_{yy} & 2Q_{ys} \\ Q_{sx} & Q_{sy} & 2Q_{ss} \end{bmatrix} = [T^{-1}] \begin{bmatrix} Q_{11} & Q_{12} & 0 \\ Q_{12} & Q_{22} & 0 \\ 0 & 0 & 2Q_{66} \end{bmatrix} [T] \tag{3.20}$$

which given the transformed reduced stiffnesses as a function of the principal lamina stiffnesses:

$$\begin{aligned}
Q_{xx} &= m^4Q_{11} + n^4Q_{22} + 2m^2n^2Q_{12} + 4m^2n^2Q_{66} \\
Q_{yy} &= n^4Q_{11} + m^4Q_{22} + 2m^2n^2Q_{12} + 4m^2n^2Q_{66} \\
Q_{xy} &= m^2n^2Q_{11} + m^2n^2Q_{22} + (m^4 + n^4)Q_{12} - 4m^2n^2Q_{66} \\
Q_{xs} &= m^3nQ_{11} - mn^3Q_{22} + (mn^3 - m^3n)Q_{12} + 2(mn^3 - m^3n)Q_{66} \\
Q_{ys} &= mn^3Q_{11} - m^3nQ_{22} + (m^3n - mn^3)Q_{12} + 2(m^3n - mn^3)Q_{66} \\
Q_{ss} &= m^2n^2Q_{11} + m^2n^2Q_{22} - 2m^2n^2Q_{12} - (m^2 - n^2)^2Q_{66}
\end{aligned} \tag{3.21}$$

Direct inversion the stress-strain equation (3.19) given

$$\begin{bmatrix} \varepsilon_x \\ \varepsilon_y \\ \gamma_{xy} \end{bmatrix} = \begin{bmatrix} S_{xx} & S_{xy} & S_{xs} \\ S_{yx} & S_{yy} & S_{ys} \\ S_{sx} & S_{sy} & S_{ss} \end{bmatrix} \begin{bmatrix} \sigma_x \\ \sigma_y \\ \tau_{xy} \end{bmatrix} \tag{3.22}$$

which lead to the transformed compliances as a function of the principal lamina compliances:

$$\begin{aligned} S_{xx} &= m^4S_{11} + n^4S_{22} + 2m^2n^2S_{12} + m^2n^2S_{66} \\ S_{yy} &= n^4S_{11} + m^4S_{22} + 2m^2n^2S_{12} + m^2n^2S_{66} \\ S_{xy} &= m^2n^2S_{11} + m^2n^2S_{22} + (m^4 + n^4)S_{12} - m^2n^2S_{66} \\ S_{xs} &= 2m^3nS_{11} - 2mn^3S_{22} + 2(mn^3 - m^3n)S_{12} + (mn^3 - m^3n)S_{66} \\ S_{ys} &= 2mn^3S_{11} - 2m^3nS_{22} + 2(m^3n - mn^3)S_{12} + (m^3n - mn^3)S_{66} \\ S_{ss} &= 4m^2n^2S_{11} + 4m^2n^2S_{22} - 8m^2n^2S_{12} + (m^2 - n^2)^2S_{66} \end{aligned} \tag{3.23}$$

### 3.2.3 ELASTIC BEHAVIOUR OF MULTIDIRECTIONAL LAMINATES

A laminate is constructed by stacking a number of laminas in the thickness direction. The overall behaviour of the laminate is a function of the geometry, material properties and stacking sequence of the individual lamina. Classical laminate theory predicts the behaviour of the laminate based on the following basic assumptions:

1. Each lamina is quasi-homogeneous, orthotropic and behaves in a linearly elastic manner.
2. The laminate is thin and wide (wide >> thickness).
3. The deformations are infinitesimal compared with the thickness.
4. A perfect interlaminar bond exists between the various layers.
5. Linear strain distribution through the thickness.
6. Displacements are continuous through the thickness.
7. Normal distances from the middle surface remain constant.

Figure 3.2 shows the geometry of a laminate which consists of *n* laminas. The geometric midplane of the laminate contains the x and y axis, and the z axis defines the thickness direction. The total thickness of the laminate is t, and the thickness of the $j^{th}$ layer is $t_j$ (j=1,2,3,....,n-1,n) where *n* is the total number of layers.

**Stress-Strain Relationship of a Layer within a Laminate**

Following assumption 5, laminate strains are linearly related to the distance from the midplane as,

$$\begin{bmatrix} \varepsilon_x \\ \varepsilon_y \\ \gamma_{xy} \end{bmatrix} = \begin{bmatrix} \varepsilon_x^0 \\ \varepsilon_y^0 \\ \gamma_{xy}^0 \end{bmatrix} + z \begin{bmatrix} \kappa_x \\ \kappa_y \\ \kappa_{xy} \end{bmatrix} \tag{3.24}$$

where: $\varepsilon_x^0$, $\varepsilon_y^0$ = midplane normal strain in the laminate

$\gamma_{xy}^0$ = midplane shear strain in the laminate

$\kappa_x$, $\kappa_y$ = bending curvature in the laminate

$\kappa_z$ = twisting curvature in the laminate

$z$ = distance from the midplane in the thickness direction

Consider an individual layer $k$ in a multidirectional laminate having a midplane at a distance $z_k$ from the laminate reference plane, the stress-strain reaction referred to the material axes are

$$\begin{bmatrix} \sigma_1 \\ \sigma_2 \\ \tau_{12} \end{bmatrix}_k = \begin{bmatrix} Q_{11} & Q_{12} & 0 \\ Q_{12} & Q_{22} & 0 \\ 0 & 0 & Q_{66} \end{bmatrix}_k \begin{bmatrix} \varepsilon_1 \\ \varepsilon_2 \\ \gamma_{12} \end{bmatrix}_k \tag{3.25}$$

and transformed into the global laminate system

$$\begin{bmatrix} \sigma_x \\ \sigma_y \\ \tau_{xy} \end{bmatrix}_k = \begin{bmatrix} Q_{xx} & Q_{xy} & Q_{xs} \\ Q_{yx} & Q_{yy} & Q_{ys} \\ Q_{sx} & Q_{sy} & Q_{ss} \end{bmatrix}_k \begin{bmatrix} \varepsilon_x \\ \varepsilon_y \\ \gamma_{xy} \end{bmatrix}_k \tag{3.26}$$

substitute equation (3.24), gives

$$\begin{bmatrix} \sigma_x \\ \sigma_y \\ \tau_{xy} \end{bmatrix}_k = \begin{bmatrix} Q_{xx} & Q_{xy} & Q_{xs} \\ Q_{yx} & Q_{yy} & Q_{ys} \\ Q_{sx} & Q_{sy} & Q_{ss} \end{bmatrix}_k \begin{bmatrix} \varepsilon_x^0 \\ \varepsilon_y^0 \\ \gamma_{xy}^0 \end{bmatrix}_k + z \begin{bmatrix} Q_{xx} & Q_{xy} & Q_{xs} \\ Q_{yx} & Q_{yy} & Q_{ys} \\ Q_{sx} & Q_{sy} & Q_{ss} \end{bmatrix}_k \begin{bmatrix} \kappa_x \\ \kappa_y \\ \kappa_{xy} \end{bmatrix}_k \tag{3.27}$$

Equations (3.24) and (3.27) show that the strain varies linearly through the thickness. In contrast, the stress does not since the discontinuous variation of the transformed stiffness matrix $[Q]_{x,y}$ from layer to layer. The average stresses in each layer are determined by knowing the reference plane strain $[\varepsilon^0]_{x,y}$ and curvatures $[\kappa]_{x,y}$, of the laminate, the location of the midplane layer $z_k$ and the transformed stiffness matrix $[Q]_{x,y}$.

The applied force and moment on a laminate, as shown in Figure 3.3, are related to the midplane strain and curvature by the following expression (Daniel and Ishai, 1994):

force-deformation relationship are

$$\begin{bmatrix} N_x \\ N_y \\ N_{xy} \end{bmatrix} = \begin{bmatrix} A_{xx} & A_{xy} & A_{xs} \\ A_{yx} & A_{yy} & A_{ys} \\ A_{sx} & A_{sy} & A_{ss} \end{bmatrix} \begin{bmatrix} \varepsilon_x^0 \\ \varepsilon_y^0 \\ \gamma_{xy}^0 \end{bmatrix} + \begin{bmatrix} B_{xx} & B_{xy} & B_{xs} \\ B_{yx} & B_{yy} & B_{ys} \\ B_{sx} & B_{sy} & B_{ss} \end{bmatrix} \begin{bmatrix} \kappa_x \\ \kappa_y \\ \kappa_{xy} \end{bmatrix} \quad (3.28)$$

and the moment-deformation relationship are

$$\begin{bmatrix} M_x \\ M_y \\ M_{xy} \end{bmatrix} = \begin{bmatrix} B_{xx} & B_{xy} & B_{xs} \\ B_{yx} & B_{yy} & B_{ys} \\ B_{sx} & B_{sy} & B_{ss} \end{bmatrix} \begin{bmatrix} \varepsilon_x^0 \\ \varepsilon_y^0 \\ \gamma_{xy}^0 \end{bmatrix} + \begin{bmatrix} D_{xx} & D_{xy} & D_{xs} \\ D_{yx} & D_{yy} & D_{ys} \\ D_{sx} & D_{sy} & D_{ss} \end{bmatrix} \begin{bmatrix} \kappa_x \\ \kappa_y \\ \kappa_{xy} \end{bmatrix} \quad (3.29)$$

where: $N_x$ = normal force resultant in the $x$-direction (per unit width)

$N_y$ = normal force resultant in the *y*-direction (per unit width)

$N_{xy}$ = shear force resultant (per unit width)

$M_x$ = bending moment resultant in the *yz*-plane (per unit width)

$M_y$ = bending moment resultant in the *xz*-plane (per unit width)

$M_{xy}$ = twisting moment resultant (per unit width)

[A] = extensional stiffness matrix for the laminate, relating in-plane loads to in-plane strain(N/m)

[B] = coupling stiffness matrix for the laminate, relating in-plane load to curvatures and moments to in-plane strain (N)

[D] = bending stiffness matrix for the laminate, relating moments to curvatures (N-m)

The elements in [A], [B] and [D] matrices are calculated from

$$A_{ij} = \sum_{k=1}^{n} Q_{ij}^{k}(h_k - h_{k-1})$$

$$B_{ij} = \frac{1}{2}\sum_{k=1}^{n} Q_{ij}^{k}(h_k^2 - h_{k-1}^2) \qquad (3.30)$$

$$D_{ij} = \frac{1}{3}\sum_{k=1}^{n} Q_{ij}^{k}(h_k^3 - h_{k-1}^3)$$

where: $n$ = total number of laminas in the laminate

$Q_{ij}^{k}$ = element in the [Q] matrix of the $k^{th}$ lamina

$h_{k-1}$ = distance from the mid plane to the top of the $k^{th}$ lamina

$h_k$ = distance from the mid plane to the bottom of the $k^{th}$ lamina

and $i, j = x, y$ or $s$.

The elements of stiffness matrix [A], [B] and [D] are functions of the elastic properties of each lamina and their location with respect to the midplane of laminate.

In the RVE modelling technique the material properties in the principal direction for each lamina are calculated from equation (3.2) and (3.3). The stiffness (or compliance) matrix of each element in the layer are transformed from local material coordinates into the global structure coordinate system using equation (3.21) (or (3.23)). From the position and thickness of each ply, the laminate stiffness matrices [A], [B] and [D] are calculated by using equation (3.30). The laminate engineering properties, referred to global coordinate system, are obtained by the inverse combination of equation (3.28) and (3.29). All the elements in the laminate model have the same value as these properties

For the layerwise modelling technique, unidirectional lamina properties are calculated using equation (3.2) and (3.3). However, the engineering properties are determined by transformation from the local material coordinate system to the global coordinate system, using equation (3.21) (or (3.23)), and integrated to form global stiffness matrix by the finite element method. Clearly, the dimensions of the stiffness matrix using this modelling technique are dependent on the number of layers, thickness of elements in the layer and the number of elements per layer.

In some cases, the elastic properties of the unidirectional lamina are determined experimentally instead of using equation (3.2) and (3.3) so as to avoid errors that arise from variations in material properties as a consequence of the manufacturing process.

## 3.3 FINITE ELEMENT FOR CONTACT MECHANICS

The finite element method has become more widely used recently in the analysis of composite material problems involving mechanical fastened joints, since this offers certain advantages over the other methods. The structure or component is modelled by a finite number of discrete elements. Groups of these elements are called meshes in which elements are connected to the contiguous elements at nodal points. The structure stiffness matrix [K] which represents the stiffness of the overall structure can then determined from the material properties. The forces that act on the body can be analysed from the basic finite element equation (Cook, 1989)

$$[K][\delta] = [R] \tag{3.31}$$

where $[\delta]$ are the nodal displacements and $[R] = \begin{bmatrix} N \\ M \end{bmatrix}$ are the loads on the structure. For the contact problems between a bolt and plate, equation (3.31) is non-linear because the stiffness matrix [K] is a function of deformation.

An iteration technique has been used by several authors in the analysis of bolt loaded composite plates that incorporate frictional effects. Since friction contact problems involve severe geometric non-linearity at the interacting surfaces, three separate iterations are required to obtain a numerical solution. The iterations developed by Wilkinson et al. (1981) are as follows:

1. Determination of the total contact area at each load step,
2. Determination of the non-sliding portion of contact area (due to friction) at each load step, and
3. Selection of incremental load steps to reach a specified load level.

The original finite element stress analysis of equation (3.31) can be reformulated through the iteration as follows,

$$
\begin{aligned}
&[\mathbf{K}^0][\Delta\delta^0]=[\Delta R^0];\\
&[\mathbf{K}^1][\Delta\delta^1]=[\Delta R^1];\\
&\quad .\quad .\quad .\\
&[\mathbf{K}^i][\Delta\delta^i]=[\Delta R^i];\\
&\quad .\quad .\quad .\\
&[\mathbf{K}^n][\Delta\delta^n]=[\Delta R^n];
\end{aligned}
\tag{3.32}
$$

where the total external load $[R]$ is given by

$$
[R]=[\Delta R^0]+[\Delta R^1]+\cdots+[\Delta R^i]+\cdots+[\Delta R^n] \tag{3.33}
$$

and the total nodal displacements vector [δ] under the full load is given by the sum of the incremental displacements [$\Delta\delta^i$], i.e.

$$[\delta]=[\Delta\delta^0]+[\Delta\delta^1]+\cdots\cdots+[\Delta\delta^i]+\cdots\cdots+[\Delta\delta^n] \tag{3.34}$$

Structural stiffness [$\mathbf{K}^n$] is based on the final deformed geometry of the (n-1) load level.

Initial displacements [$\Delta\delta^0$] are obtained from the first part of equations (3.34) using the initial stiffness [$\mathbf{K}^0$] and loading [$\Delta R^0$]. Contact conditions are then implemented. Contact of a node is established whenever it numerically penetrates or touches the surface of the bolt. Numerical iteration using the finite element method is repeated at every load increment of equation (3.34) to guarantee that no nodes lie inside the bolt and until no bolt surface is contacted. The change in boundary conditions are therefore reflected completely in the final displacements for each loading step.

The contact boundary conditions for slip and non-slip nodes in each step can be determined by computing the normal and shear stresses for the contacting nodes. Stick or slip of each of these contacting nodes can then be resolved according to the following criteria. If,

$$|\mu\sigma_r|-|\tau_{r\theta}|<0 \tag{3.35}$$

a node continues to slide at this level, where $\mu$ is coefficient of friction $\sigma_r$ and $\tau_{r\theta}$ are the normal and shear stresses, in terms of the local polar coordinates, as illustrated in Figure. 3.4.

If,

$$0 \leq |\mu\sigma_r| - |\tau_{r\theta}| \leq \beta \tag{3.36}$$

where $\beta$ is a prescribed tolerance stress magnitude, having a value in the range of 7-35 kPa (Rahman, 1993), then this node becomes fixed to the bolt at current displacement. If,

$$|\mu\sigma_r| - |\tau_{r\theta}| \leq \beta \tag{3.37}$$

the available friction force $F_f$ is significantly greater than the actual shear forces $F_s$ and the node becomes fixed to the bolt surface. However, this node is fixed to an interpolated position on the bolt surface between the tangential component of the displacement for this node, corresponding to the current and immediately previous load levels. The interpolation formula for the displacement $u^i$ used for this situation is,

$$u_\theta^i = (1-\alpha)u_\theta^{i-1} + \alpha u_\theta^i \tag{3.38}$$

where $i$ represents the $i^{th}$ load iteration, $u_\theta^i$ is the displacement tangential to the contacting surface of the $i^{th}$ load iteration, and

$$\alpha = \frac{\beta}{|\mu\sigma_r| - |\tau_{r\theta}|} \tag{3.39}$$

For relatively small load increments, any node in which new contact is made on the bolt surface slides before it becomes fixed. Once a node does become fixed, it remains at that position on the bolt throughout all subsequent structural loading.

In this study, the commercial available finite element code I-DEAS 1.3 MS. has been used. The subroutine for gap element was utilized to calculate the contact condition. The concept of incremental loading is similar to the method. described above, however, instead of the prescribed load required by Wilkinson et al. (1981) a prediction of the initial contact point is needed.

For all the finite element models used in this investigation the validity of the elements used was tested by undertaking a patch test (Cook, 1995) to ensure that the discretization error was reduced as the mesh was refined. The convergence test was satisfied using the $Z^2$ error estimator method which evaluates the error in the computed stresses using a strain energy balance. The optimum mesh refinement for each model was achieved using this procedure.

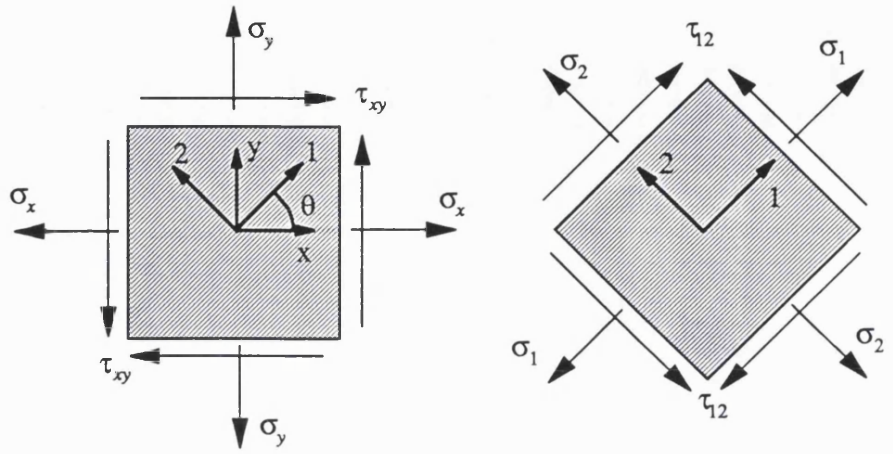


Figure 3.1 Stress component in a unidirectional lamina referred to loading and material axes

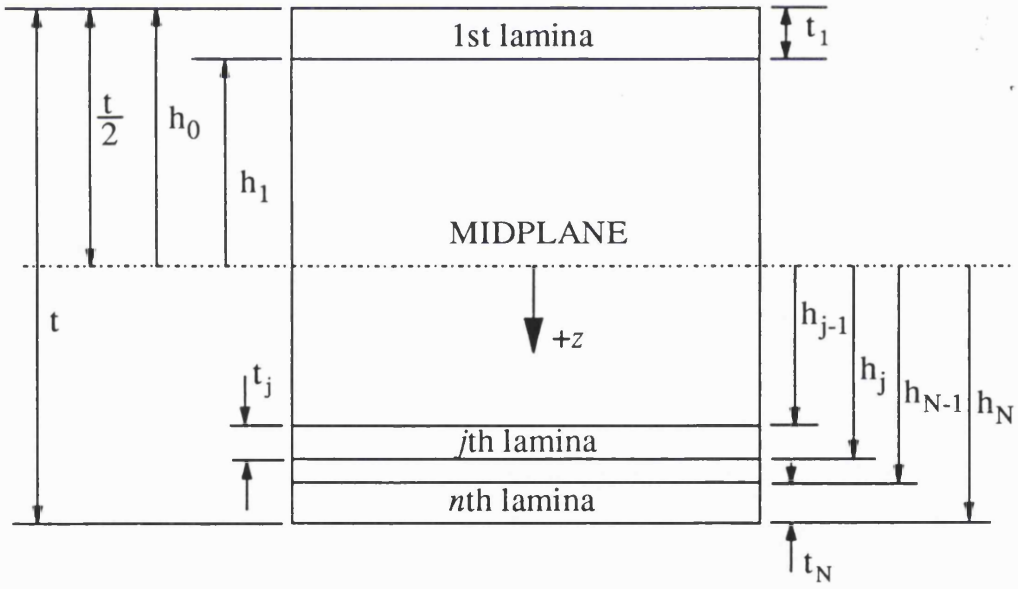


Figure 3.2 Laminate geometry

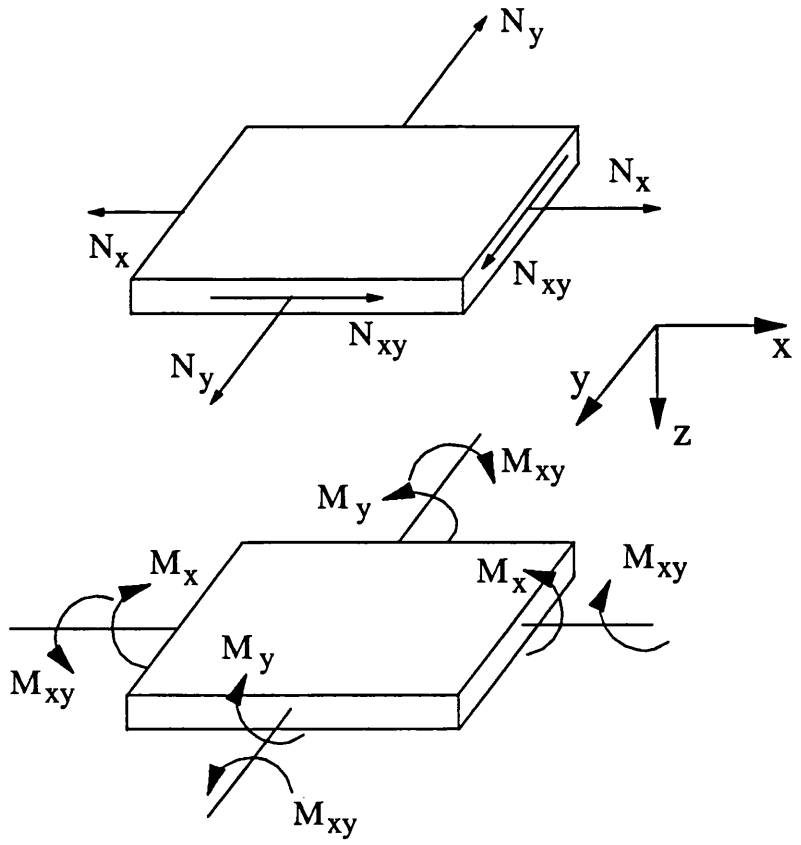


Figure 3.3 In-plane, bending, and twisting loads applied on a laminate

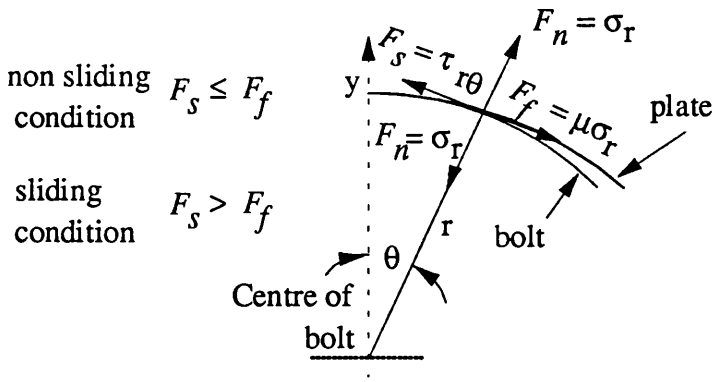


Figure 3.4 Normal and shear forces at the contacting node

# CHAPTER 4

# TWO-DIMENSIONAL SINGLE FASTENER MODEL

## 4.1 INTRODUCTION

In the development of a three-dimensional model for a single fastened double lap joint, two-dimensional modelling was investigated to evaluate the reliability of the analytical technique by comparing the results with the previously published experimental data. Provided a suitable correlation could be established this would assure the applicability of the modelling procedure and provide firm support for the further investigation. For the two-dimensional analysis a model consisting of a single fastened composite laminate joined in the double lap fashion was examined. Details of the model as well as the results and conclusions obtained from the analysis are given in the following section.

The methodology employed to assess the contact stress distribution between the mechanical fastener and the composite laminate involved carrying out two different analytical procedures for verification purposes. Firstly, the accuracy of the commercial computational code used in the investigation was confirmed by comparing the results with those derived from an alternative computational code. Secondly, the confidence of the modelling technique employed in this investigation was assessed by comparing the results of this analysis with the experimental results and data available in the literature.

## 4.2. MODEL

Eriksson (1986) used two-dimensional models of a composite laminate conforming with the T300/914C graphite/epoxy, laminate types A, B and C having material properties given in Table 4.1. In the present study, for comparison purposes, the same model was analysed using the commercial finite element analysis code I-DEAS Master Series 1.3c for all three laminate types.

The model incorporated a deformable pin and no clearance between the pin and the composite laminate. The effect of friction at the contact interface was examined using a friction coefficient of 0.0 and 0.3.

Figure 4.1 shows the physical model of T300/914C graphite/epoxy laminate. The finite element model with meshes generated using 4-node quadrilateral shell elements for the composite laminate is given in Figure 4.2. Adjacent nodes along the hole boundary subtend an angle of 5° at the centre of the bolt. For the elasto-plastic pin (titanium) 3-node triangular elements were applied where the angular separation between adjacent nodes along the hole boundary was the same as that used for the composite laminate. The interface of coincident nodes between the laminate plate and pin along the anticipated contact length on the hole boundary (i.e. along the second quadrant) was modelled using node to node type gap elements.

A tensile force of 2 kN was applied at the one end of the plate and the centre of the pin was restrained in all directions. Symmetry permits analysis of only half of the physical laminate model, as shown in Figure 4.2. In the case of laminate A joined to an elasto-plastic pin, the finite element model has a total 523 elements consisting of 468 four-node quadrilateral elements, 36 three-node triangular elements and 19 node to node type gap element.

Using this model, the case of a rigid pin, having an interfacial friction coefficient of 0.3, was also considered to compare the accuracy of I-DEAS MS 1.3c with an alternative finite element computational code, ABAQUS 5.2. In this case, the model developed using I-DEAS MS 1.3c. incorporated gap elements of node to ground type at the interface between the rigid pin and the laminate, whereas, in the model developed using ABAQUS 5.2 a rigid interface line was employed to simulate the contact boundary.

Table 4.1 Material properties of T300/914C graphite/epoxy (Eriksson 1986), titanium pin and rigid pin

| Percentage of piles in direction 0°/90°/±45° | $E_x$ (GPa) | $E_y$ (GPa) | $G_{xy}$ (GPa) | $\nu_{xy}$ |
|---|---|---|---|---|
| laminate A: 25/25/50 | 51.4 | 51.4 | 19.3 | 0.33 |
| laminate B: 69/06/25 | 102 | 24.2 | 111 | 0.44 |
| laminate C: 06/69/25 | 24.2 | 102 | 112 | 0.10 |
| laminate D: 20/60/20 | 40.6 | 91.4 | 9.6 | 0.10 |
| titanium pin | 110 | 110 | | 0.29 |
| rigid pin | $\propto$ | $\propto$ | | $\propto$ |

Eriksson (1986) reported both experimental and analytical results for a second model, of the type shown in Figure 4.3, conforming to laminate type D, having a different stacking sequence (20/60/20 percentage ply distribution) and properties, as shown in Table 4.1. A similar model was also constructed in this study, applying 4-node quadrilateral elements to represent the composite laminate. Adjacent nodes along the hole boundary subtended an angle of 5° at the centre of the bolt, as described in the previous model. A smooth rigid pin and an elasto-plastic (titanium) pin having a perfect fit were studied. A model of titanium pin was constructed using 3-node triangular element.

The finite element model, presented in Figure 4.4, was loaded in compression using an applied load of 3.0 kN at the end of the plate furthest from the pin. In this model, a total of 577 elements were employed and included 522 four-node quadrilateral elements for laminate D, 36 three-node triangular elements for titanium pin and 19 node to node type gap elements, joining coincident nodes of laminate D and the titanium pin.

Using the I-DEAS MS 1.3c code, node to node type gap elements, with the following coefficients of friction: 0.0, 0.01, 0.05, 0.1 and 0.3, were used to model the contact between coincident nodes of the laminate and the deformable pin along the third quadrant of the hole boundary. In the analysis using a rigid pin, the gap elements of node to ground type were used to connect the nodes along the third quadrant of the laminate plate. Symmetric boundary conditions comparable with the previous model was also applied.

## 4.3 RESULTS AND DISCUSSION

For comparative assessment stresses were normalized according to the following definitions. Contact stresses were normalized by the average bearing stress, $\bar{\sigma}_b$

$$\bar{\sigma}_b = \frac{\text{load transferred on a specific hole}}{d \times t} \tag{4.1}$$

where $d$ denotes the hole diameter and $t$ is the laminate thickness. The shear stresses along the shear-out plane were normalized by the average shear stress, $\bar{\tau}$

$$\bar{\tau} = \frac{\text{applied load}}{2e \times t} \tag{4.2}.$$

where, $e$ is the distance from the centre of the hole to the edge of the plate. The axial stresses along the bearing plane were normalized by the gross tensile stress, $\sigma_T$

$$\sigma_T = \frac{\text{applied load}}{w \times t} \tag{4.3}$$

where $w$ is the plate width. For the case of the maximum principal stresses, these were also normalized using the nominal far field stress, as given in equation (4.3).

### 4.3.1 ACCURACY OF THE MODELLING TECHNIQUES

The results of the analysis using I-DEAS MS 1.3c and ABAQUS 5.2 finite element code are shown in Figures 4.5, 4.6 and 4.7, which show the normalized axial stress, normalized maximum principal stress at (a) the critical distance ($A_0$) and at (b) the hole interface, respectively. In both cases, involving a smooth rigid pin and friction, the results obtained using I-DEAS MS 1.3c and ABAQUS 5.2, shown in Figure 4.5 and 4.6, are almost identical. For the nodes in contact, shown in Figure 4.7, a small difference was recorded. This may be attributed to the different interfacial element used in ABAQUS 5.2 compared with the gap element utilized in I-DEAS MS 1.3c which affects the deformation geometry. Clearly, there is very little difference between the two solutions; the main advantages of using I-DEAS MS 1.3c as opposed to ABAQUS 5.2 is that associated with the ease in which post-processing may be carried out.

### 4.3.2 CONFIDENCE IN THE MODELLING TECHNIQUES

The results of this investigation were compared with those obtained in the analytical and experimental examination undertaken by Eriksson (1986); the results of this comparison are summerised below.

Experimental and analytical results obtained by Eriksson for laminate D are compared with the results obtained in this study, in Figure 4.8. These results

show the normalized axial strain $\varepsilon_x / \overline{\varepsilon_x}$, where $\overline{\varepsilon_x}$ is the far field strain, along the bearing plane plotted against the normalized distance from the hole interface.

Generally, good agreement is found for an elastic pin with a friction coefficient equal to 0.3. The results also show that effect of increasing friction in reducing the axial strain at the pin-composite laminate interface. The results for the rigid and elastic pin are comparable with the exception of the case involving a high friction coefficient of 0.3. This arises from the higher contact area for rigid pin in conjunction with a high circumferential friction force producing a significantly lower axial contact pressure. It is noticeable that the rigid pin assumption employed by many investigators is applicable for this particular contact problem, provided the friction coefficient at the interface is less than a value of 0.2.

In addition to the comparison given above for laminate D, analytical data taken from Eriksson (1986) for laminate A, B and C are compared with the results obtained in this study, as shown in Figure 4.9, 4.10 and 4.11. In all of these figures the variation in the normalized radial stress at the hole boundary of the laminate is plotted against angular position, with respect to the centre of the pin. For comparison purposes the normalized radial, tangential and shear stresses at the critical distance $A_0$, equivalent to 1.26 mm. from the hole boundary, as a function of angular position are also given.

The results obtained for the normalized radial stress at the hole boundary and the normalized radial and tangential stress at the distance $A_0$ for laminate A, using an elastic pin without friction, compare favourably with the results obtained from Erikssson (1986) which employed a friction coefficient of 0.3. In contrast, using the same friction coefficient of 0.3 in this analysis shows that the stress are consistently lower than those obtained by Eriksson (1986) for angular positions between zero and seventy-five degrees, with respect to the positive x-direction. However, the converse applies to the normalized shear stresses at the distance $A_0$. Furthermore, it is interesting to note that the maximum shear stress was not given by Eriksson (1986), since only the first quadrant was examined. In the present study the maximum shear stress for laminate A was recorded in the second quadrant, as shown in Figure 4.8 (d).

Comparison of the various stress components in laminate A at the distance $A_0$ shows that the maximum normalized tangential stress (corresponding to zero normalized shear and radial stresses) occurred at an angular position of 85 degrees, with respect to the positive x-direction. This is also the case for laminate B and C as shown in Figure 4.10 and 4.11. This is in agreement with previously published work (Hyer and Klang 1984) showing that the maximum tangential stress occurs at the end of the contact zone, i.e. when $\theta \equiv 85$ degrees. In general, the trend in the normalized stress values for laminate B and C are compatible with the work of Eriksson (1986).

The normalized axial stress along the bearing plane for laminates A, B and C is shown in Figure 4.12. The results show good agreement with Eriksson's work (1986) except at normalized distances less than, approximately, 0.1 (i.e. half the critical distance) where the stresses are lower. The results of the current work show that the axial stress peaks at a normalized distance equivalent to 0.1. For comparison purposes the normalized axial stress as a function of normalized distance for all three laminates is shown in Figure 4.12 (d). At any distance from the hole boundary the axial stress on the bearing plane of laminate B is greater than the corresponding axial stresses in either laminate A or C.

### 4.3.3 COMPARATIVE ASSESSMENT OF LAMINATES A, B AND C

The normalized radial, tangential and shear stresses at angular position between 0 and 180 degrees at, (a) the hole boundary, (b) the critical distance, for laminates A, B and C is given in Figure 4.13 and 4.14, respectively. The variation in the normalized tangential and radial stresses are similar at both the hole boundary and the critical distance, although the magnitude is greater at the hole boundary compared with the critical distance. The shear stress distribution is somewhat different, exhibiting a minimum value at an angular position of 60 degrees at the hole boundary, compared with a maximum value at an angular position of 130 degrees at the critical distance.

At the hole boundary the tangential stress is a maximum at an angular position of 80 degrees, whereas, the radial and shear stress components exhibit intermediate values. At the critical distance and the same angular position these stresses diminish to zero while the tangential stress maintains a maximum value, although of a reduced magnitude compared with the stress at the hole boundary.

The tangential and shear stresses for each laminate are similar at any specific angular position, at either the hole boundary or the critical distance, however, the radial stress distribution is different for each laminate. The maximum radial stress on the hole boundary occurs at angular positions of 50, 25 and 75 degrees from the positive x-direction for laminates A, B and C, respectively, whereas, at the critical distance the maximum stress corresponds to an angular position of 0 and 55 degrees, as shown Figure 4.14 (a). The angular variation in peak stress for each laminate is attributed to the different fibre content in the principal direction of the laminate, as identified in Table 4.1

## 4.4 CONCLUDING REMARKS

Comparison of the results obtained in this study, for a single pin fastened joint, with previously published work has validated the finite element code together with the modelling technique. Furthermore, it may be concluded that the stresses imposed on the laminate are influenced by some specific parameters concerned with the modelling of the joint interface.

### 4.4.1 ACCURACY AND RELIABILITY

Though different interfacial elements were utilized in the finite element model using I-DEAS MS 1.3c and ABAQUS 5.2 code, the resulting analytical solutions for a pin loaded laminate joint compared favourably. I-DEAS MS 1.3c was adopted for subsequent investigations since it provides special features for post processing. The results obtained from the model incorporating a deformable pin were shown to be compatible with previously published experimental and analytical data given by Eriksson (1986), thus further verifying the modelling technique employed.

### 4.4.2 EFFECTS OF PIN RIGIDITY AND FRICTION

In the analysis of a pin jointed laminate, most investigators have assumed a rigid pin and/or a smooth pin-laminate interface. Figure 4.8 shows that these assumptions produce a conservative result. The rigid pin assumption gives higher axial contact stresses compared with a smooth deformable pin because of the reduced contact area. The reduction in the axial contact stress is significant when friction is introduced at the pin interface; a higher friction coefficient lowers the contact stress.

Obviously, the principal effect of friction is to reduce the contact stress on the bearing plane, thereby, increasing the frictional force in the circumferential direction and, as a result of the equilibrium conditions, the hoop stress

decreases. The identical effect was demonstrated in the analytical works by de Jong (1982) and Hyer et al (1987). Also in this study, it was shown that the maximum circumferential stress occurs at the end of the contact zone which corroborates earlier work done on similar laminate models (Hyer and Klang 1984).

### 4.4.3 EFFECTS OF LAMINATE PROPERTIES

The ply orientation has a considerable influence on the stress distribution in the composite laminate. Figure 4.13 shows that (a) the radial stresses, (b) tangential stresses and (c) shear stresses, on the hole boundary for three types of laminates A, B and C. Clearly, laminate A, having quasi-isotropic material properties, has a lower maximum radial stress compared with laminates B and C, which have orthotropic properties. This is due to the higher percentage of plies aligned in the 45° direction that cause a more uniform stress distribution with in the laminate. The maximum radial stress occurs in the 45° direction in case of laminate A, the 25° direction for laminate B and the 75° direction for laminate C. The mode of failure of a composite laminate is strongly dependent on the angular position of this specific stress component. Laminate B has fewer piles in the 90° direction and exhibits the lowest tangential stress. In contrast, Figure 4.13(b) shows that laminate C, with the largest number of fibres in the direction perpendicular to the applied load, exhibits the largest tangential stress. The same conclusion can be made in assessing the variation in radial stresses, tangential stresses and shear stresses at the critical distance, $A_0$, as shown in Figure 4.14.

The resultant element stresses obtained in the analysis, in conjunction with a suitable failure criterion, will enable ply failure indices to be derived for each of the laminates considered in this study. The procedure to achieve the failure index is given in Chapter 6.

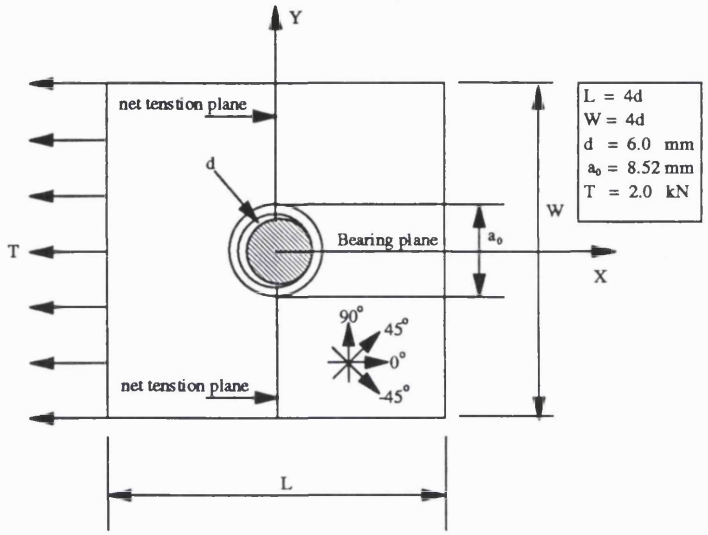


Figure 4.1 Physical model of laminate A under tensile load (Eriksson 1986)

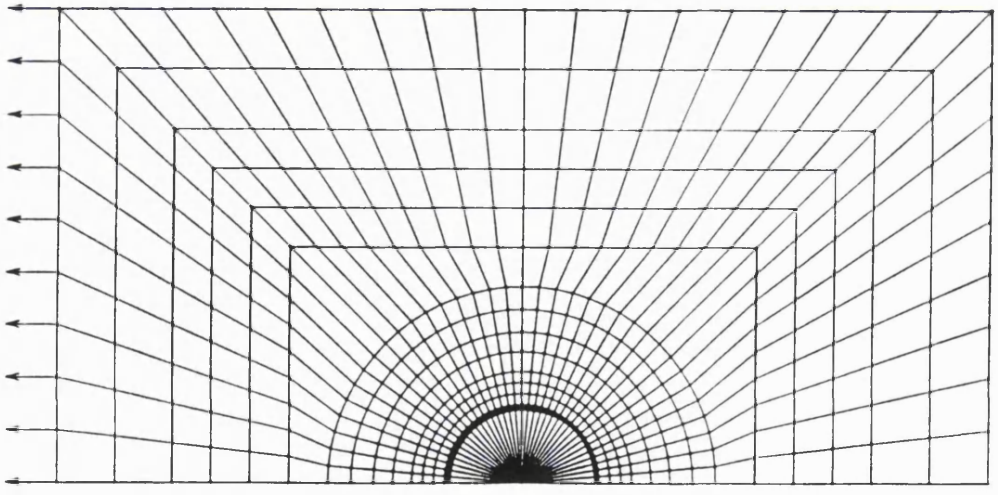

Figure 4.2 Typical finite element model of laminate A

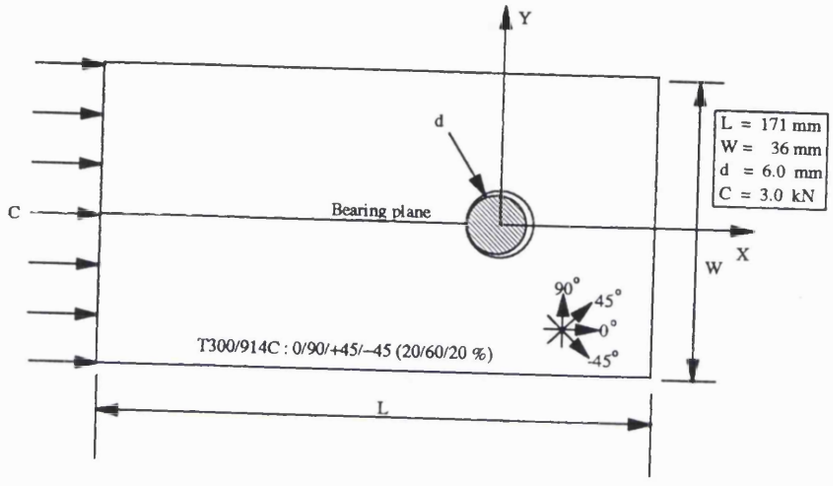


Figure 4.3 Experimental model for laminate D (Eriksson 1986)

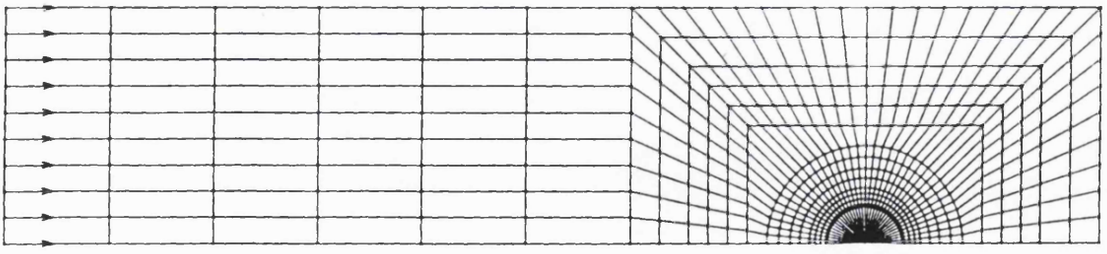

Figure 4.4 Two dimensional finite element model of laminate D

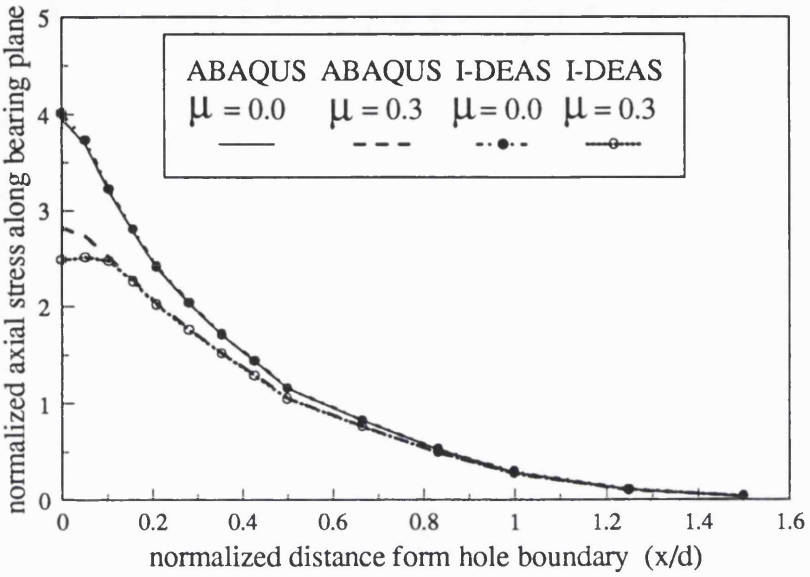


Figure 4.5 Comparison of normalized axial stress

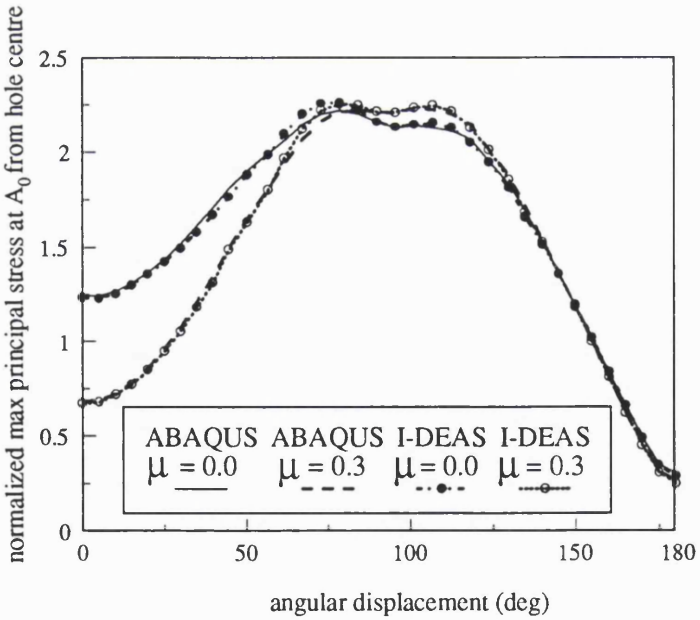


Figure 4.6 Results for the maximum principal stress at distance $A_0$ from the hole centre

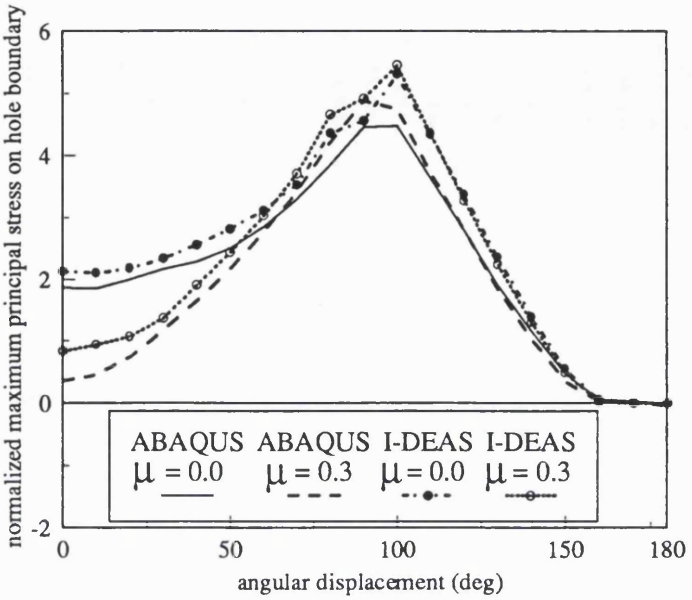


Figure 4.7 Normalized maximum principal stress of nodes on hole boundary

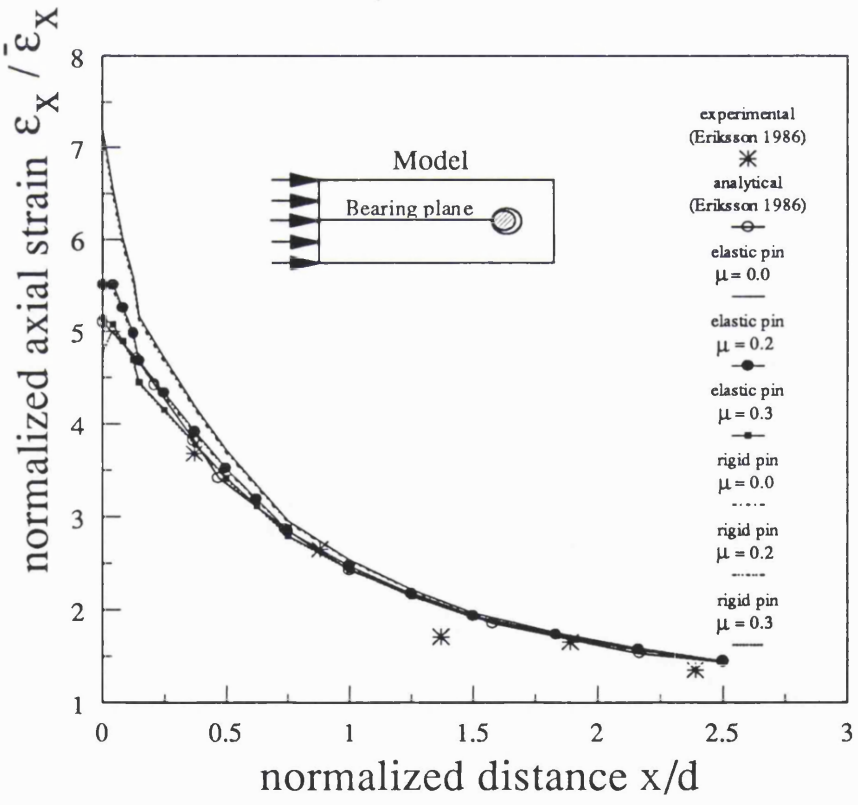


Figure 4.8 Effect of pin rigidity and coefficient of friction on axial strain of laminate D

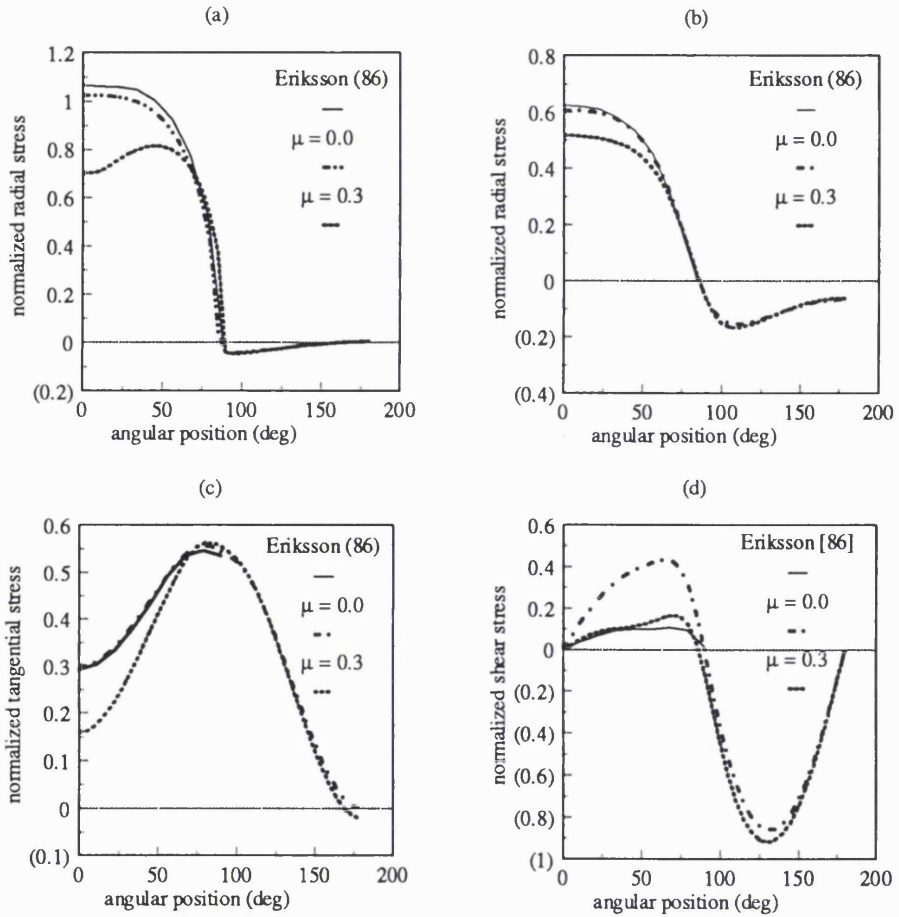


Figure 4.9 Analytical comparison of stresses for laminate A at (a) hole boundary, (b), (c) and (d) at the critical distance, $A_0$

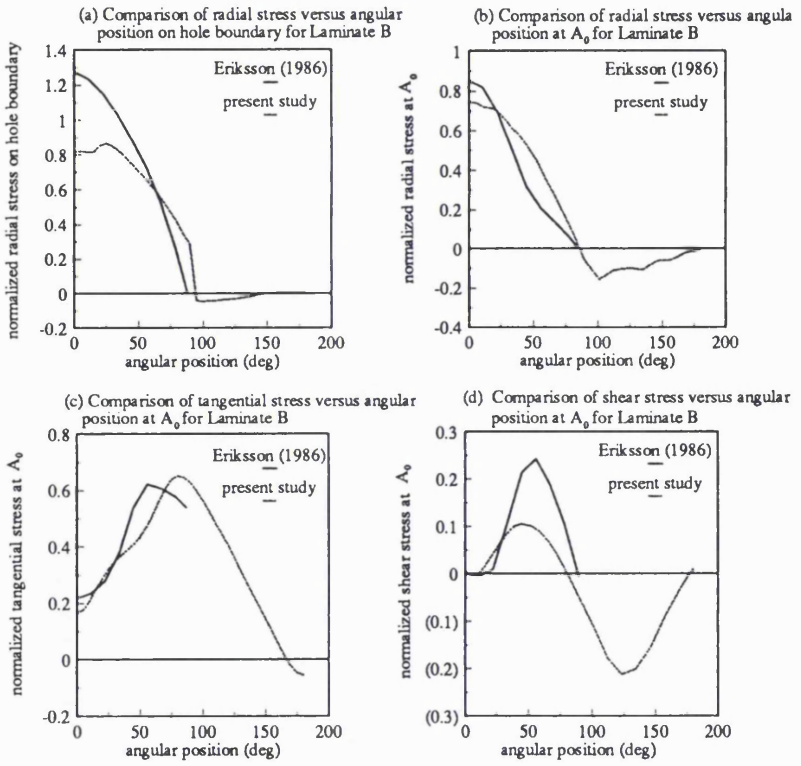


Figure 4.10 Analytical comparison of stresses for laminate B at (a) hole boundary, (b), (c) and (d) at the critical distance, $A_0$

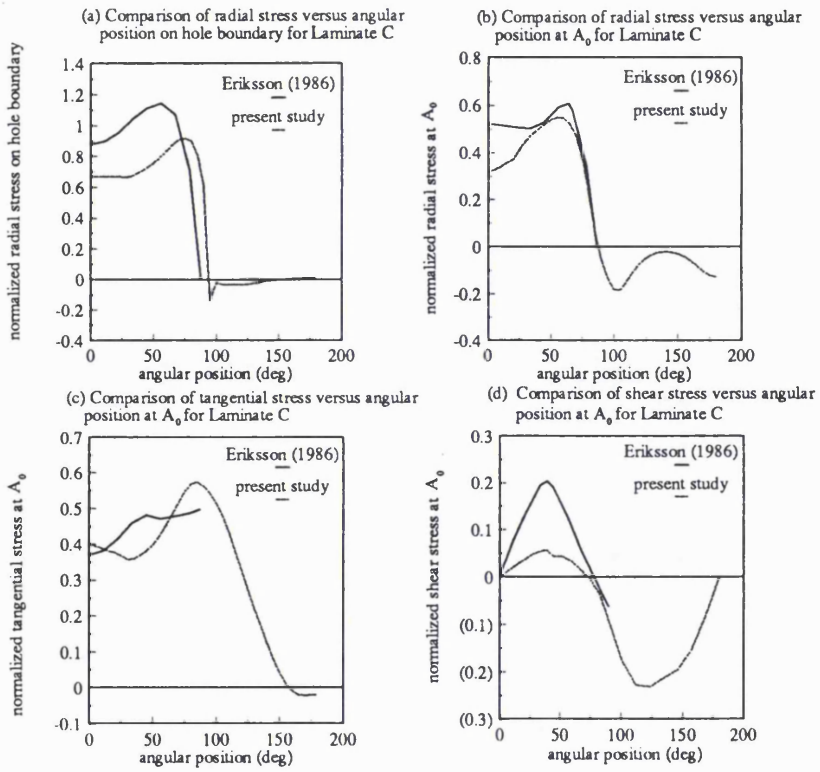


Figure 4.11 Analytical comparison of stresses for laminate C at (a) hole boundary, (b), (c) and (d) at the critical distance, $A_0$

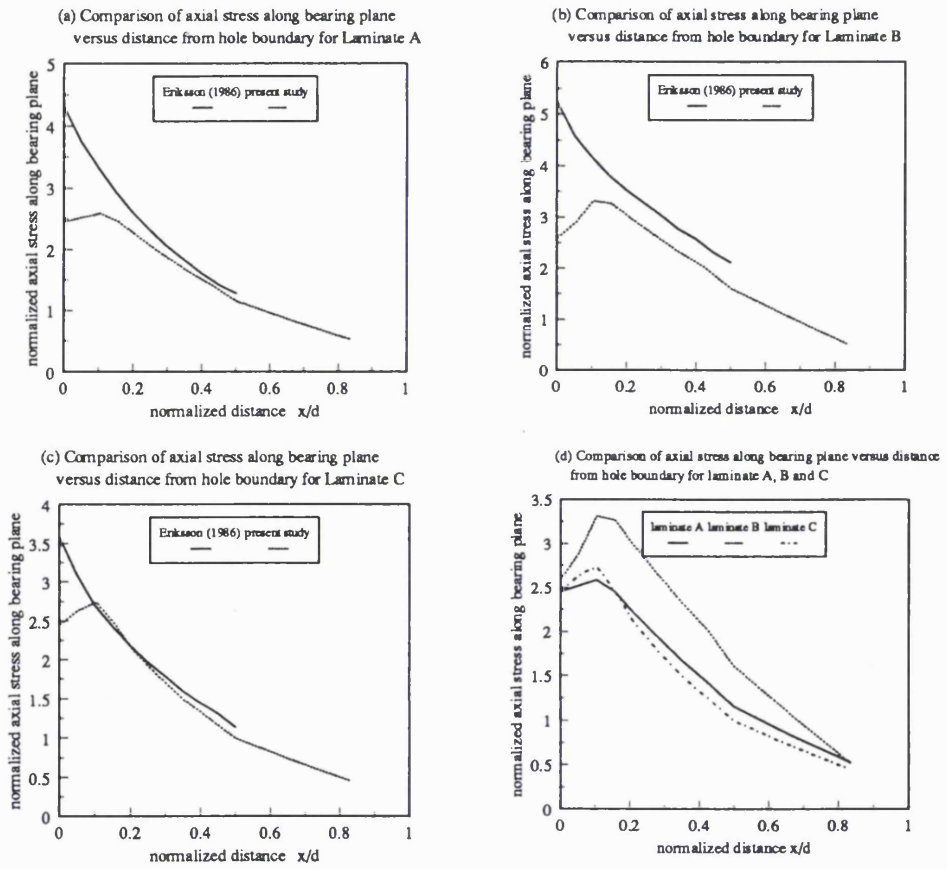


Figure 4.12 Comparison of normalized axial stress versus normalized distance for (a) laminate A, (b) laminate B, (c) laminate C and (d) laminate A, B and C

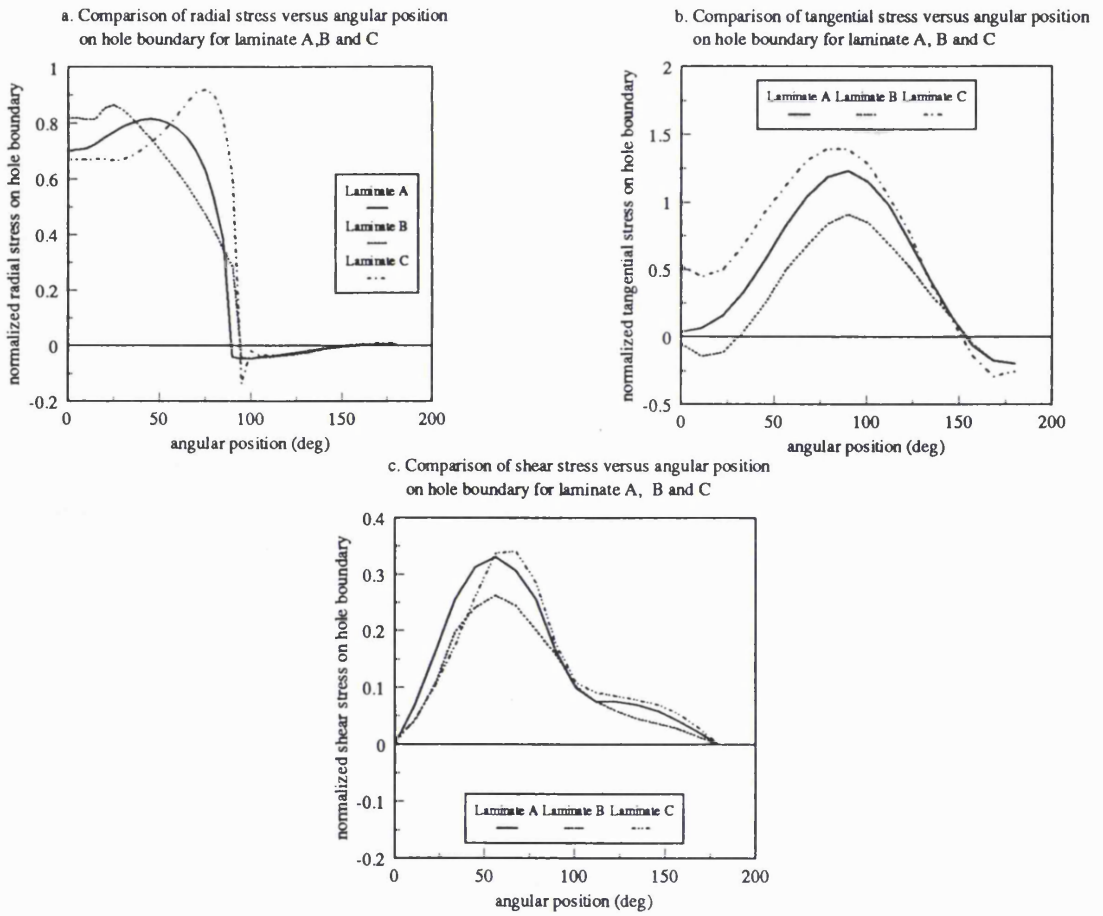


Figure 4.13 Comparison of (a) radial stress, (b) tangential stress and (c) shear stress on the hole boundary for laminate A, B and C

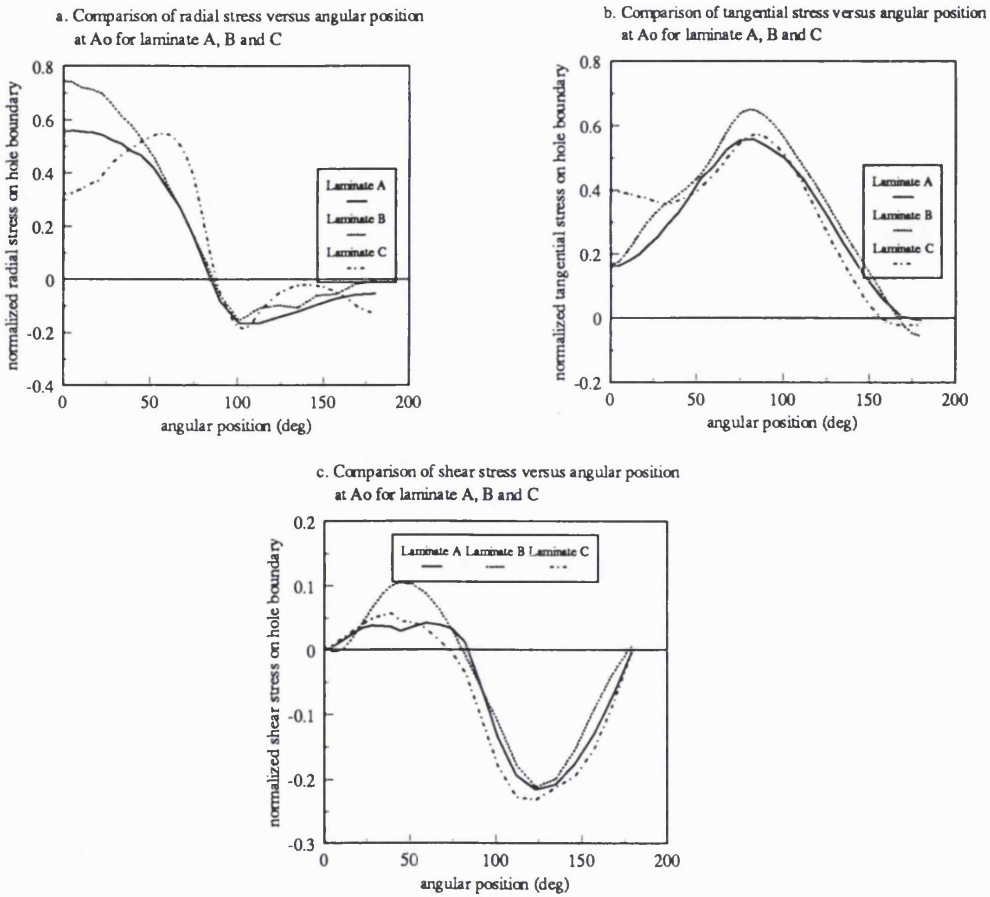


Figure 4.14 Comparison of (a) radial stress at $A_0$, (b) tangential stress at $A_0$ and (c) shear stress at $A_0$ for laminate A, B and C

# CHAPTER 5

# TWO-DIMENSIONAL MULTI-FASTENER MODEL

## 5.1 INTRODUCTION

Although considerable work has been undertaken in the analysis of single bolt fastened laminates, in many practical applications multi-fasteners are commonly utilized. One of the major problems concerned with this type of joint is the load transferred by each specific fastener. Wang and Han (1988), Fan and Qui (1993) and Oakeshott and Matthews (1994) have addressed this problem and investigated analytically the load distribution occurring in multi-fastened joints. However the localized contact stress distribution was not considered in any of these previous studies.

This chapter describes a general two dimensional finite element model which was used to determine the local stress distribution at the pin/hole interface and the load transferred on each pin in multi-fastened composite plates. Pin elasticity and interfacial friction are taken into account. A multi-fastened double lap joint consisting of two elastic plates and a composite laminate joined by rigid pins as well as a composite laminate joined to a rigid fixture were also examined.

## 5.2 METHOD OF ASSESSMENT

Two models of a double lap joint were constructed in this analysis, the first consisted of two high modulus elastic plates connected to an inner lap composite laminate by several rigid fasteners (Rowlands et al. 1982 and Griffin et al. 1994), thereby, confining the deformation to the inner lap plate. A second model, consisting of a joint between an inner lap composite laminate and a rigid fixture connected by a series of elastic pins, providing zero relative displacement between the centre of the fastener and the outer lap, was also analysed. Either rigid elements (Kim and Kim 1995) or deformable elements were employed to model the fasteners. In this respect, considering elastic fasteners in the model offers an advantage in that they provide a more realistic contact stress distribution at the interface.

### 5.2.1 RIGID FASTENERS

For comparison purposes, the geometric configuration of a double row 7 pin multi-fastened double lap joint, in a double lap fashion as utilized by Griffin et al. (1994) was adopted in this study. The length of the CFRP and steel plates was 260.35 mm., with widths of 190.5 mm. and 202.4 mm., respectively. These plates were connected using rigid pins of 19.05 mm. diameter with centre distances on the same row (pitch distance) of 47.625 mm. The edge distance and row spacing were 44.45 mm. and 38.1 mm., respectively, as shown in Figure 5.1. The mode of loading and identification number assigned to each hole in the

laminate are also shown in this figure. The row closest to the end of the plate being referred to as the outboard row and the row furthest from the end as the inboard row.

The material properties chosen for the model of a composite laminate and elastic plates were similar to those used in the experimental work conducted by Griffin et al. (1994) and are given in Table 5.1. The composite plate (laminate E) and the steel plate were modelled with 4-node quadrilateral shell elements. The finite element model for the multi-row cases employed a lower number of elements on each hole boundary than the single pin models due to the restriction on the number of gap elements that can be incorporated in the analysis. In these meshes an element on hole boundary subtended an angle of 11.25° at the pin centre. The rigid pins were constructed having the same number of nodes along the hole boundary as the laminate.

Table 5.1 Material properties of two-dimensional multi-fastened model (Griffin Jr., 1994)

| Material | plies and orientation | $E_x$ (GPa) | $E_y$ (GPa) | $G_{xy}$ (GPa) | $\nu_{xy}$ |
|---|---|---|---|---|---|
| IM7G/3501-6 Laminate E | $\{[(\pm 15)_3/90_2/0/(\pm 45/0)_5/90_3]_6/(\pm 15)_3\}_T$ | 86.05 | 48.06 | 21.03 | 0.191 |
| Steel plate | | 206.84 | 206.84 | 80.15 | 0.30 |

Using the I-DEAS MS 1.3c code, gap elements were used to model the contact between coincident nodes of the plates and the rigid pins, in the first and fourth quadrant for the pin/composite laminate interface and in the second and third quadrant for pin/steel plate interface; the tolerance of the pins was disregarded. Gap elements that modelled the interaction between the rigid pin and composite plate were defined using the local coordinates of each pin. In this analysis, the friction coefficient at the interface was chosen as either 0.0 or 0.3. Symmetry permits analysis of only half of the physical joint, as shown in Figure 5.2.

A model of multi-fastened composite laminate inner lap joined to steel plate outer laps by rigid pins was also constructed, having a line of symmetry along the mid-plane of the physical model. The 7 pin model consisted of 3278 elements, which included 3218 four-node quadrilateral shell elements, 2098 elements for the steel plate and 1120 elements for laminate E and 60 of the node to node type gap elements.

### 5.2.2 ELASTO-PLASTIC FASTENERS

A model of a multi-fastener composite plate using laminate D with titanium pins, having material properties given in Table 4.1, was used to investigate the effect of the joint geometry on the stress distribution and load transferred to the laminate. A multi-pin fastening between a rigid fixture and a composite laminate was examined as it represents the extreme case for load transfer to the laminate

via the inboard fasteners (Chang and Scott 1984a.). Models containing a single row of either 2, 3, or 4 pins, as shown in Figure 5.3, were constructed for analysis, each pin having the same diameter, $d$. A constant edge distance of $2d$ was adopted with two pitch distances: $3d$ and $4d$, corresponding to side distances of $1.5d$ and $2d$, respectively. The latter dimensions were adopted to provide an equivalent stress on the net section area of the plate while maintaining average bearing, shear and far field stresses for each configuration.

The double row configurations were also constructed incorporating 5 and 7 pins in two patterns A and B, as shown in Figure 5.3. Pattern A has the greater number of pins on the inboard row while pattern B has the greater number on the outboard row. The row spacing used in this configuration was $3d$ with the same edge distance used for the single row joint ($2d$); pitch distances of $3d$ and $4d$ were investigated. For all the multi-fastener configurations, tensile forces were applied at the end furthest from the hole and the pin centres were fully constrained. Only half of the model width was analysed since symmetric boundary conditions applied along the centre line of the joint.

A model to study the effects of pitch distance, row spacing, end distance and pin diameter on the percentage of load transferred via the inboard and outboard rows for a joint of infinite width was also constructed. The condition of an infinite width, quasi isotropic, laminate was utilized to exclude the influence of free edge effects. The material properties of the composite plate (laminate D), having an overall length of 69.85 mm., and the

titanium pins used as fasteners are identical to the previous model. A constant hole diameter of 6.35 mm. was used in this model while the pitch distance was varied between 3*d* and 14*d*, the row spacing between 2*d* and 4*d* and the edge distance between 1*d* and 3*d*. The effect of the bolt diameter on the stress distribution in the joint was investigated by varying the diameter between 5 mm. and 16 mm. whilst maintaining a constant pitch distance, row spacing and edge distance of 38.10 mm., 19.05 mm. and 12.70 mm., respectively. These values were considered to be close to the optimum values derived from the previous analysis for a single fastener model having pin diameter of 6.35 mm. The geometric configuration of the laminate considered in this study is shown in Figure 5.4.

The rigid outer lap model was constructed using 4-node quadrilateral shell elements for the laminate plate, while the deformable pins were represented by 3-node triangular shell elements. An angle of 11.25 degrees was subtended at the centre of the hole by adjacent nodes along the hole boundary, as used in all the two-dimensional finite element models of the multi-fastened composite laminate. Gap elements, having a friction coefficient equal to 0.3, were used to connect coincident nodes between the composite plate and the pins. A plate of infinite width allowed symmetric boundary conditions to be applied along the centre line of the pins parallel to the load direction. A uniform tensile load was applied at the edge furthest from the inboard row. A typical finite element model is shown in Figure 5.5.

## 5.3 RESULTS

The radial contact stress on each hole was normalized for comparative assessment of the results using the nominal bearing stress which is given by equation (4.1).

### 5.3.1 RESULTS FOR MULTI-FASTENED COMPOSITE LAMINATES JOINED BY RIGID PINS

The results obtained in this study for the percentage of load transferred to each pin in a multi-fastened double lap joint, consisting of two steel outer laps joined by either three or seven rigid pins to an inner lap composite laminate, are given in Table 5.2. The load transferred to each pin was calculated by numerically intergrating the load-direction components of the contact stresses obtained from the gap elements. The results show that, for a composite inner lap, the load transferred is highest on the outer most hole on the outboard row (hole 1 for the case of 3 pin and hole 3 for the case of 7 pin configuration). For the 3 pin configuration, the load transferred to the pin on the outboard row (hole 1) is 41.3% higher than the load transferred to the pin on the inboard row (hole 2). It can be seen that the 7 pin configuration exhibits the more uniform load transferred.

The results obtained for the frictionless condition compare well, for both the three and seven pin configurations, with the earlier work of Griffin et al. (1994) on which this model was based. The introduction of interfacial friction

between the pin and composite plate is shown to have a negligible effect on the load transferred to each pin.

The variation in the normalized radial stress at the hole boundary for the seven pin double lap joint is given in Figure 5.6. These results show that when friction is incorporated in the model there is a reduction in the stress on the bearing plane but negligible effect on the maximum stress on the inboard row, whereas, the maximum stress decreases at both holes on the outboard row. Although the peak stresses are symmetric about the bearing plane for both the inboard and outboard rows the maximum stress for holes 2 and 4 on the outboard row occurs at ±45 degrees with respect to the loading direction. The observed changes in location of the peak stress, arising from considering friction at the fastener interface, will clearly have a consequential effect on the failure mode of the joint.

Table 5.2 Comparison of load transferred by each pin in a multi-fastened composite laminate

| | hole 1 (%) | | | hole 2 (%) | | | hole 3 (%) | | | hole 4 (%) | | |
|---|---|---|---|---|---|---|---|---|---|---|---|---|
| Model | *1** | *2** | *3** | *1** | *2** | *3** | *1** | *2** | *3** | *1** | *2** | *3** |
| 3H μ=0.0 | 38 | 41 | 41.4 | 32 | 31 | 29.3 | - | - | - | - | - | - |
| 3H μ=0.3 | - | - | 42.1 | - | - | 29 | - | - | - | - | - | - |
| 7H μ=0.0 | 15 | 15 | 15.1 | 12 | 10 | 9.6 | 16 | 18 | 17.8 | 15 | 15 | 15 |
| 7H μ=0.3 | - | - | 15.2 | - | - | 9.4 | - | - | 18 | - | - | 14.9 |

*1** and *2** Experimental and analytical results after Griffin et al. (1994)

*3** Results obtained in this study

### 5.3.2 RESULTS FOR MULTI-FASTENED COMPOSITE LAMINATE OUTER LAP JOINED TO A RIGID INNER LAP

For purposes of comparison the results for the normalized radial stress on the hole boundary in the single row multi-fastened joint are shown in Figure 5.7. The four-pin single row, with a pitch of 4*d*, exhibits the highest normalized radial stress at the interface of the hole nearest the side of the plate, i.e. the outer most hole (hole 1), which is slightly higher than that recorded for the 3*d* pitch configuration. This is reflected in the nonuniform distribution of load transferred across the joint and demonstrates that the results obtained for single pin joints cannot be extrapolated to cases involving multi-pin fastenings.

The results obtained for double row multi-fasteners containing 5 pins are shown in Figure 5.8, 5.9, 5.10 and 5.11. Figure 5.8 compares the normalized radial stress on the hole boundary for pattern A and B with pitch distances of 3*d* and 4*d*. For both patterns and pitch, the maximum radial stress occurs at the outer most hole on the inboard row (hole 1, h1).

Figure 5.9 shows the normalized hoop stress on the hole boundary to be zero at an angular position of 0° (i.e. localized bearing plane) but then dramatically increase to a peak value at an angular position of 90°(i.e. localized tension plane). This stress then decreases to a minimum value at an angular position of 180°. The maximum tangential stress occurs in the joint configuration with the largest pitch distance (4*d*).

The normalized shear stress component, shows in Figure 5.10, exhibits maximum and minimum values at angular positions of ±45° which diminishes to about zero at angular positions of ±90°. A second peak is obtained, although lower in magnitude, at an angular position of 135°.

In all these cases an asymmetric stress distribution about the bearing plane may be observed with hole 1 pattern B - 4*d* pitch, showing the highest recorded stress.

The Von Mises stress is shown for the double row 5 pin configuration on the deformation model in Figure 5.11. From this stress distribution it is apparent that the often used assumption of equivalent load transfer on each pin is erroneous. The stress contour plot and the deformation associated with each hole indicates that a high proportion of the load is transferred via the inboard pins and, in particular, the outer most pin of the outer lap plate. The percentage of load transfer via each pin is referred to in a later section.

The results obtained for the double row, 7 pin joint configurations are shown in Figure 5.12, 5.13, 5.14 and 5.15. The maximum normalized radial stress (Figure 5.12) is recorded on the inboard row at the outer most hole (hole 1) for pattern B, with a pitch of 4*d*. This is consistent with the observation made in the case of the 5 pin joint.

The variation in the radial stress, tangential stress (Figure 5.13) and shear stress (Figure 5.14) along the hole boundary, for all the configurations investigated corresponds with the stress distributions observed for the 5 pin multi-fastened joint, although the peak stresses in this case are greater.

Figure 5.15 shows that significant deformation occurs in the 7 pin joint configuration, particularly around the hole closest to the side of the plate on the inboard row. As in the case of 5 pin joint the highest load is transferred via the inboard pins, as shown by the Von Mises stress contour plot.

The load transferred in a multi-fastened joint having a single row is shown in Figure 5.16. It may be observed that the load transferred is slightly higher when the number of pins is increased from 3 to 4. The load transfer for a double row fasteners is shown in Figure. 5.17. For these joints the range in stress levels between the maximum normalized radial stress on each hole in the same model increases with the number of pins and the load transferred to the outmost hole appears proportional to the number of pins used. It is also apparent from these results, which further confirms earlier analysis of multi-fastened composite joints using rigid pins, that for the outer lap plate the percentage of load transferred is more significant on the outer most pin on the inboard row.

For an infinite width composite laminate connected to a rigid fixture the effect of varying the row spacing, and edge distance on the percentage of load transferred to the inboard and outboard rows, for various values of pitch

distance, is shown in Figure 5.18 and Figure 5.19, respectively. These results show that the variation in load transfer as a function of pitch distance is the same for all the row spacings investigated and that the higher row spacing (as a function of pin diameter) gives a more uniform load distribution across both the inboard and outboard rows.

It is also evident from Figure 5.18 and Figure 5.19 that, for all row spacing and edge distances shown, the load transfer is almost unaffected when the pitch distance exceeds, approximately, six times the pin diameter. Varying the edge distance between one and three times the pin diameter, as shown in Figure 5.19, produced a more uniform transfer of the load for both the inboard and outboard rows, although very little change was observed for edge distances greater than $2d$, where $d$ is the hole diameter.

For perfect fit pins the change in radial contact stress, normalized with respect to the gross tensile stress (equation 4.3), at the pin-hole interface is shown in Figure 5.20 for a range of pin diameters. In the case of the inboard row (Figure 5.20a) the angular position of the maximum stress, with respect to the pin centre, increases from 30 degrees for the smallest pin diameter (5 mm) to 40 degrees for pin diameters of 8 mm and above. It is apparent that this stress rapidly decays once the maximum value is attained, with the exception of the larger pins diameters (13 mm and 16 mm). The angular position of the maximum radial contact stress on the outboard row, as shown in Figure 5.20b, exhibits a trend similar to that observed for the inboard row, however, the magnitude of

the normalized stress is considerably lower. Once the maximum stress has been reached, unlike the trend observed on the inboard row, there is a gradual reduction with increasing contact angle; for the larger pin diameters the stress only drops significantly when the contact angle exceeds 90 degrees. This is to be expected since the hoop stress is also comparatively low resulting in lower slip at the interface and prolonged contact.

The normalized stress on the net tension plane (local stress divided by the gross tensile stress) is shown in Figure 5.21 for a range of pin diameters. This value is clearly important since it is likely to determine the functionality of the joint (since only tensile loading has been considered here). These results show that the stress at the pin-hole interface systematically decreases as the pin diameter increases in the range of 5 mm to 8 mm. However, this represents the limit in pin diameter for this joint configuration since a further increase to 16 mm raises the interfacial stress as a consequence of the increasing influence of the net tension stress.

The effect of increasing the pin diameter on the load transferred on both the inboard and outboard rows is shown in Figure 5.22. A more uniform load distribution across the joint is observed for the smallest pin diameter, with increasing asymmetric loading occurring as the pin diameter is increased. This result cannot be considered in isolation since the optimum joint geometry is dependent on several other parameters, particularly the net tension stress at the hole boundary, as shown earlier.

## 5.4 CONCLUDING REMARKS

From the results given in the previous section, the following conclusions may be made concerning some of the specific geometric parameters of a multi-fastened joint.

### 5.4.1 EFFECT OF FRICTION AT THE INTERFACE

Interfacial friction appears to exert a negligible effect on the percentage of load transferred in a multi-fastened double lap joint, consisting of two high modulus elastic plates and a composite laminate inner lap, connected by either three or seven, perfect fit, rigid pins. However, friction does significantly effect the normalized radial contact stress on the bearing plane, in some cases reducing the value by approximately 50%.

### 5.4.2 EFFECT OF NUMBER OF PINS

The normalized radial stress distribution for a single row multi-fastened joint, as shown in Figure 5.7, was observed to increase at the hole nearest the side of the plate (hole 1) as a result of increasing the number of pins. However, the variation in the maximum normalized radial stress on each hole on the same model is limited to a narrow range. This leads to the conclusion that for the single row array, increasing the number of pins will slightly increase the load

transferred at hole 1 relative to the single pin joint, as measured by the percentage of load transferred, shown in Figure 5.16. The load transfer for double row fasteners is shown in Figure 5.17. For these joints the range in stress levels between the maximum normalized radial stress on each hole in the same model increases with the number of pins and the load transferred to the outermost hole on the outer lap plate appears proportional to the number of pins used.

### 5.4.3 EFFECT OF NUMBER OF ROWS AND PATTERNS

The results obtained in Figure 5.16 show that although the loads are not uniformly distributed through all the pins in the single row multi-fastened joint, the variation is low resulting in a slightly higher load transferred at the outmost hole (hole 1) compared with that obtained in a single pin joint. For the double row configurations the results are somewhat different exhibiting reductions up to 40% of load transferred by a single pin (pattern B with a 5 pin array and $4d$ pitch). These results also show that increasing the number of rows in the joint has a considerable effect on the load distribution, and for the cases studied, significantly increasing the load transferred via the outer most hole.

Comparing the results obtained for the double row joint configuration, conforming to either pattern A or B, shows that, for a pitch distance of $3d$, pattern A gives the better load distribution, for both 5 pin and 7 pin configurations. Increasing the pitch distance to $4d$ considerably improved the

load distribution, particularly for pattern B. The implication is that for both 5 and 7 pin configurations there is greater potential for improving the joint performance of pattern B compared with A. It may be concluded that in mechanically fastened joints between a composite laminate and rigid fixture, pattern B is the preferred configuration since it gives a more uniform stress distribution across the joint.

### 5.4.4 EFFECT OF PITCH DISTANCE, ROW SPACING AND EDGE DISTANCE

Single row multi-fastened composite laminates with a pitch distance of $4d$ exhibit slightly higher normalized radial stresses compared with similar joint configurations with lower pitch distances. However, as the hole interspacing is reduced closer attention must be given to the influence of the stress distribution from the neighbouring holes and the reduced net section area. The results of 5 and 7 pin double row multi-fastened joint configurations, conforming to either pattern A or B, indicate that when the value of pitch distance is increased from $3d$ to $4d$ the joint performance is improved. For the infinite width multi-fastened double lap joint, consisting of a composite laminate inner lap fastened to rigid outer lap plate the more suitable pitch distance was found to be approximately six times the pin diameter, although some maginal benefit may be gained by increasing this parameter. The preferred row spacing and edge distance was found to be twice the pin diameter, provided that uniform transfer of load for both rows is the design objective.

Since tensile failure represents the catastrophic failure mode for composite laminates it is important to consider the magnitude of the net tension stress. Thus, having chosen the optimum pitch and edge distances the most suitable pin diameter can be selected by considering both the peak net tension stress at the hole boundary, with a view to minimising this value, and the percentage of load transferred to the inboard and outboard rows of the joint. From the results of the latter model it is clear that 8 mm diameter pins give the lowest normalized tensile stress at the hole boundary these also give an acceptable load distribution across the joint. An optimum pin diameter of 8 mm may be considered suitable for this paticular type of joint.

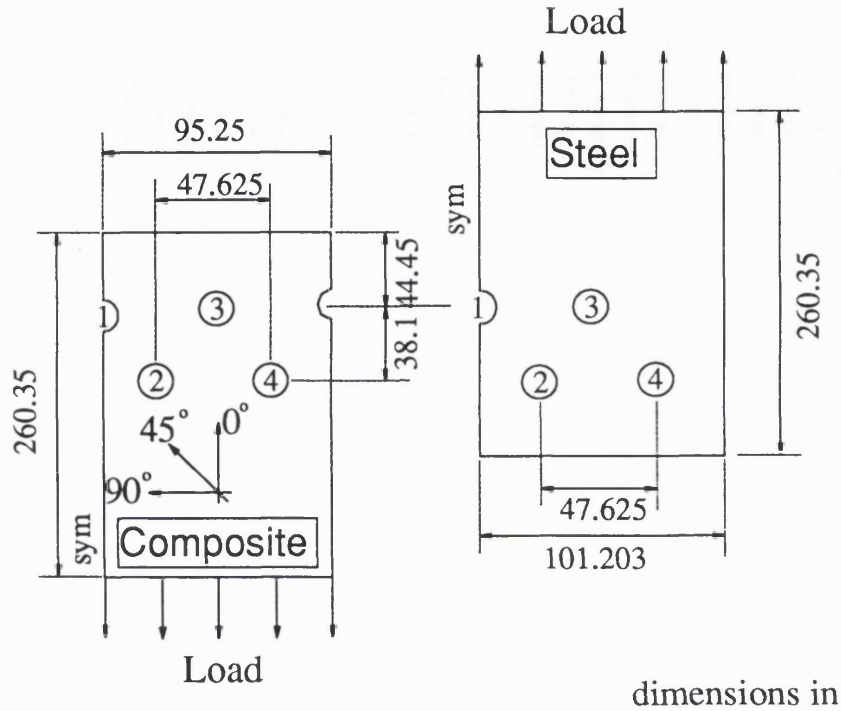


Figure 5.1 Geometric configuration of composite laminate and steel plate

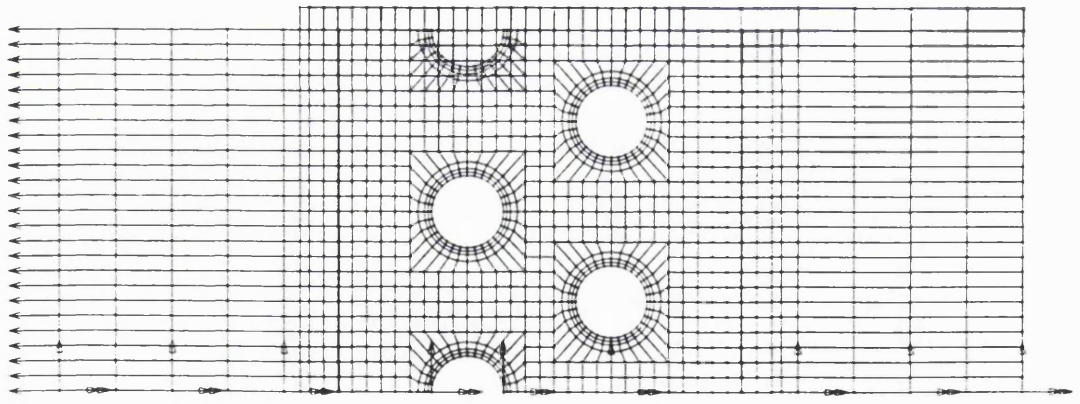

Figure 5.2 Finite element model representing a composite laminate joined to steel plates outer lap

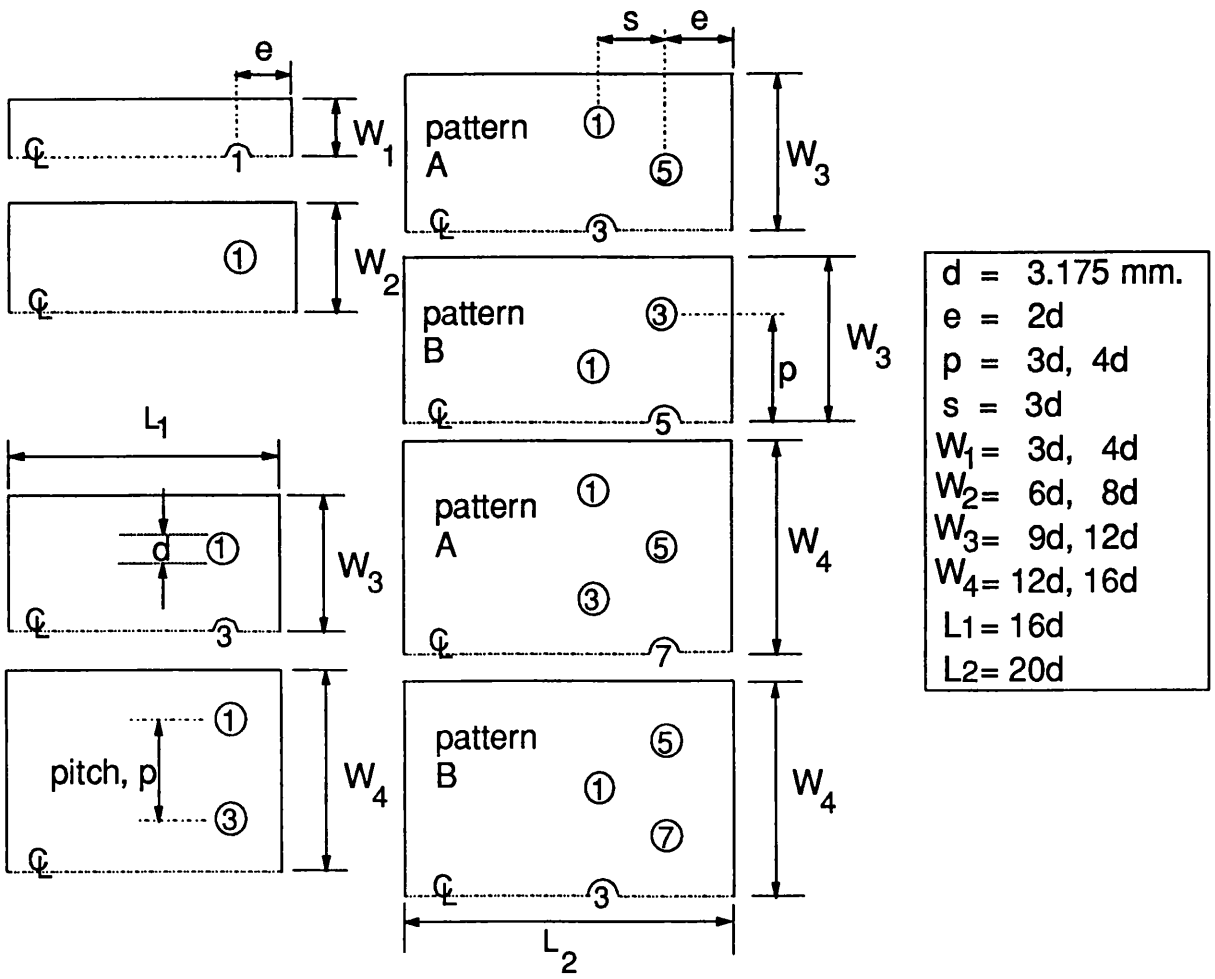


Figure 5.3 Configuration for two-dimensional multi-fastened joints using deformable pin

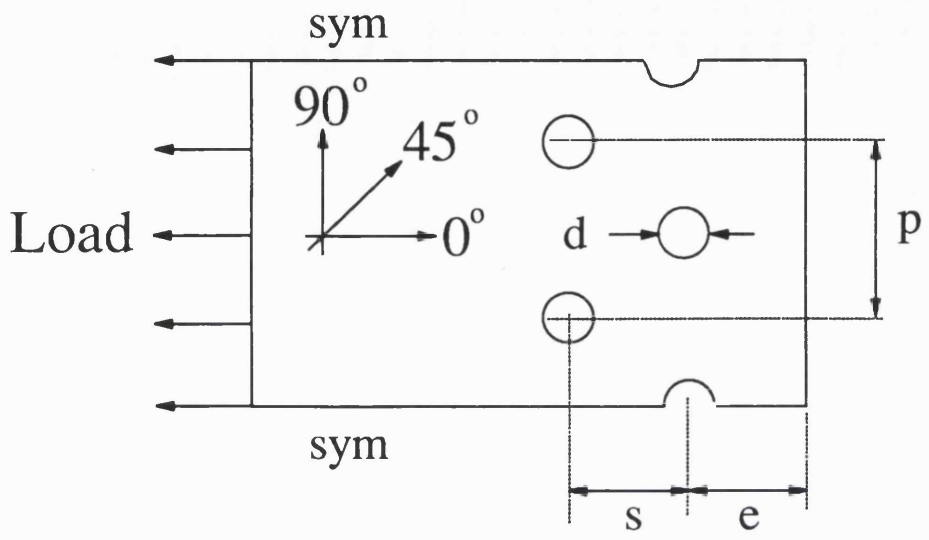


Figure 5.4 Geometric configuration for double row multi-fastened laminate of infinite width

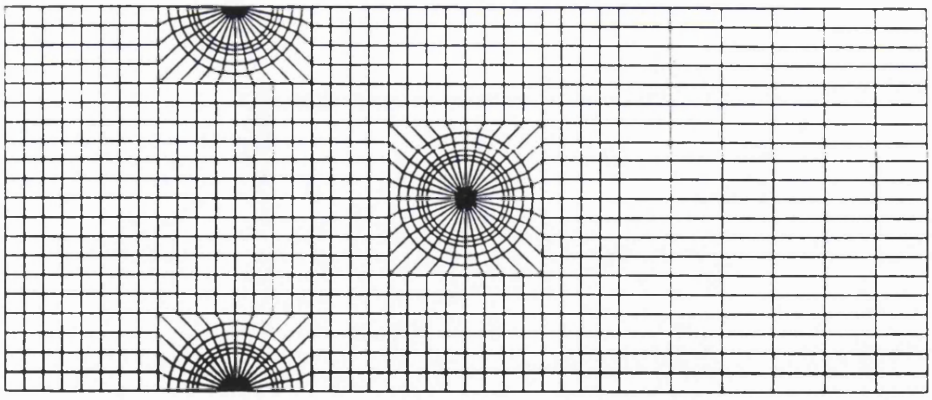

Figure 5.5 Typical model for composite plate fastened with elastic pins

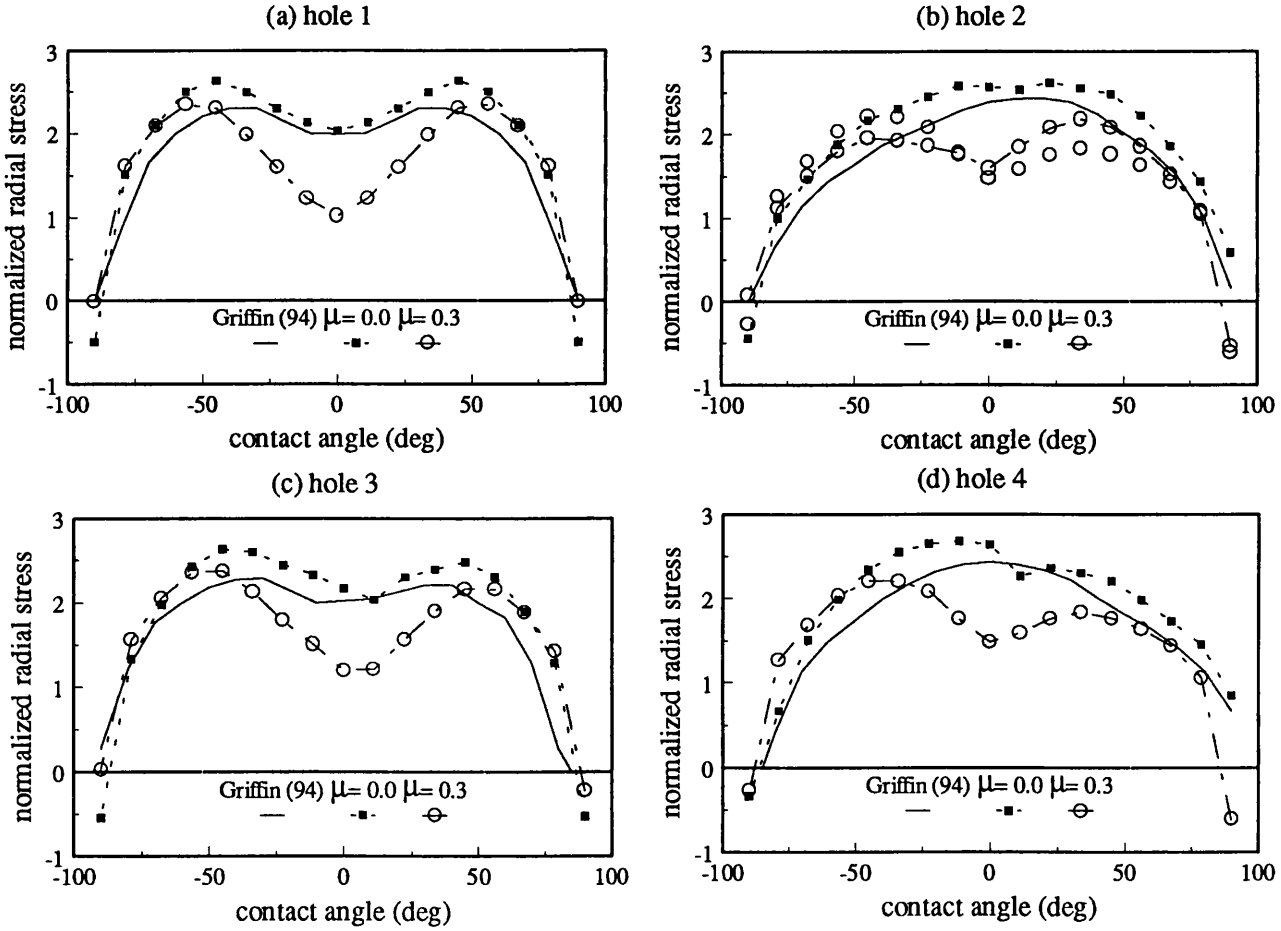


Figure 5.6 Contact stress on the hole boundary of a seven pin double lap joint

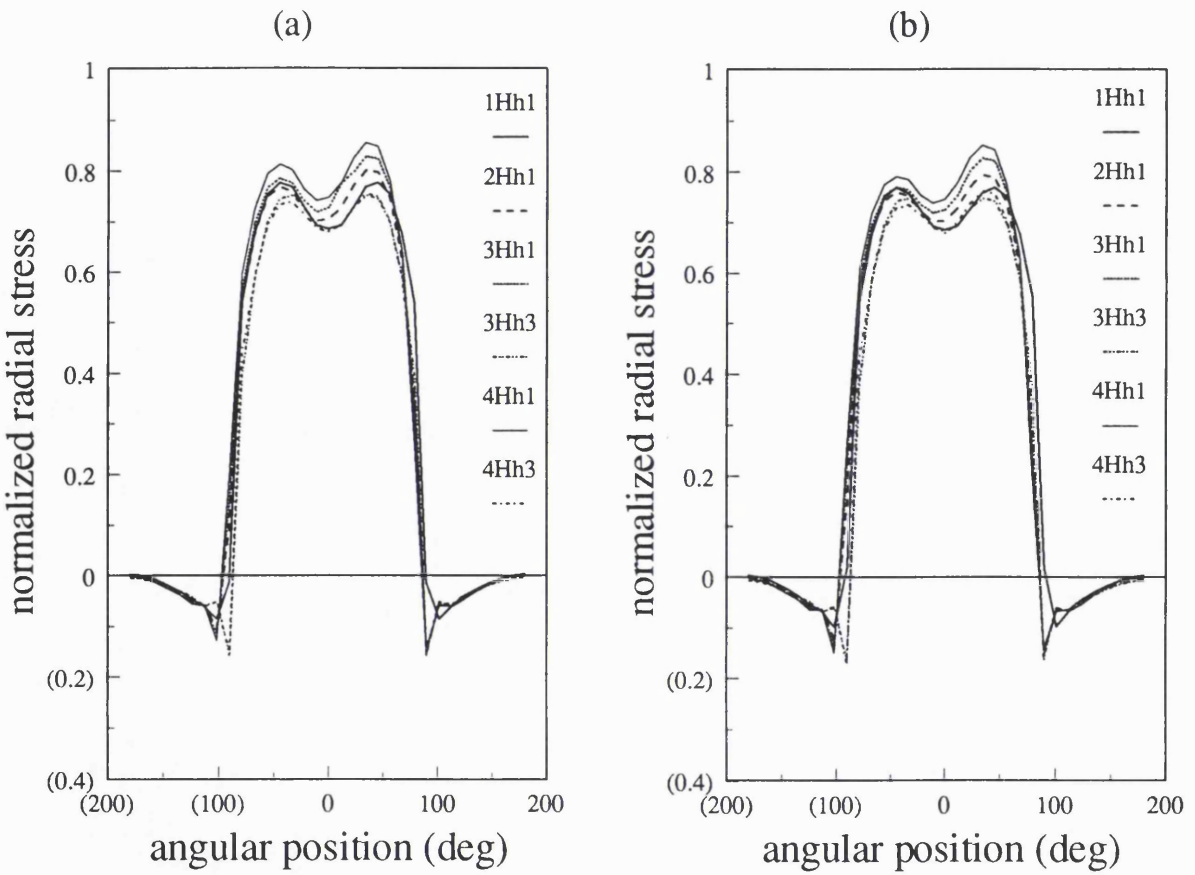


Figure 5.7 Normalized radial stress on the hole boundary for a single row multi-fastener with pitch distance (a) 4*d* and (b) 3*d*

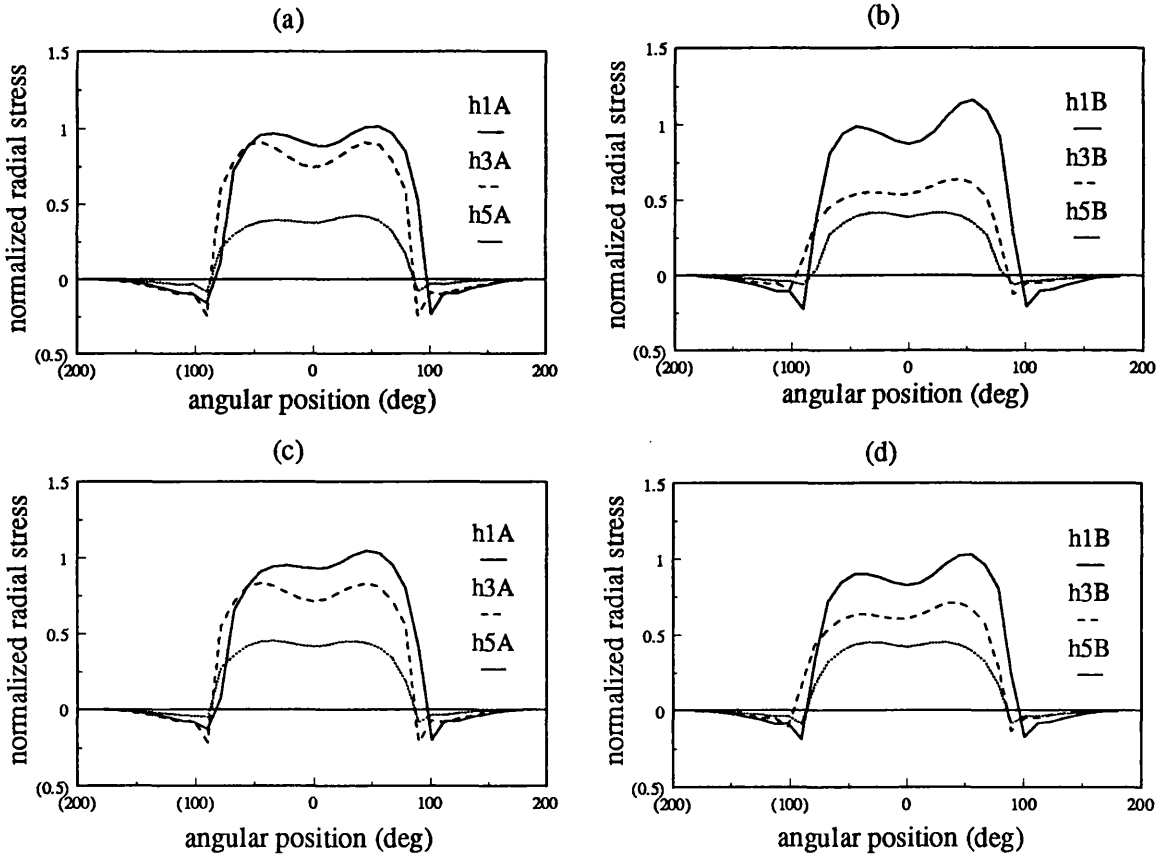


Figure 5.8 Normalized radial stress for double row, 5 pin joint configurations (a) pattern A, pitch 4*d*, (b) pattern B, pitch 4*d*, (c) pattern A, pitch 3*d* and (d) pattern B, pitch 3*d*

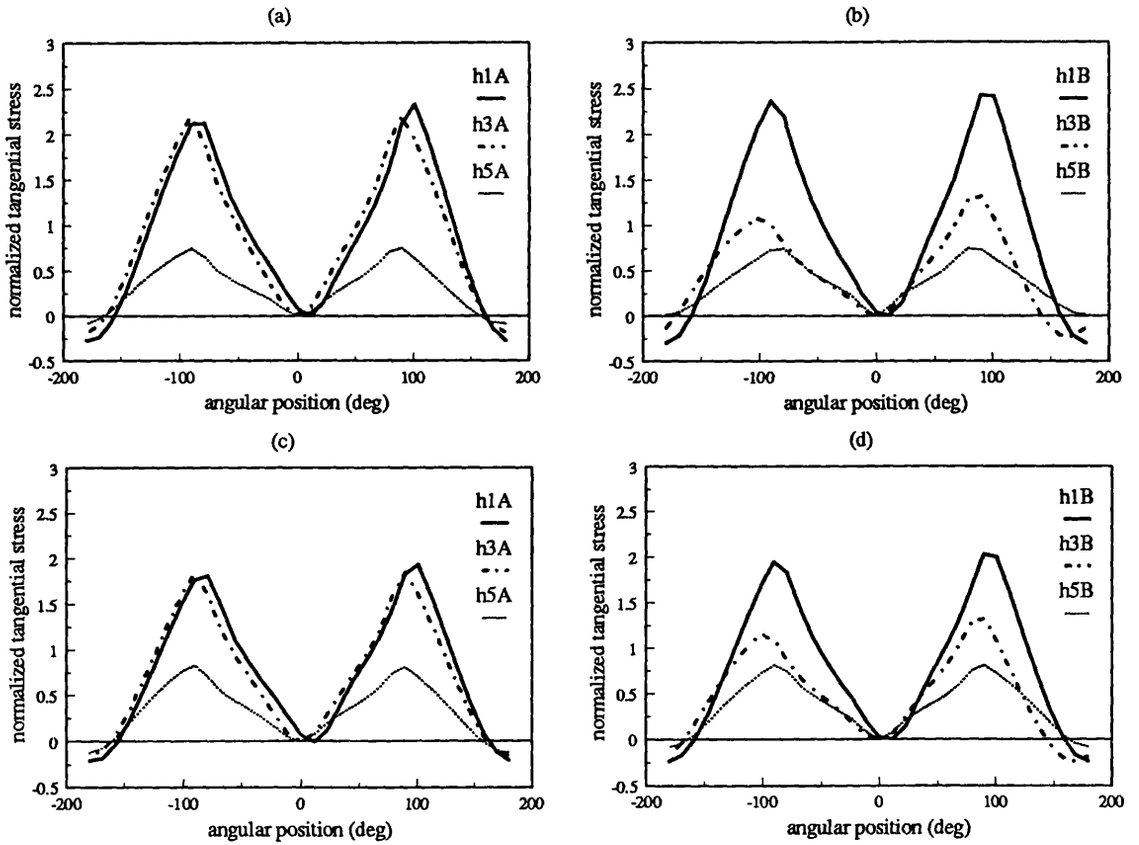


Figure 5.9 Normalized tangential stress for double row, 5 pin joint configurations (a) pattern A, pitch 4*d*, (b) pattern B, pitch 4*d*, (c) pattern A, pitch 3*d* and (d) pattern B, pitch 3*d*

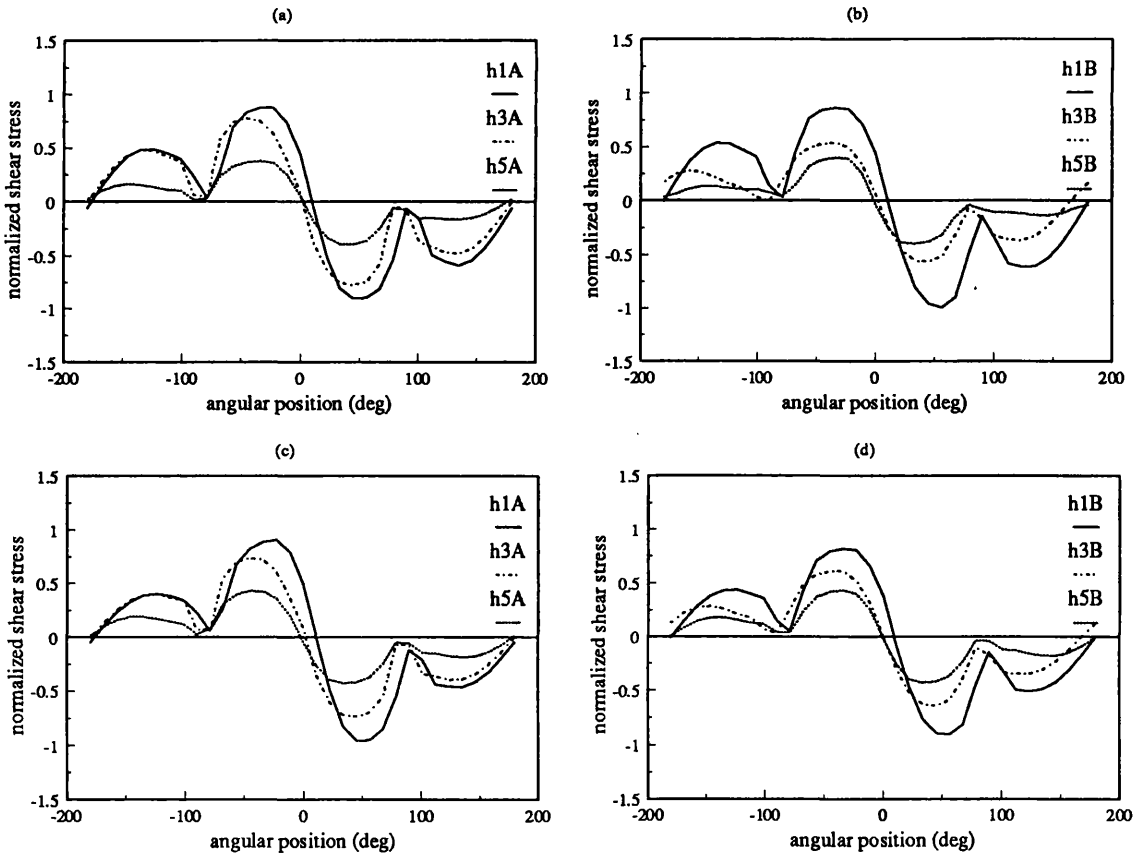


Figure 5.10 Normalized shear stress for double row, 5 pin joint configurations (a) pattern A, pitch 4*d*, (b) pattern B, pitch 4*d*, (c) pattern A, pitch 3*d* and (d) pattern B, pitch 3*d*

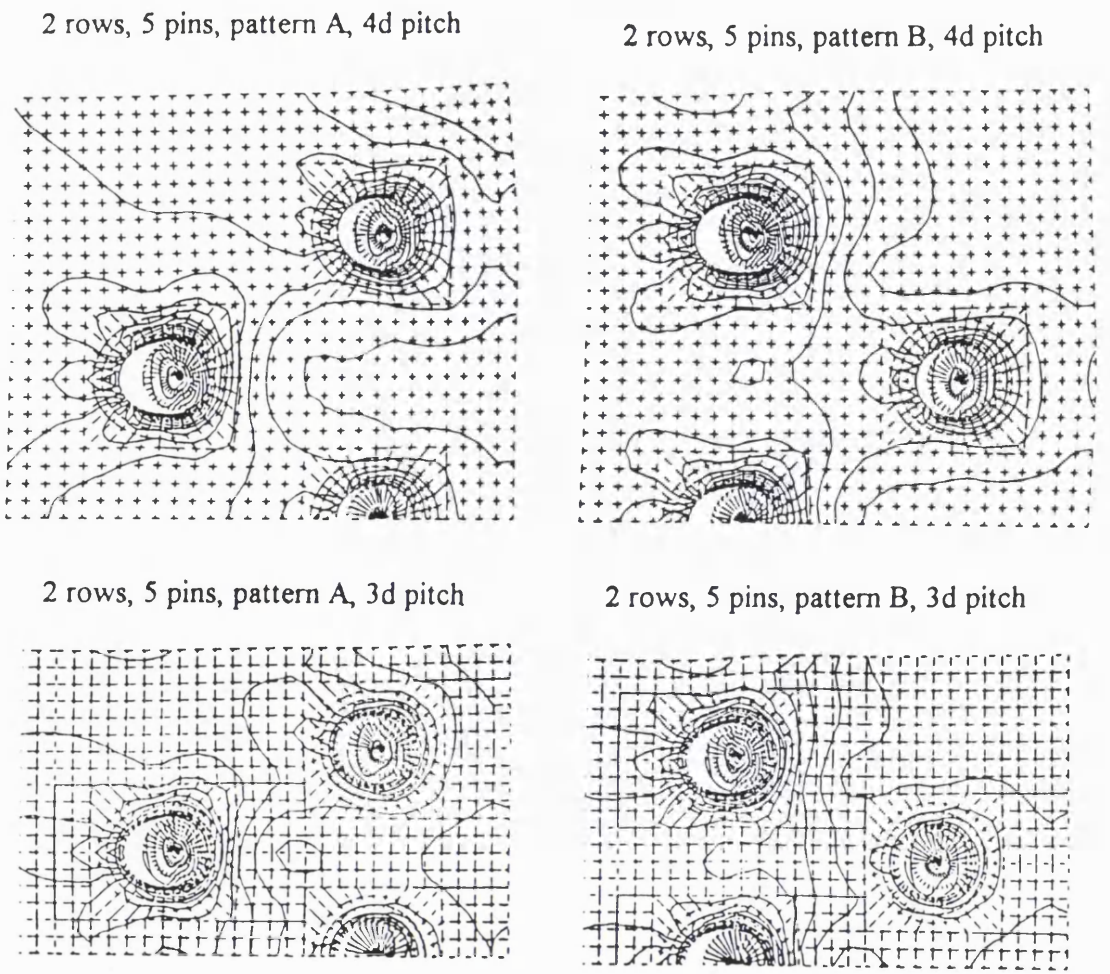


Figure 5.11 Contour plot of Von Mises stress on the deformed model for the double row 5 pin configuration

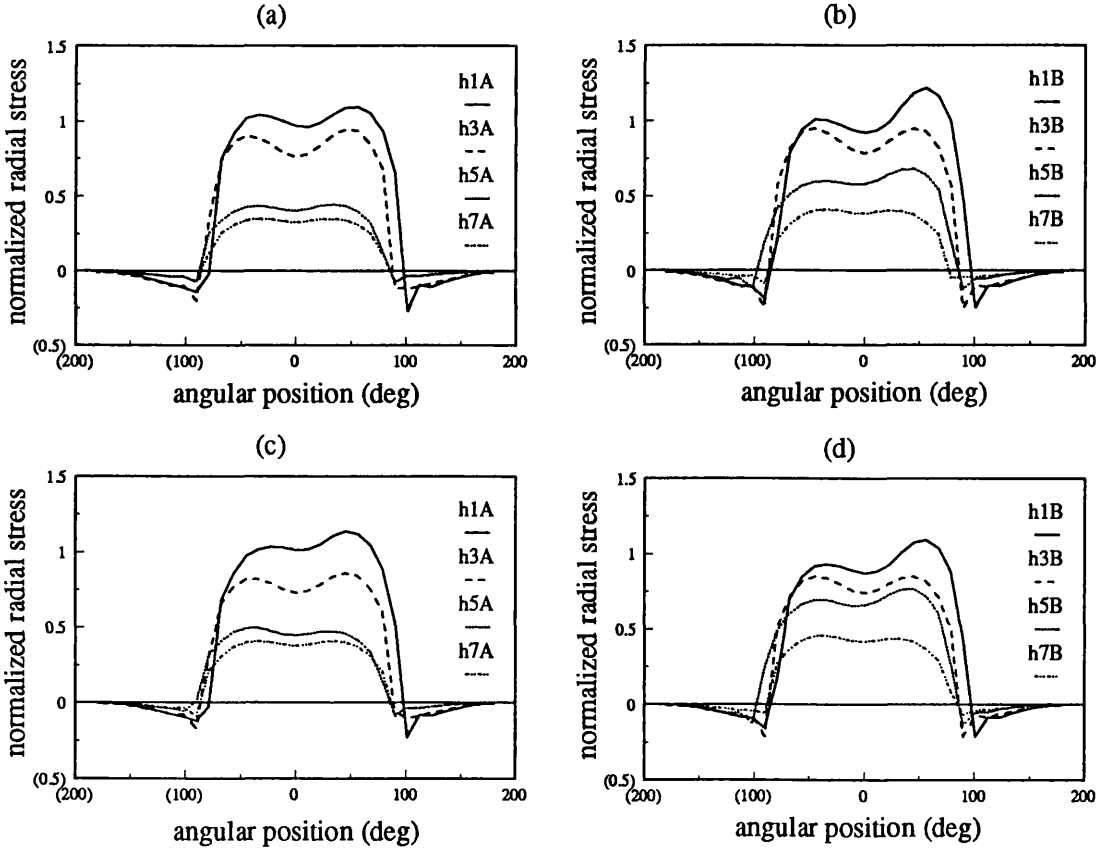


Figure 5.12 Normalized radial stress for double row, 7 pin joint configurations (a). pattern A, pitch 4*d*, (b). pattern B, pitch 4*d*, (c). pattern A, pitch 3*d* and (d). pattern B, pitch 3*d*

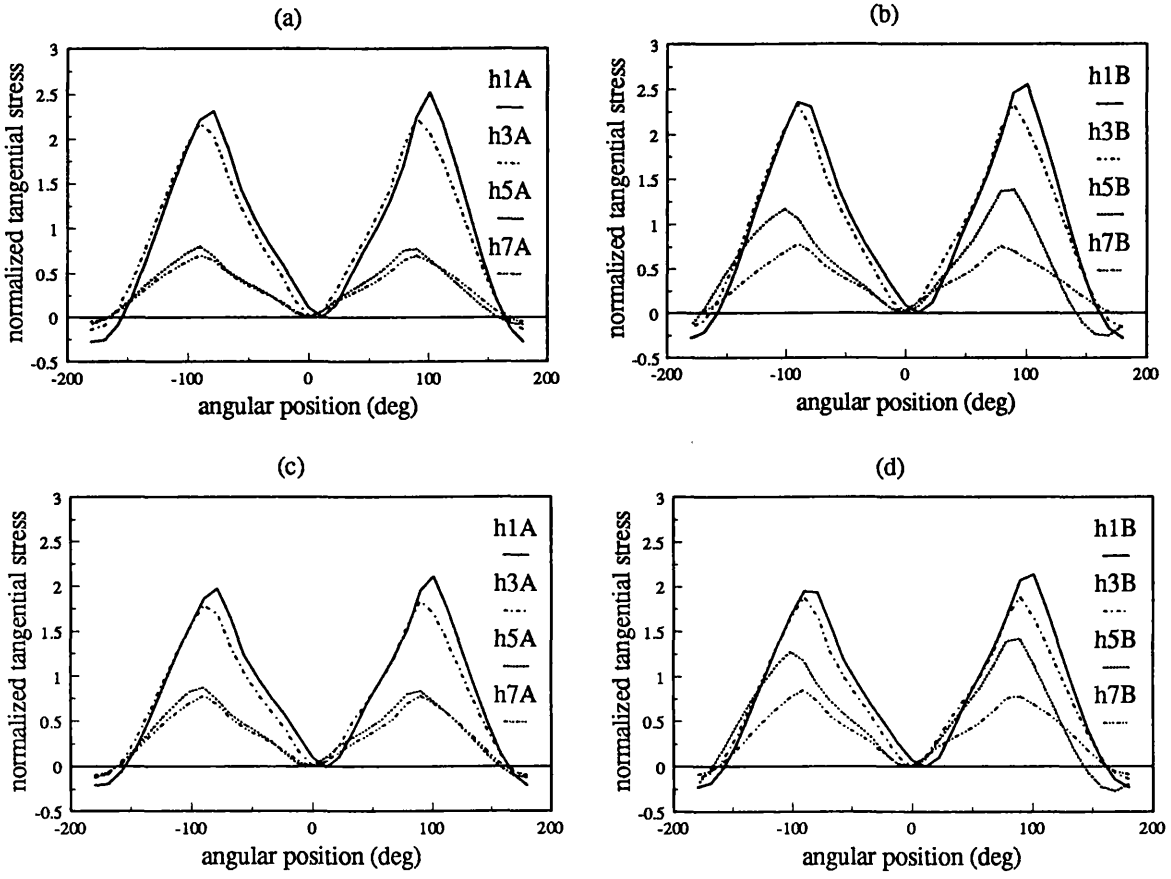


Figure 5.13 Normalized tangential stress for double row, 7 pin joint configurations (a). pattern A, pitch 4*d*, (b). pattern B, pitch 4*d*, (c). pattern A, pitch 3*d* and (d). pattern B, pitch 3*d*

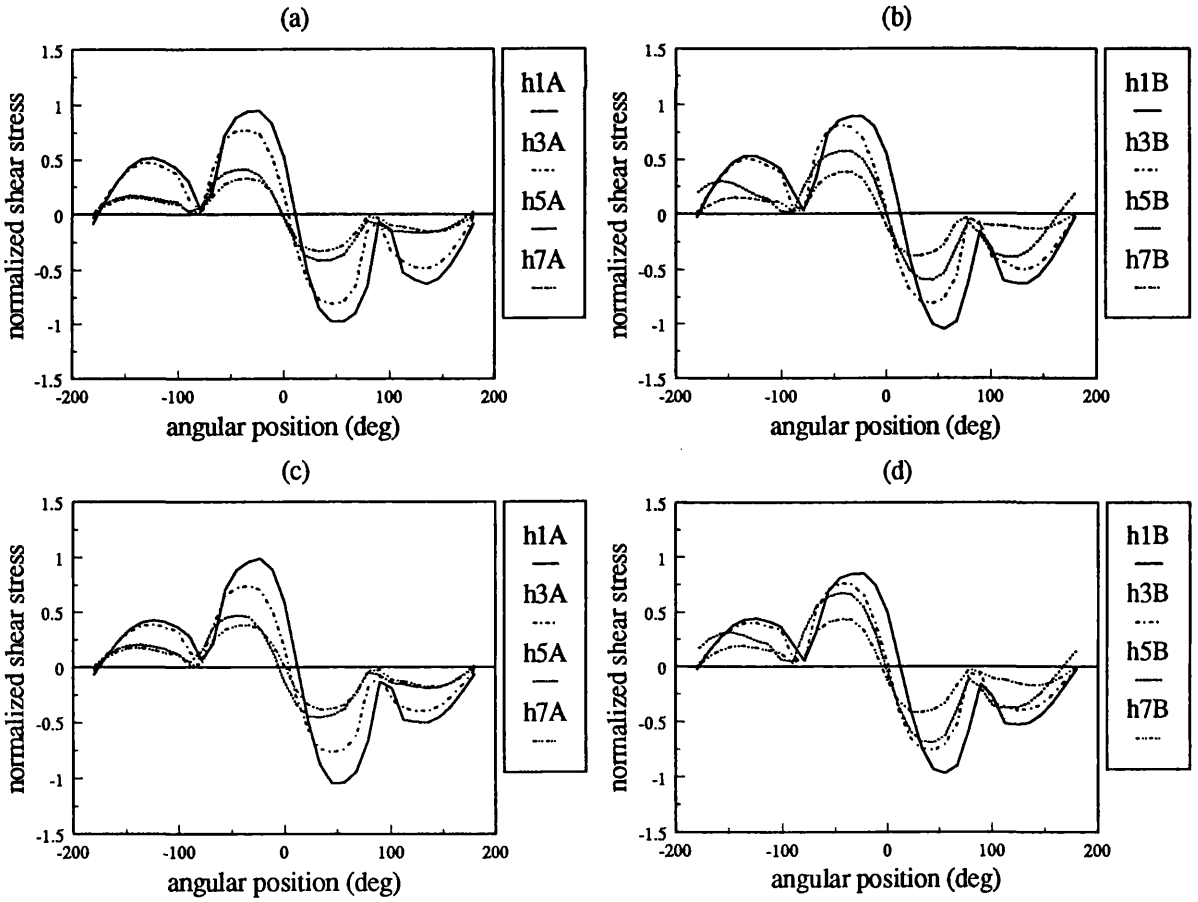


Figure 5.14 Normalized shear stress for double row, 7 pin joint configurations (a). pattern A, pitch 4*d*, (b). pattern B, pitch 4*d*, (c). pattern A, pitch 3*d* and (d). pattern B, pitch 3*d*

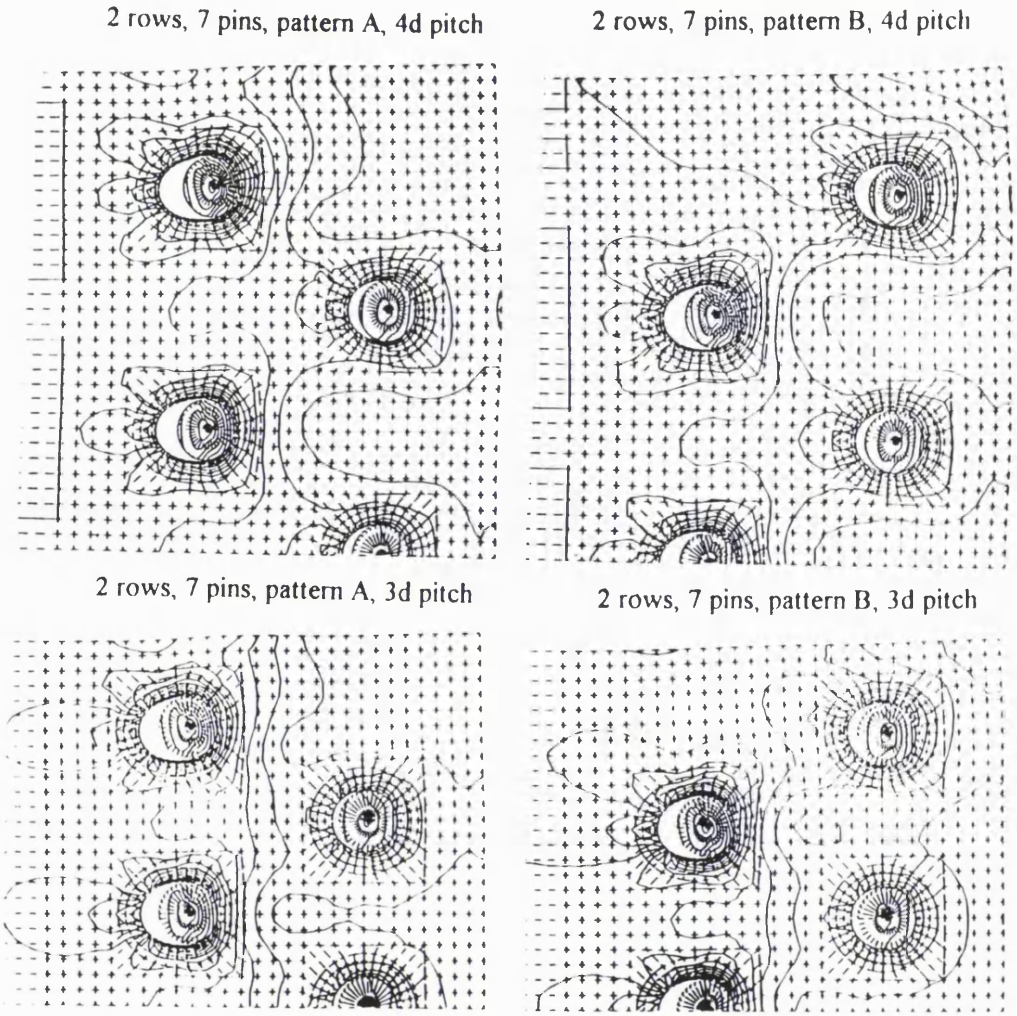


Figure 5.15 Contour plot of Von Mises stress on the deformed model for the double row 7 pin configuration

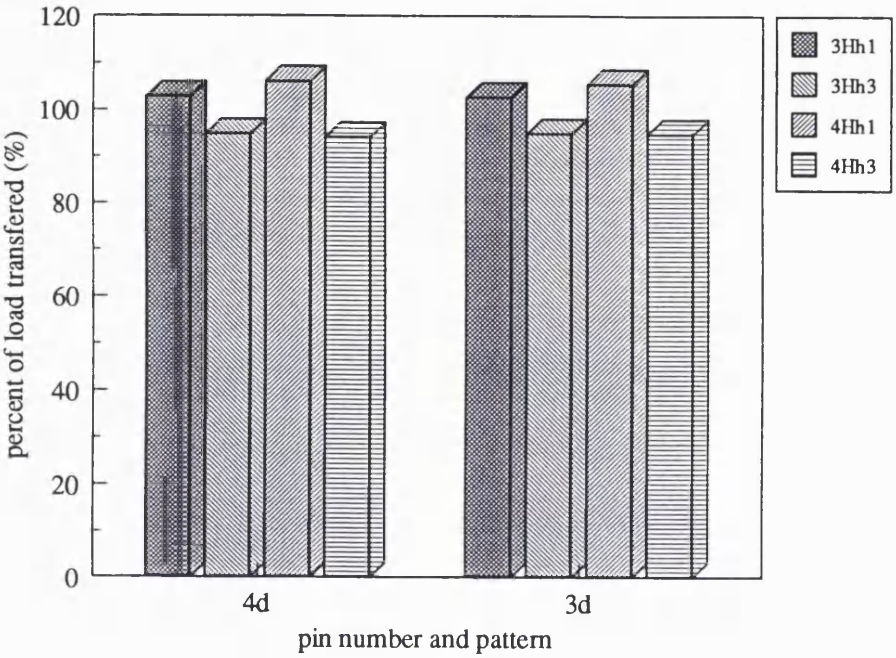


Figure 5.16 Percentage of load transfer for single row joints compared with a single pin configuration

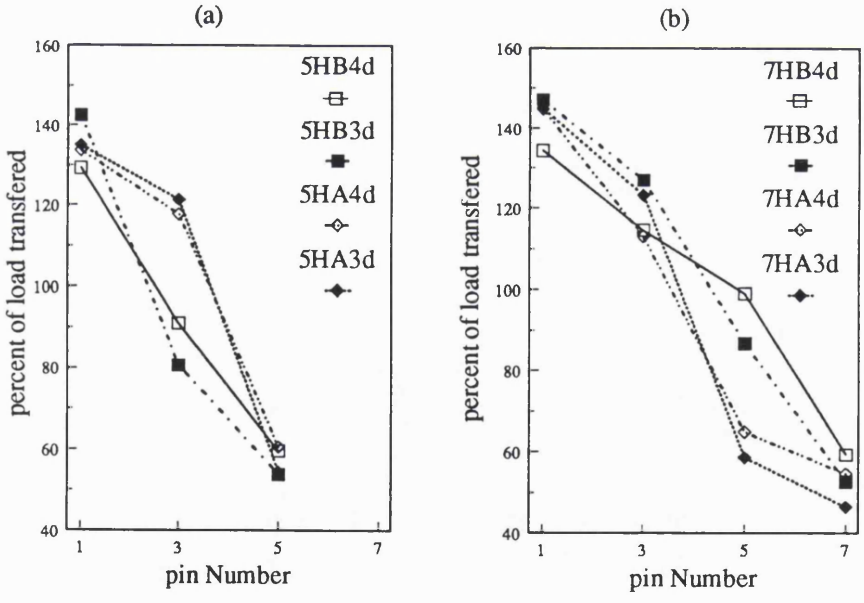


Figure 5.17 Percentage of load transfer for double row joints compared with a single pin configuration (a) 5 pin and (b) 7 pin

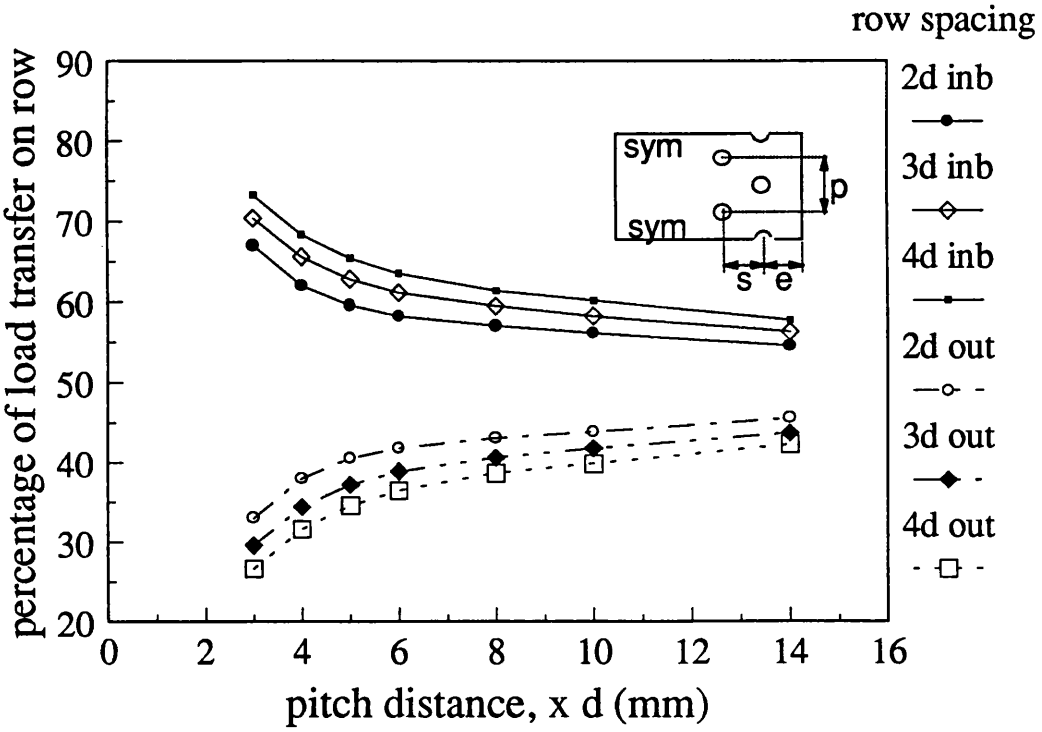


Figure 5.18 Effect of variable pitch distance and row spacing on load transferred to in board and outboard rows (constant $e = 2d$)

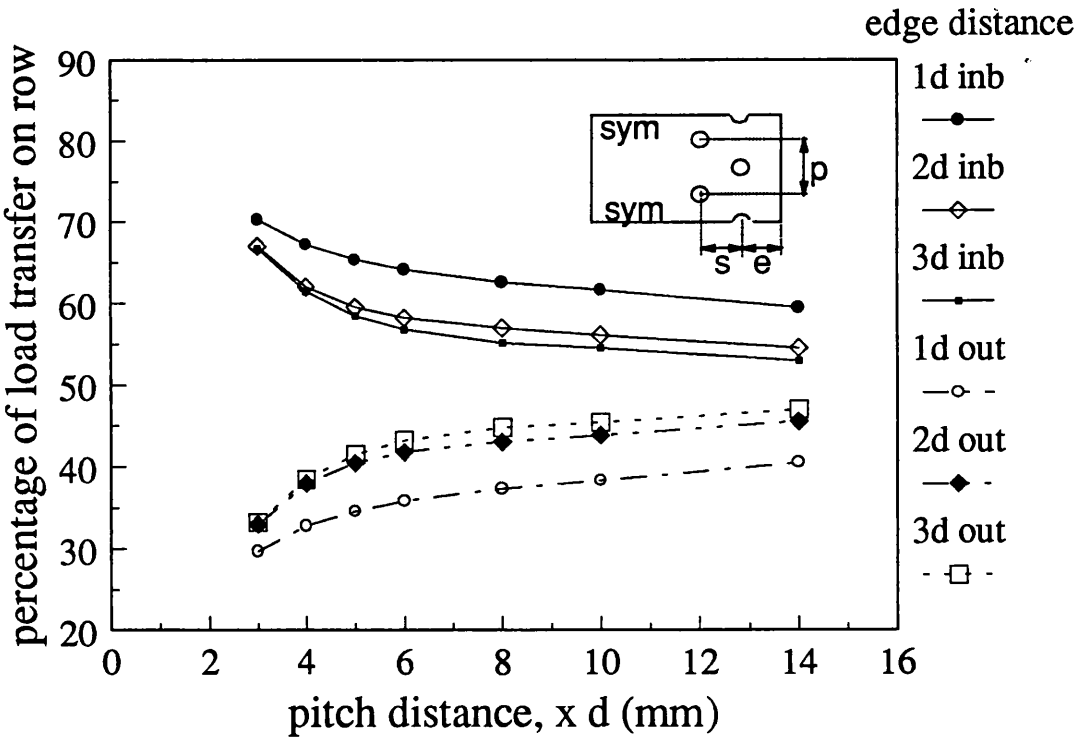


Figure 5.19 Effect of variable pitch distance and edge distance on load transferred to in board and outboard rows (constant $e = 2d$)

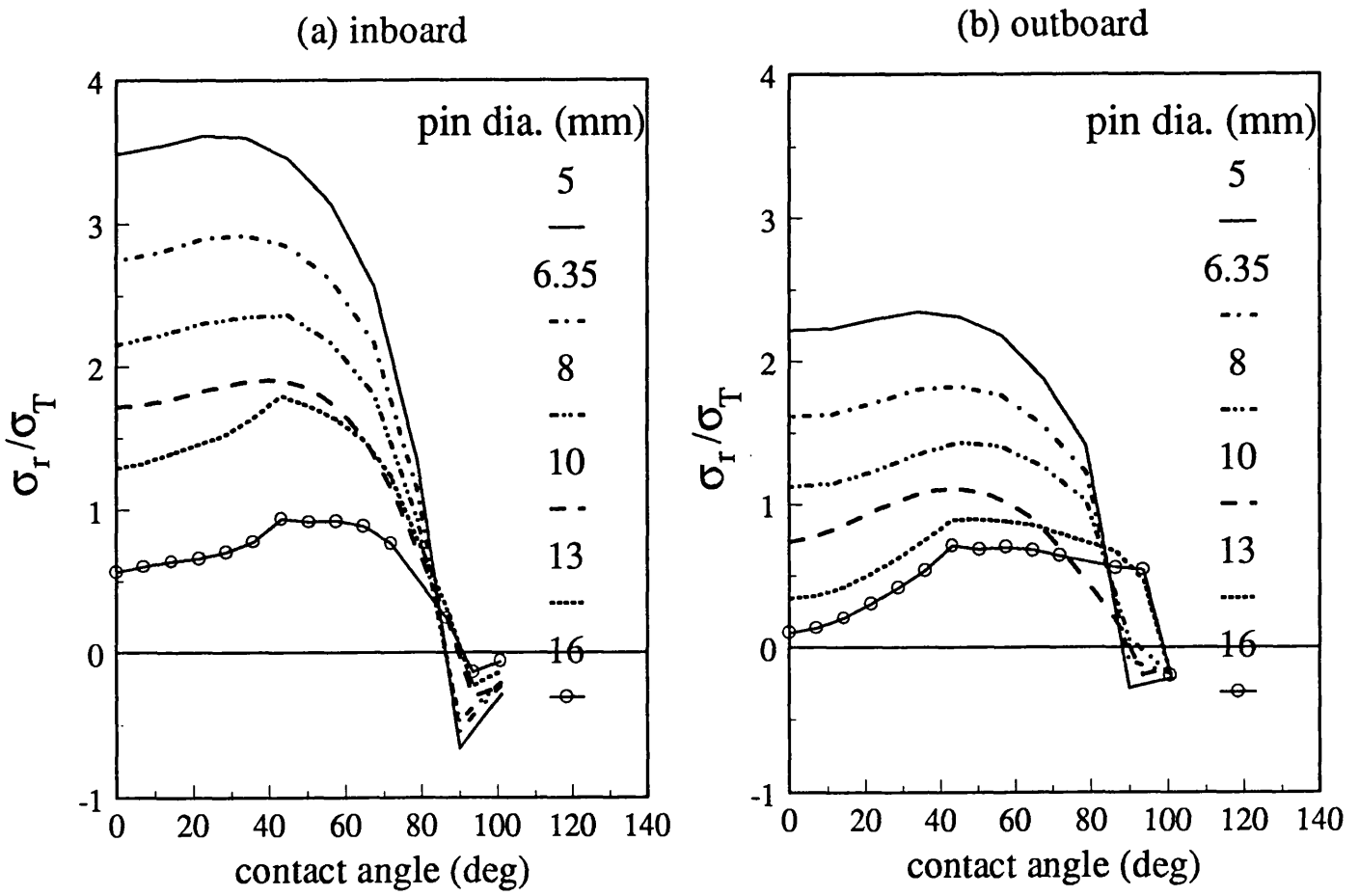


Figure 5.20 Comparison of radial stress/gross tensile stress at the hole boundary for different pin diameters

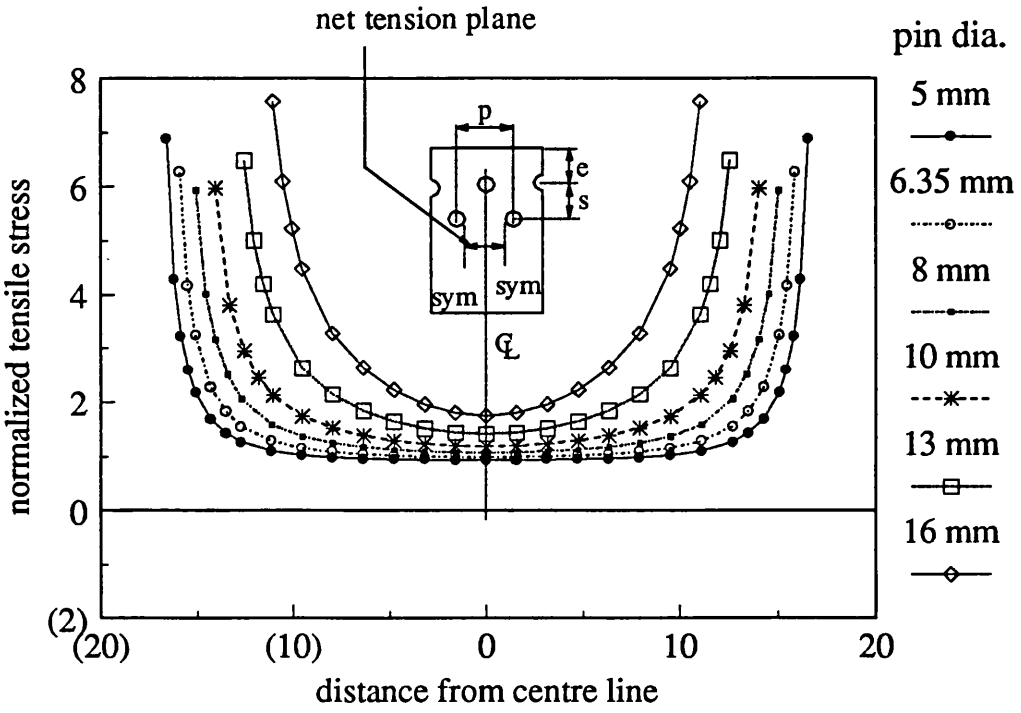


Figure 5.21 Stress distribution across net tension area on the inboard row

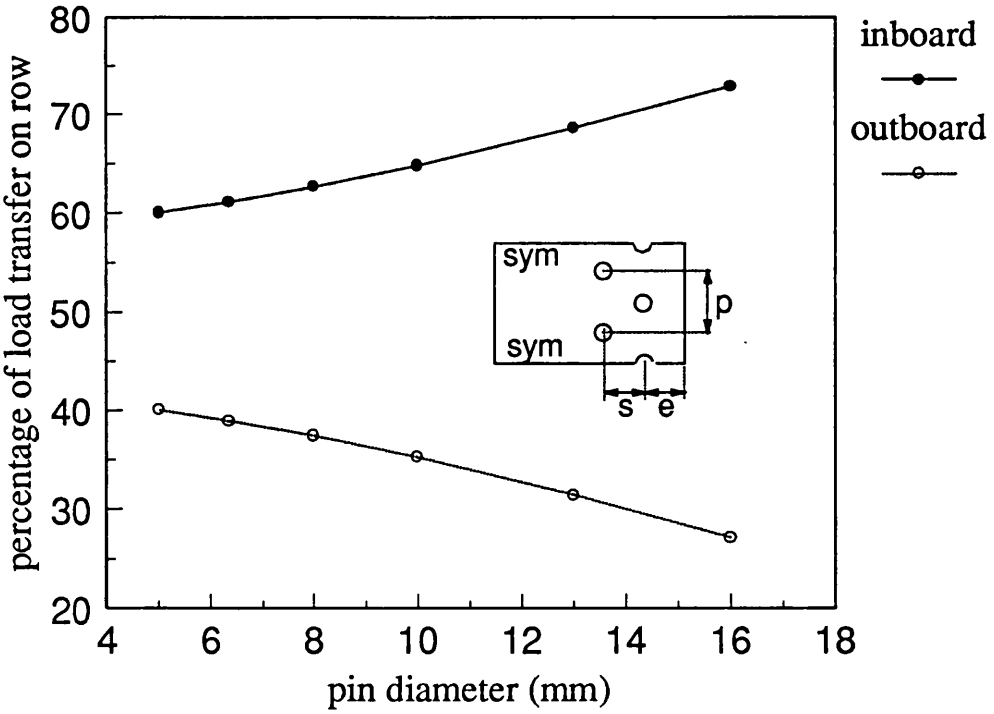


Figure 5.22 Effect of pin diameter on load transferred to inboard and outboard rows

# CHAPTER 6

# THREE-DIMENSIONAL SINGLE FASTENER MODEL

## 6.1 INTRODUCTION

Though the results obtained from the investigation using two-dimensional modelling, as described in the preceding chapter, showed reasonably good agreement with previously published experimental investigations this does, however, present certain limitations in the applicability of the analysis. The principal assumption in two dimensional modelling was that only in-plane deformation, without transverse shear and normal stresses, is considered, therefore, an accurate assessment of the true stress resultant is impossible. Consequently, suitable prediction of failure initiation, joint strength and failure mode, are also limited.

This chapter describes the validation procedure utilised for the three-dimensional modelling technique adopted in this study, by comparing the results with previously published experimental work of Marshall et al. (1989) and Smith et al. (1986). The subsequent modelling techniques were then used in the modelling of a single bolted composite laminate joint connected in a double lap configuration. The investigation was concerned especially with the effects of laminate stacking sequence, joint geometry (width, row spacing and end distance) and clamping pressure, on the stress distribution around the fastener and the percentage of load transferred through the joint. Ply failure indices were

calculated from the resultant ply stress and these were used to indicate the effect of joint geometry and clamping pressure on specific ply failure. Finally, the minimum load required to initiate first ply failure was determined.

## 6.2 METHOD OF ASSESSMENT

Mathematically there is a very straightforward development from two-dimensional shell elements to solid elements. The formulation of a three-dimensional element is a simple extension of that proposed for the two-dimensional case. However, the application of three-dimensional finite element analysis is more difficult. These difficulties arise from the complexity of constructing the three-dimensional finite element model, which results in a large matrix of equations that requires significantly more computer resource, and display capability for visualizing the results (Knight, 1993). Although the modelling is a difficult process, the technique is the only practical numerical approach that can be used to evaluate the effects of the interlaminar shear and through thickness stresses occurring in mechanically fastened composite laminates.

### 6.2.1 SINGLE LAMINATE MODEL

Many of the previous experimental investigations into the performance of double lap single-bolted joints have been specifically concerned with the behaviour of the composite inner lap, for example Marshall et al. (1989),

Hamada et al. (1995) and Cooper and Turvey (1995). This enabled finite element simulations to be performed by considering only a single laminate in contact with the bolt.

In the current study two models were developed to validate the three-dimensional modelling techniques; both consisted of a double lap composite laminate joint connected using a single bolt fastening. In the first model a thick GRP ($0_4/90_4$) laminate joined by an aluminum bolt (6061-T1) was considered, as proposed in the work by Marshall et al. (1989). The second model consisted of an eight ply thin quasi-isotropic CFRP laminate connected using a steel bolt, after Smith et al. (1986). Table 6.1 shows the mechanical properties of the materials used in this investigation. Figure 6.1 shows a representation of the physical model investigated by Marshall et al. (1989).

Table 6.1 Material properties for GRP (Marshall et al., 1989) and bolt (Chen et al., 1995)

| Material properties | $E_1$ GPa | $E_2$ GPa | $E_3$ GPa | $G_{12}$ GPa | $G_{23}$ GPa | $G_{31}$ GPa | $\nu_{12}$ | $\nu_{23}$ | $\nu_{31}$ |
|---|---|---|---|---|---|---|---|---|---|
| GRP | 31.8 | 10.2 | 7.14 | 2.14 | 2.14 | 2.14 | .328 | .199 | .045 |
| 6061-T6 | 68.3 | 68.3 | 68.3 | 25.7 | 25.7 | 25.7 | .33 | .33 | .33 |

Before undertaking the finite element analysis the findings of the cited experimental work were examined in order to anticipate the requirements of the

finite element model. Clearly, for the model represented in Figure 6.1 only the laminate-bolt contact needs to be considered and, using the symmetric plane of the joint, only a quarter of the physical model was employed in the numerical analysis. The resultant finite element model used in this study is shown in Figure 6.2.

The model consists of 480 eight-node brick elements, 32 six-node wedge elements and 27 node-to-node type gap elements, representing the laminate plate, a perfect fit bolt and interfacial boundary, respectively. In this model two layers of elements were used: one layer consisting of four plies of 0° orientation and the other of four plies oriented at 90°, with respect to the loading direction. The element material properties were calculated from the properties of each of the plies and the stacking sequence, using classical laminate plate theory, as described in Chapter 3. Adjacent nodes along the hole boundary subtended an angle of 11.25° at the centre of the hole. Node-to-node type gap elements connected coincident nodes on the bolt-laminate interface, in the first quadrant. An interfacial friction coefficient of 0.2 was used.

In addition, the effect of bolt clearance was investigated using the same model. A clearance ratio, $\lambda$ , as defined by Hayer and Klang (1984), equivalent to 0.2% was used, where:

$$\lambda = \frac{d - d_{bo}}{d} x100 \qquad (6.1)$$

and $d$ is the hole diameter, $d_{bo}$ is the bolt diameter.

The boundary conditions were selected as follows: for the first plane of symmetry, parallel to the $xy$-plane and at half the laminate thickness, for the second plane of symmetry, parallel to the $xz$-plane and coincident with the centreline of the hole. Nodes along the edge of the laminate furthest from the hole centre were considered as having a fixed displacement. A line loading range from 0 to 2.5 kN was applied at the centre of the bolt in the positive $x$ direction, parallel to the longitudinal axis of the composite laminate.

The second model, consisting of an 8-ply thin quasi-isotropic CFRP $(45/0/-45/90)_s$ laminate joined by a AISI 4130 bolt, having the material properties given in Table 6.2, was constructed for comparison with the work undertaken by Smith et al. (1986). The physical representation of this model is shown in Figure 6.3.

Table 6.2 Material properties for CFRP (Smith et al., 1986) and bolt (Chen et al., 1995)

| Material properties | $E_1$ GPa | $E_2$ GPa | $E_3$ GPa | $G_{12}$ GPa | $G_{23}$ GPa | $G_{31}$ GPa | $\nu_{12}$ | $\nu_{23}$ | $\nu_{31}$ |
|---|---|---|---|---|---|---|---|---|---|
| CFRP | 150 | 9.5 | 9.5 | 3.5 | 3.5 | 3.5 | .263 | .253 | .0167 |
| AISI 4130 | 200 | 200 | 200 | 75.8 | 75.8 | 75.8 | .32 | .32 | .32 |

In this model a CFRP laminate, 60 mm in length, 40 mm width and 2 mm thickness having a 5 mm diameter hole, and 10 mm washer, was subjected to a tensile load. The clamping pressure applied to the washer was equivalent to a bolt tightening torque of 5.6 Nm. Analysis of the experimental investigation indicated that only a finite element model representing the composite laminate inner lap was necessary for a suitable comparison to be achieved. This reduced the complexity of the model since only two deformable bodies in contact are needed. Gap elements were used to join coincident nodes on the laminate-bolt surface corresponding to the first quadrant on the circumference of the hole boundary. A perfect fit bolt was assumed in the subsequent analysis.

The planes of symmetry utilized in this analysis corresponded to an *xz* plane, along the centreline of the hole, in conjunction with an *xy* plane, at half of the laminate thickness. A quarter of the physical model was required for the three-dimensional finite element investigation which incorporated a total of 686 elements: 636 eight-node brick elements, 24 six-node wedge elements and 26 node-to-node gap elements. Elements along the hole boundary subtended an angle of 7.5° at the hole centre. Layers of elements corresponding to half the laminate thickness were used in the model. Global laminate plate properties were determined using classical laminate plate theory, as described in Chapter 3. A coefficient of friction at the laminate-bolt interface of 0.0 and 0.2 was adopted in this study.

Compressive forces ranging from 0 to 5 kN were applied to centre of the bolt in the positive $x$ direction, parallel to the longitudinal axis of the composite laminate. A clamping pressure equivalent to a bolt tightening torque of 5.6 Nm was applied to the nodal points of the plate under the washer. The nodes at the end of the laminate furthest from the bolt were ground, simulating rigid clamping at this point. A corresponding finite element model is presented in Figure 6.4.

### 6.2.2 DOUBLE LAMINATE MODEL

The benefit of a double lap mechanically fastened joint is not only that this configuration minimizes the bending of the joint due to non-coplanar loading, but also that a fraction of the load can be transferred from the inner lap directly to the outer lap, through interfacial friction at the laminate contact surface (bypass load). The latter effect arises as a consequence of bolt pre-load, which increases the normal compressive force between the plates and thereby increases the frictional force. Accordingly, the contact stress at the hole boundary, due to the load transferred via the bolt, is reduced.

This investigation was concerned with the stress distribution in a double lap joint consisting of an inner lap GRP laminate, having the material properties given in Table 6.1, fastened to an outer lap of the same material by a perfect fit aluminum bolt. A tensile load was applied at the end of composite outer lap furthest from the bolt, while the end of the inner lap was fixed. The lateral constraint, as represented by the bolt tightening torque, T, was applied to the

laminate in the form of a clamping pressure $p_w$, exerted by the washer, and is given by Stewart (1965):

$$T = kd_{bo}p_w\left(\frac{\pi}{4}(w_a^2 - d_{bo}^{\ 2})\right) \tag{6.2}$$

where $k$ is the torque coefficient equal to 0.2, $d_{bo}$ is the bolt diameter and $w_a$ is the outside diameter of the washer, which in the current study was taken as equal to $2d_{bo}$. A typical physical model for a single bolt composite laminate joined in a double lap fashion, as described is shown in Figure 6.5.

The effects of laminate stacking sequence, joint geometry and clamping pressure on the stress distribution in the joint were evaluated, as well as the effects of interfacial friction at the contact surface. The ply failure index and the onset of delamination were derived using the Azzi-Tsai-Hill theory (Azzi and Tsai, 1965) and Hashin-Rotem (1974), respectively. The first ply failure load was also determined based on the strength in the principal directions of the GRP laminate, as given in Table 6.3.

Table 6.3 Material strengths of the GRP laminate (Chen et al., 1995)

| Properties | $X$ MPa | $Y$ MPa | $S$ MPa | $R$ MPa |
|---|---|---|---|---|
| Estimated value | 60 | 60 | 60 | 60 |

$X$ and $Y$ are the laminate strength in the principal direction (1 and 2)

$S$ is the in-plane shear strength

$R$ is the interlamina shear strength

A GRP laminate outer lap, having a total thickness ($t$) of 6 mm, and an inner lap having a total thickness of 12 mm and with the stacking sequences given in Table 6.4, were adopted to examine the effect of ply orientation on the stress distribution in the vicinity of the hole boundary. Figure 6.6 shows the ply designation of the laminate used in this study. An in-plane force having a magnitude of 1 kN was applied to the extremities of each laminate, as shown in Figure 6.5. Analysis was undertaken, in the first instance, using a coefficient of friction at the contact interfaces of 0.2 and without any lateral constraint. The geometric configuration of the laminates was the same for each stacking sequence, having a width and edge distance equivalent to 6$d$.

Table 6.4 Laminate ply orientations

| Designation | ply orientation |
|---|---|
| *seq. A* | $(0/45/-45/90)_s$ |
| *seq. B* | $(45/90/0/-45)_s$ |
| *seq. C* | $(0/90/45/-45)_s$ |
| *seq. D* | $(0_2/90_2)_s$ |
| *seq. E* | $(90_2/0_2)_s$ |
| *seq. F* | unidirectional $(0_8)$ |

The quasi-isotropic laminate, $(0/45/-45/90)_s$, was subsequently utilized to evaluate the influence of joint geometry on various parameters. A constant hole

diameter, $d$, of 6.35 mm was used, while the laminate width ($w$) was varied between $3d$ and $6d$ and the edge distance between $2d$ and $6d$.

The effect of bolt tightening was also examined using this model. The bolt tightening torque was varied from 0 to 8 Nm and was represented by a uniform clamping pressure applied directly to an annulus representing the washer contact area on the outer layer of the laminate. An in-plane tensile load was applied at the ends of the outer lap, furthest from the fastening.

In the analysis fixed boundary conditions in the $y$- and $z$- directions were specified for nodes on the loaded edge, permitting displacement only in the $x$-direction. Symmetric boundary conditions were selected coincident with the $xz$-plane along the longitudinal centreline of the bolt and the $xy$-plane through the mid-plane of the double lap configuration. Further, fixed displacement boundary conditions were applied to the nodes at the end of the inner lap furthest from the hole.

A typical finite element model as used in this investigation is shown in Figure 6.7(a) and details of the model around the fastener is given in Figure 6.7(b). For this configuration, having a width and edge distance of $6d$, the model includes 1248 eight-node linear solid elements, representing a single outer lap and half thickness of the inner lap; each element having a thickness equal to the ply thickness. Thus, the eight ply laminate was represented by eight layers of elements aligned so that the specified material properties were consistent with

the ply orientation. The aluminum bolts were modelled using six-node linear solid elements, having the material properties as given in Table 6.1. The bolt nodes were constructed initially to be coincident with the laminate nodes along the hole boundary, representing a perfect fit bolt. A total of 204 six-node solid element were used to represent the bolt.

Node to node type gap elements were used to model the contact between coincident nodes of: the inner lap and the bolt in the first quadrant, the outer lap and the bolt in the second quadrant and the inner lap and outer lap contact surface. The gap elements included 202 elements between the bolt-laminate interface and 77 elements between coincident nodes of both laminates. Interfacial friction at the hole boundary between the bolt and the composite inner and outer laps was considered only in the circumferential direction, while friction at the laminate planar contact surfaces was confined to the loading direction. A coefficient of friction equal to 0.2 was adopted.

Loading was applied to the model in two steps: firstly, the clamping pressure was applied and the stiffness matrix and deformed nodal displacements computed. These values were subsequently used in the second step, the application of a 1 kN tensile in-plane load at the end of the outer lap furthest from the joint.

This model was also utilized to determine the onset and location of failure in the laminate for a fixed joint geometry and bolt pre-load, having a width and

edge distance of $6d$ and a clamping pressure equivalent to the bolt tightening torque of 4 Nm.

## 6.3 RESULTS AND DISCUSSION

The results obtained from the three-dimensional finite element analysis are given in the following section:

### 6.3.1 COMPARATIVE ASSESSMENT

Figure 6.8 shows the results obtained in this study for the load-axial strain relationship at a point on the bearing plane 10 mm from the edge of the thick GRP, $(0_4/90_4)_s$, laminate (as shown in Figure 6.1) compared with the experimental results reported by Marshall et al. (1989). The result for both cases, a perfect fit bolt and a bolt with a clearance ratio of 0.2%, show generally good agreement.

It is interesting to note that the results obtained by Marshall et al. (1989) show a non-linear load-strain relationship at very low applied loads. This may be attributed either to the influence of the bolt-hole tolerance or to the non-linear properties of the GRP. However, the numerical results shows that this may be due to the bolt clearance, since the data for this condition is closer to the slope of the experimental data than the slope of the curve representing the perfect fit bolt condition.

The strain values at points a and b on the bearing plane (Figure 6.3) obtained from the analysis of the CFRP, having a stacking sequence $(45/0/-45/0)_s$, are shown in Figure 6.9. The results indicate that the effect of considering interfacial friction is to marginally reduce the strain at these locations, for any given value of load. It should be noted that in the analytical examination a tensile strain was recorded at these locations even in the absence of an applied tensile load. This was wholly attributed to the clamping pressure exerted on an annulus of the laminate beneath the washer and accounts for the marginal difference in these results, at low load, compared with the experimental data (Smith et al., 1986).

Clearly, these results illustrate that although the laminate properties in this analysis were computed using classical laminate theory (Jones, 1975) reasonably good agreement was achieved with previously published work (Marshall et al., 1989 and Smith et al., 1986). This correlation provided the confidence to use the three-dimensional modelling technique as part of a further investigation into a more realistic analysis of joint behaviour.

### 6.3.2 DOUBLE LAMINATE MODEL RESULTS

In order to obtain a ply-by-ply failure index, the -Hill-Tsai expression (Azzi and Tsai, 1965) having the following form was used:

$$\frac{\sigma_1^2}{X^2} - \frac{\sigma_1\sigma_2}{XY} + \frac{\sigma_2^2}{Y^2} + \frac{\tau_{12}^2}{S^2} = 1 \qquad (6.1)$$

where, $\sigma_i$ = stress in the principal direction (1 and 2), $X$ and $Y$ are the laminate strengths in the principal direction 1 and 2, respectively and $S$ is the laminata shear strength. For the onset of delamination the following expression applies (Hashin and Rotem, 1974):

when $\overline{\sigma_3} > 0$

$$\left(\frac{\overline{\sigma}_3}{Y}\right)^2 + \left(\frac{\overline{\tau}_{13}}{S}\right)^2 + \left(\frac{\overline{\tau}_{23}}{R}\right)^2 = 1 \qquad (6.2a)$$

when $\overline{\sigma_3} \leq 0$

$$\left(\frac{\overline{\tau}_{13}}{S}\right)^2 + \left(\frac{\overline{\tau}_{23}}{R}\right)^2 = 1 \qquad (6.2b)$$

where 3 denotes the thickness direction and $R$ is the interlaminar shear strength.

**The effect of ply orientation**

The effect of the ply orientation on the radial contact stress at the hole boundary at various positions through the thickness, of both the outer and inner lap laminate, is shown in Figure 6.10 and Figure 6.11, respectively. In almost all of the stacking sequences investigated, with the exception of the *seq. B* and *seq. E* laminates, the maximum radial contact stress for the outer lap was recorded on the bearing plane at the laminate interface. As the angular position increases,

with respect to the bearing plane, the radial contact stress decreases continuously at this location and becomes zero at the end of the contact zone (approximately 85° in all stacking sequences). Beyond this point the radial stress becomes tensile and peaks at position on the hole boundary coincident with the net tension plane. The results for the *seq. B* are somewhat different, attaining a maximum value on the hole boundary at an angular position of 30°, which diminishes to zero at the end of the contact zone.

In contrast the orthotropic laminate of *seq. E*, $(90_2/0_2)_s$, exhibits the maximum radial contact stress at the bearing plane between layers 5A and 6A, where the fibres are aligned with the loading direction (load carrying fibres). These results suggest that the peak radial contact stress only occurs at the laminate plate interface on the bearing plane of the outer lap when the fibre orientation of the outer ply of the laminate corresponds with the loading direction.

The maximum radial contact stress for the inner lap (Figure 6.11) occurs on the bearing plane at the laminate interface for all the stacking sequences investigated. Unlike the outer lap, the maximum radial stress for the cross ply laminate of *seq. E* also occurs at this location. However, for this laminate the contact stress does not decreases continuously around the contact interface but peaks at an angular position of about 60°, before diminishing to zero at larger angular positions. It is apparent that the magnitude of the maximum radial contact stress for each stacking sequence on the inner lap is considerably higher

than the value on the outer lap. This is considered to be the effect of bolt bending caused by the peeling moment on the outer lap.

It is recognised that the radial contact stress is the predominant stress component contributing to the failure of the joint. Although prediction of the laminate strength was not performed in this particular analysis the magnitude of the radial contact stress for the cross-ply laminates (*seq. E* and *seq. D*) indicates that a fibre orientation of 90° on the outer layer would improve the joint strength. This is in agreement with an observation made in an experimental examination conducted by Marshall et al. (1989) using an identical material. Quinn and Matthews (1977) also showed that for GFRP 0°, ±45° and 90° laminates, with a stacking sequence having a 90° ply at, or near, the surface produced a higher strength than any other configuration.

The effect of laminate stacking sequence on the inter-lamina shear stress distribution on the hole boundary of the outer lap and the inner lap is shown in Figure 6.12 and 6.13, respectively. The maximum shear stress for both the outer lap and inner lap of the *seq. B*, the cross ply laminate (*seq. D* and *seq. E*) and the unidirectional laminate (*seq. F*) was recorded at the laminate plate interface. However, the maximum inter-lamina shear stress for the quasi-isotropic laminate of *seq. A* and *seq. C* was recorded at the interface between the two plies designated as 6 and 7 for *seq. A* and 5 and 6 for *seq. C*, for both the outer and inner lap. This peak stress occurs at a lamina interface where there is a 90° difference in orientation between adjacent plies. For all the ply orientations

studied, the maximum inter-lamina shear stress occurs at a similar angular position on the hole boundary and peaks at approximately 45°, with respect to the positive $x$-direction. However, the magnitude of the peak stress at any given interface for the *seq. A* and *seq. B* laminates is somewhat different. In the case of the *seq. A* the interlaminar shear stress is higher compared with the other lay-ups for low and intermediate angular positions (<60°), whereas for *seq. B* the shear stress exhibits significantly higher values at all angular positions around the hole boundary.

The percentage of load transferred via the bolt for each stacking sequence is shown in Figure 6.14. These results show that the lowest value was recorded for *seq. B*, which also exhibits the lowest maximum radial contact stress and highest maximum shear stress of all the lay-up examined. In contrast, the unidirectional laminate *seq. F*, which was shown to have the highest radial contact stress and lowest interlaminar shear stress, exhibits the highest percentage of load transferred via the bolt. The different in the percentage of load transferred via the bolt for each of the laminates shown is considered to be the consequence of different degrees of bending of the outer lap, which increases the normal contact force at the laminate plate interface. Thus, it may be inferred that for *seq. F* there is limited contact at the laminate plate interface.

The quasi-isotropic laminate, *seq. A* $(0/45/-45/90)_s$, was chosen for the second phase of this study which was concerned with determining the effects of friction and bolt pre-load on the stress distribution around the bolt interface and

failure of the laminates. This particular lay-up was chosen since it exhibited extremely high radial contact stresses compared to all of the other stacking sequences investigated.

**The effect of laminate width, edge distance and clamping pressure**

The effect of varying the joint geometry on the maximum normalised radial contact stress at the laminate plate interface, recorded by the application of an in-plane load to a quasi-isotropic inner lap and outer lap laminate with interfacial friction at the contact surfaces, is shown in Figure 6.15. The effect of varying the edge distance, as a function of hole diameter ($d$) between $2d$ and $4d$, shown in Figure 6.15a and 6.15b for the inner lap and outer lap, respectively, was to marginally increase the maximum radial contact stress at the laminate plate interface for all the laminate widths examined. However, a further increase in edge distance to $6d$ showed no significant effect on the contact stress. In contrast, the results obtained for the outer lap showed that increasing the laminate width, as a function of hole diameter, for a range in edge distances from $2d$ to $6d$ (Figure 6.15b) caused a continuous increase in the maximum radial contact stress. However, the opposite effect was observed at the top surface of the outer lap, where increasing the laminate width from $2d$ to $6d$ lowered the radial contact stress on the bearing plane, as shown in Figure 6.16. This figure presents the variation in radial contact stress at the hole boundary and through the outer lap thickness for these laminates.

Thus, the stress gradient through the outer lap thickness, on the bearing plane or close to it on the hole boundary, increases as the laminate width is increased. This is considered to arise from the excessive longitudinal bending sustained by the narrow laminate ($w$=3$d$) in comparison with a laminate of greater width ($w$=6$d$), which has a tendency to reduce the radial contact stress on the bearing plane at the laminate plate interface.

The effect of joint geometry on the maximum interlaminar shear stress which was recorded between layers 6A-7A for the outer lap and layers 6B-7B for the inner lap, at an angular position of 45° to the bearing plane, is shown in Figure 6.17a and 6.17b, respectively. The maximum interlaminar shear stress is reduced as a result of increasing the end distance from 2$d$ to 4$d$, for both the inner lap and the outer lap. A further increase in edge distance to 6$d$ has no effect on the maximum interlaminar shear stress. From these results it is clear that the interlaminar shear stress is greatest for outer lap having the smallest width, whereas the minimum value occurs in the inner lap having the largest width. Increasing the width of the outer lap has a very little effect on interlaminar shear stress at low edge distances, whereas, the converse applies in the case of the inner lap.

Figure 6.18a and 6.18b shows the normalized tensile stress at the laminate plate interface on the net tension plane for the inner and outer lap laminates, respectively. For a range of laminate widths, between 3$d$ and 6$d$, increasing the edge distance from 2$d$ to 4$d$ caused a reduction in the tensile stress for both the

inner lap and the outer lap. Increasing the edge distance beyond $4d$ has a negligible effect on the magnitude of the tensile stress. Clearly, increasing the width of the laminate lowers the net tensile stress on the net tension plane and for a given laminate width the inner lap sustains a greater tensile stress compared with the outer lap.

In summary, although a slightly higher radial stress was found for the laminate with an edge distance equivalent to $4d$ compared with $2d$, the results obtained for the variation in interlaminar shear and tensile stress indicate that a minimum edge distance of $4d$ is preferred for this type of lap joint. As a tensile failure mode in the laminate is induced by high stresses on the net tension plane an edge distance of $6d$ may be considered to be the most suitable since this give the minimum tensile stress values.

The effect of bolt pre-load on the stress distribution in a laminate having a width and edge distance of $6d$, was examined by applying a uniform lateral pressure on an annulus representing the washer contact area on the top surface of the laminate. The pressure applied was equivalent to a bolt tightening torque of 4 Nm and 8 Nm. The normalised radial contact stress distribution on the laminate surface and at each ply interface on the bolt-hole boundary, for both the inner lap and the outer lap, is given in Figure 6.19a and 6.19b, respectively. These results show that the maximum radial contact stress occurs on the bearing plane at the laminate plate interface for both the inner lap and the outer lap, and

corresponds with the observation made for the same case without the pre-loading the bolt.

However, it is quite apparent that pre-loading the bolt, by applying a tightening torque of 4 Nm, dramatically reduces the maximum radial stress on the bearing plane at the laminate plate interface of the inner lap. In contrast, the maximum radial stress at the same location for the outer lap is increased. In the case of the outer lap it interesting to note that on the top surface of the laminate the radial stress on the bearing plane is considerably higher than that obtained in the joint with no bolt pre-load. Comparing the radial stress variation on the hole boundary for both laminates shows that the stress decreases continuously with angular position at the surface of the inner lap, whereas, the stress remains constant on the top surface of the outer lap. In the latter case the radial stress peaks near an angular position of 90° with respect to the positive $x$-direction. The high radial stress at this position arises from the increased contact pressure between the laminate and the bolt as a consequence of the clamping pressure exerted by the washer, causing the hole boundary to deform in the radial direction. This effect is more pronounced in the case of highest clamping pressure, as shown in Figure 6.19b (iii), which clearly, shows that the maximum radial stress occurs at the angular position of 90° on the top surface. In this particular case the maximum radial stress at the laminate plate interface is significantly lower as a consequence of the high radial stress on the opposite surface.

These results indicate that it is essential to examine the stress distribution for both the inner lap and the outer lap to assess the full impact of bolt tightening on joint performance.

For the range of the bolt tightening torques investigated, the maximum interlaminar shear stress on the hole boundary was recorded at the interface between layers 6 and 7, at an angular position of 45°, with respect to the positive $x$-direction, for both the inner and outer lap laminates, as shown in Figure 6.20. It is interesting to note that there is a difference in orientation of 90° between adjacent plies at this position. Increasing the bolt tightening torque results in a reduction in the maximum interlaminar shear stress for both the inner lap and outer lap laminates. This is to be expected since the bolt pre-load acts to increase the interfacial pressure between adjacent plies.

Figure 6.21 shows the through thickness stress as a function of the angular position for both the outer lap (6.21a and 6.21b) and the inner lap (6.21c and 6.21d) laminates for bolt tightening torques of 4 Nm and 8 Nm. In all the cases for the outer lap the through thickness stress decreases from the top surface of the laminate towards the centre (layer 4A-5A) and exhibits a peak value on the bearing plane. This stress diminishes around the hole boundary reaching a minimum at an angular position of approximately 15° and, thereafter, increases marginally up to an angular position of approximately 90°. The variation in through thickness stresses from the centre of the laminate (layer 5A-6A) towards the joint interface exhibits minimum values at angular positions of 30° before

increasing continuously up to angular positions of 180°. At this location it is noticeable that the through thickness stress on the laminate plate interface is higher than at the other ply interfaces. This is consistent with the effect produced by bending of the outer lap which causes an additional compressive stress in the through thickness direction at this location on the hole boundary.

The through thickness stress for the inner lap (Figure 6.21c and 6.21d) shows a gradual reduction in magnitude from the laminate plate interface to the mid-plane position. The stress variation around the hole boundary for the four plies nearest to the laminate plate interface is consistent with that observed for the corresponding position in the outer lap. However, there appears to be negligible change in the interlaminar normal stress from layer 4B towards the mid-plane of the laminate at all angular positions.

The results obtained for the variation in the tensile stress along the net tension plane as a consequence of changing the clamping pressure over a range equivalent to a bolt tightening torque of 0 to 8 Nm, are given in Figure 6.22. These results show that the maximum tensile stress on the inner lap (Figure 6.22a.) at the laminate plate interface is significantly reduced as the tightening torque is increased. This is also the case at all other interfaces considered for the inner lap, however, the magnitude of the reduction is different and dependent on the position of the interface with respect to the laminate surface. This may be explained as the result of the through thickness stress contributing an additional compressive component to the tensile stress. The higher the through thickness

stress at the interface between the plies, the greater the reduction in the maximum tensile stress.

The clamping pressure on the outer lap, as shown in Figure 6.22b, exerts a significant effect on the maximum tensile stress recorded at the top surface of the laminate and results in a high compressive component on the hole boundary. In contrast, the maximum tensile stress at the laminate plate interface exhibits an increase in magnitude with increasing tightening torque. This is considered to be the effect of the bolt pre-load causing longitudinal bending of the laminate as the clamping pressure was applied.

The effect of joint geometry on the maximum radial contact stress for the inner lap and outer lap, with bolt tightening torques of 4 Nm and 8 Nm, is summarized in Figure 6.23. With the exception of the result for the outer lap having tightening torque of 8 Nm, these results are comparable with those obtained for the same joint with no bolt pre-load (Figure 6.15). The maximum radial contact stress occurs on the bearing plane at the laminate plate interface and marginally increases as the edge distance is increased from $2d$ to $4d$. This stress remains relatively constant for an increase in edge distance from $4d$ to $6d$. In the case of the outer lap subjected to the higher bolt tightening torque of 8 Nm, an increase in edge distance results in only a minor reduction in the maximum radial stress, as shown in Figure 6.23d.

Figure 6.24 presents the effect of joint geometry on the maximum inter laminar shear stress for the inner lap and outer lap, having bolt tightening torques of 4 Nm and 8 Nm. For the entire range of the geometries considered, increasing the edge distance from $2d$ to $4d$ reduced the maximum inter laminar shear stress. A further increase in the edge distance from $4d$ to $6d$ produced an insignificant change in the magnitude of this stress. The edge distance and laminate width had no effect on changing either the angular position of the maximum stress, relative to the bearing plane, or the interlaminar position on the hole boundary. Figure 6.24 also shows that for intermediate and high edge distances the maximum shear stress is reduced as the laminate width is increased.

The effect of joint geometry on the maximum tensile stress for the inner lap and outer lap subjected to bolt tightening torques of 4 Nm and 8 Nm, is shown in Figure 6.25. The trend in these results is comparable to that observed in Figure 6.24 for the maximum interlaminar shear stress.

Although not presented here the through thickness stress distribution for the inner lap and the outer lap were almost insensitive to changes in the joint geometry and only marginal changes in magnitude were recorded.

A quantitative evaluation of the deformation produced as a consequence of bolt clamping and in-plane loading of the composite outer lap, at the laminate plate interface, is shown in Figures 6.26 to 6.28. The displacement in the $z$-direction at specific longitudinal positions across the plate width has been

recorded. For all the examples shown a constant edge distance equivalent to $6d$ was adopted and the laminate width varied from $6d$, $4d$ and $3d$, as shown in Figure 6.26, 6.27 and 6.28, respectively. For each specific laminate width a bolt tightening torque of 0, 4 Nm and 8 Nm was investigated. These results show that the maximum out-of-plane displacement was recorded when no clamping pressure was applied to the laminate. In this case considerable deformation was recorded in the $+z$ direction in the vicinity of the hole boundary due to excessive bending of the bolt as a result of the applied load.

Applying a clamping pressure, equivalent to a tightening torque of 8 Nm, significantly reduced the deformation, especially near the washer and reversed the out-of-plane deflection from a positive to a negative displacement. In addition transverse bending of the laminate was also recorded. Increasing the tightening torque to 8 Nm caused greater deformation of the laminate than that sustained for the lower torque value. Clearly, for a constant clamping pressure the deformation in the z-direction was more significant for the narrower laminate and confirms an earlier hypothesis concerning the observation of the higher stress gradient in the through thickness direction for this joint configuration.

The displacement due to bending in the $z$-direction at the free edge of the outer lap, relative to the centreline of the laminate, is shown in Figure 6.29. For the narrow outer lap, having a laminate width of 3d, transverse bending causes displacement in a negative direction, with respect to the centre line of the plate,

whereas, displacement of the wider laminates is in the opposite sense; i.e. causing further separation of the laminate plate interface.

The effect of joint geometry on the percentage of load transferred via the bolt as a function of clamping pressure, is shown in Figure 6.30. As anticipated, the results for the double lap single bolt fastened joint clearly indicate that increasing the bolt tightening torque substantially reduces the percentage of load transferred via the bolt. Varying the edge distance ($2d$-$6d$) and laminate width ($3d$-$6d$) has an insignificant effect on the percentage of load transferred.

As the percentage of load transferred via the bolt is approximately inversely linearly proportional to the clamping pressure this demonstrates that the effectiveness of the joint may be readily established from an assessment of the bolt pre-load. However, the influence of the bolt pre-load on the magnitude of the various stress components in the vicinity of the bolt-hole interface, such as the radial contact stress and tensile stress, should also be considered for optimum joint design.

The ply failure and delamination indices were investigated using the stress resultant in conjunction with the failure (Azzi and Tsai , 1965) and delamination criterion (Hashin and Rotem, 1974) described earlier. The element stresses, as opposed to the average contact stresses, were used to calculate the failure indices based on the strength of GRP, as shown in Table 6.3.

Since the delamination index, as used by Hashin and Rotem (1974), is determined from the element stresses this may only be used as an indication of failure within each lamina and not the delamination at the ply interface, which is more common mode of failure. The other limitation of this analysis is that linear elastic behaviour through the thickness is assumed and hence the derived shear stress is only a first approximation to the actual value. This clearly restricts the application of this failure criterion in determining the onset of delamination and the results presented in the current study should be viewed with some scepticism.

The failure indices for elements on the hole boundary, representing the surface plies at the laminate plate interface for both the inner lap and outer lap, are shown in Figure 6.31 to 6.33. This surface was selected since stress analysis indicated that failure of the laminate could be initiated at this site. The effect of joint geometry on a single bolted double lap composite joint without bolt tightening and with tightening torques of 4 and 8 Nm, for both the inner lap and outer lap, are also shown in these figures.

In all the cases the peak failure index was recorded in the element adjacent to the bearing plane (element 1) or in the element adjacent to the net tension plane (element 6). For the inner lap laminate (a. b. and c. in Figure 6.31 to 6.33), the effect of bolt pre-load was to lower the failure indices at all the elements on the hole boundary. Increasing the edge distance results in an increase in the failure index of the element adjacent to the bearing plane whilst the failure index for the element having a mid-point at an angular position of 97.5° (element

position 6), with respect to the bearing plane, was decreased. This result is consistent with the influence of joint geometry on the maximum radial contact stress and maximum tensile stress of the inner lap, as given earlier.

The effect of increasing the clamping pressure on the outer lap laminate (d. e. and f. in Figure 6.31 to 6.33) was to lower the failure index of the element adjacent to the bearing plane. However, the opposite effect was observed for the element located at an angular position of 97.5°; increasing the edge distance was found to raise the maximum ply failure index at the site adjacent to the bearing plane for all clamping pressures applied but the peak index value for element 6 was reduced.

For elements adjacent to the bearing plane and net tension plane the change in the ply failure index as a consequence of changing the laminate width, for all the clamping pressures applied, conforms with the results obtained for the variation in the maximum radial contact stress and maximum tensile stress for the outer lap. This observation confirms that this stress parameter may be used as a first approximation in determining the location of the failure initiation site within the laminate.

Finally, it can be seen from Figure 6.31 to 6.33 that an increase in bolt tightening torque reduces the number of elements on the hole boundary having ply failure indices exceeding unity. In terms of joint performance, this confirms the benefit afforded by preloading the fasteners.

Figure 6.34 shows the onset of delamination for the elements on the hole boundary of the inner and outer lap at the laminate plate interface. In this example a laminate having a width and edge distance of $6d$ was subjected to an in-plane tensile load of 1 kN and a range of bolt tightening torques was considered. The results obtained for the inner lap with no bolt pre-load showed that the onset of delamination was most likely to occur at the element adjacent to the bearing plane, with the index falling to zero further around the interface. Pre-loading the bolt reduced the delamination index for the element adjacent to the bearing plane which remained almost constant, at a low value, around the interface. For the outer lap, shown in Figure 6.34b, the effect of increasing the bolt tightening torque was to increase the onset of delamination index for the element adjacent to the bearing plane.

Although not presented here, the variation in the delamination indicies on the hole boundary, for both the inner lap and outer lap, exhibits identical characteristics for the entire range of joint geometries and clamping pressures investigated. The relatively low magnitude of this index indicates that ply failure, as opposed to delamination, is the predominant failure mechanism for this particular double lap configuration.

The comparative assessment of the ply failure indicies on the hole boundary presented in these figures fails to account for the load shedding that occurs as a consequence of failure initiation at any given site on the hole boundary. A more suitable evaluation of the failure initiation site can be

undertaken by examining the load case when the failure index for any given element exceeds unity.

A series of trial loads were undertaken to determine the minimum value to initiate first ply failure of the laminate. In this instance a double lap laminate having a width and edge distance of 6*d* fastened with a 4 Nm bolt tightening torque was used. Figure 6.35 shows the resultant ply failure index for a range of in-plane loads from 0.6 to 0.7 kN. Clearly, a tensile in-plane load of 0.65 kN was sufficient to cause failure of the outer lap at an element position adjacent to the net tension plane. Therefore, it may be concluded that a tensile failure mode predominates for this specific joint configuration, despite the outer lap having a large width to diameter ratio.

A means of reducing the likelihood of a catastopic tensile failure on the outer lap would be to increase the laminate width. This demonstrates the overriding influence of this parameter upon the ply failure index on the net tension plane (as observed earlier in evaluating the effect of joint geometry on the failure index). In contrast, Figure 6.35 reveals that a bearing failure mode is the controlling failure criterion for the inner lap.

## 6.4 CONCLUDING REMARKS

The results obtained in this study, using the laminate properties computed from classical laminate theory (Jones, 1975), show good agreement with

previously published work (Marshall et al., 1989 and Smith et al., 1986) and, thereby, validated the modelling technique adopted in the three-dimensional finite element investigation. However, to predict the laminate failure mode and evaluate the joint strength a full three-dimensional stress investigation, using ply-by-ply properties (layerwise), as shown in the previous section is required.

Three dimensional stress analysis for a range of different laminates forming the inner and outer lap of a mechanically fastened joint, connected by a single bolt without pre-loading, has shown that the maximum radial contact and interlaminar shear stresses occur on the hole boundary of the inner lap at the laminate plate interface. This has been attributed to the effect of bolt bending and interfacial friction at the laminate contact surface and the bolt-laminate interface. The location of the peak radial stress on the hole boundary was shown to be coincident with the bearing plane. For a quasi-isotropic laminate the magnitude of this stress was found to be higher than any of other laminate lay-ups considered in this investigation. The peak radial stress for the outer lap was also shown to occur on the bearing plane for all laminates except the $(45/90/0/-45)_s$ lay-up (*seq. B*) which displayed a peak value at a angular position of 30°, with respect to the bearing plane.

The peak interlaminar shear stress on the laminate plate interface of the inner lap and outer lap occurred at an angular position of 45°, with respect to the bearing plane, for all the laminates investigated. For the quasi-isotropic laminate

the maximum shear stress was recorded at the interface between layer 6B and 7B.

The effect of increasing the bolt tightening torque, up to a maximum value of 8 Nm, on the radial contact and interlaminar stresses for the quasi-isotropic laminate was to lower the peak stress at the laminate plate interface, with the exception of the through thickness stress, which shows the converse effect.

Although only an in-plane tensile load was applied to the joint significant out-of-plane displacements were recorded on the outer lap due to bending of the fastener. Applying bolt pre-load reduced the magnitude of these displacements. However, preloading the fasteners was shown to cause small transverse deflections in the laminate.

The laminate width and edge distance was shown to influence the ply and delamination failure indices and the results suggest that the laminate width should be maximized, consistent with an appraisal of the net tension stress. The optimum edge distance on the other hand was considered to be equivalent to four times the bolt diameter. Comparison of the ply and interlaminar failure indices indicated that ply failure was the predominant failure mode for the quasi-isotropic laminate and that first ply failure would occur at an angular position close to 90°, with respect to the bearing plane, on the hole boundary. The first ply failure load for the joint configuration examined in this study was 0.65 kN.

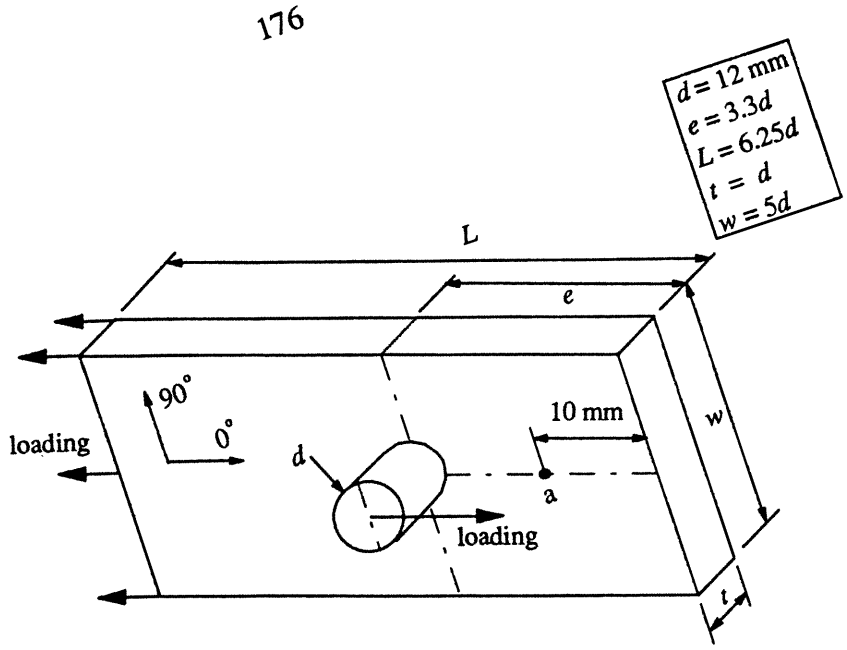


Figure 6.1 An experimental configuration of GRP $(0_4/90_4)_s$ joint, after Marshall et al. (1989)

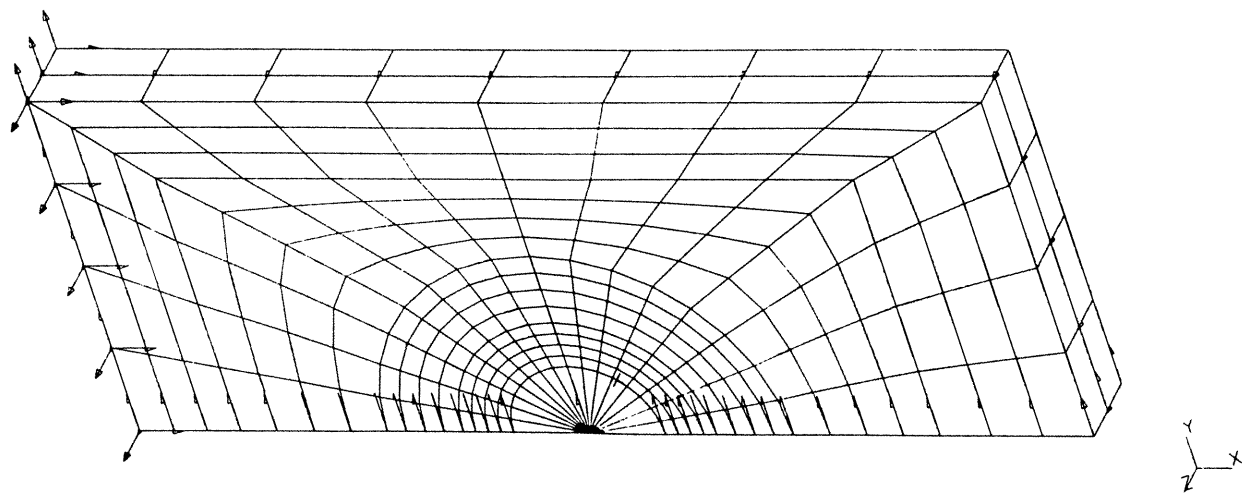


Figure 6.2 Finite element model of thick GRP laminate

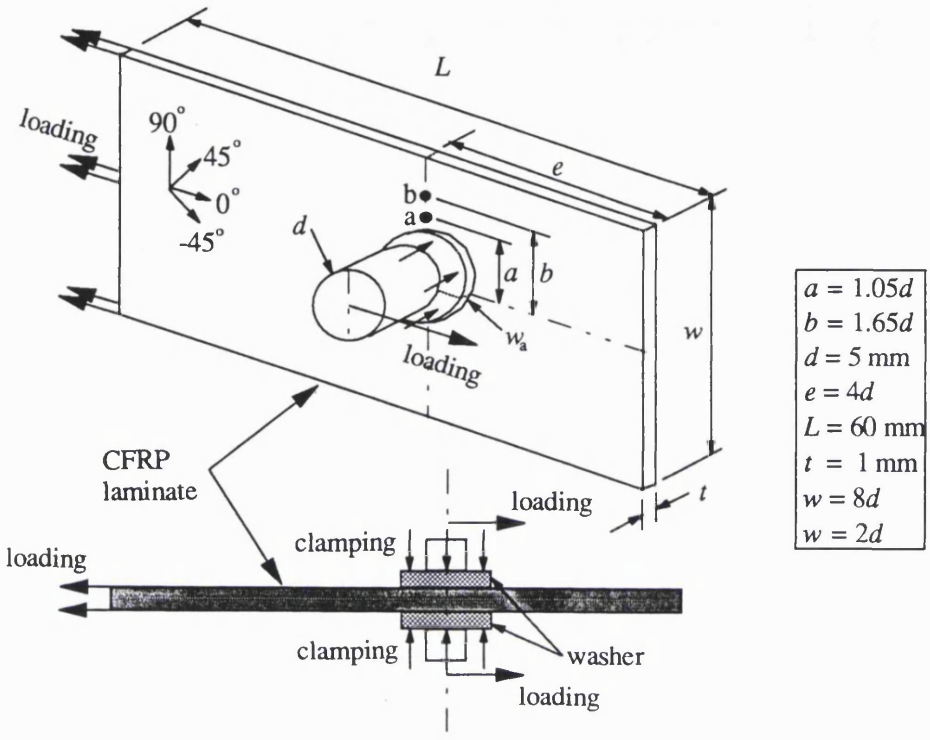


Figure 6.3 An experimental configuration of a CFRP laminate, $(45/0/-45/90)_s$ joint after Smith et al. (1986)

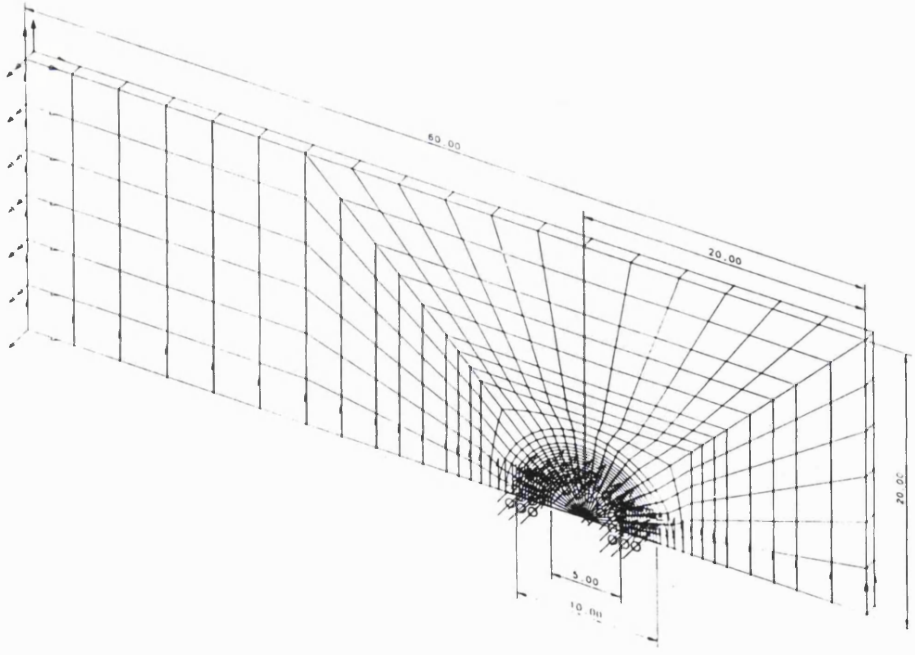

Figure 6.4 Finite element model for CFRP laminate of $(45/0/-45/90)_s$

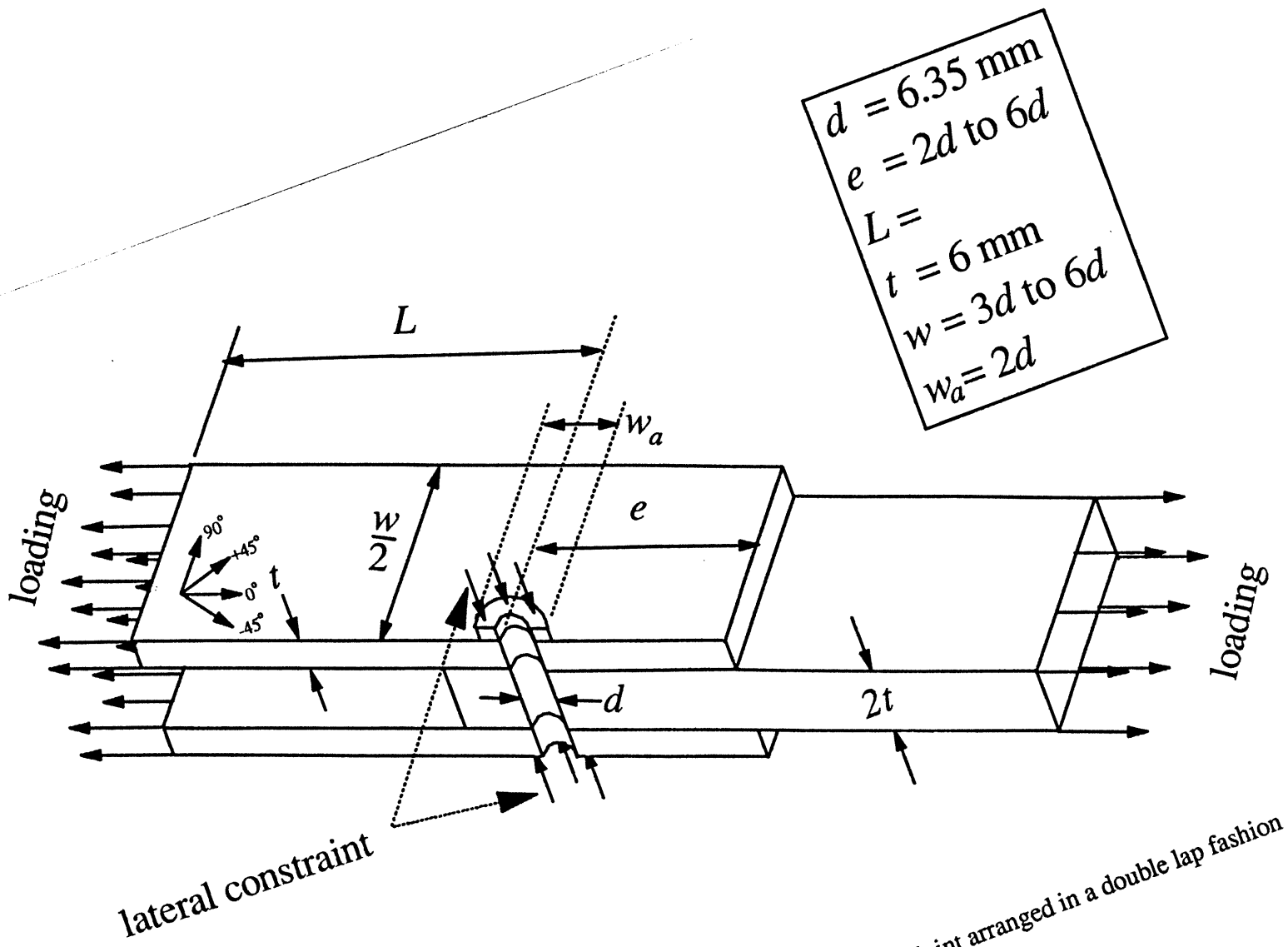


Figure 6.5. Physical model of a single bolt composite laminate joint arranged in a double lap fashion

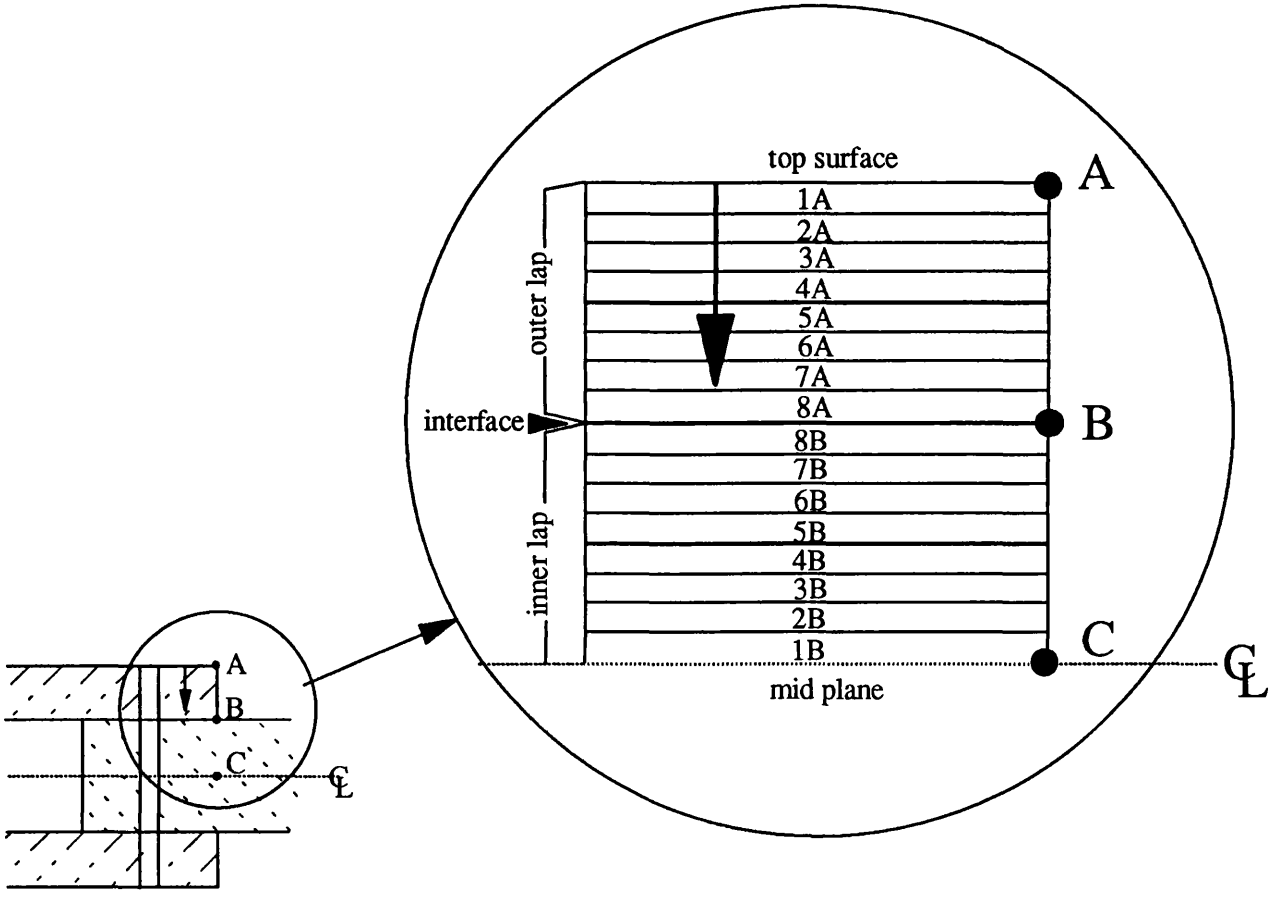


Figure 6.6. Lay-up designation of composite laminate used in this investigation

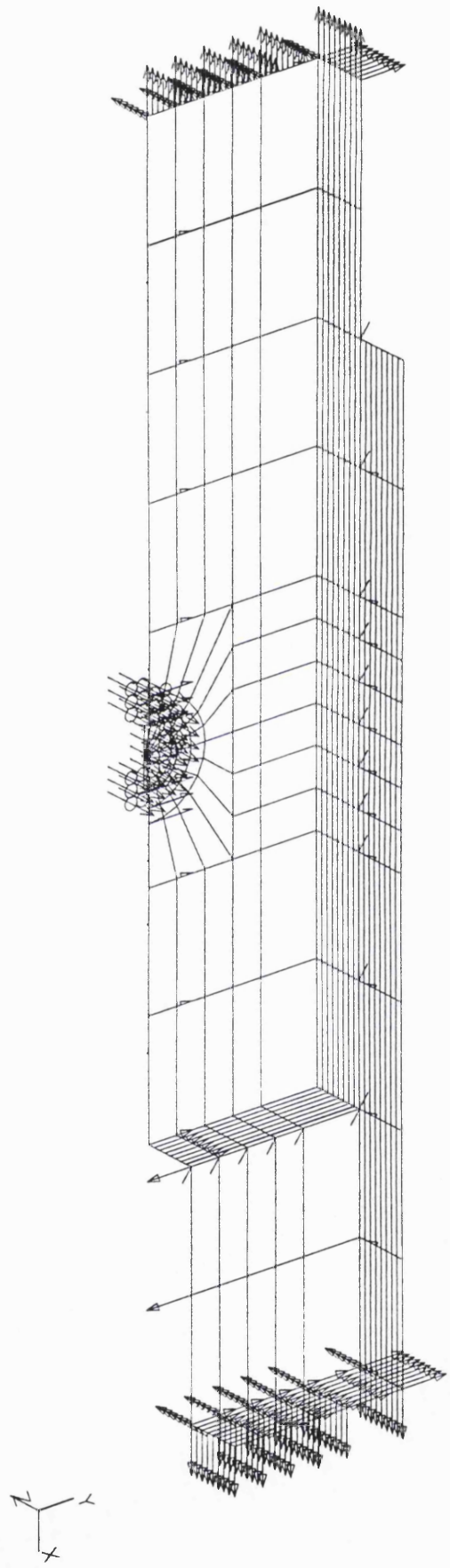


Fig 6.7a. Finite element model of double lap joint

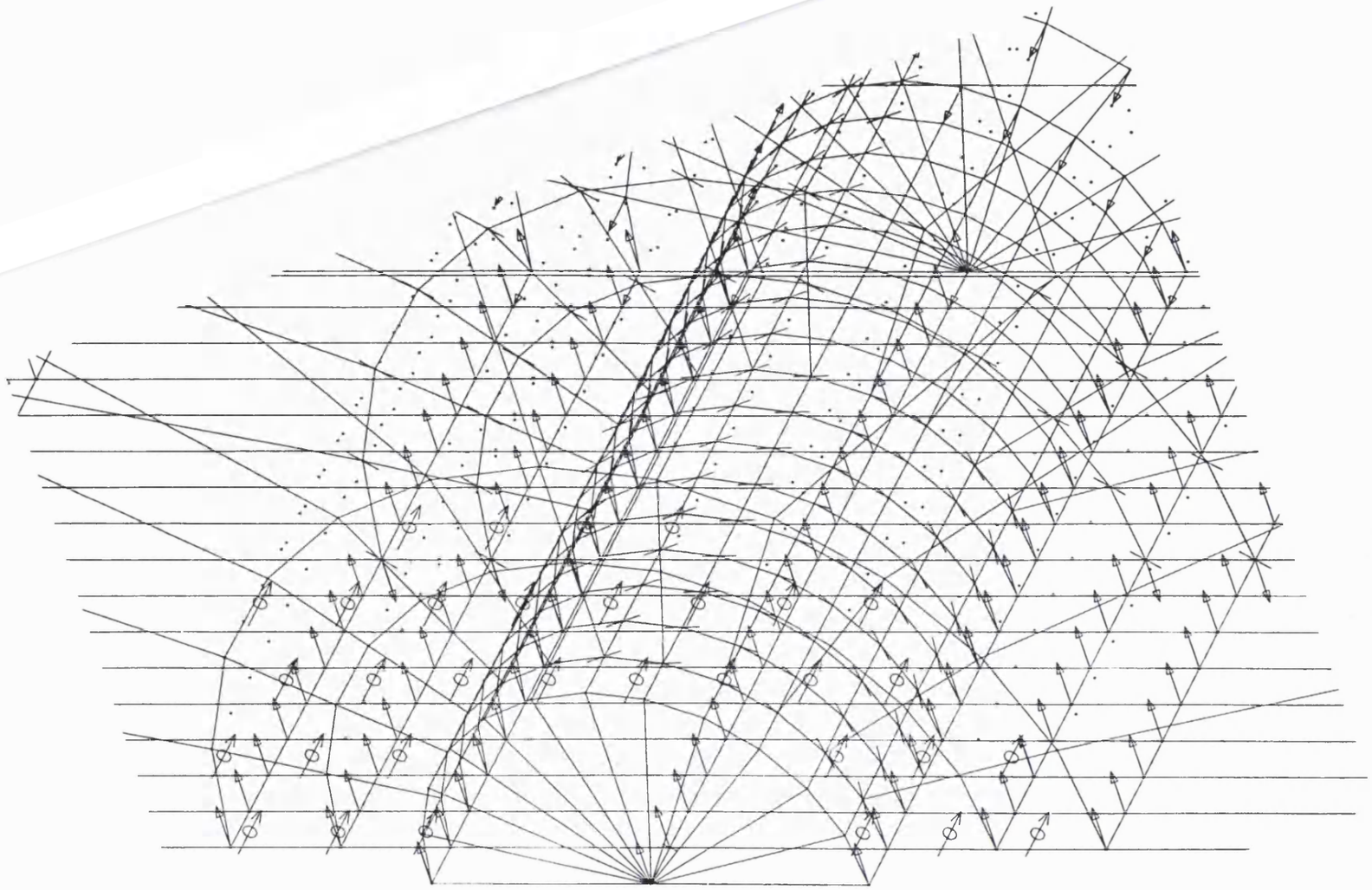

Fig 6.7b. Detail of finite element model at the bolt-laminate interface

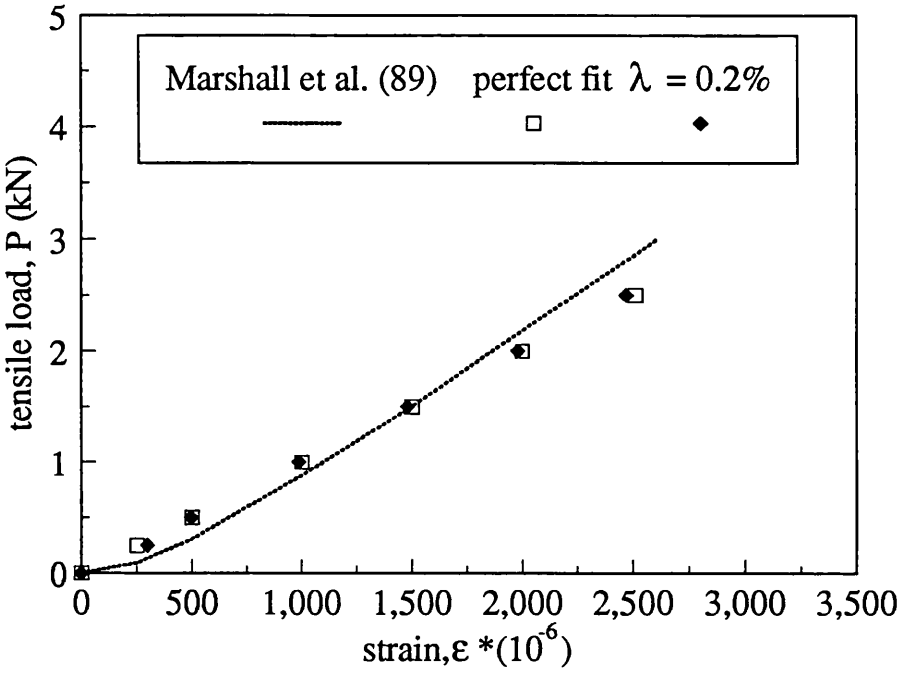


Figure 6.8 Comparison of axial strain (point a) on the bearing plane for GRP ($0_4/90_4$) with Marshall et al. (1989)

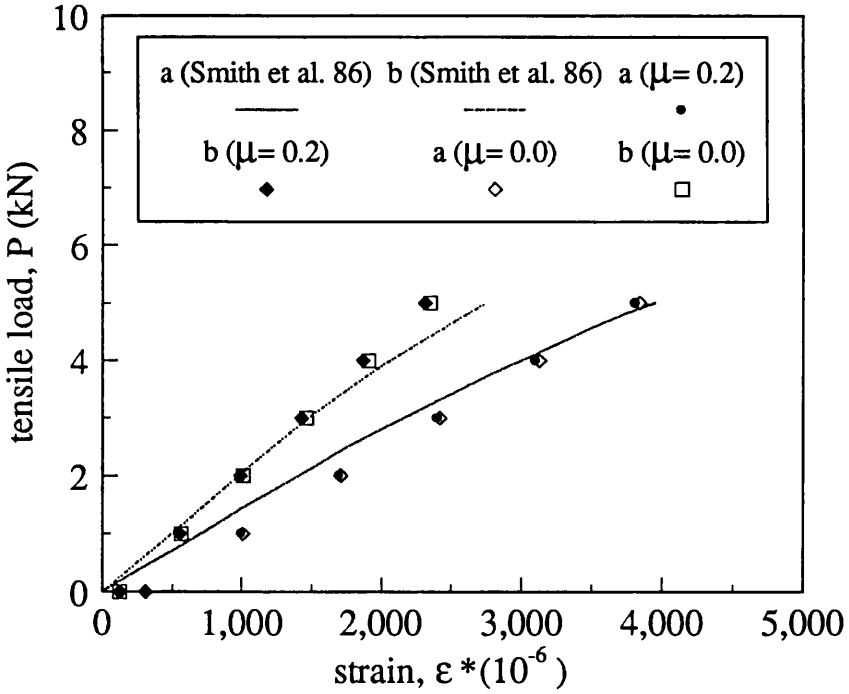


Figure 6.9 Relation between load and strain at point a and b for CFRP $(45/0/-45/90)_s$ compared with Smith et al. (1986)

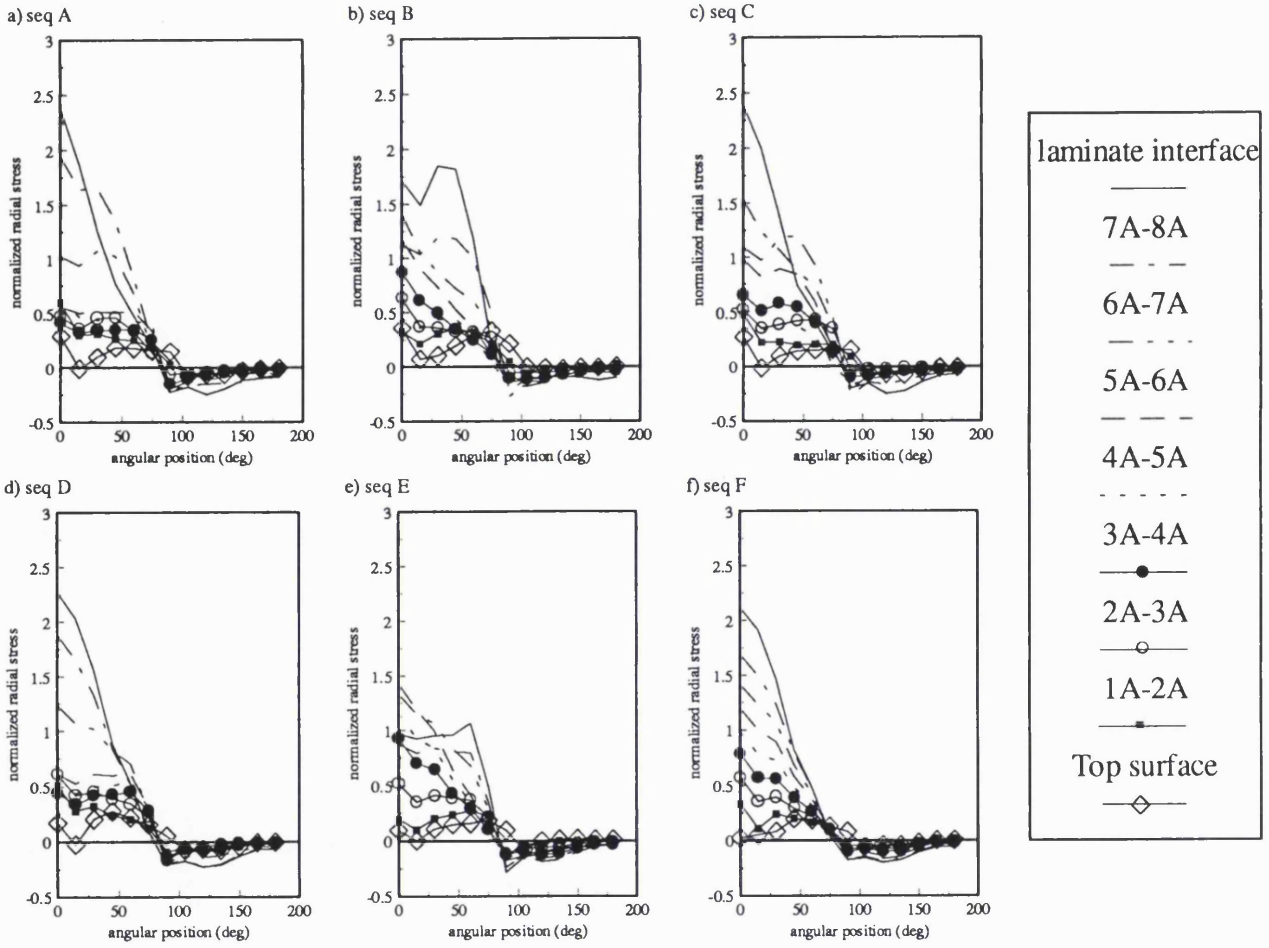


Figure 6.10 The effect of laminate stacking sequence on the normalized radial stress distribution of the outer lap

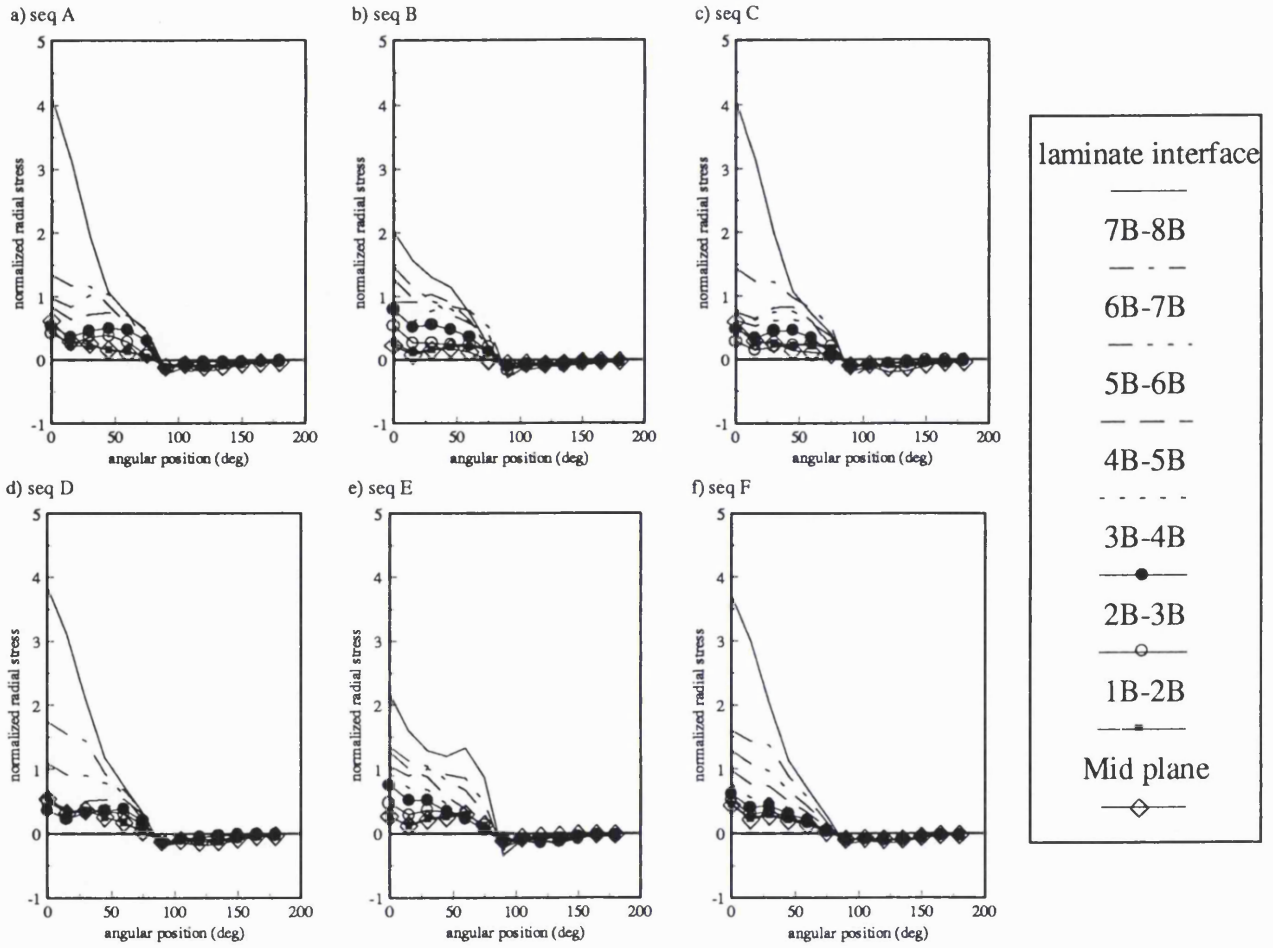


Figure 6.11 The effect of laminate stacking sequence on the normalized radial stress distribution of the inner lap

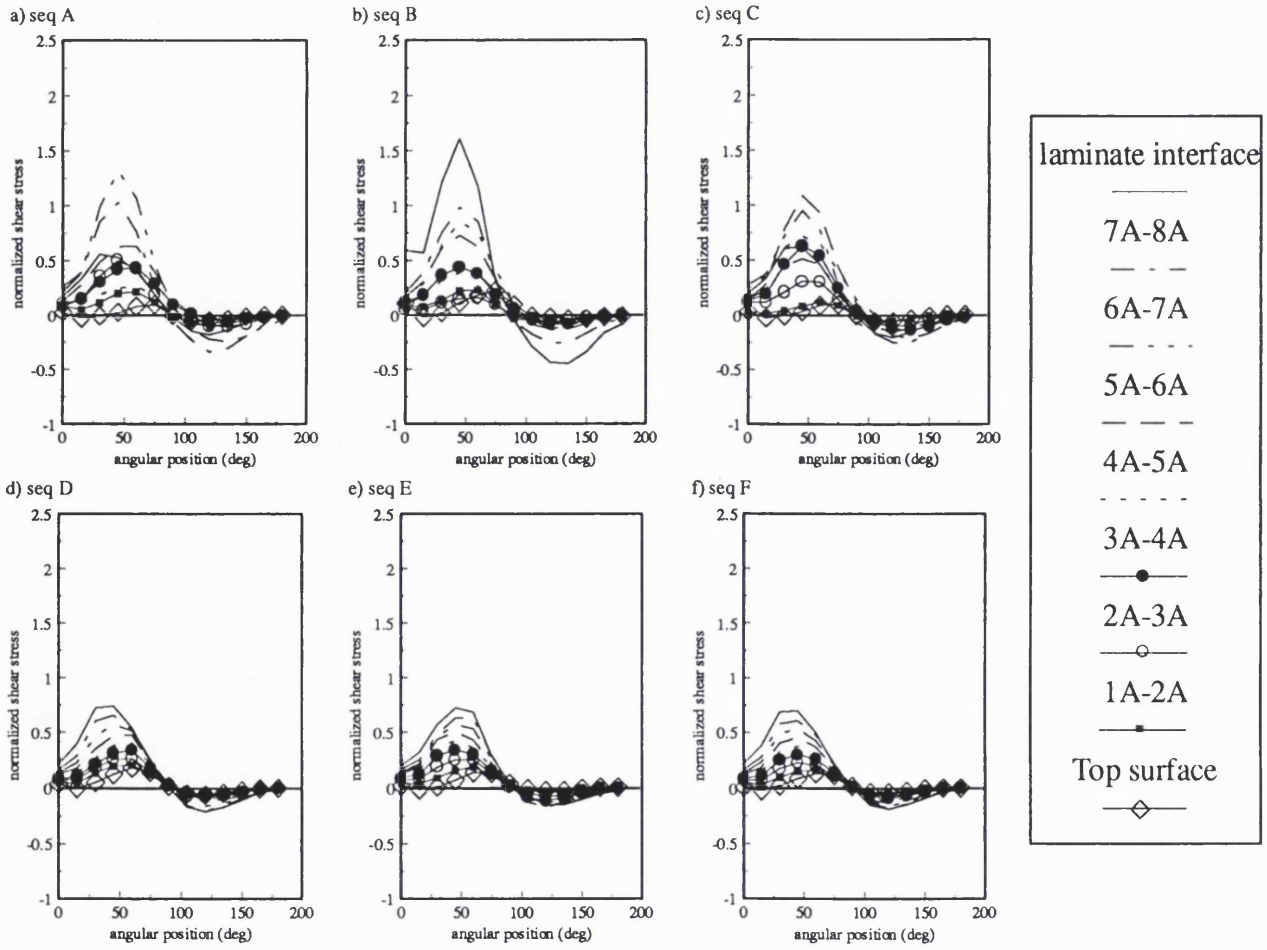


Figure 6.12 The effect of laminate stacking sequence on the normalized shear stress distribution of the outer lap

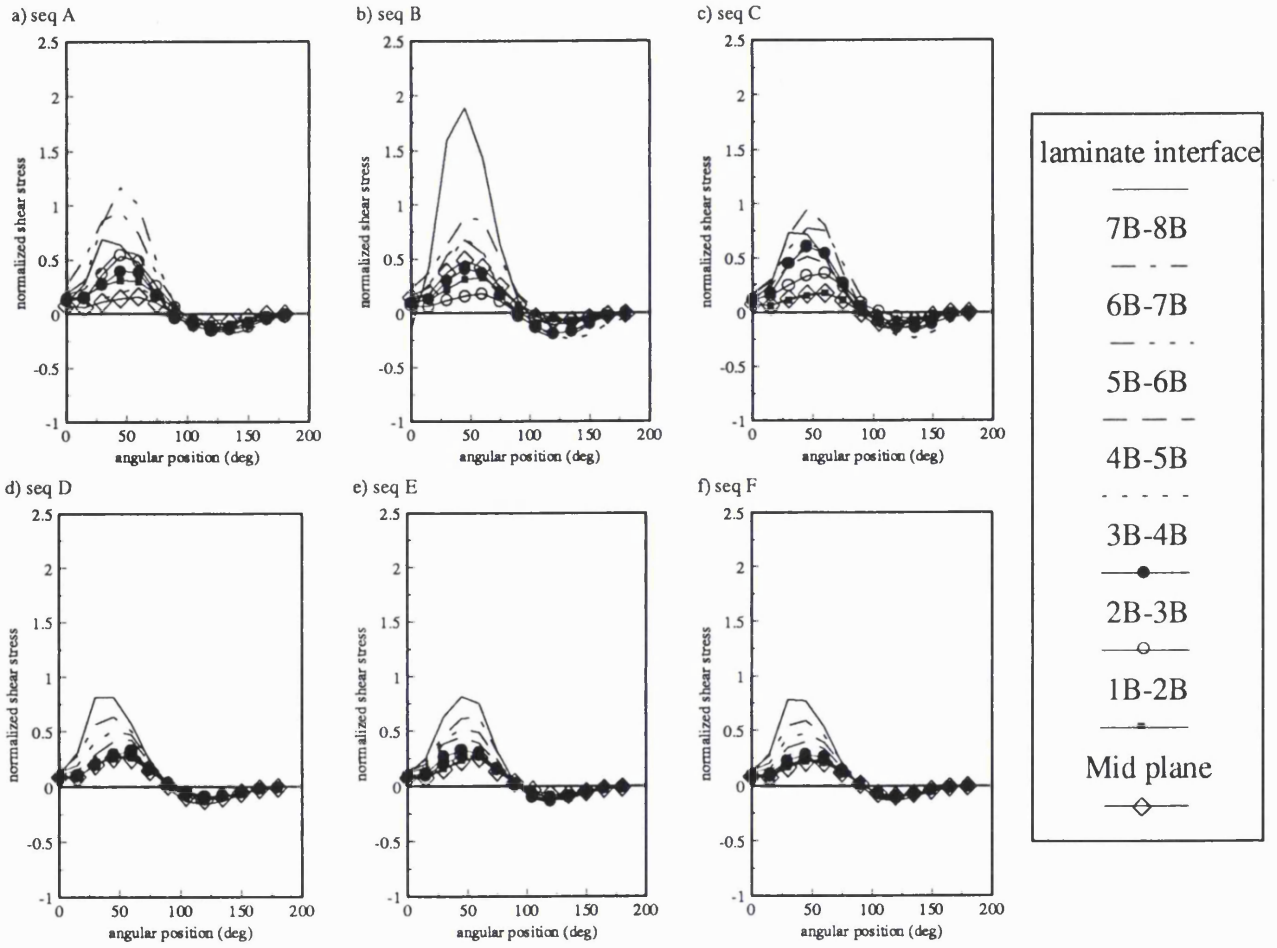


Figure 6.13 The effect of laminate stacking sequence on the normalized shear stress distribution of the inner lap

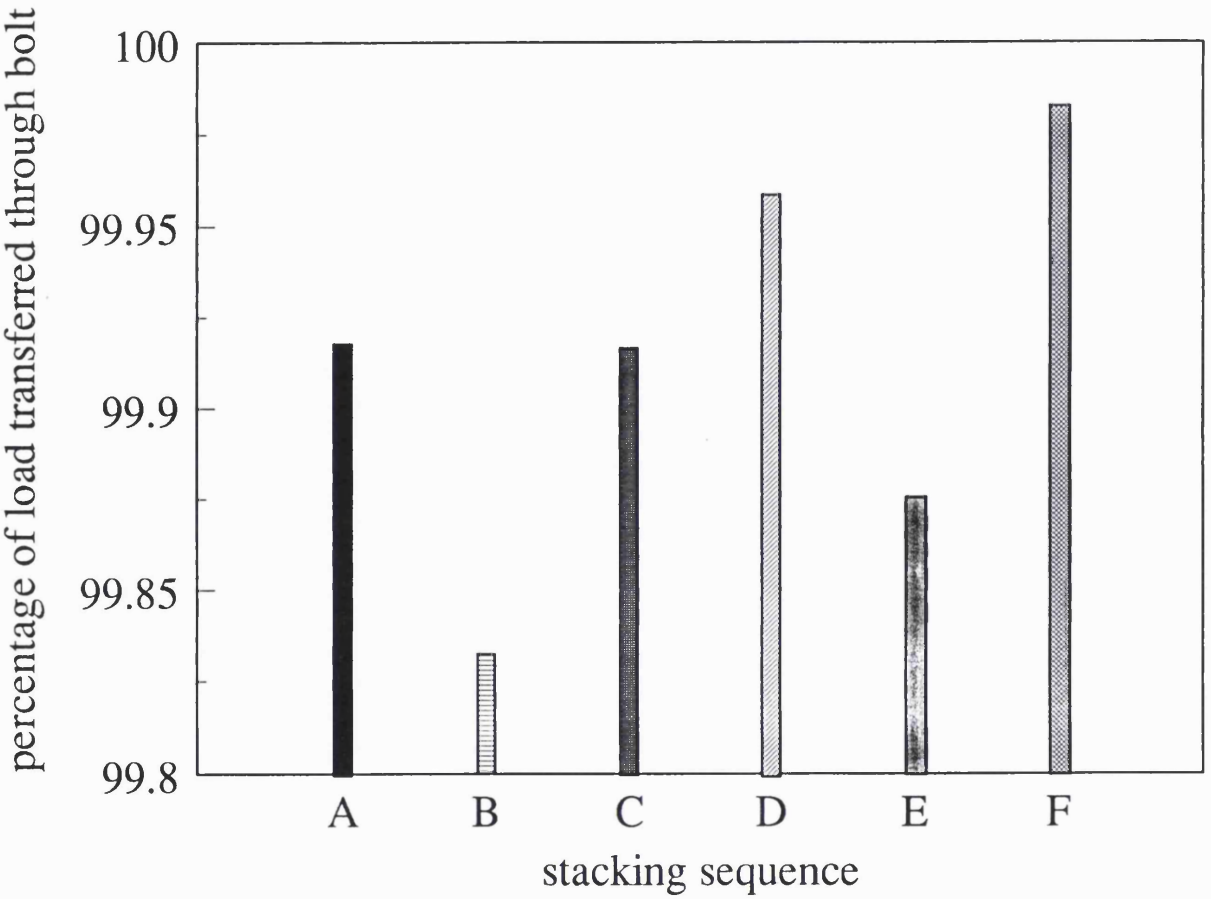


Figure 6.14 Percentage of load transferred through the bolt for different stacking sequences

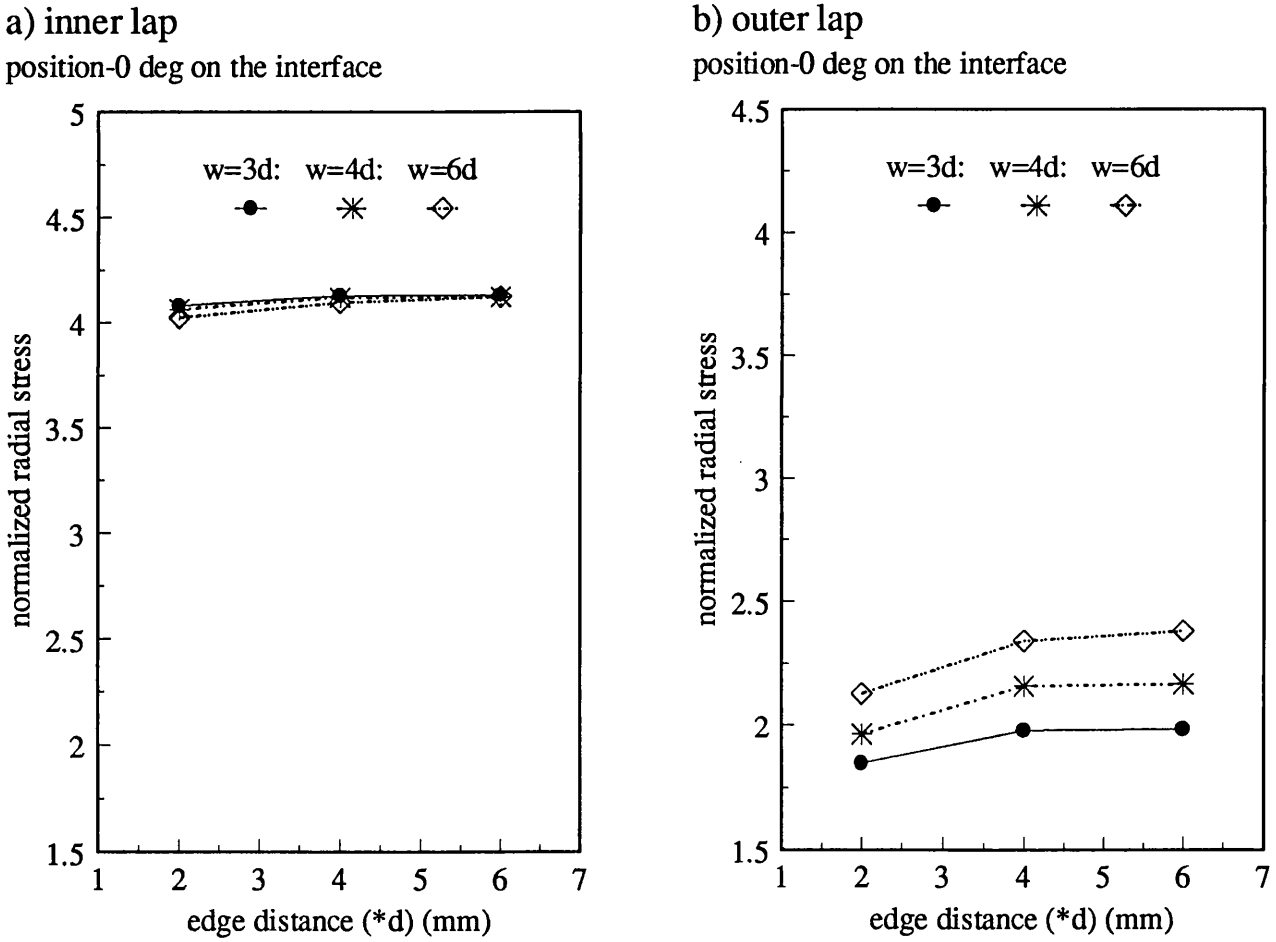


Figure 6.15 Effect of laminate width and edge distance on normalized radial stress

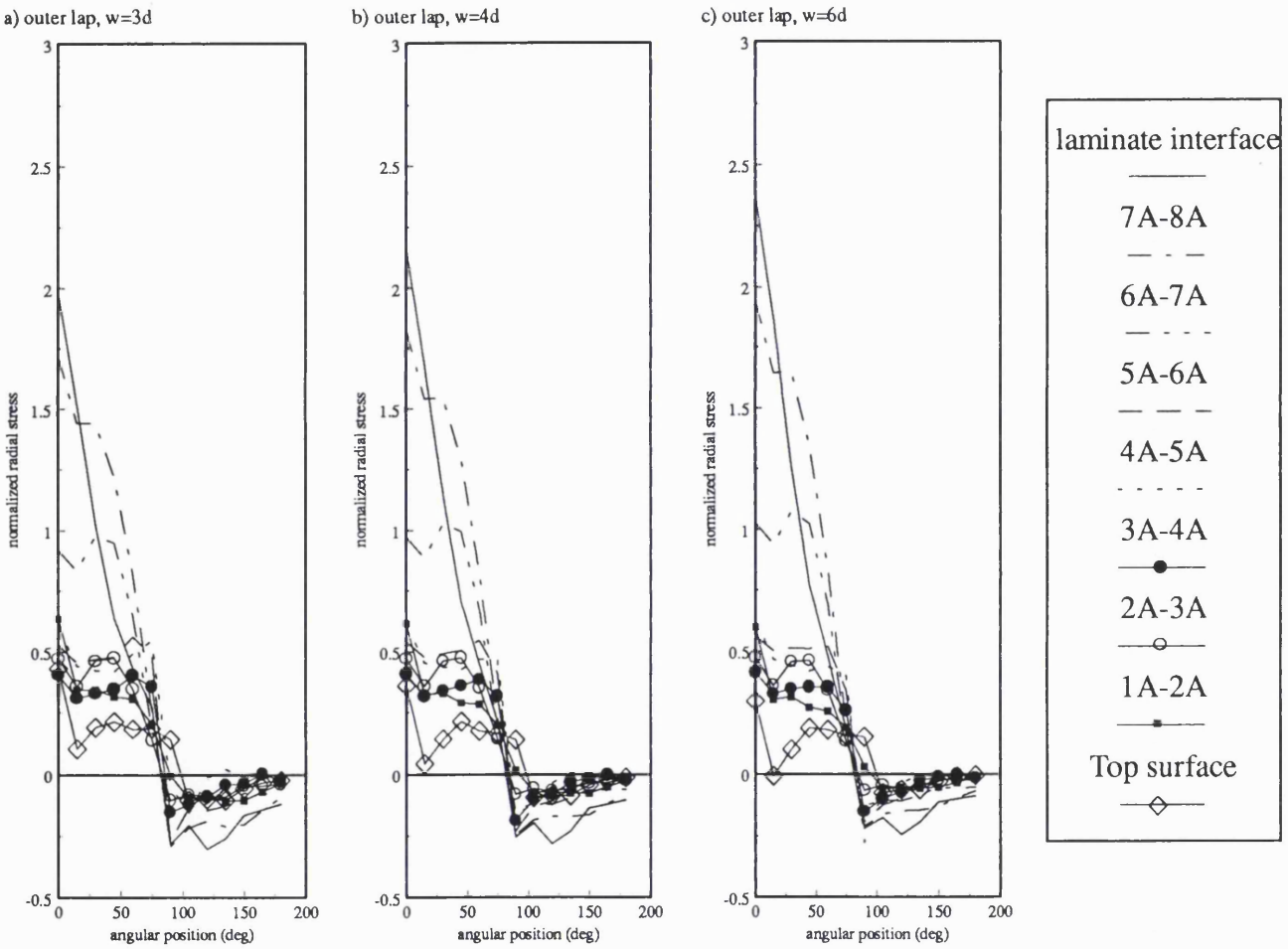


Figure 6.16 Normalized radial contact stress through the thickness of the outer lap laminate without bolt tightening torque

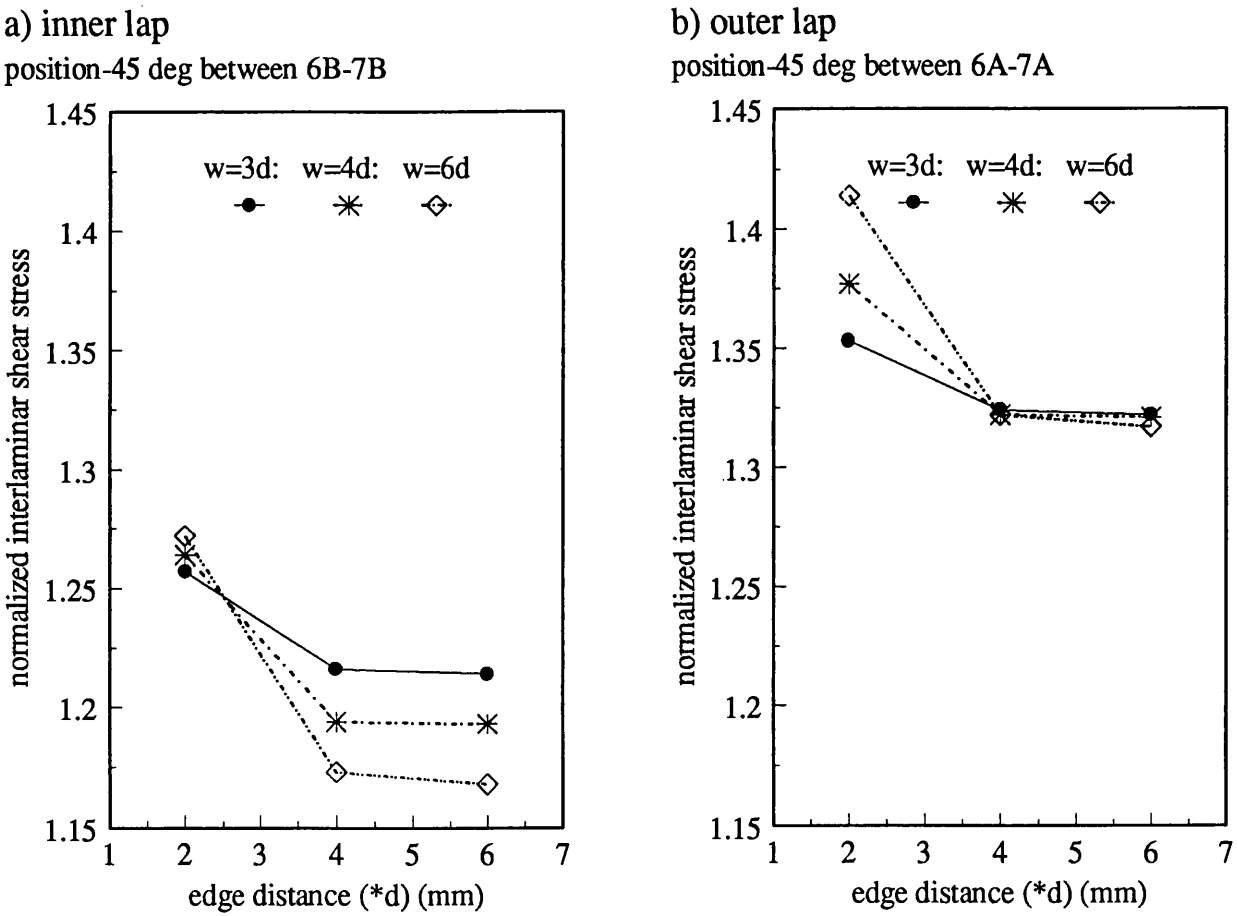


Figure 6.17 The effect of laminate width and edge distance on normalized interlaminar shear stress

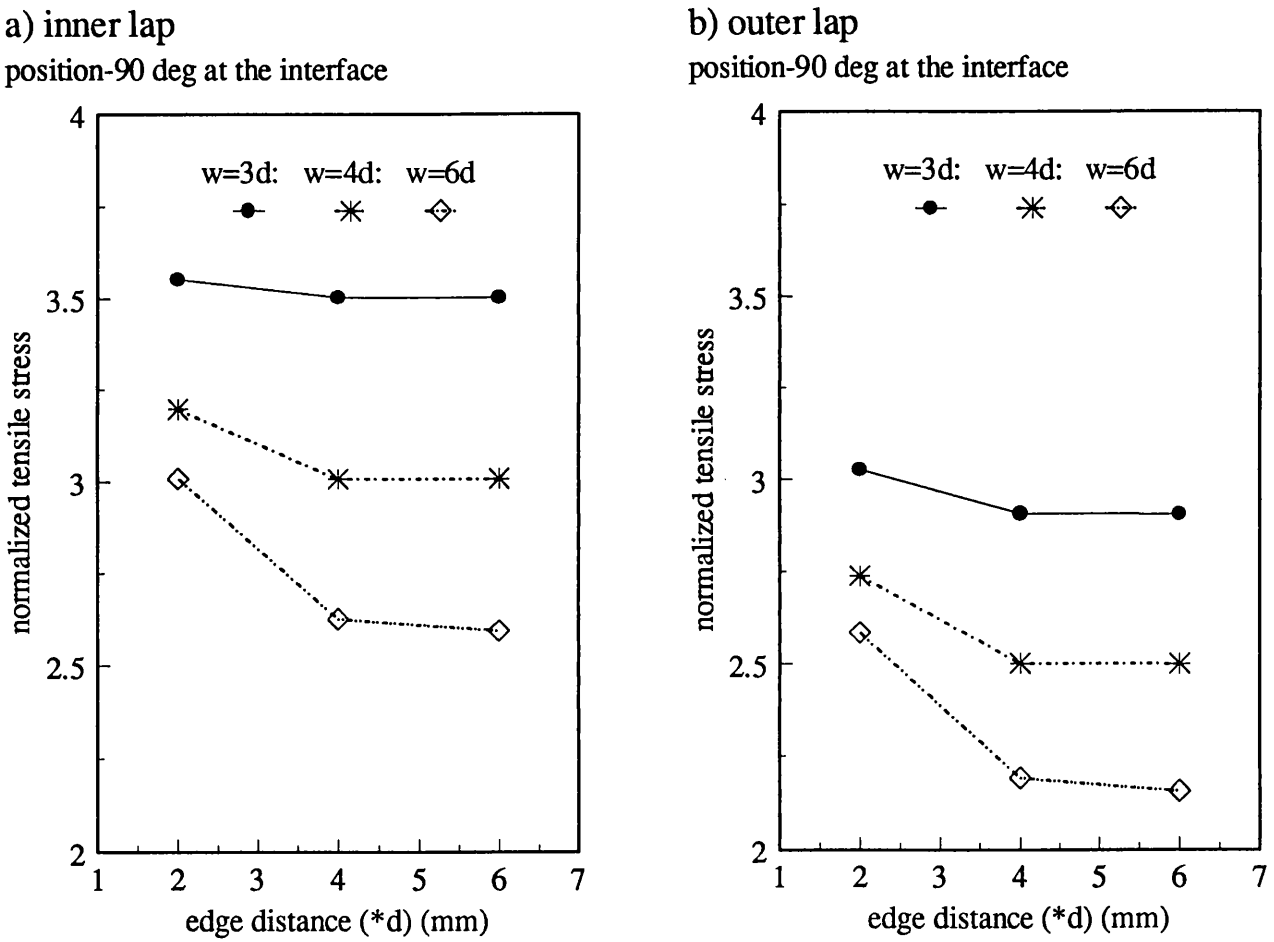


Figure 6.18 The effect of laminate width and edge distance on the normalized tensile stress on the net tension plane

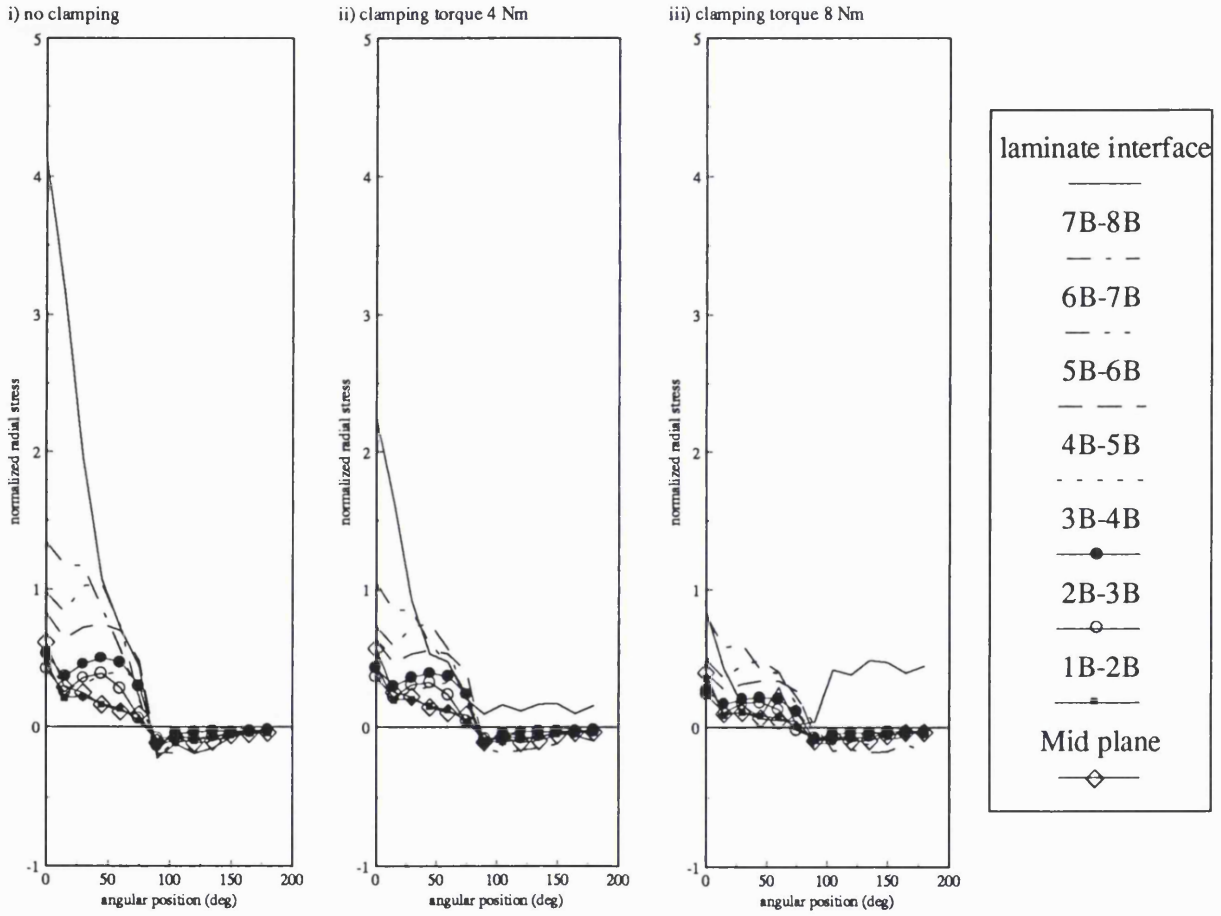


Figure 6.19a. Normalized radial contact stress on the hole boundary in the through thickness direction of the inner lap(i, ii and iii), for a range of bolt tightening torques

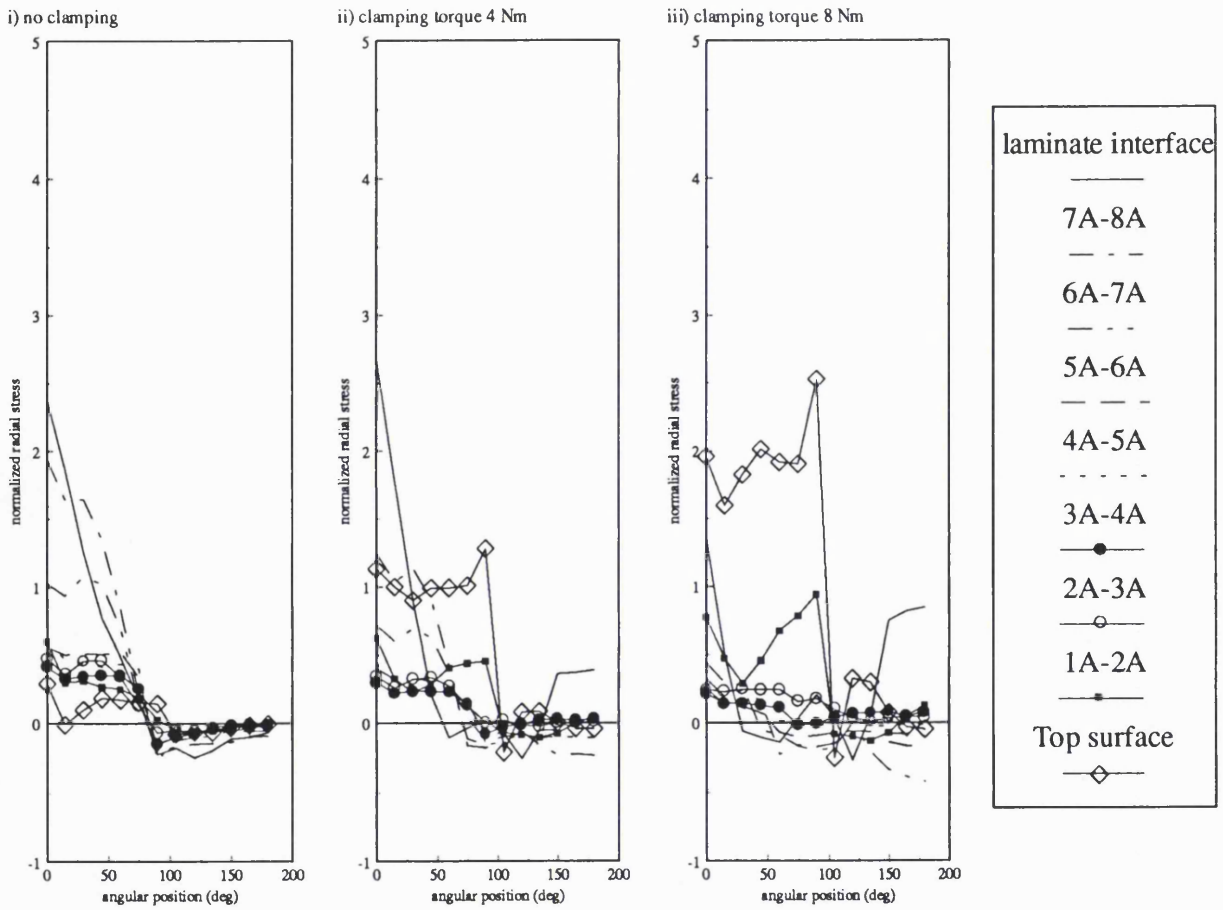


Figure 6.19b. Normalized radial contact stress on the hole boundary in the through thickness direction of the outer lap, (i, ii and iii) for a range of bolt tightening torques

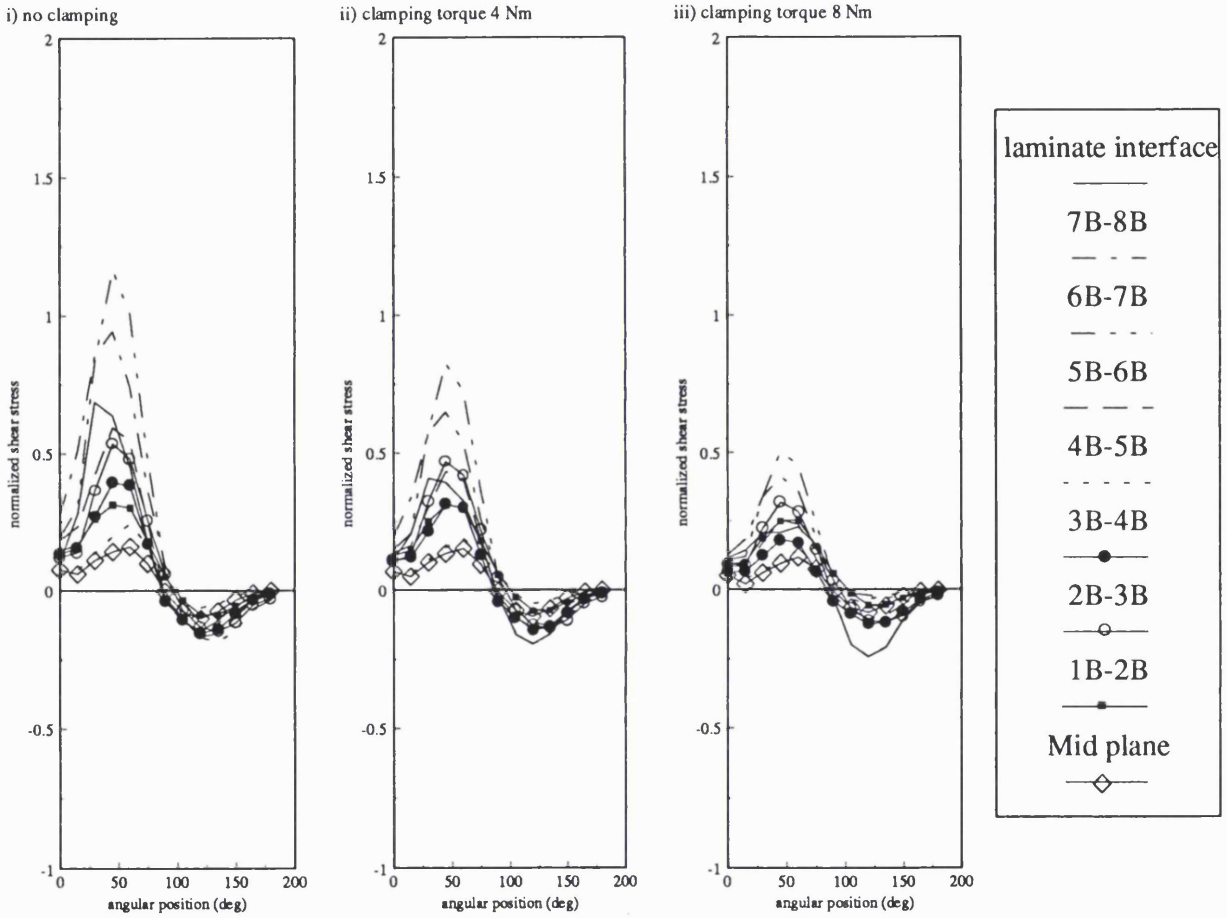


Figure 6.20a. Normalized interlaminar shear stress on the hole boundary in the through thickness direction of the inner lap for a range of bolt tightening torques

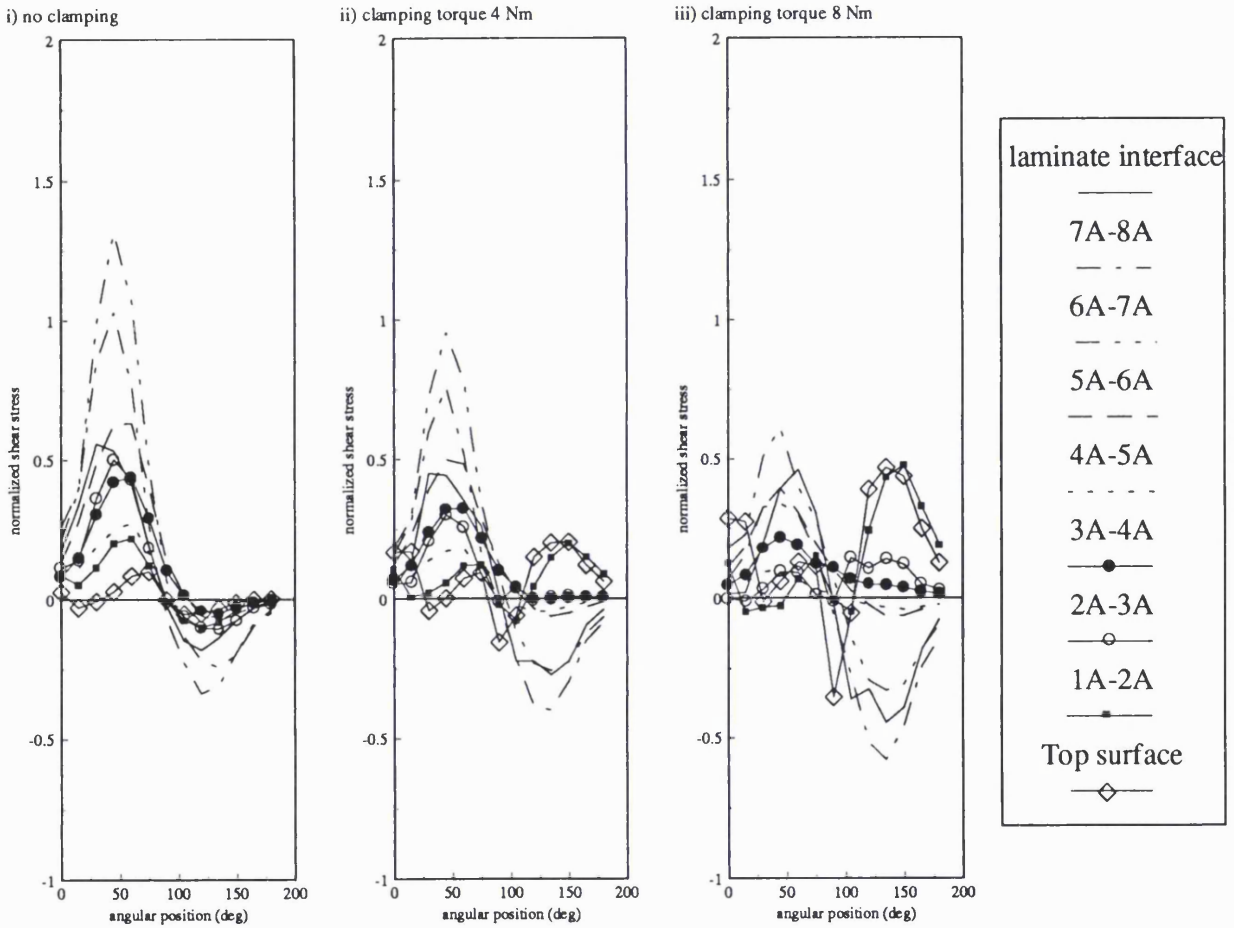


Figure 6.20b. Normalized interlaminar shear stress on the hole boundary in the through thickness direction of the outer lap for a range of bolt tightening torques

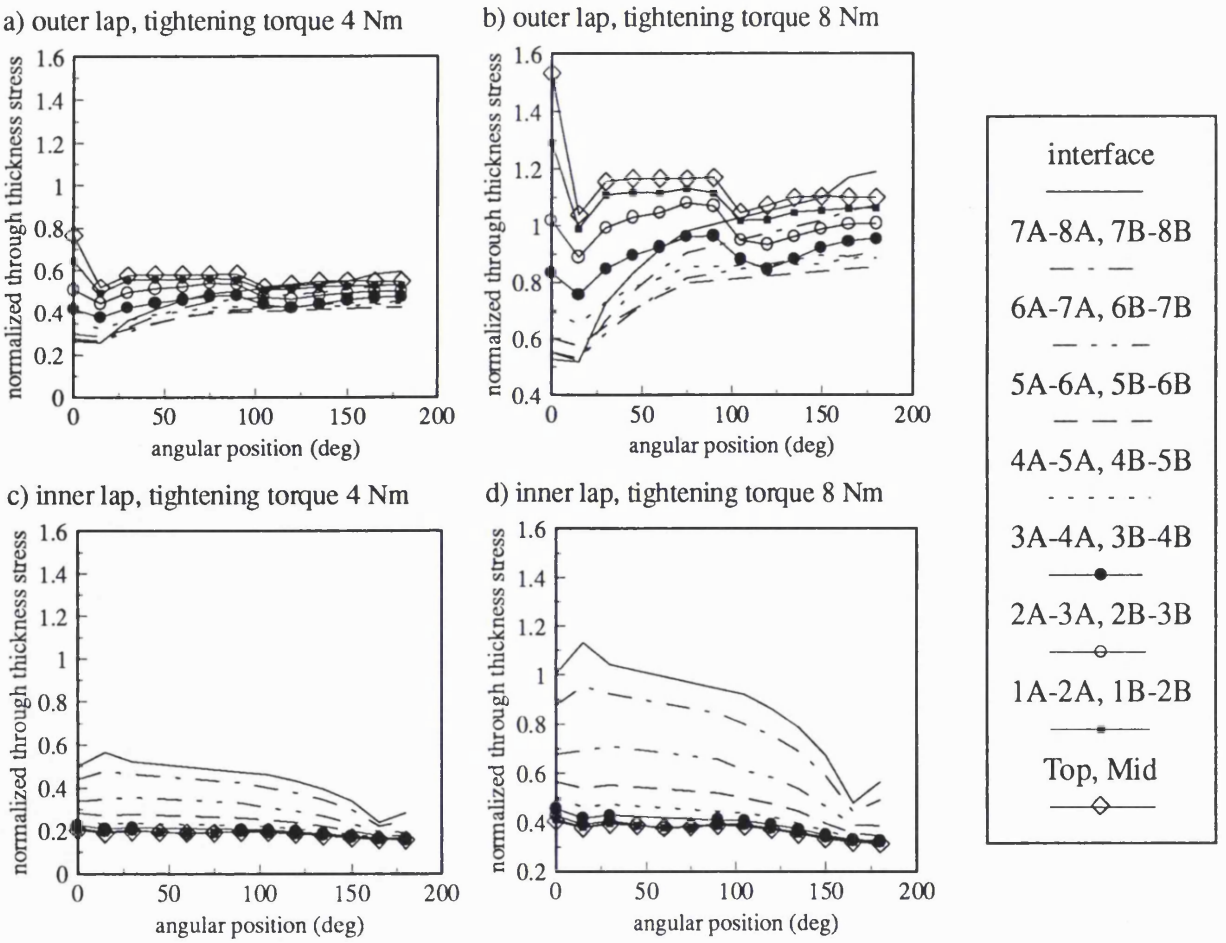


Figure 6.21 The effect of bolt tightening torque on the through thickness stress of the inner lap and outer lap laminate

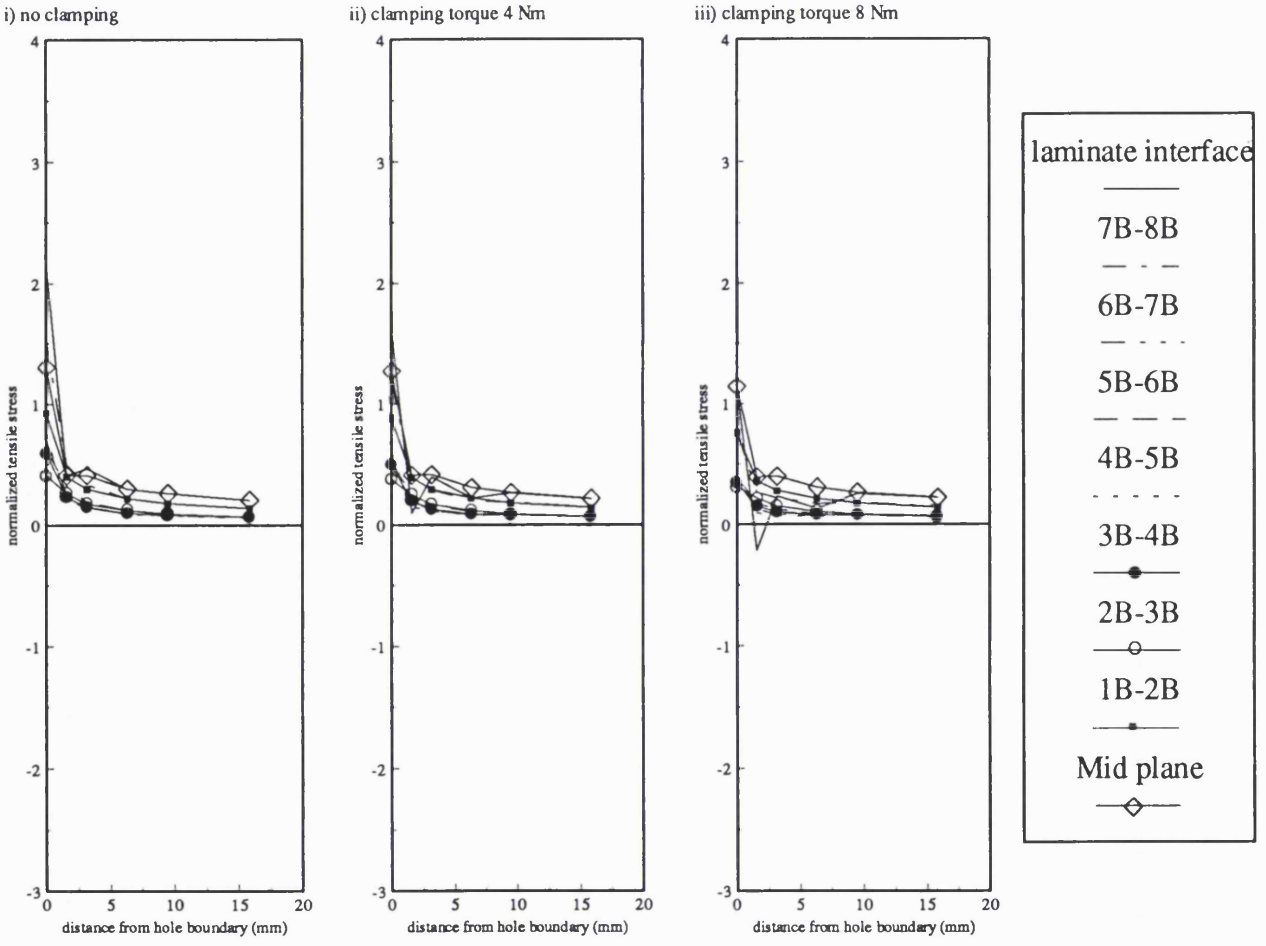


Figure 6.22a Normalized tensile stress along the net tension plane of the inner lap for a range of bolt tightening torques (0 to 8 Nm)

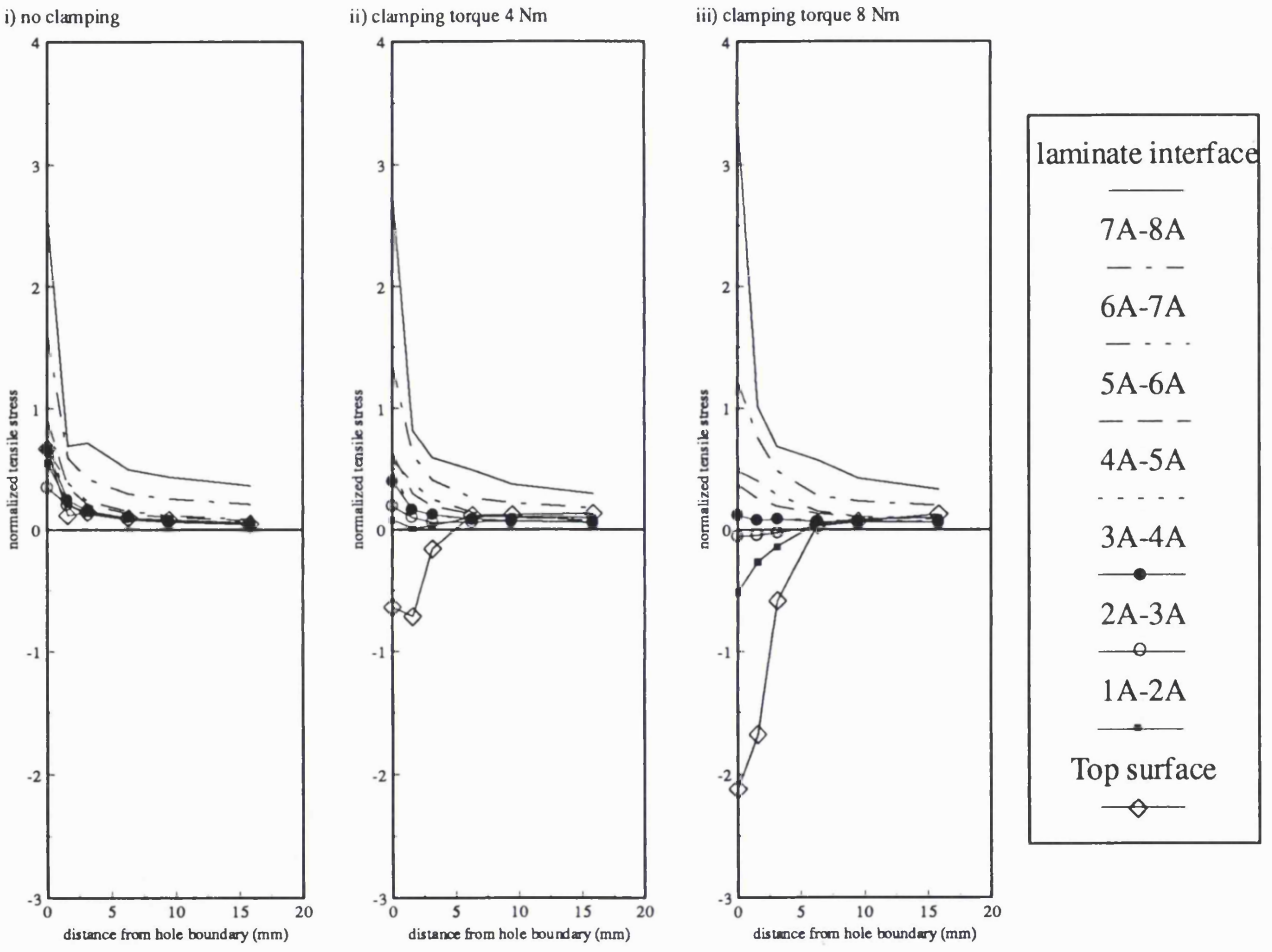


Figure 6.22b Normalized tensile stress along the net tension plane of the outer lap for a range of bolt tightening torques (0 to 8 Nm)

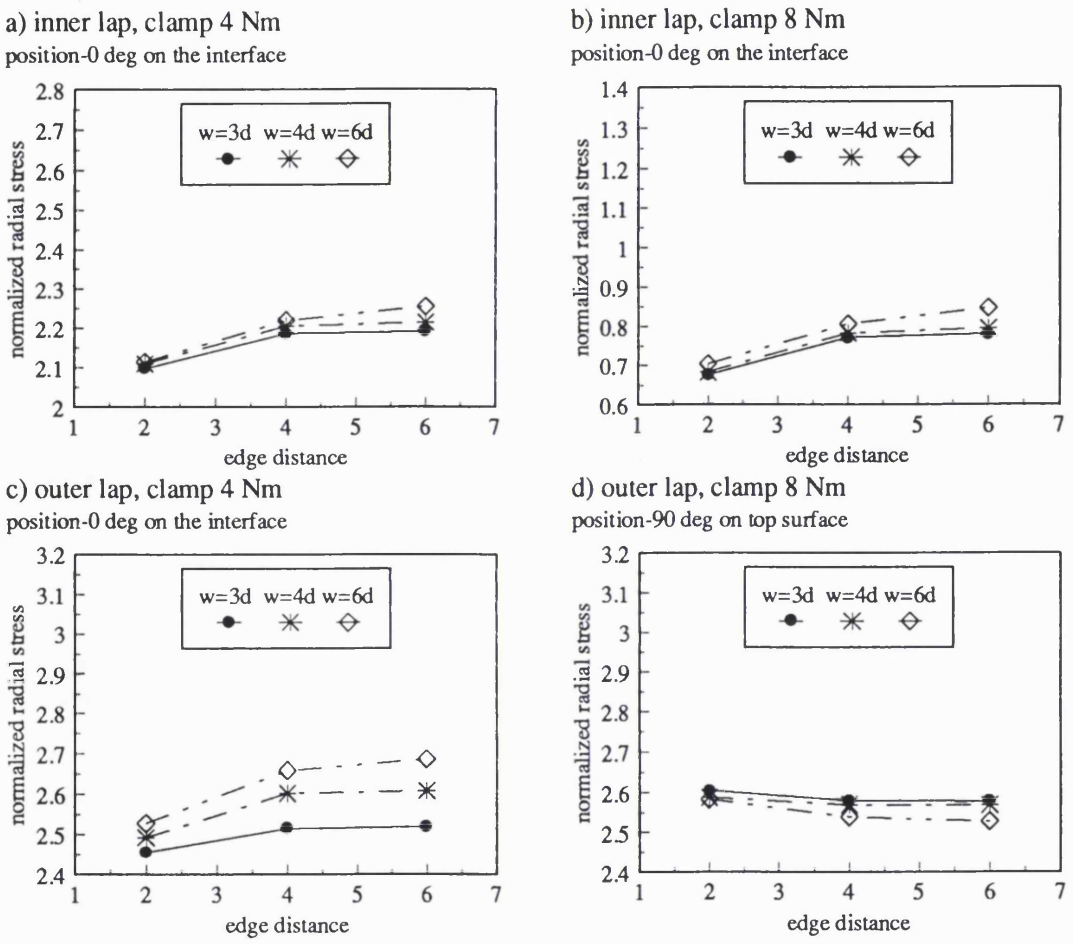


Figure 6.23 The effect of joint geometry on the maximum radial contact stress for the inner lap and outer lap having the bolt tightening torques of 4 Nm and 8 Nm

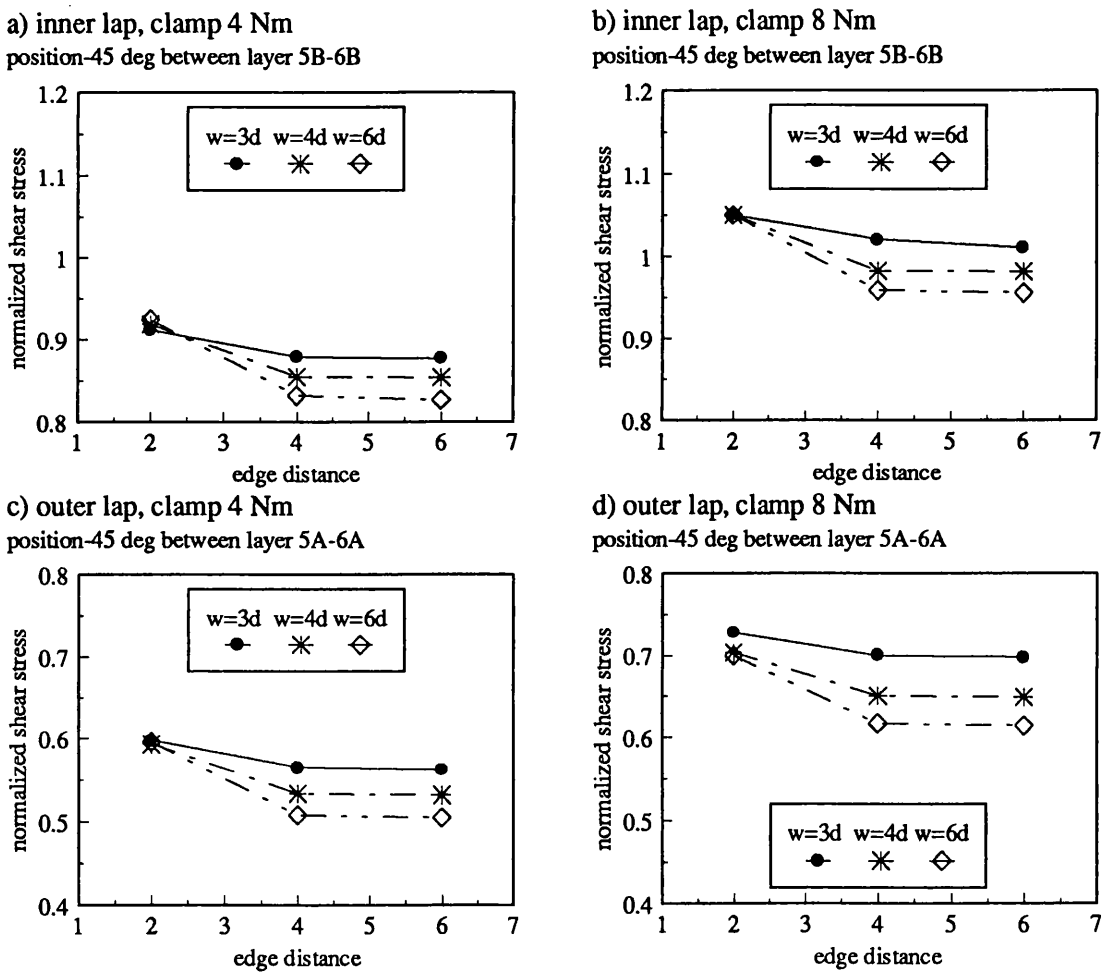


Figure 6.24 The effect of joint geometry on the maximum inter laminar shear stress for the inner lap and outer lap having the bolt tightening torques of 4 Nm and 8 Nm

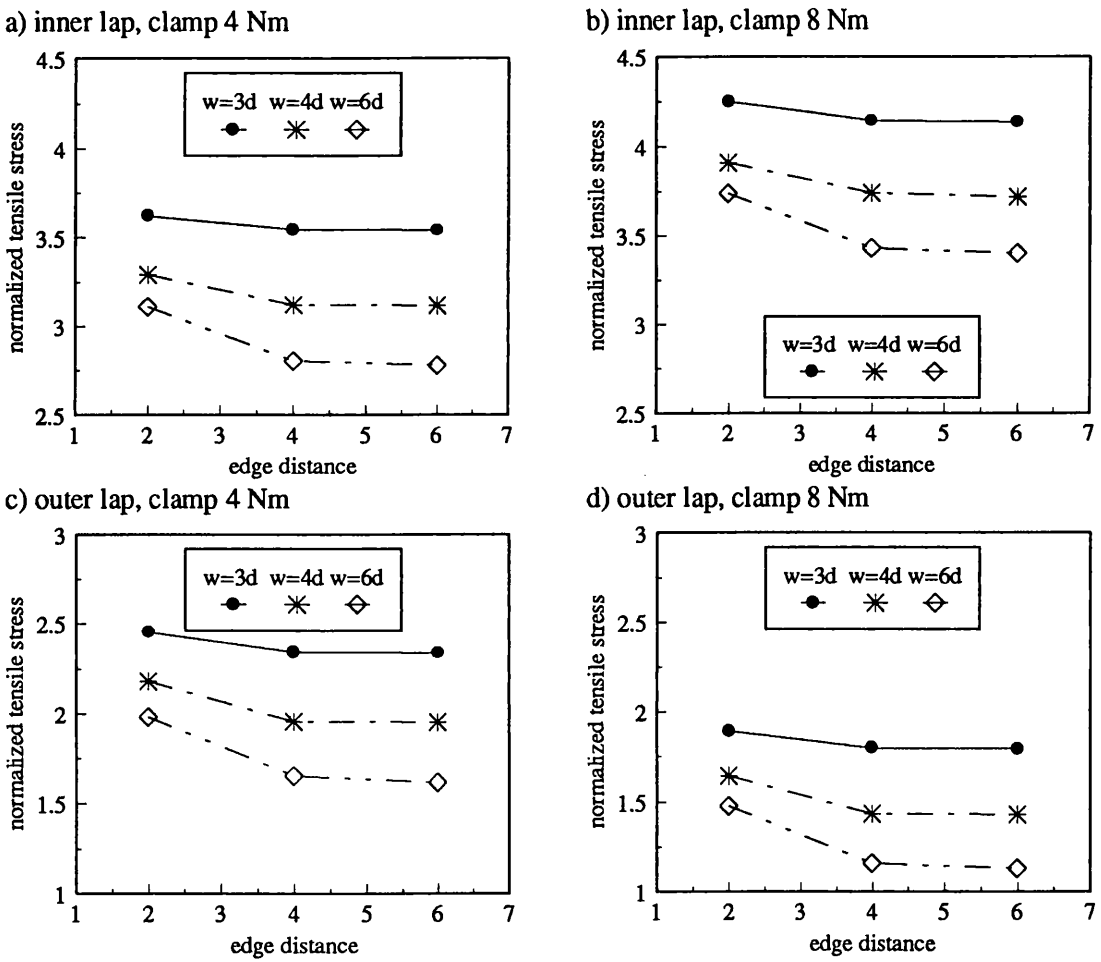


Figure 6.25 The effect of joint geometry on the maximum tensile stress for the inner lap and outer lap having the bolt tightening torques of 4 Nm and 8 Nm

a) without bolt tightening

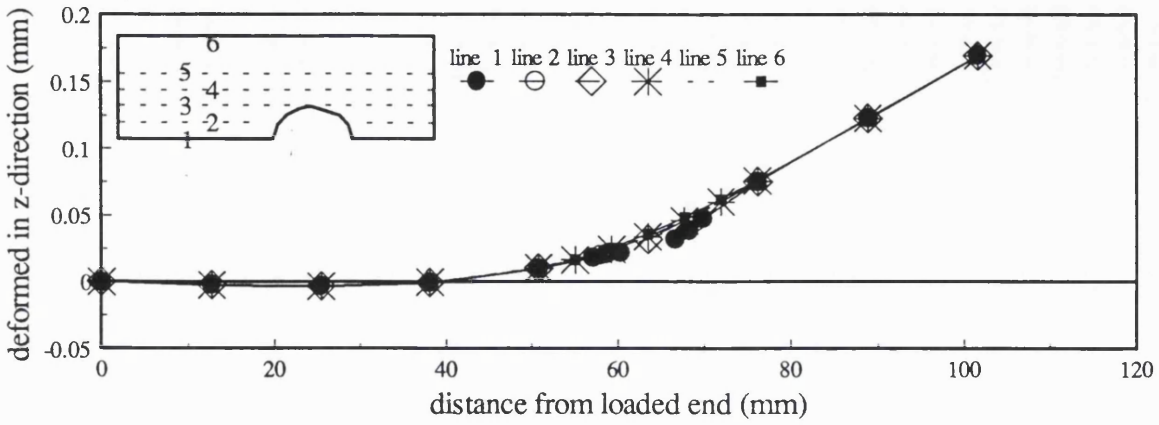


b) 4 Nm bolt tightening torque

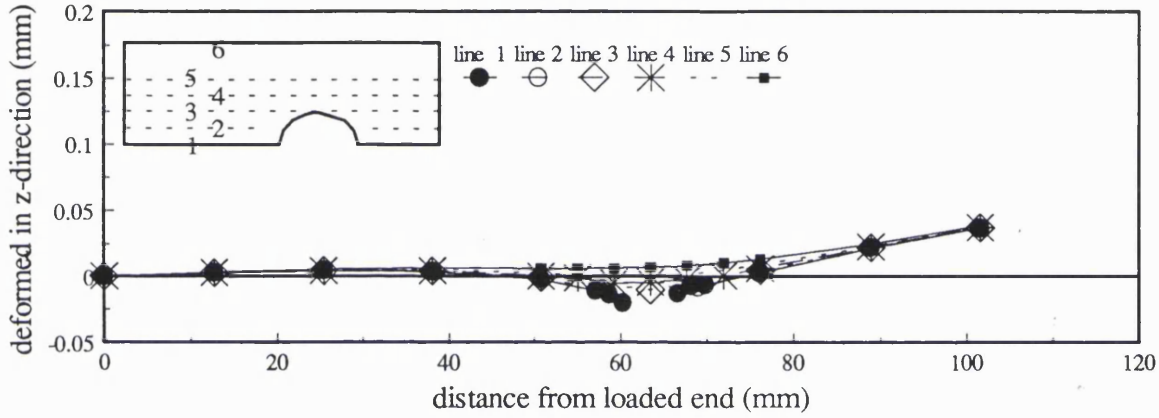


c) 8 Nm bolt tightening torque

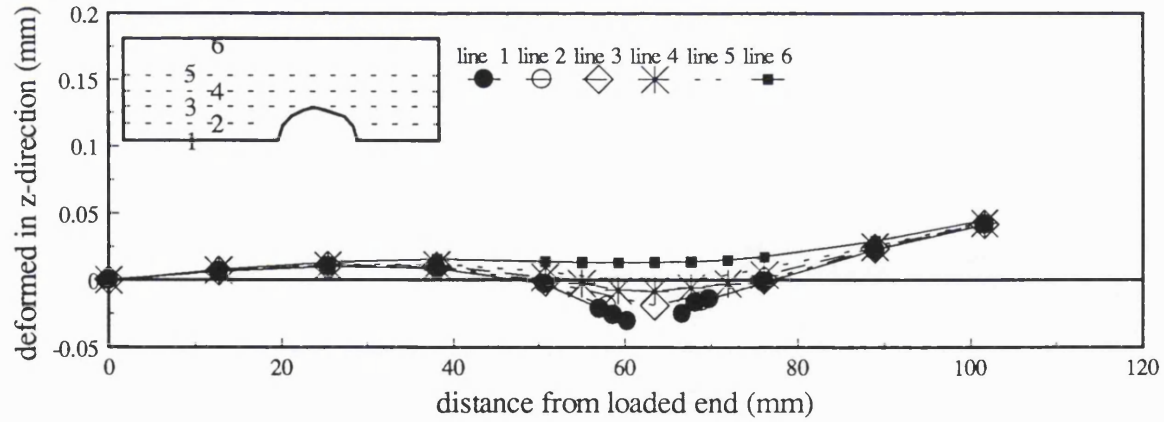


w=6d : e=6d (outer lap at the laminate plate interface)

Figure 6.26 Deformed shape in the *z*-direction for (a) without bolt tightening, (b) 4 Nm and (c) 8 Nm tightening torque; laminate width = 6d: edge distance = 6d

a) without bolt tightening

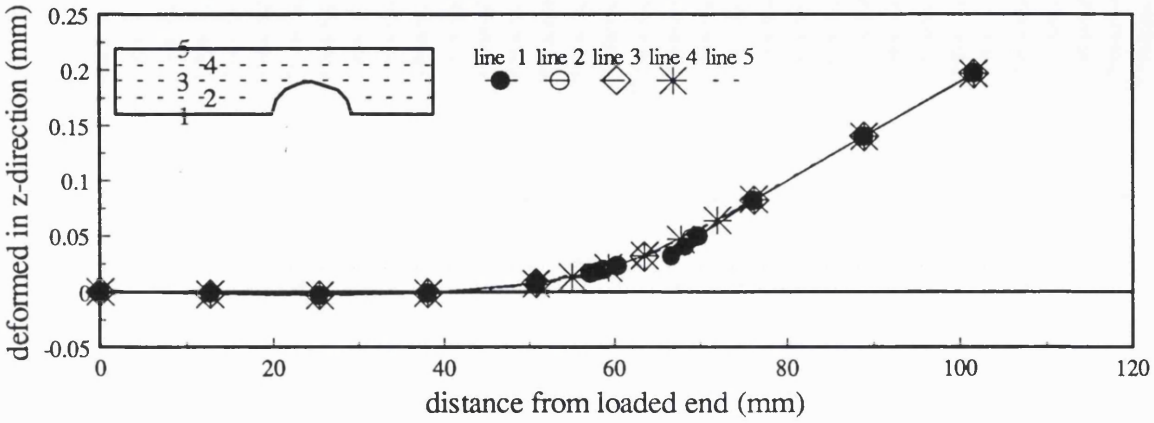


b) 4 Nm bolt tightening torque

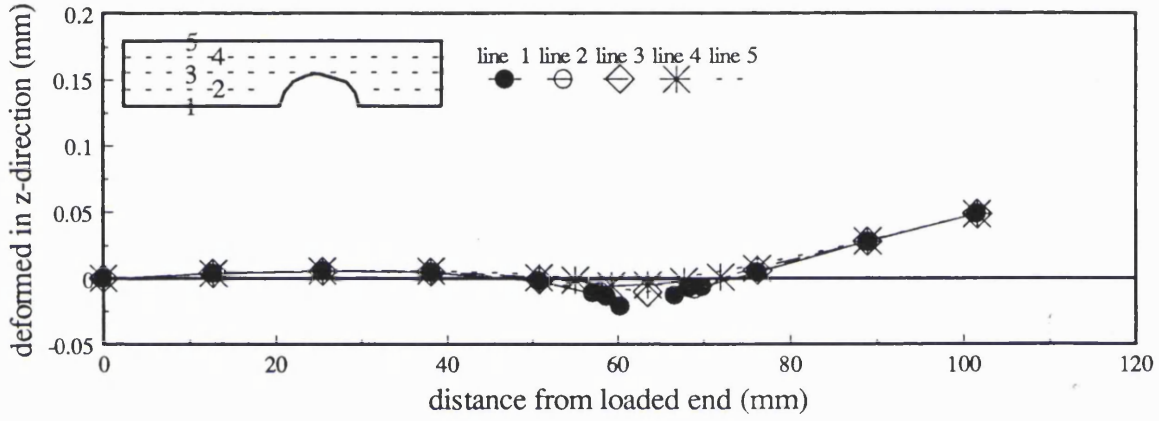


c) 8 Nm bolt tightening torque

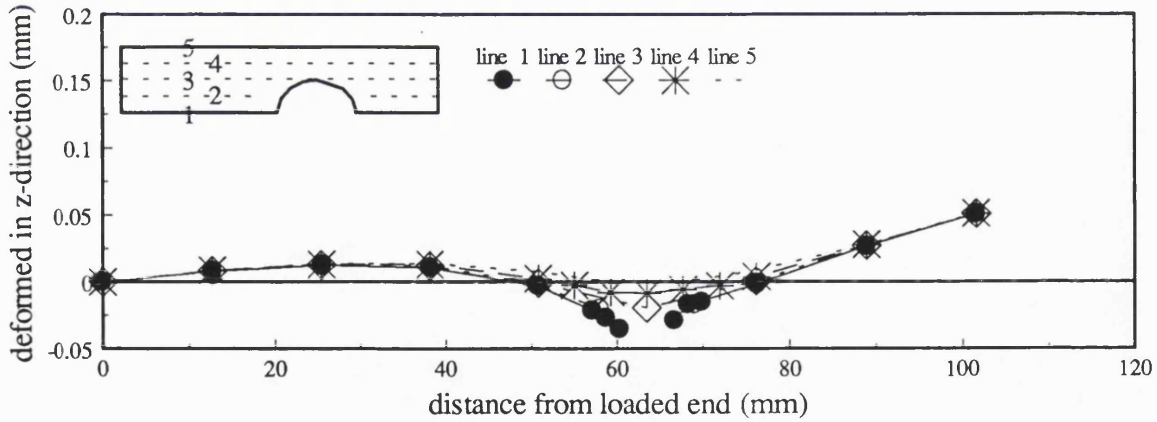


w=4d : e=6d (outer lap at the laminate plate interface)

Figure 6.27 Deformed shape in the z-direction for (a) without bolt tightening, (b) 4 Nm and (c) 8 Nm tightening torque; laminate width = 4d: edge distance = 6d

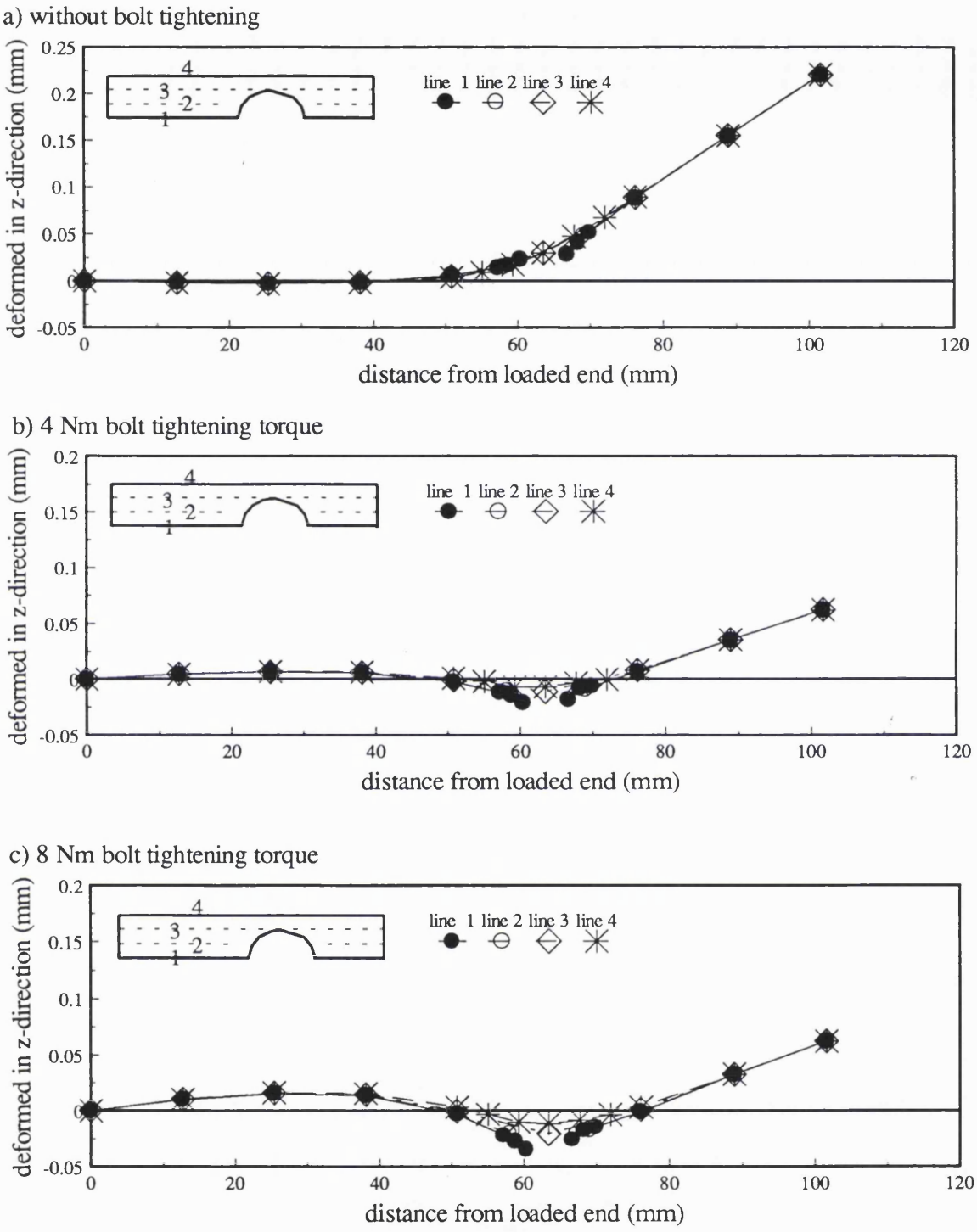


Figure 6.28 Deformed shape in the z-direction for (a) without bolt tightening, (b) 4 Nm and (c) 8 Nm tightening torque; laminate width = 3d: edge distance = 6d

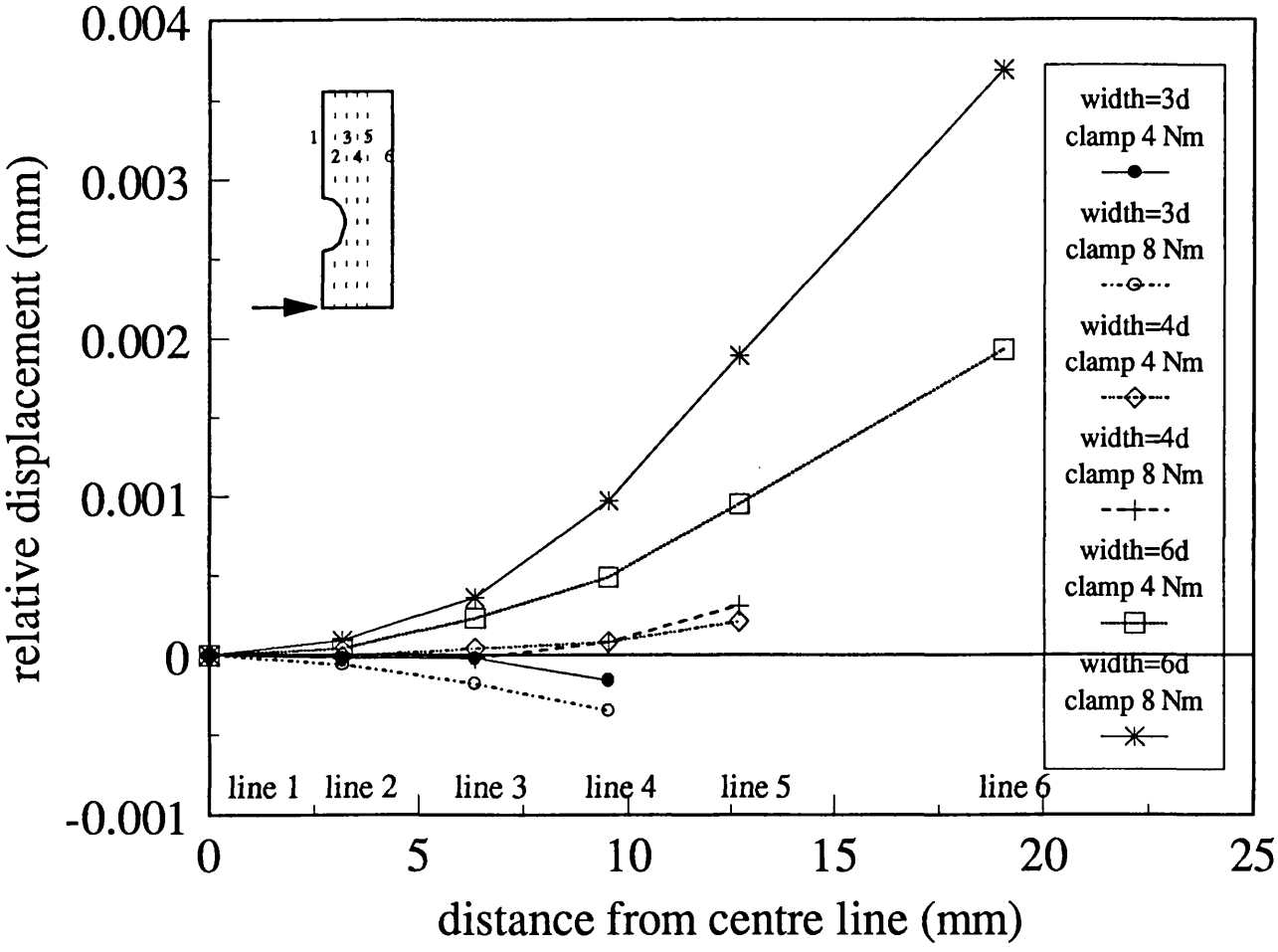


Figure 6.29 Relative displacement in the *z*-direction at the free end of the outer lap compared with displacement at the centreline

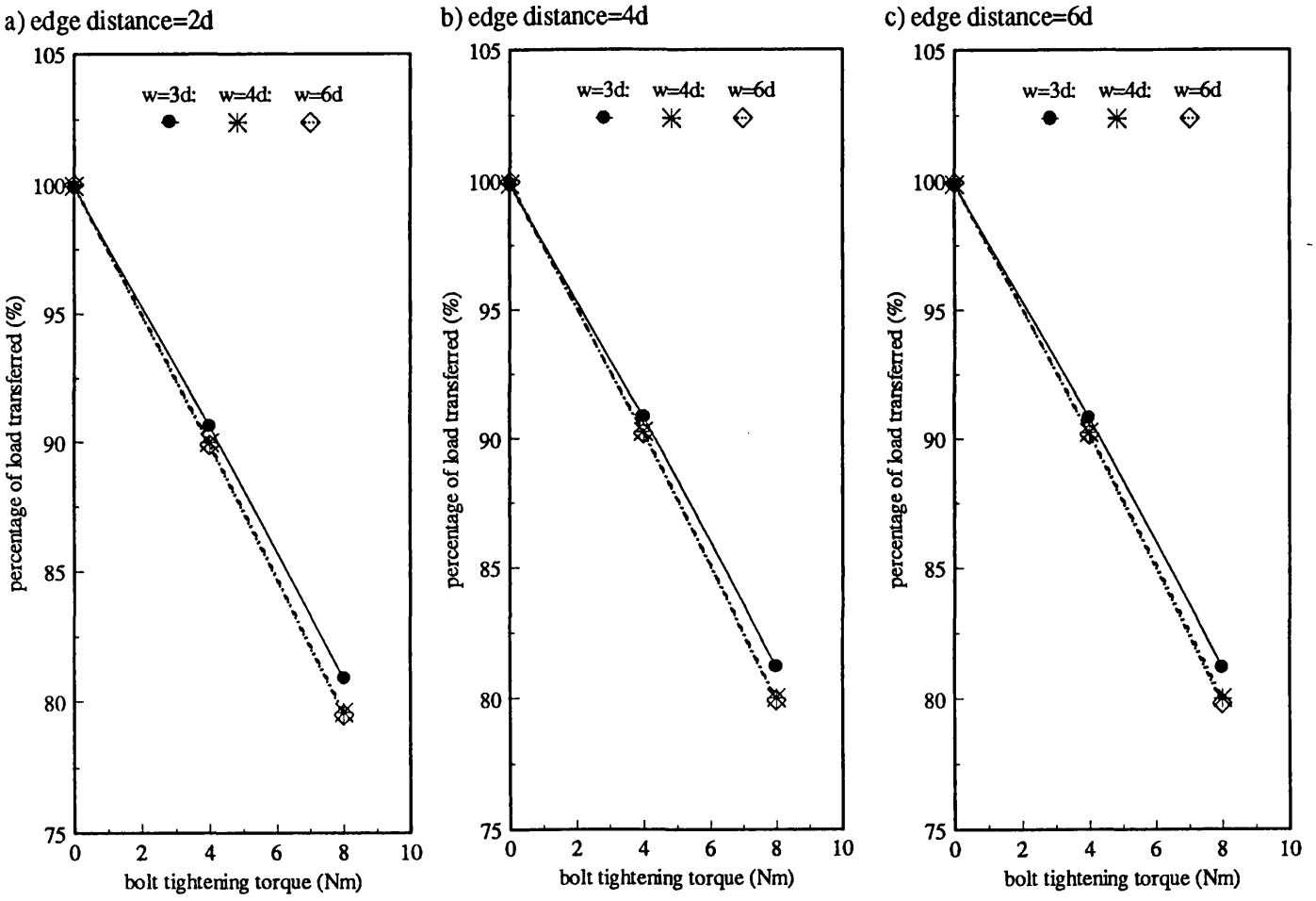


Figure 6.30 The effect of clamping pressure on the percentage of load transferred via the bolt

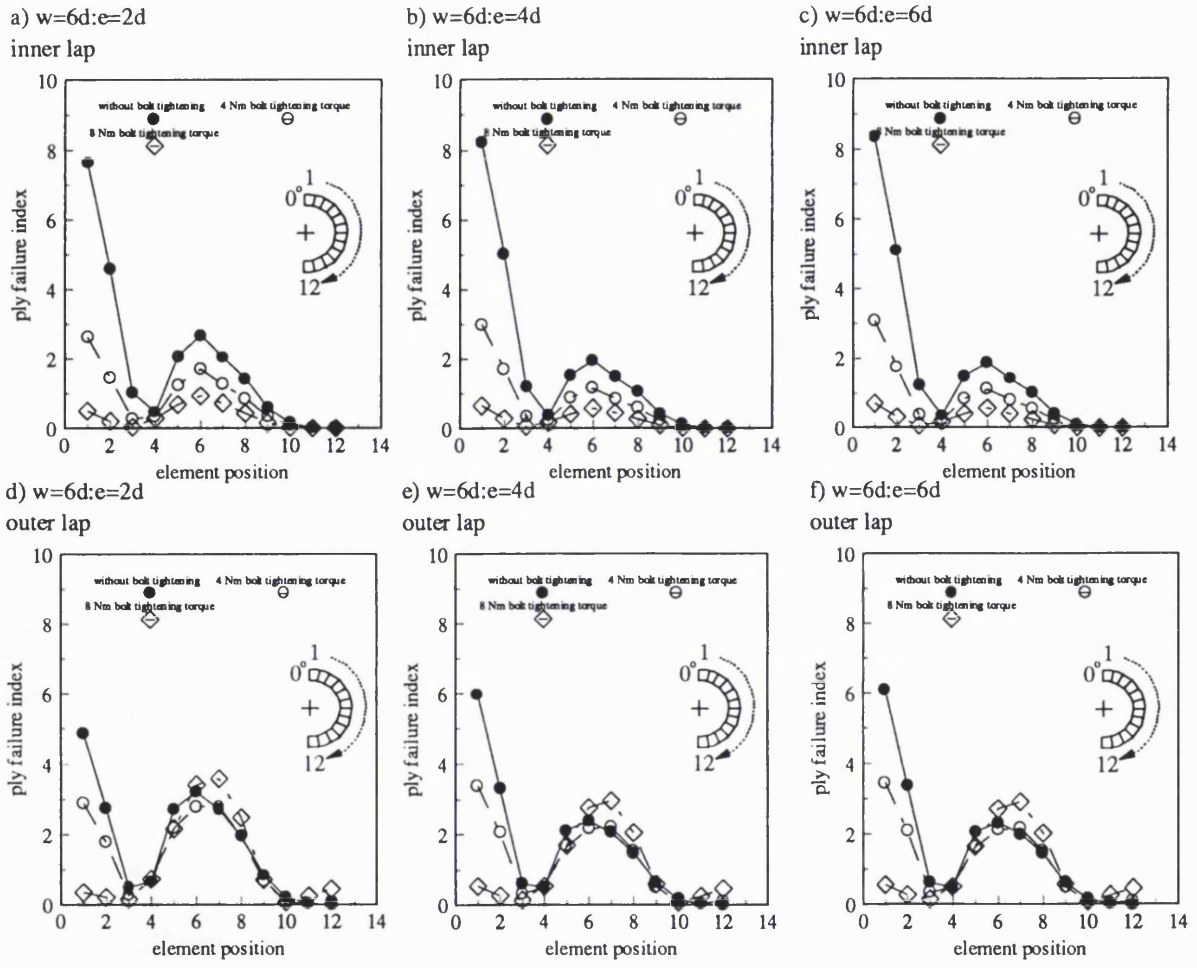


Figure 6.31 The effect of edge distance on the ply failure index for the elements at the interface between the inner lap and the outer lap, having a range of bolt tightening torques (constant width of 6*d*)

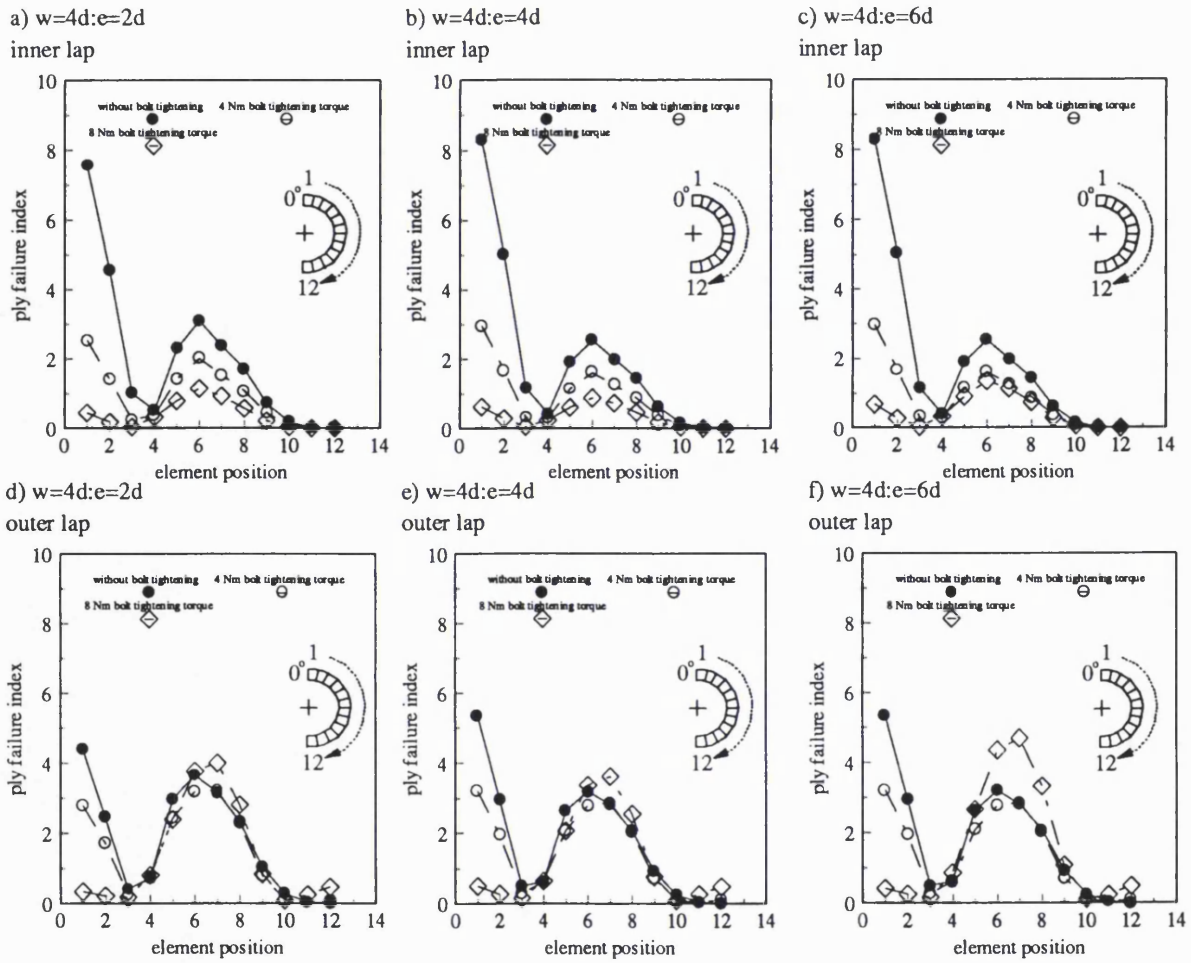


Figure 6.32 The effect of edge distance on the ply failure index for the elements at the interface between the inner lap and the outer lap, having a range of bolt tightening torque (constant width of 4*d*)

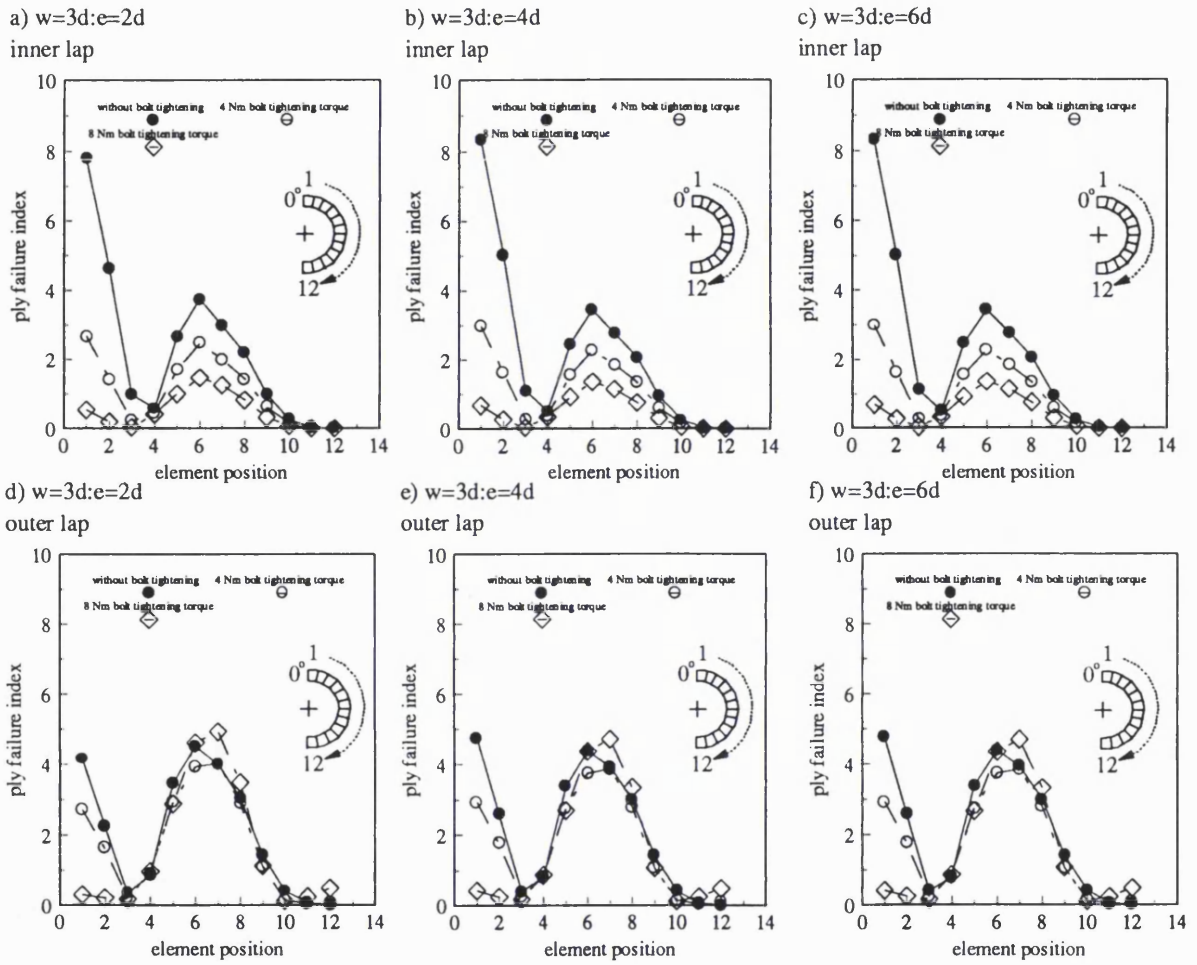


Figure 6.33 The effect of edge distance on the ply failure index for the elements at the interface between the inner lap and the outer lap, having a range of bolt tightening torques (constant width of 3*d*)

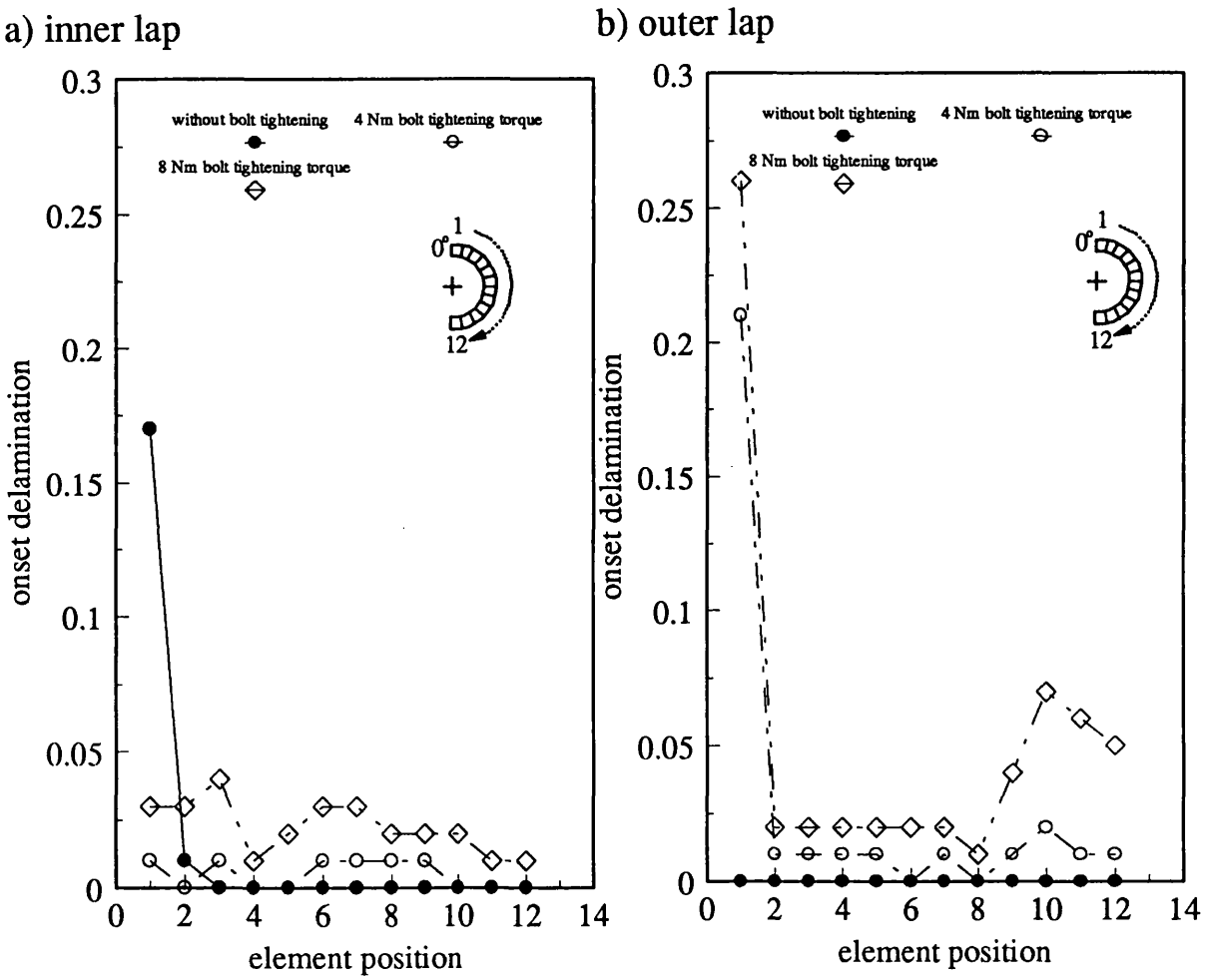


Figure 6.34 Onset of delamination for the elements of the inner lap and the outer lap on the hole boundary (w=6d: e=6d)

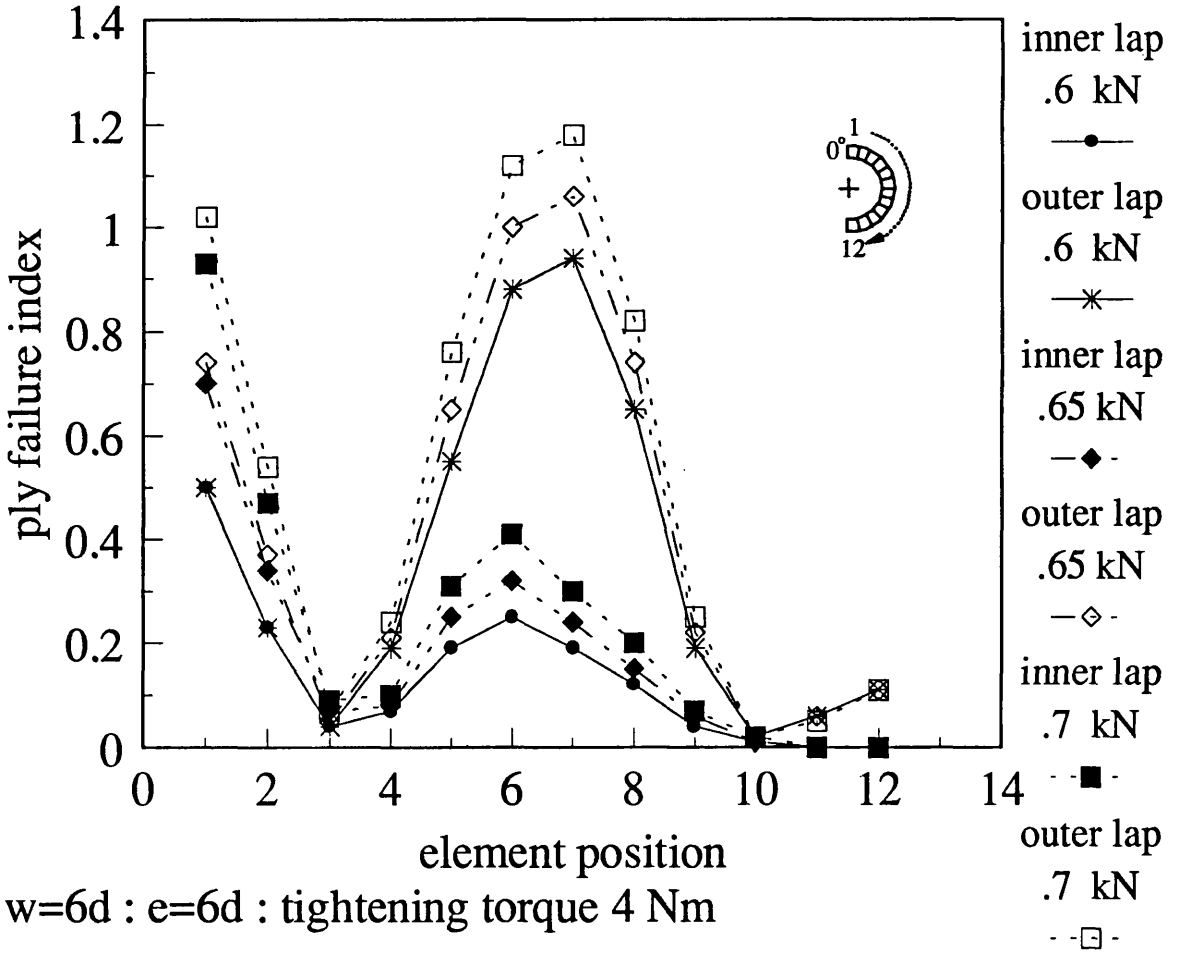


Figure 6.35 Failure index for elements on the hole boundary of the outer lap at the laminate plate interface (w=6d: e=6d: bolt tightening torque 4 Nm)

# CHAPTER 7

# CONCLUSIONS AND SUGGESTIONS FOR FURTHER RESEARCH

In this chapter a summary of each of the previous chapters is provided. This is followed by a brief overall appraisal of the results and an assessment of the relevance of this work to the current understanding of the behaviour of mechanically fastened composite laminates. Finally, suggestions are made for extending the current work.

## 7.1 CONCLUSIONS

### 7.1.1 CHAPTER 2

This chapter presented a literature review of the current developments in both experimental and analytical investigations of the stress distribution and failure analysis of mechanically fastened joints. Experimental examinations concerned with assessing the effect of joint geometry, material composition and fastener configuration on the joint strength and failure mode were discussed.

In the case of the analytical studies it is apparent that many researchers have attempted to use the boundary element method as well as the finite element method, as a means of evaluating the stress distribution around the fasteners and, thereby, the joint strength. However, in the application of the boundary element method, the requirement to prescribe the contact condition at the joint interface

limits the suitability for this type of problem. The finite element method, however, utilises numerical techniques to solve the interfacial contact condition and consequently has been shown to be the most appropriate method to date in the analysis of mechanically fastened composite laminates.

The accuracy of the results obtained from a finite element analysis of this problem are dependent on the assumptions made in the modelling process. To achieve a more realistic model, the contact conditions at the interface should be solved analytically using an incremental loading scheme. Moreover, the layerwise technique for modelling the laminate should be utilised so that the effects of the interlaminar normal and shear stresses may be incorporated. These additional features will not only increase the complexity of the modelling process but will normally increase the time required to construct the model, as well as to perform the analysis and post-processing of the results.

### 7.1.2 CHAPTER 3

In this chapter the theoretical aspects concerning the laminate plate theory and the contact mechanism concept in the analysis of mechanically fastened joints was presented. Layerwise modelling was considered more suitable for three-dimensional modelling than the RVE modelling technique since interlaminar shear and through thickness stresses can be directly evaluated for each lay-up. However, this technique requires considerable time in model construction, carrying out the analysis and then post-processing the results.

### 7.1.3 CHAPTER 4

The results obtained from two-dimensional finite element modelling of a single pin, double lap, composite laminate joint subjected to an in-plane load was described in this chapter. The modelling technique was verified by comparing the results obtained for a specific joint configuration with those given in previously published studies.

The influence of interfacial friction, pin elasticity and the laminate properties on the stress distribution at the hole boundary were assessed. The combined effect of interfacial friction and pin elasticity, which have not been previously assessed, were considered to have a significant influence on the joint performance. This is confirmed by the results which showed that an increase in the friction coefficient lowered the radial contact stress, thereby, reducing the pin deformation and increasing the pin-laminate contact area. Moreover, the angular position of the peak radial, interlaminar shear and through thickness stresses was shown to be dependent on the stacking sequence of the laminate.

### 7.1.4 CHAPTER 5

In this chapter a two-dimensional multi-fastener model of a double lap joint was presented. The special features of this model enabled a realistic evaluation of the load transfer via each fastener to be derived from the local contact pressure distribution. These results indicate that for the specific joint configurations

considered the outermost hole on the inboard row of the inner lap was subjected to the highest load transfer.

The non-uniform transfer of load through the fasteners demonstrates that results obtained in the analysis of single fastened joints can not be extrapolated to multi-fastened configurations, since the stress distribution is affected by the proximity and location of adjacent fasteners.

### 7.1.5 CHAPTER 6

Two types of three-dimensional model were given in chapter 6 in which; (a) a representative volume element (RVE) technique was used in the modelling of an inner lap laminate in contact with a single bolt and (b) replica (layerwise) modelling was utilized to construct models for both the inner and outer lap laminates in a double lap joint.

The modelling technique was validated by comparing the analytical results with previously published work. The effect produced by varying bolt pre-load and tolerance demonstrated that good correlation may be obtained between analytical and experimental results when the model includes most of the physical attributes of the joint.

Although good agreement was obtained using the RVE procedure, the layerwise technique was employed in the subsequent analysis since this allows

consideration of the interlaminar stress and, thereby, enables failure analysis of the joint to be carried out.

The proportion of load transferred due to the interfacial friction at the laminate plate interface and the out-of-plane deformation that occurs under load, highlights the importance of three-dimensional modelling for this type of joint. Bolt pre-load showed a considerable influence on the stress distribution on the hole boundary and the load transferred by the bolt. For the case without bolt pre-loading the maximum radial contact stress was recorded on the inner lap, whereas, for a bolt tightening torque of 4 Nm and 8 Nm the maximum radial contact stress occurred in the outer lap. Despite the contrary practice these results demonstrate that it is essential to perform a comprehensive stress analysis on both the inner and outer lap of the joint when undertaking three-dimensional modelling.

## 7.2 ACHIEVEMENTS OF THIS WORK

This thesis outlines the application of three-dimensional finite element modelling in studying the stress and strain produced during loading of mechanically fastened composite laminates. An original model of a double lap single bolted joint, consisting of an inner lap and outer lap laminate joined by an elastic bolt, was constructed. The model incorporated the analysis of the interlaminar shear and through thickness stresses imposed on the laminate by the application of bolt pre-load and an applied tensile load. A realistic contact stress

distribution at the joint interfaces was modelled which included the effect of friction at the bolt-hole interface as well as at the laminate plate interface.

Comprehensive stress analysis of the laminates showed the influential effect of stacking sequence, joint geometry and bolt pre-load on the stress distribution in the vicinity of the fastener. This analytical work is the first study to demonstrate out-of-plane bending of the outer lap as function of bolt pre-load and laminate width. Finally, on the basis of examining a variety of joint geometries design guidelines were proposed for this particular double lap joint configuration.

## 7.3 SUGGESTIONS FOR FURTHER WORK

As a result of this study, the following recommendations are made to extend the work presented here.

### 7.3.1 MODELLING TECHNIQUES

In this study the bolt pre-load was applied directly on the surface nodes corresponding to the washer contact area. This assumption is violated when the laminate deforms out-of-plane in the *z*-direction. A more accurate result could be obtained by modelling the washer as an individual elastic body and subsequently carrying out the contact analysis at the washer-laminate interface. However, this proposal increases the complexity of the model and may cause a non-

convergence in the numerical iteration loop when the frictional contact analysis is undertaken.

In predicting laminate failure the average stress on an element was used in the appropriate failure criteria. Clearly, the finer the mesh, especially in vicinity of the hole boundary, the more accurate is the prediction of the initiation site. This is, however, dependent on the number of contact elements that can be incorporated in the finite element simulation. Further work should be undertaken to investigate the optimum mesh size to give the appropriate resolution for investigating failure initiation.

### 7.3.2 MATERIAL AND FASTENER PARAMETERS

The application of different laminate stacking sequences and or material combinations under various clamping conditions should be investigated. The effect of bolt elasticity and tolerance should also be considered as bolt bending influences the radial contact stress distribution through the laminate thickness. The effect of washer size is another parameter to study since this governs the through thickness stress. Moreover, a three-dimensional analysis of a multi-fastened joint should be examined since this is more appropriate to practical applications. This assessment is considered essential to enhance joint performance and to evolve a more useful design methodology of composite bolted joints.

### 7.3.3 FAILURE CRITERIA AND STRENGTH PREDICTION

This study has shown that it is possible to predict the failure initiation for this particular type of joint using existing failure criteria. Further development in the procedures for predicting joint strength and failure mode are required. This may be included into the analytical simulation by recalculating the stiffness of the laminate immediately after an element has failed and adopting an iterative loading procedure to check for subsequent element failure. The reliability of this type of assessment must dependent on the accuracy of the damage mechanics model that is used to recalculate the laminate stiffness near the damaged zone.

# REFERENCES

**ABAQUS** Finite Element Computer program, Hibbitt, Karlsson, and Sorensen, Inc., Providence, RI

**Abd-El-Naby, S. F. M., Hollaway, L. and Gunn, M.** (1991): "Load distribution in two-pinned polymer composite joints", Composite Structures 6 (Ed. Marshall, I. H.), pp. 553

**Abd-El-Naby, S. F. M., and Hollaway, L.** (1993a.): "The experimental behaviour of bolted joints in pultruded glass/polyester material. Part 1: Single-bolt joints", Composites, Vol. 24, pp. 531-538

**Abd-El-Naby, S. F. M., and Hollaway, L.** (1993b.): "The experimental behaviour of bolted joints in pultruded glass/polyester material. Part 2: Two-bolt joints", Composites, Vol. 24, pp. 539-546

**Agarwal, B. L.** (1980): "Behaviour of multifastener bolted joints in composite materials", AIAA-80-0307

**Azzi, V. D. and Tsai, S. W.** (1965): "Anisotropic strength of composites.", Experimential Mechanics, Vol. 5, pp. 283-298

**Bencheckchou, B and White, R. G.** (1995a.): "Stress around fasteners in composite structures in flexure and effects on fatigue damage initiation part 1: cheese-head bolts", Composite Structures, Vol. 33, pp. 95-108

**Bencheckchou, B and White, R. G.** (1995b.): "Stress around fasteners in composite structures in flexure and effects on fatigue damage initiation part 1: countersunk bolts", Composite Structures, Vol. 33, pp. 109-119

**Chamis, C. C.** (1974): "Micromechanics strength theories", Composite Materials, Vol. 5, Fracture and Fatigue (Ed. Broutman, L. J.), Academic Press, New York, pp. 93-115

**Chamis, C. C. and Sendeckyj, G. P.** (1968): "Critique on theories predicting thermoelastic properties of fibrous composites", Journal of Composite Materials, Vol. 2, pp. 332-348

**Chang, F. K. and Chang, K. Y.** (1987): "Post-failure analysis of bolted composite joints in tension or shear-out mode failure", Journal of Composite Materials, Vol. 21, pp. 809-833

**Chang, F. K., Scott, R. A. and Springer, G. S.** (1982): "Strength of mechanically fastened composite joints", Journal of Composite Materials, Vol. 16, pp. 470-494

**Chang, F. K., Scott, R. A. and Springer, G. S.** (1984a.): "Failure of composite laminates containing pin loaded holes - method of solution", Journal of Composite Materials, Vol. 18, pp. 255-278

**Chang, F. K., Scott, R. A. and Springer, G. S.** (1984b.): "Design of composite laminates containing pin loaded holes", Journal of Composite Materials, Vol. 18, pp. 279-289

**Chen, W. H. and Lee, S. S.** (1995): "Numerical and experimental failure analysis of composite laminates with bolted joints under bending loads", Journal of Composite Materials, Vol. 29, pp. 15-36

**Chen, W. H., Lee, S. S. and Yeh, J. T.** (1995): "Three-dimensonal contact stress analysis of a composite laminate with bolted joint", Composite Structures, Vol. 30, pp. 287-297

**Cohen, D., Norton, F.M. and Hodgson, M.E.** (1989): "Experimental investigation of failure loads in thick composite joints", Proceedings of the Fourth Technical Conference of the American Society for Composites, Blacksburg, VA, October, pp. 72-81

**Cohen, D., Hayer, M. W., Shuart, M. J., Griffin, O. H., Prasad, C. and Yalamanchili, S. R.** (1995): "Failure criterion for thick multifastener graphite-epoxy composite joints", Journal of Composites Technology & Research, Vol. 17, pp. 237-248

**Cole, R. T., Bateh, E. J. and Potter, J.** (1982): "Fasteners for composite structures", Composites, Vol. 13, pp. 233-240

**Collings, T. A.** (1977): "The strength of bolted joints in multi-directional CFRP laminates", Composites,Vol. 8, pp. 43-55

**Collings, T. A.** (1982): "On the bearing strengths of CFRP laminates", Composites, Vol. 13, pp. 241-252

**Collings, T. A.** (1987): "Experimentally determined strength of mechanically fastened joints", Jointing fibre-reinforced plastics (Ed. Matthews, F. L.), Elsevier, London

**Conti, P.** (1986): "Influence of geometric parameters on the stress distribution around a pin-loaded hole in a composite laminate," Composite Science and Technology, Vol. 25, pp. 83-101

**Cook, R. D., Malkus, D. S. and Plesha, M. E.** (1989): "Concepts and applications of finite element analysis", 3rd Edition, John Wiley, New York

**Cooper, C. and Turvey, G. J.** (1995): "Effects of joint geometry and bolt torque on the structural performance of single bolt tension joints in pultruded GRP sheet material" Composite Structures, Vol. 32, pp. 217-226

**Crews, J. H., Jr.** (1981): "Bolted bearing fatigue of a graphite/epoxy laminate", Joining of Composite Materials ASTM STP 749 (Ed. Kedward, K. T.), American Society for Testing and Materials, pp. 131-144

**Crews, J. H., Jr. and Naik, R. A.** (1986): "Combined bearing and bypass loading on a graphite/epoxy laminate", Composite Structures, Vol. 6, pp. 21-40

**Curtis, P. T.** (1993): "Theoretical prediction of failure mechanism and strength", Composite materials in maritime structures (Fundamental aspect) (Ed. Shenoi, R. A., Wellicom, J. F.), Cambridge University Press, Cambridge, Vol. 1. , pp. 280-307

**de Jong, T.** (1977): "Stresses around pin-loaded holes in elastically orthotropic or isotropic plates", Journal of Composite Materials, Vol. 11, pp. 313-331

**de Jong, T.** (1982): "Stresses around pin-loaded holes in composite materials", in Mechanics of Composite Materials, Recent Advances, Pergamon Press, pp. 339-348

**de Jong, T.** (1987): "On the calculation of stresses in pin-loaded anisotropic plates", TU Delft, Report LR-529, November

**Daniel, I. M. and Ishai, O.** (1994): "Engineering mechanics of Composite Materials", Oxford University Press, New York

**Eisenmann, J. R.** (1976): "Bolted joint static strength model for composite materials", NASA TM-X-3377, April, pp. 563-602

**Eriksson, I.** (1990): "On the bearing strength of bolted graphite/epoxy laminates", Journal of Composite Materials, Vol. 24, pp.1246-1269

**Eriksson, L. I.** (1986): "Contact stresses in bolted joints of composites laminates", Composite Structures, Vol. 6, pp. 57-75

**Fan, W. and Qiu, C.** (1993): "Load distribution of multi-fastener laminated composite joints", International Journal of Solids Structures, Vol. 30, pp. 3010-3023

**Garbo, S. P. and Ogonowski, J. M.** (1981): "Effect of variances and manufacturing tolerances on the design strength and life of mechanically fastened composite joints", AFWAL-TR-81-3041, Air Force Wright Aeronautical Laboratory, Dayton, OH, Vol. 1 & 2 & 3, April

**Godwin, E. W. and Matthews, F. L.** (1980): "A review of the strength of joints in fibre reinforced plastics. Part I: Mechanically fastened joints", Composites, Vol. 11, pp. 155-160

**Godwin, E. W., Matthews, F. L. and Kilty, P. L.** (1982): "Strength of multi-bolt joints in GRP", Composites, Vol. 13, pp. 268-272

**Graham, U., Wisnom, M. R. and Webber, J. P. H.** (1994): "A novel finite element investigation of the effects of washer friction in composite plates with bolted filled holes", Composite Structures, Vol. 29, pp. 329-339

**Griffin Jr., O.H., Hyer, M.W., Cohen, D., Shuart, M.J., Yalamanchili, S.R. and Prasad, C.B.** (1994): "Analysis of multifastener composite joints", Journal of Spacecraft and Rockets, Vol. 31, pp. 278-284

**Hamada, H., Haruna, K. and Maekawa, Z.-I.** (1995): "Effect of stacking sequences on mechanically fastened joint strength in quasi-isotropic carbon-epoxy laminates", Journal of Composites Technology & Research, Vol 17, pp. 249-259

**Hart-Smith, L. J.** (1977): "Bolted joints in graphite-epoxy composites", Douglas Aircraft Company, NASA Langley Contract Report, NASA CR-144899, January

**Hart-Smith, L. J.** (1980): "Mechanically fastened joints for advanced composites - Phenomenological considerations and simple analysis", Fibrous composites in structural design (Ed. Lenoe, E. M., Oplinger, D. W. and Burke, J. J.), Plenum Press, New York

**Hart-Smith, L. J.** (1987): "Design and empirical analysis of bolted or riveted joints", Jointing fibre-reinforced plastics (Ed. Matthews, F. L.), Elsevier, London

**Hashin, Z. and Rotem, A.** (1974): "A fatigue failure criterion for fibre reinforced materials", Journal of Composite Material, Vol. 7, pp. 448-504

**Herrera-Franco, P. J. and Cloud, G. L.** (1986): "Experimental Analysis of Multiple-Hole Arrays of Composite Material Fasteners", Proceedings of the 1986 SEM Spring Conference on Experimental Mechanics, New Orleans, Louisiana, June, pp. 621-629

**Hodgkinson, J. M.** (1985): "The strength of bolted joints in Kevlar RP, Proc. Conf., Composite design for space application, 15-18, ESA SP-243, European Space Agency, Noordwijk, Netherlands

**Holister, G. S. and Thomas, C.** (1966): "Fibre reinforced materials", Elsevier Publishing Co., London

**Humphris, N. P.** (1978): "Migration of the point of maximum stress in a laminate composite lug structure - A stepwise approach", Symposium: Jointing in Fibre Reinforced plastics, Imperial College, London, September, pp. 79-86

**Hyer, M. W. and Klang, E. C.,** (1984): "Contact stresses in pin loaded orthotropic plates" Virginia Polytechnic and State University, VPI-E-84-14, April

**Hyer, M. W., Klang, E. C. and Cooper, D. C.** (1987): "The effect of pin elasticity, clearance and friction on the stresses in a pin-loaded orthotropic plate", Journal of Composite Materials, Vol. 21, pp. 190-206

**Hyer, M. W. and Liu, D.** (1983): "Photoelastic determination of stresses in multiple-pin connectors", Experimental Mechanics, Vol. 23, pp. 249-256

**Hyer, M. W. and Liu, D.** (1984): "Stresses in a quasi isotropic pin-loaded connectors using photoelasticity", Experimental Mechanics, Vol. 23, pp. 48-53

**Hyer, M. W. and Liu, D.** (1985): "Stresses in pin-loaded orthotropic plates: Photoelastic results", Journal of Composite Materials, Vol. 19, pp. 138-153

**I-DEAS Master Series 1.3c.** (1993), 2000 Eastman Drive, Milford, OH 45150, USA,

**Jones, R. M.** (1975): "Mechanics of composite materials", Hemisphere Publ. Co., New York

**Jurf, R. A. and Vinson J. R.** (1990): "Failure analysis of bolted joints in composite laminates", Composite Material: Testing and Design (Ninth Volume), ASTM STP 1059 (Ed. Garbo, S. P.), American Society for Testing and Materials, Philadelphia, pp. 165-190

**Kretsis, G. and Matthews, F. L.** (1985): "The strength of bolted joints in glass fibre/epoxy laminates", Composites, Vol. 16, pp.92-102

**Kim, S.J. and Kim, J.H.** (1995): "Finite element analysis of laminated composite plates with multi-pin joints considering friction", Computer and Structures, Vol. 55, pp. 507-514

**Knight, C. E., Jr.** (1993) "The finite element in mechanical design" PWS-KENT Publishing Company, Boston, U. S. A.

**Kortschot, M. T., Beaumont, P. W. R.** (1990): "Damage mechanics of composite materials: 1.-Measurement of damage and strength, 2.-A damage based notched strength model", Composite Science and Technology, Vol. 39, pp. 289-326

**Lehman, G. M. and Hawley, A. V.** (1969): "Investigation of joints in advanced fibrous composites for aircraft structures", McDonnel-Douglas Coporation, Contract F33615-67-C-1582, June

**Lekhnitskii, S. G.** (1968): "Anisotropic plates", Translated from Russian by Tsai, S. W. and Cheron, T., Gordon and Breach Science Publishing, New York

**Lessard, L. B.** (1991): "Bearing failure of composite pinned joints using progressive damage modeling", ICCM/8, International Conference on Composite Materials, Honolulu, HI, July 15-19, pp. 9E1-9E10

**Lessard, L. B., Poon, C. and Fahr, A.** (1992): "Composite pinned joint failure modes under progressive damage", ECCM-V Fifth European Conference on Composite Materials and Exhibition, Bordeaux, France, April 7-10

**Lessard, L. B. and Mahmood, M. S.** (1995): "Two-dimensional modeling of composite pinned-joint failure", Journal of Composite Materials, Vol. 29, pp. 671-697

**Lin, Chien-Chang and Lin, Chuen-Horng** (1993): "Stress and strength analysis of composite joints using direct boundary element method", Composite Structures, Vol. 25, pp. 209-215

**Mahayerin, E. and Sikarskin, D. L.** (1986): "Boundary element study of loaded hole in an orthotropic plate", Journal of Composite Materials, Vol. 20, pp. 375-389

**Mallick, P. K.** 1988: "Fiber-reinforced composites: materials, manufacturing and design", Marcel Dekker Inc., New York

**Mangalgiri, P. D.** (1984): "Pin-loaded holes in large orthotropic plates" AIAA Journal, Vol. 22, pp. 1478-1484

**Mangalgiri, P. D. and Dattaguru, B.** (1986): "A large orthotropic plate with misfit pin under arbitrary oriented biaxial loading" Composite Structures, Vol. 6, pp 271-281

**Marshall, I. H., Arnold, W. S., Wood, J. and Mousley, R. F.** (1989): "Observations on bolted connections in composite structures", Composite Structures, Vol. 13, pp. 133-151

**Matthews, F. L., Nixon, A. and Want, G. R.** (1976): "Bolting and riveting in fibre reinforced plastics", Proceedings of Reinforced Plastics Congress, British Plastics Federation, Brighton, November

**Murthy, A. V., Dattaguru, B., Narayana, H. V. L. and Rao, A. K.** (1990): "An improved iterative finite element solution for pin-joints", Computer and Structures, Vol. 36, pp. 1121-1128

**Murthy, A. V., Dattaguru, B., Narayana, H. V. L. and Rao, A. K.** (1991): "Stress and strength analysis of pin joints in laminated anisotropic plates", Composite Structures, Vol. 19, pp. 299-312

**Nahas, M. N.** (1986): "Survey of failure and post-failure theories of laminated fibre-reinforced composites", Journal of Composites Technology & Research", Vol. 8, pp. 138-153

**Oakeshott, J. L. and Matthews, F. L.** (1994): "Determination of fastener load distribution in double lap composite joints", American Society of Mechanical Engineers, PD-Vol. 64-2, Engineering Systems Design and Analysis, Vol. 2, pp. 243-251

**Oplinger, D. W.** (1978): "On the structural behavior of mechanically fastened joints in composite structures", Conference Proceedings: Fibrous Composites in Structure Design, San Diego, California, Nov. 14-17, pp. 575-602

**Oplinger, D. W. and Gandhi, K. R.,** (1974): "Analytical study of structural performance in mechanically fastened fibre-reinforced plates", Army Symposium Proceedings: Solid Mechanics, 1974; The role of mechanics in design-structural joints, Army Materials and Mechanics Research Center, Report No AMMRC MS 74-8 (AD 786 543), pp. 211-242

**Pagano, N. J. and Pipes, R. B.** (1971): "The influence of stacking sequence on laminate strength", Journal of Composite Materials, Vol. 5, pp. 50-62

**Pipes, R. B. and Pagano N. J.** (1970): "Interlamina stresses in composite laminates under uniform axial extension", Journal of Composite Materials, Vol. 4, pp. 538-548

**Poon, C.** (1986): "Literature review on the design of mechanically fastened joints", National Aeronautical Establishment Canada, Aeronautical Note NAE-AN-37, NCR No-25442, February

**Pradhakaran, R.** (1982): "Photoelastic investigation of bolted joints in composite", Composites, Vol. 13, pp. 253-256

**Quinn, W. J. and Matthews, F. L.** (1977): "The effect of stacking sequence on the pin bearing strength in glass fibre reinforced plastic", Journal of Composite Materials, Vol. 11, pp. 139-145

**Rahman, M. U., Chiang, Y. J. and Rowlands, R. E.** (1991): "Stress and failure analysis of double-bolted joints in douglas-fir and sitka spruce", Wood and Fiber Science, Vol. 23, pp. 567-589

**Rahman, M. U. and Rowlands, R. E.** (1993): "Finite element analysis of multiple-bolted joints in orthotropic plates", Computers and Structures, Vol. 46, pp. 859-867

**Ramakrishna, S., Hamada, H. and Nishiwaki, M.** (1995): "Bolted joints of pultruded sandwich composite laminates", Composite Structures, Vol. 32, pp. 227-235

**Ramkumar, R. L. and Tossavainen, E. W.** (1984): "Bolted joints in composite structures: Design, analysis and verification task I test result- single fastener joints", AFWAL-TR-84-3047

**Reddy, J. N. and Pandey, A. K.** (1987): "A first-ply failure analysis of composite laminates", Computer and Structures, Vol. 25 pp. 371-393

**Rowlands, R. E., Rahman, M. U., Wilkinson, T. L. and Ching, Y. I.** (1982): "Single- and multiple-bolted joints in orthotropic materials", Composites, Vol. 13, pp. 273-279

**Sandhu, R. S.** (1972): "A survey of failure theories of isotropic and anisotropic materials", Air Force Flight Dynamics Laboratory, Technical Report AFFDL-TR-72-71, Wright Aeronautical Labs, Dayton, OH

**Serabian, S. M. and Oplinger, D. W.** (1987): "An experimental and finite element investigation into the mechanical response of 0/90 pin-loaded laminates", Journal of Composite Materials, Vol. 21, pp. 631-649

**Serabian, S. M. and Anastasi, R. F.** (1991): "Out-of-plane deflections of metallic and composite pin-loaded coupons", Experimental Mechanics, March 1991, pp. 25-32

**Serabian, S. M.** (1991): "The effect of nonlinear interlaminar shear behavior on the modeling accuracy of $[(0/90)_3,0]_s$ and $[(+45/-45)]_{3s}$ pin-loaded laminates", Journal of Composite Technology & Research, Vol. 13, pp. 236-248

**Smith, P. A.** (1985): "Aspects of the static and fatigue behaviour of composite laminates, including bolted joints", PhD Thesis, Cambridge University Engineering Department, Cambridge, UK

**Smith, P. A., Pascoe, K. S.** (1985): "Behaviour of bolted joints in $(0/90)_{ns}$ laminates, Cambridge University Engineering Department Technical Report (CUED/C/MATS/TR.121), UK

**Smith, P. A., Pascoe, K. S., Polak, C. and Stroud, D. O.** (1986): "The behaviour of single-lap bolted joints in CFRP laminates", Composite Structures, Vol. 6, pp. 41-55

**Smith, P. A., Ashby, M. F. and Pascoe, K. S.** (1987): "Modelling clamp-up effects in composite bolted joints", Journal of Composite Materials, Vol. 21, pp. 878-897

**Stewart, W. C.** (1965): "Metals Engineering Design", ASME Handbook (Ed.Horger, O. J.), McGraw-Hill, New York

**Stockdale, J. H. and Matthews, F. L.** (1976): "The effect of clamping pressure on bolt bearing loads in glass fibre reinforced plastics", Composites, Vol. 7, pp. 34-38

**Tsai, W. S.** (1965): "Strength characteristics of composite materials", NACA CR-224

**Tsai, S. W. and Hahn, H. T.** (1975): "Failure analysis of composite materials", Inelastic behaviour of composite materials (Ed. Herakovich, C. T.), American Society of Mechanical Engineer, New York

**Tsai, W. S. and Wu, E. M.** (1971): "A general theory of strength of anisotropic materials", Journal of Composite Materials, Vol. 5, pp. 58-80

**Tsieng, T. H. and Mandell, J. F.** (1985): "Damage development in bolt bearing of composite laminates", AIAA Journal, Vol. 23(10), pp. 1570-1577

**Tsujimoto, Y and Wilson, D.** (1986): "Elasto-plastic failure analysis of bolted joints", Journal of Composite Materials, Vol 20, pp. 236-252

**Waddoups, M. E., Eisenmann, J. R. and Kaminski, B. E.** (1971): "Macoscopic fracture mechanics of advanced composite materials", Journal of Composite Materials, Vol. 5, pp. 446-455

**Wang, S. and Han, Y.** (1988): "Finite element analysis for load distribution of multi-fastener joints", Journal of Composite Materials, Vol. 22, pp. 124-135

**Waszczak, J. P. and Cruse, T. A.** (1971): "Failure mode of strength predictions of anisotropic bolt bearing specimens", Journal of Composite Materials,Vol. 5, pp. 421-425

**Waszczak, J. P. and Cruse, T. A.** (1973): "A synthesis procedure for mechanically fastened joints in advanced composite materials", AFML-TR-73-145, Vol. II, September, 1973.

**Wilkinson, T. L., Rowlands, R. E. and Cook, R. D** (1981): "An incremental finite element determination of stresses around loaded holes in wood plates", Computers and Structures, Vol. 14, pp. 123-128

**Wilson, D. W. and Pipes, R. B.** (1981): "Analysis of shearout failure mode in composite bolted joints", Composite Structure 1 (Ed. Marshall, I.H.), pp. 34

**Wilson, D. W. and Tsujimoto, Y.** (1986): "On Phenomenological failure criteria for composite bolt joint analysis" Journal of Composite Science and Technology" Vol. 26, pp. 283-305

**Whitney, J. M. and Nuismer, R. J.** (1974): "Stress fracture criteria for laminated composites containing stress concentrations", Journal of Composite Materials, Vol. 8, pp. 253-265

**Wood, J** (1994): "Finite element analysis of composite structures", Composite Structures, Vol. 29, pp. 219-230

**Yamada, S. E. and Sun, C. T.** (1978): "Analysis of laminate strength and its distribution", Journal of Composite Materials, Vol. 12, pp. 275-284

**Ye, L.** (1988): "Role of matrix resin in delamination onset and growth in composite laminates", Composite Science & Technology, Vol. 33, pp. 257-277

**Yogeswaran, E. R. and Reddy, J. N.** (1988): "A study of contact stresses in pin loaded plates", Computers and Structures, Vol. 30, pp. 1067-1077.

**Zimmerman, K. B.** (1991): "Mechanical fastening of GFRP composites", AIAA J., Vol. 29, pp. 1009-1011

# APPENDIX A

# MACROMECHANICAL FAILURE THEORIES

Macromechanical failure theories for composites lamina have been proposed by extending and adapting isotropic failure theories, such as maximum normal stress (Rankine), maximum shear stress (Tresca), and maximum distortional energy (Von Mises), to account for the anisotropy in stiffness and strength of composite lamina. Sandhu (1972) and Nahas (1986) have surveyed the literature on anisotropic failure theories, the latter containing a summary of more than forty such theories.

All existing failure theories are based on a phenomenological design criteria because of its simple and direct approach. It is often assumed that failure criteria can be established and strength predicted for a composite lamina, subjected to a combination of stresses, if the strength of the five loading modes of a unidirectional lamina, i.e., longitudinal tension and compression, transverse tension and compression and longitudinal shear, have been determined. Of all failure theories available, the most frequently used failure criteria theories used in predicting the strengths of composite lamina are presented below.

## MAXIMUM STRESS FAILURE THEORY

According to the maximum stress failure theory, a ply is considered to have failed when any stress in the principal material directions is equal to, or greater than, the corresponding allowable strength. Thus, no failure will occur if:

$$\begin{aligned} -X_c < \sigma_1 < X_t \\ -Y_c < \sigma_2 < Y_t \\ -S < \tau_{12} < S \end{aligned} \qquad \text{(A.1)}$$

Where $\sigma_1$ and $\sigma_2$ are the normal principal stress components; $\tau_{12}$ is the shear stress component; $X_c$, $X_t$, $Y_c$ and $Y_t$ are the longitudinal compressive and tensile strengths and transverse compressive and tensile strengths, respectively; $S$ is in-plane shear strength. Failure surfaces for the maximum stress criterion are shown schematically in Figure A.1.

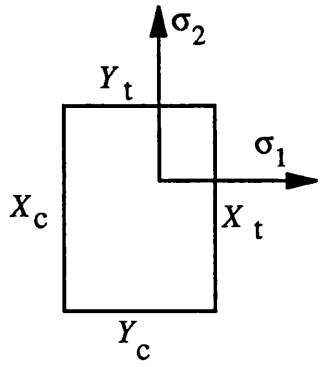


Figure A.1 Schematic failure surface for maximum stress

The maximum stress theory is more applicable for the brittle modes of failure of the material, closer to transverse and longitudinal tension, and does not take into account any stress interaction under a general biaxial state of stress.

## MAXIMUM STRAIN FAILURE THEORY

Similar to the maximum stress failure theory, the maximum strain failure theory is probably the most widely accepted lamina strength prediction theory and is commonly used in the aerospace industry. Failure of a ply arises when any strain in the principal material directions is equal to, or greater than, the allowable strain in same direction. Failure is avoided if the following conditions are satisfied:

$$\begin{aligned} -\varepsilon_{Lc} < \varepsilon_1 &< \varepsilon_{Lt} \\ -\varepsilon_{Tc} < \varepsilon_2 &< \varepsilon_{Tt} \\ -\gamma_s < \gamma_{12} &< \gamma_s \end{aligned} \qquad \text{(A.2)}$$

where $\varepsilon$ and $\gamma$ are the normal and shear strains respectively; subscripts Lc and Lt denote the longitudinal compressive and tensile components, respectively; Tc and Tt the transverse compressive and tensile components and s is the shear in corresponding plane. The maximum strain failure theory is often preferred over the maximum stress theory because the allowable strain data is usually more accurate than the allowable stress data for certain types of material. The failure surface is shown schematically in Figure A.2.

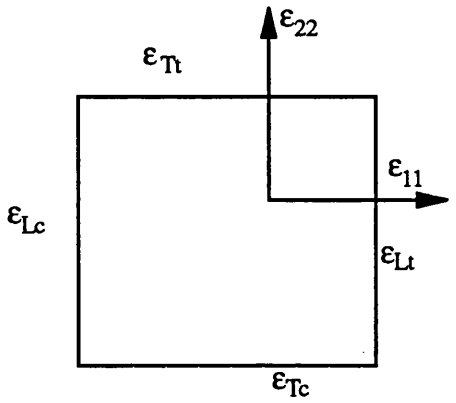


Figure A.2 Schematic failure surface for maximum strain

## AZZI-TSAI-HILL FAILURE THEORY

Azzi and Tsai (1965) proposed this failure criterion after Hill's generalized Von Mises isotropic yield failure criterion for anisotropic materials. The criterion for unidirectional lamina states that failure occurs in an orthotropic lamina if and when the following equality is satisfied,

$$\frac{\sigma_1^2}{X^2}-\frac{\sigma_1\sigma_2}{XY}+\frac{\sigma_2^2}{Y^2}+\frac{\tau_{12}^2}{S^2}=1 \qquad \text{(A.3)}$$

where $\sigma_1$ and $\sigma_2$ are both tensile (positive) stresses. When $\sigma_1$ and or $\sigma_2$ are compressive (negative) stresses, the corresponding compressive strength are used in this equation. Graphic representations of Azzi-Tsai-Hill theory in the stress coordinate system or failure envelope for a general anisotropic lamina is shown in Figure A.3, for various values of the $\tau_{12}/S$ ratio.

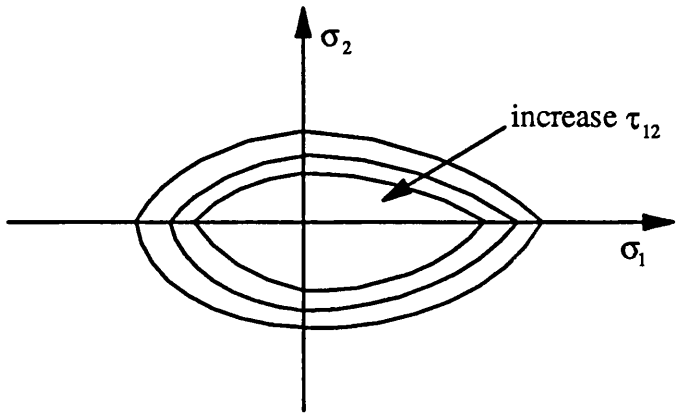


Figure A.3 Failure envelope of Azzi-Tsai-Hill theory

The Azzi-Tsai-Hill failure theory is expressed in terms of a single criterion instead of the three subcriteria required in the maximum stress and maximum strain theories. The Azzi-Tsai-Hill theory allows for considerable interaction between the stress components. One disadvantage, however, is that it does not distinguish between tensile and compressive strengths. The strength parameters in Eq. (A.3) must be specified according to the given state of stress.

## HOFFMAN FAILURE THEORY

The Hoffman failure criterion is similar to the Azzi-Tsai-Hill criterion, but accounts for different strengths in tension and compression. This failure criterion is expressed as:

$$\frac{\sigma_1^2 - \sigma_1\sigma_2}{X_t X_c} + \frac{\sigma_2^2}{Y_t Y_c} + \frac{X_c - X_t}{X_t X_c}\sigma_1 + \frac{Y_t - Y_c}{Y_t Y_c}\sigma_2 + \frac{\tau_{12}^2}{S^2} = 1 \tag{A.4}$$

## TSAI-WU FAILURE THEORY

The most general failure criterion for composite materials is the tensor polynomial criterion given by Tsai (1965) and Tsai and Wu (1971). Failure in an orthotropic lamina is predicted when the following equality is satisfied:

$$F_1\sigma_1 + F_2\sigma_2 + F_6\tau_{12} + F_{11}\sigma_1^2 + F_{22}\sigma_2^2 + F_{66}\tau_{12}^2 + 2F_{12}\sigma_1\sigma_2 = 1 \qquad \text{(A.5)}$$

Here, $\sigma_{ii}$ are the stress tensor components in the material principal coordinate directions and $F_i$ and $F_{ij}$ are the component of the strength tensors, such that:

$$F_1 = \frac{1}{X_t} - \frac{1}{X_c} \;:\; F_2 = \frac{1}{Y_t} - \frac{1}{Y_c} \;:\; F_6 = 0$$
$$F_{11} = \frac{1}{X_t X_c} \;:\; F_{22} = \frac{1}{Y_t Y_c} \;:\; F_{66} = \frac{1}{S^2} \qquad \text{(A.7)}$$

where $F_{12}$ is a strength interaction term between $\sigma_1$ and $\sigma_2$ which is determined experimentally. All these components are referenced with respect to the principal axes of the material. This equation assumes that there is no interaction between shear stresses and normal stresses.

Since reliable experimental data are not always easy to obtain an approximate range of $F_{12}$ has been recommended by Tsai and Hahn (1975).

$$-\frac{1}{2}(F_{11}F_{22})^{\frac{1}{2}} \le F_{12} \le 0 \qquad \text{(A.8)}$$

The lower limit of this equation is frequently used for $F_{12}$ in absence of experimental data.

Typical comparison of the failure envelopes of five failure criterion theories is shown in Figure A.4. All the stress tensors described here have been used for special cases, which are a reduced form of the Tsai-Wu tensor polynomial theory (Reddy and Pandey, 1987)

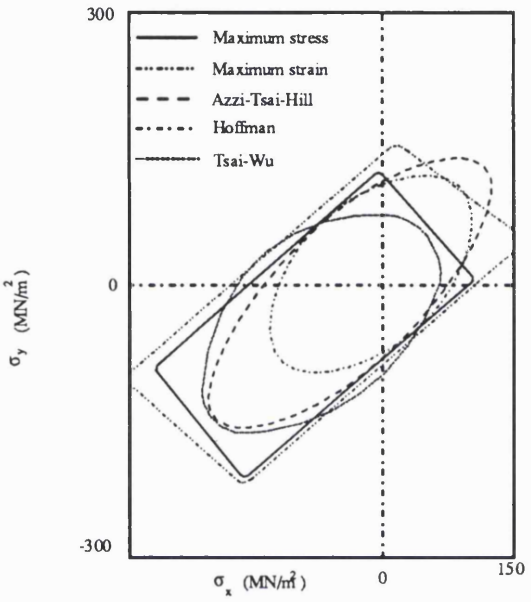


Figure A.4 Comparison of the failure envelope of the most often used failure theories

The failure theories previously given are representative and the most widely used. The validity and applicability of a specific theory depends on the convenience of application and agreement with the experimental results. Since the failure mode depends on the material properties and loading condition, the applicability of the various theories must also be related to the type of material and failure mode.

For example, the maximum stress and maximum strain theories are more applicable when brittle behaviour is predominant. Although the concept of these theories is simple, they are not suitable for computational operation since there are three subcriteria involved.

The interactive theories, such as Azzi-Tsai-Hill, Hoffman and Tsai-Wu theories, are more applicable when ductile behaviour under shear or compression loading is predominant. For the Tsai-Wu failure theory, a comprehensive material characterization program is desirable to determine accurately the numerous material parameters required.

## ANALYTICAL STRENGTH PREDICTION

The failure criterion theories reviewed previously in this appendix only apply to individual laminate layers, with the assumption that the lamina or ply forming part of the laminate exhibits the same behaviour as a unidirectional isolated ply. The stresses and strains in each lamina, that may be computed, are transformed into stresses and strains in the principal material directions. These results may be compared with the failure envelope produced by one of the methods described above to determine which lamina has failed first.

If the laminate strength is considered as the initial failure of a single lamina in either the fibre direction or in the direction perpendicular to the fibres, the method is termed: first ply failure (FPF). On the other hand, if the strength is

considered after the structure has degraded to the point where it is no longer capable of carrying additional load, the method is called last ply failure (LPF).

For the last ply failure approach, reduced stiffness and strains, determined by either the total discount method, limited discount method or residuary property method, are assign to the failed laminate. The stresses and strains of remaining laminas are recalculated and then the process is repeated by comparing the stress or strain with the appropriate failure envelope until the ultimate failure of the laminate takes place.

In many composite laminates, first ply failure occurs just before ultimate failure (Mallick, 1988), and this is considered as justification of the first ply failure design approach. In other materials, the last ply failure approach may be more suitable, since the first ply approach can be considered rather conservative. If the laminate stresses are $\sigma_x$, $\sigma_y$ and $\tau_{xy}$ the transformations of laminae stress of the $n^{th}$ ply are,

$$\begin{aligned}
\sigma_1^{(n)} &= \sigma_x \cos^2\theta_n + \sigma_y \sin^2\theta_n + 2\tau_{xy}\cos\theta_n \sin\theta_n \\
\sigma_2^{(n)} &= \sigma_x \sin^2\theta_n + \sigma_y \cos^2\theta_n - 2\tau_{xy}\cos\theta_n \sin\theta_n \\
\tau_{12}^{(n)} &= (-\sigma_x + \sigma_y)\sin\theta_n \cos\theta_n + \tau_{xy}(\cos^2\theta_n - \sin^2\theta_n)
\end{aligned} \qquad \text{(A.9)}$$

when $\theta_n$ is the ply orientation of $n^{th}$ lamina. If the failure criterion is satisfied in a ply of an element, the individual contribution, or failure indices, of each stress component to the tensor polynomial are computed. For example, if the

contribution of the $\sigma_1^{(n)}$ to the polynomial is larger than the contribution of the other stress components, then it is assumed that failure in that ply is caused by the tension or compression in the 1 direction depending on the sign of $\sigma_1^{(n)}$. The failure indices can also be used to reduce the stiffness in post first ply failure (FPF) analysis.